TRANSPORT PHENOMENA IN THE HUMAN SKIN

by

Kosmas Kretsos

October 23 2003

A dissertation submitted to the

Faculty of the Graduate School of State

University of New York at Buffalo

in partial fulfillment of the requirements for the

degree of

Doctor of Philosophy

Department of Chemical Engineering

INFORMATION TO USERS

The quality of this reproduction is dependent upon the quality of the copy submitted. Broken or indistinct print, colored or poor quality illustrations and photographs, print bleed-through, substandard margins, and improper alignment can adversely affect reproduction.

In the unlikely event that the author did not send a complete manuscript and there are missing pages, these will be noted. Also, if unauthorized copyright material had to be removed, a note will indicate the deletion.

ProQuest Information and Learning Company
300 North Zeeb Road
P.O. Box 1346
Ann Arbor, MI 48106-1346

Στην ιερη μνημη του πατερα μου

Abstract

Drugs and chemicals applied to the skin surface permeate deeper tissue layers, and also pass into the body's systemic circulation by entering blood vessels in the dermis. Quantitative aspects of the dermal diffusion and capillary clearance processes are key to the effective development of transdermally delivered drugs, as well as to risk assessment of chemical exposure in applications ranging from cosmetics and other consumer products, to protection against biological warfare agents. The present work addresses three major aspects of these phenomena:

A comprehensive macroscopic transient model of transdermal diffusion is developed (Chaps. 3 and 4). It specifically accounts for the spatial distribution of blood vessels (in terms of convection-enhanced volumetric dispersion and clearance coefficients), and explicitly incorporates transport through deeper tissue. Comparisons with published experimental results show the manner in which the model improves upon existing models.

The first steps toward the development of a microscopic model of the dermis are presented (Chap. 5). The model is based on dermal physiology, and it will encompass physical processes such as protein binding and hindered diffusion of solute. The end result will be a framework for correlating and predicting the effective "background" transport properties (solute diffusivity and partition coefficient) of the dermis, within the context of the medium in which blood vessels and appendages are embedded.

A new geometrical model is developed to describe the dermal capillary clearance process (Chaps. 6 and 7). The real physiological structure is modeled in terms of a doubly periodic array of absorbing capillaries. Convection-dominated transport in the blood flow within is coupled with diffusion outside, the latter process being quantified using a slender-body-theory approach. Convective transport across the capillary wall and in the surrounding interstitial space is also considered. The model

accounts for the finite permeability of the capillary wall, as well as for the geometry of the capillary array, based on realistic values of physiological parameters. The ultimate outcome is a prediction of the dermal flux (or rate of absorption) per unit area of skin. Parametric studies quantify the importance of the capillary permeability and blood flow velocity in the process of the microvascular clearance.

Acknowledgments

Four years of work do not pass without the help and support of mentors, friends and family. Therefore, I would like to thank those who have been constant guides in my studies and work.

I will be forever grateful to my advisor, Dr. Johannes Nitsche for everything that he taught me. A friend told me once that it is the duty of a student to try to be better than the teacher; it was not long until I realized that this was impossible. Nevertheless, he inspired me to be better, as a person and as a scientist, and I am certain that my work will always reflect what I have learned from him. I feel privileged to have called myself his student.

Another positive scholastic influence has been Dr. Gerald Kasting. He created an awareness of pharmaceuticals in my work and my interaction with him throughout my studies have made this thesis more holistic than it may have otherwise been. I am looking forward to working with him again soon. Many thanks also to Dr. Michael Roberts whose communications about salicylic acid were invaluable.

I am unable to find the right words when I try to express my gratitude to my family. My father, Ioannis, and my mother, Chrisanthi, taught me to be who I am through their love and constant support. In order to give me more opportunities and a better future, they endured great suffering. I only hope that I will someday be able to give the same gifts to my children. My big brother, Giorgos, was always keeping an eye on me and kept me out of trouble in numerous occasions! I feel lucky that he continues to be a positive role model for me. Both he and my sister-in-law, Eirini,were a constant source of encouragement through this journey. They also gave me a great gift in my little nephew Ioannis, who managed to put a smile in my heart during difficult times. My love, Kristin, offered me constant support, comfort and managed to endure my strange self. Her love and the kindness of her heart make me

want to be a better man. I feel blessed that she is in my life.

During my studies, I was fortunate enough to have good friends that were always there when I needed them. Many thanks to my roomates, Chris and Yanni, for the gift of their friendship. I would also like to thank Aris, Fanis, Greg and Tara, Maria and Vicki, George and Chrisaugi for the privilege of calling them my friends.

Contents

List of Figures

List of Tables

Chapter 1

Introduction

1.1 Motivation

The study of permeation of, and transport through, human skin has many important applications. If we consider the vast array of substances with which we come into contact, we may facilely arrive at the conclusion that skin is a formidable barrier. However, it became apparent, as early as the late 19th century, that skin is not absolutely impermeable [324]. In more recent years, this "vulnerability" triggered a large amount of research [8, 90, 119, 172, 224, 238, 331, 389, 404], motivated by the quest for effective transdermal drug delivery. The momentum that the transdermal delivery has gained is considerable. In 2001, 40% of the drug delivery candidate products under clinical evaluation were transdermal systems, while the worldwide transdermal patch market is worth $\simeq 2\pounds$ billion [23]. Given the very limited number of FDA approved, transdermal drug formulations that exist currently [134, 236], one can imagine the potential of this industry.

Drug administration through skin offers a very attractive alternative to the more traditional oral and intravenous routes. Compared to injections, it offers a painless analogue that does not require any assistance to the patient. Compared to oral administration, it eliminates losses due to gastrointestinal metabolism. Compared to

both of the latter, it has the great advantage of a controlled-release, steady-state process that may be sustained for days [165, 178, 341]. However, the optimism stemming from the potential advantages is counterbalanced by the remarkable barrier properties of skin [178]. The limitations are considerable; there is a general consensus on that an effective drug delivery by passive (unassisted) permeation through skin, is restricted to small substances that possess "ideal" properties, e.g, high potency and certain solubility characteristics [23, 134, 341]. Furthermore, there is always the danger of eliciting an irritant or allergic reaction [178, 236].

We should note at this point the existence of an important branch of transdermal delivery research which deals with the enhancement of drug administration. This may be done either by altering the (passive) barrier properties of skin, or by inventing donor formulations/devices that interact in a desired manner with skin. Thus, research has developed in electrically-assisted transport [295], the most popular approach being iontophoresis [341], as well as sonicated transport (ultrasound) [165] and hydration of skin prior to treatment [23]. Devices that enhance delivery include highly specialized and complex membranes-patches [178], liposomes that carry the drug through skin and subsequently release it [23], high velocity particles that are fired into skin [280], sorption-promoting chemicals that temporarily diminish the skin's barrier ability [44], and microneedles [280].

Besides the intense interest in the ways to deliver drugs through the skin, there is an equally important interest in assessing, and consequently planning preventive strategies of, transdermal permeation of noxious substances. The main goal of the risk assessment field is to determine whether the absorption of chemicals into, or penetration through, the skin can have a local or systemic, toxic effect [272]. Compared with other ways by which systemic toxicity may occur (oral and/or inhalation exposures), dermal exposure or the percentage of the total exposure that can be attributed

to it is not easily measured and probably not so acute. This is exemplified by the fact that, out of 30,000 chemicals in commercial use, only 275 have a skin notation in their label, with no quantitative information [272]. The picture is certainly clearer for substances that are intended to be applied to skin. A good review ([6]) reports a very long list of topically applied drugs and cosmetic agents that have been proven to have systemic, toxic, side-effects after their application. Furthermore, dermal exposure to chemicals may be critical if it has a local effect, i.e., irritation and allergic reaction [124] and/or it occurs over a prolonged period of time, i.e., in a working environment [219]. Surprisingly enough, even the common bathing/showering has been recently put under the microscope in order to determine if there is substantial, potentially toxic, exposure to substances like chloroform [213].

A third area that makes the study of transport through skin important, became apparent to the general population after the recent events of September 11. The subsequent attacks via anthrax-contaminated mail renewed the research interest in protection against biological warfare. Several of the known, potentially weaponized, viruses and bacteria either enter the human body through skin, or manifest themselves on the skin. Examples include cutaneous anthrax [71], smallpox, and influenza (both of the latter being spread respiratory and by skin contact) [70]. Surely, for these substances the most important aspect is the immunological response of the host. However, these are substances that are transported through skin. Thus, by studying their pattern of absorption one may be able to invent ways of preventing it.

1.2 The study of transport through human skin

Research in the literature to date has focused on selected aspects of the big picture of transdermal transport. The leading target of study has been the steady-state permeability coefficient $P_{sc/w}$ (or closely related properties) of the outermost stra-

tum corneum ("SC") layer of skin, which serves as the primary barrier to molecular passage. A vast body of *in vitro* experimentation has yielded empirical determinations of $P_{sc/w}$ over wide ranges of permeant molecular structure, species- and body site-variations in skin type, and permeation conditions. Corresponding theoretical studies have produced models for $P_{sc/w}$ taking the form of approximate correlations in terms of molecular solubility, size/mobility and other parameters [42, 58, 172, 173, 276, 277, 324, 395]. Microscopic "brick-and-mortar" diffusion models [111, 120, 147, 164, 197, 224, 365] represent a more mechanistic approach to understanding the basis of $P_{sc/w}$ in SC structure and the physicochemical and transport properties of its constituent phases. The intercellular pathway through the extracellular lipid ("lipid pathway") is often regarded as the dominant route for transport [5, 45, 112] and emphasized both in corellations [275, 276] and "brick - and - mortar" models [164, 365]. However, strong evidence for parallel transcellular and polar pathways exists [2, 10, 11, 43, 79, 143, 144, 177, 194, 261, 262, 357, 400, 403], and such pathways have been included, at least approximately, in some permeability correlations [172, 173, 177, 200, 380, 395, 400].

Although the stratum corneum is the primary barrier, transport processes occurring below this membrane can dramatically affect transdermal fluxes, as well as the pharmacologically important local concentration levels. These processes are operative in *in vivo* permeation studies in which the outcome of SC permeability is manifested only in convoluted form [5]. Kasting et al. [172] included a resistance in series for an aqueous layer below the SC (representing an approximate model for the epidermal and dermal layers) in their model for steady transdermal flux. They concluded that this additional aqueous layer resistance sets an upper limit on the flux for very lipophilic compounds, which would otherwise be predicted to be very large owing to high solubility in the intercellular lipid. In addition, experimental

results [188] have shown that, although studies focused on SC adequately predict the steady-state transdermal flux and the overall skin permeability coefficient, they underestimate other important parameters such as the half-life of the drug and the lag time following application to skin. Furthermore, recent experimental findings revealed that the common assumption of a perfect clearance through the bloodstream, occuring at a certain depth in the superficial dermis, may not be valid, depending on the solute [215, 233], environmental and pathological conditions [119, 302], and cooadministration of vasoconstrictive drugs [35, 47, 237, 338]. The papers cited raise major questions regarding the role played by deeper tissue layers. These questions are particularly tantalizing because they arise even in highly simplified representations where only molecular diffusion (and not convection by capillary blood flow) is allowed for. The reality of deeper tissue dispersion and clearance processes is likely to have considerably richer physics, in part because the permeable blood capillaries are distributed over the volume of the dermis and hypodermis. Moreover, the outcome of this physics for transient permeation (as opposed to steady permeation considered in existing models including an aqueous series resistance) is likely to be even more interesting.

1.3 Overview

There exist numerous physiological descriptions of the human skin; however, most of them deal with the structure in a qualitative manner. Chapter 2 approaches skin physiology in a quantitative, coincise, "engineering" way, suitable for providing the necessary metrics for a practical, modeling attempt. Chapter 3 introduces a new, whole-skin, non-steady state, transport model in which the processes of diffusion and blood clearance are treated as spatially distributed phenomena. This model is used in Chapter 4 for the deduction of dermal transport parameters through the fitting of

published experimental results on the dermal absorption of salicylic acid. Chapter 5 provides the initial steps toward the construction of a geometrical, physiologically accurate model that predicts the transport characteristics of the dermal layer. Several topics on the capillary exchange field are debated in Chapter 6. A plethora of quantitative information is reported and key theoretical issues are discussed. Finally, Chapter 7 introduces a microscopic, theoretical model of the clearance process occuring through the dermal blood capillaries. It is a three-dimensional, steady-state model in which capillary-capillary interactions are accounted for, and both diffusive and convective transport processes are included. Results on the clearance of salicylic acid from the dermal capillary array show the manner by which this model improves upon existing models. The way by which the capillary model may be used in conjuction with a macroscopic representation of skin is also investigated.

Chapter 2

Normal Skin Physiology

2.1 Introduction

The scope of this chapter is to provide a brief physiological description of the normal (non-pathological) human skin from an engineering/quantitative point of view with emphasis on the dermis and the microcirculation. Skin is the largest and most versatile organ of the body, having a surface of ~ 2 m^2 [241, 294] and totaling more than 10 % of body weight [302, 401]. It has unique functions since it is our almost exclusive "contact" with the environment. It :

- Protects from mechanical stresses
- Prohibits entrance of noxious substances.
- Acts as a permeability barrier preventing losses of internal fluid/substances.
- Regulates the temperature via its blood flow and perspiration.
- Senses external signals with its nerves.
- Serves as a food reserve (hypodermis).

Skin has three separate layers that are quite different from each other. The superficial epidermis may be viewed as a thin cellular wall. The underlying layer is the fibrous

water-based dermis, host to numerous integral structures. The last skin layer is the lipid-rich hypodermis. It should be noted that there are well recognized variations of the skin's "normal" features associated with species, sex, age, nutrition, climate and a marked individual variability [49, 69, 113, 193, 232, 259, 347, 378]. Also, one should bear in mind that the skin is a living organ, constantly changing and responding to its environment. Furthermore, many of the experimental studies that are cited here were performed *ex vivo* with techniques that potentially destroy or extract skin moieties [176]. The reader may consider the herein reported characteristics as quantitative guidelines but not as absolute limits. However, the following analysis is essential to a modeling attempt of skin's functions and properties.

2.2 Epidermis

The epidermis is a highly cellular, avascular, continuous stratified sheet. It consists of roughly cuboidal cells that are stacked together. The intercellular space is filled with a "glue substance" [104], suggested to be comprised from a mixture of polysaccharides, proteins, and lipid-rich secretory products of cells in aqueous solution [113, 157, 258]. The cells are mostly keratinocytes (at least 80 % [137]), named after the fibrous keratin proteins which are the end product of differentiation. Other epidermal cells include melanocytes, Langerhans' cells and Merkel cells [113, 241, 302].

Its thickness varies with anatomical site; for the better part of the body it is $O(100)\mu$m thick [8, 36, 113, 137, 241, 316, 324] with the exception of palms and soles where it can be several times thicker [8, 241, 294].

Epidermis is constantly replenished. Keratinocytes are produced at the dermal-epidermal junction by proliferation, ascend into the superficial layers as they differentiate, and finally reach the outermost layer and die [157, 302, 335]; it takes about

one to two months for all cells to be completely replaced [241, 335].

As keratinocytes differentiate/mature, they experience an orderly succession of biochemical and structural changes such as water content [113, 125, 383] and shape. Depending on the stage of differentiation and depth, epidermis is divided into distinct sublayers [137, 157, 241, 294, 335]: The basal layer (*stratum basale*), which is a single row of columnar cells, is the site where cell growth begins. The prickle layer (*stratum spinosum*) consists of polyhedral cells and is the thickest of them all; it has a variable thickness but is usually five-cells thick. The granular layer (*stratum granulosum*) can be thought of as the transition from life to death, as the cell characteristics change and keratin is produced. Some authors report an additional, one-cell thick layer, the hyalin layer (*stratum lucidum*).

The outermost layer is called the horny or keratin layer (*stratum corneum*) and has been identified as the principal barrier for skin permeation [8, 137, 294, 324, 325, 368]. It is composed of $\sim$ 15 layers of closely stacked, flattened, lipid-depleted, protein-enriched, dead keratinocytes also known as corneocytes, each one of them being $\sim 1\mu$m thick [222] and 30μm wide [241, 294, 302, 325]. The extracellular space ($\sim$ 30 % by volume [8]) is filled with highly ordered lamellar lipids. Some of stratum corneum's properties that may explain its low permeability are its low hydration ($15 - 20\%$), its high density (1.4g/cm^3 in the dry state) and its low surface area available for solute transport [302].

2.3 Dermal-epidermal junction

The cutaneous basement membrane has received attention as a separate, specialized structure with its own properties [55, 60, 229, 374, 397]. It is a network of interconnecting proteins with the main feature being the anchoring fibrils that extend into

the dermis and are partly responsible for skin's integrity [60]. Its basic functions are a) attachment of epidermis to dermis, b) mechanical support to epidermis. It has also been hypothesized that it may act as permeability barrier for macromolecules [8, 60, 397]. However, it is known that Langerhans cells are able to get across during an immune response.

2.4 Dermis

The dermis, which may be regarded as the main body of the skin, supports the epidermis by providing the necessary nutrients, regulates temperature, pressure, and pain, and offers structural integrity and elasticity to the whole skin in general. It is a relatively acellular connective tissue, enclosing two separate yet interwoven fiber meshes (collagen-elastin fibers), extensive microvascular- and lymphatic-vessel networks, a nerve network, and structures such as hair follicles and sweat glands. The rest of the space is occupied by a complex mixture of proteins and polysaccharides that forms a gelatinous amorphous matrix named ground substance. Apart from this, there is a percentage of plasma proteins extravascularly [259] that are originated from plasma leaks and are probably present inside liquid pools. The dermis varies substantially in thickness, being the thickest on the back and thigh and the thinnest on the face [347]; on the average it is ~ 2 mm thick [302, 316, 347]. The water content of dermis is $550 - 650$ mg/g fresh weight [259].

Based on physiological differences, dermis is divided in two regions. The superficial one is called papillary, while the underlying one is called reticular. The papillary dermis is molded against the epidermis forming papillae (approximately conical, fingerlike elevations existing at a number density of $O(100)/\text{mm}^2$ skin surface [15, 113] being $0.1 - 0.2$mm in height [113]) and thus conforms to the epidermal basal ridges and grooves [241]. It is $\sim 100 - 200\mu$m thick [137, 324] (or 1/10 of full dermal thick-

ness [347]) and has a water content of 71% [125]. It is richer in cells, nerves and vascular vessels [125, 241], and the collagen and elastin fibers are thinner, fewer, and molecularly different from those in the deeper dermis [137, 158, 241, 347].

The reticular layer has denser fibrillar networks, sparse vasculature and cell populations, and a proportionately smaller amount of ground substance [241]. The collagen fiber bundles are aligned with the skin surface, contrary to the ones in the papillary where they are randomly oriented [241, 316]. Reticular dermis is also drier (61% water [125]).

Notably, the papillary dermis "invades" its reticular neighbor forming sheaths around hair follicles, sweat glands and ducts. These extensions collectively go by the name periadnexal dermis while the term adventitial dermis is used to describe both the papillary and periadnexal dermis [347].

2.4.1 Collagen fibers

Collagen is the dominant extracellular constituent of the dermis (90 % of the total protein [270]) (Table 2.1) providing both tensile strength and elasticity. It is very hydrophilic with an "astonishing capacity to bind and release water depending on pH, temperature, ionic strength of the surrounding medium" [125]. Experiments have shown that H_2O binds to collagen in two ways; mostly weakly ("swelling water", 79% of bonds), and firmly (21%) [125].

Collagen molecules align into a highly precise organized pattern [270] to form a fibril $15 - 200$ nm in diameter depending on location. These fibrils, in turn, are packed closely with each other (the space between them is similar to, or less than, their diameter [368]) making the collagen fibers which are predominantly organized in bundles. Both the fibers and the bundles thereof are larger in the reticular region

Fiber diameter(μm)	% Skin weight	% Skin volume	% Skin area	Source
$1-35^b$ $3-90^c$			93.35 ± 4.6 89.2 ± 5.5	[49]
	$\sim 75^a$			[137]
		$\sim 70^a$		[378]
$5-30$ $\sim 25^c$				[115]
	75^a	$18-30$		[368]
	$70^{a,d}$			[125]
	30			[257]
	20			[69]
	$70-80^a$			[245]

Table 2.1: Dermal collagen properties; [a]dry dermis, [b]papillary, [c]reticular, [d]fat-free

[137] and they are slightly [115] or predominately [241] oriented in the plane of the skin. There are 25 genetically different types of collagen so far identified, 6 of which are present in skin [374]. The main types are I and III, their content ratio in dermis being 5 : 1 or 6 : 1. Type I collagen forms the majority of reticular dermis (thick fibers, diameter $60-100$ nm) whereas type III makes $10-15\%$ of dermal content (thin fibers, diameter $20-40$ nm). Type III is enriched in the papillary dermis [137, 270, 347, 374]

2.4.2 Elastin fibers

Elastin fibers form highly branching superstructures around, but not connected to, bundles of collagen that are, at least partly, responsible for skin's mechanical behavior [249]. In reticular dermis there are mature, bandlike elastin fibers whereas in the papillary dermis the common type is thin immature (oxytalan) fibers [137]. The fibers have two components: the elastin core which formulates 90% of the fiber and microfibrils that surround the core [137, 347, 305, 373]. The fibers' diameter increases with depth. There is no apparent orientation preference (random network) except in the dermoepidermal junction region where they are predominantly perpendicular to

the skin's surface [81, 374].

Fiber diameter(μm)	% Skin weight[a]	% Skin volume	% Skin area	Source
	$1-2$			[245]
$\sim 0.8^b$ $\sim 1.75^c$		0.75^b 2.5^c		[378]
2.5		2.1 ± 1.1	5.4 ± 2.9	[373]
	4	1		[368]
	$2-4$			[305]
	$2-4$			[374]
	4			[137]
	2			[125]

Table 2.2: Elastin fibers properties; [a]dry dermis, [b]papillary, [c]reticular

2.4.3 Ground substance

The archaic term "ground substance" is an indication of the difficulty in defining the extracellular, extrafibrillar, extravascular component of skin. In fact, most of the information available in the literature to date refers to human cartilage. This difficulty originally lead to the misconception that since dermis is more than 50 % water, it may be considered an aqueous well-mixed solution. It has been debated that the fraction of freely movable fluid is small, found in the form of thin films no more than $\sim 0.5 - 1$ μm thick [168, 311, 390]. The ground substance is a gelatinous or semi-gelatinous complex mixture of polysaccharides (glycosaminoglycans) and polysaccharide-protein complexes (proteoglycans) [125] that have an enormous ability to bind water. There are also other sugar-containing glycoproteins with properties resembling those of the plasma proteins [258]. Measurements have showed that ground substance comprises 10% of dermis dry weight [159].

Glycosaminoglycans (GAGs) constitute $\sim$ 0.2 % of the dry weight of skin [137, 245, 258]. They are anionic polysaccharides (glycan) containing hexosamines (glycosamino) [333]. The principal GAG is hyaluronic acid ($\sim$ 25 mg/100g fresh

dermis weight [125, 258]) that can exist both free and bound to protein. Other GAGs include dermatan sulfate, keratan sulfate, chondroitin 4 (and 6-) -sulfate [76, 159, 258, 260]. The combination of GAGs with a protein yields a unit called proteoglycan (PG). They are large molecules (MW may be more than 10^6) consisting of the core protein and usually numerous (50 or more) GAG chains of various sizes and compositions that covalently bind to the molecule in a "bottle brush" configuration. PGs, in turn, may attach non-covalently to a large molecule of hyaluronic acid ($O(10^5)$ MW) to create proteoglycan aggregates of $O(10^8)$ MW [76, 333]. These extremely hydrophilic structures can bind up to 1000 (hyaluronic acid) or 100 (proteoglycan) times their volume, thus regulating the dermal water content, volume, and compressibility [76, 137]. Other important properties include interpenetration in, and binding to, the collagen and elastin fiber networks that lead to their immobilization, interactions with dermal cells, and volume exclusion of macromolecules like leaked plasma proteins [76, 137].

2.4.4 Cells

Most of the dermal cells can be found in their greatest density in the papillary region and surrounding vessels. The regular residents of the dermis are fibroblasts, macrophages and mast cells [125, 137]. The majority of the dermal cells are fibroblasts [193]. They migrate within the tissue producing tissue components such as collagen, laminin and fibronectin. The second most popular type is the macrophage (constituting $70-85\%$ of the total population together with the fibroblast [15]) that have a variety of functions including phagocytosis, wound healing and tissue remodeling [137]. Mast cells ($O(50)/\text{mm}^2$ skin surface [82]) are specialized secretory cells involved in immune responses. There are also fat cells , sparsely distributed, with the total fat content being $\sim$ 25 mg/g fresh weight [113, 259]. Naturally, there are

also cells associated with the existing vessels such endothelial cells and pericytes that form/surround the microvasculature, lymphocytes that form the lymphatics and leukocytes from blood at inflammation sites [125, 137].

2.4.5 Lymphatics

The lymphatic may be characterized as the drainage network that takes away the "debris" of daily wear and tear in a tissue [241, 312, 326]. Protein leaks from the blood vessels (mostly in the venular part [313]) along with plasma, and it has to be removed both for recycling and tissue pressure control purposes [302]. This is done by the lymphatic system, a tree-like collection of vessels (similar to the blood microcirculatory/circulatory system) that confines, removes, and eventually recycles back to the circulation the extravascular plasma leaks working hand in hand with the macrophages, cell-incinerators of proteins [137, 312]. The importance of the lymphatics is readily obvious from the fact that $50 - 60\%$ of plasma and $\sim 45\%$ of plasma proteins are leaked daily from blood [312, 313].

Lymphatics in the human skin first appear at the subpapillary dermis [137, 314, 326] while their presence in the dermal papillae has been associated with abnormal skin [312]. These initial lymphatic vessels are cylindrical microtubules ~ 50 μm in diameter [326, 349] that are composed of attenuated endothelial cells, with a discontinuous basement membrane surrounding them [241, 326]. The density of the network decreases with the depth while the diameter of the vessels increases. Thus, each part of the system drains into fewer, larger vessels that are equipped with flow regulating valves [326]. On the average the number density of lymphatic channels is $0.3 - 1.5$ per μm^2 [313].

2.5 Hypodermis

The subcutaneous fat has diverse functions. It serves as an energy reserve (a well-fed person can live without food for many weeks), a heat insulator (although recent findings suggest that fat can be more of an electric blanket/heat generator than a simple insulator), and a protective padding since it can absorb mechanical stress. It also affects the cosmetic appearance of skin since it is directly associated with wrinkles and lumps [137, 294, 302, 348]. Hypodermal fat is also important in the distribution and storage of drugs [40, 279].

Hypodermis is bounded above by the reticular dermis and below usually by deep fascia covering skeletal muscle. It is composed of loose areolar connective tissue with broad collagen bundles as its structural framework [348] and consists of 30 % water [125]. The extracellular space contains glycosaminoglycans and glycoproteins like the dermis [258].

Most of the cells are adipocytes (fat cells) [294]. They are either spherical white (mature) fat cells enclosing one big fat droplet, or polygonal brown fat cells enclosing several small droplets. On the average a white cell is 100 μm in diameter and encloses $0.04 - 0.06$ μg of fat [348].

Other subcutaneous structures include some hair follicles, nerves, mammary glands, lymphatics, some striated muscles and blood vessels with an extensive capillary network around fat cells [348].

2.6 Appendages

There are three primary types of appendages present in the skin: hair follicles, sebaceous glands and sweat glands. All of them have a microvascular supply net around

them.

2.6.1 Hair

Hairs are keratinous fibers that grow out from follicles all over the skin surface except the palms, soles and lips [241, 302]. There are two kinds: the terminal hair which may mainly be found in the scalp, and the fine body hair called vellus. Each hair goes through recurring metabolic stages of growth (anagen), regression (catagen), rest (telogen). The fiber is comprised from closely packed keratinized cells and can vary from a few μm to a hundred μm in diameter [241]. Most of the hairs originate from the reticular dermis. They are kept in place by attached smooth muscles that also erect the fibers in response to fear [302]. On the average, there are $O(100)$ fibers/cm^2 [302, 324] with the exception of the scalp where there are approximately 250 hairs/cm^2, 60 μm in diameter [106]

2.6.2 Sebaceous glands

These glands are directly associated with hair since they empty through a short duct into the follicular canal. They can be found anywhere except the palms, soles and feet dorsum [353]. There are usually $\sim 50-100/$ cm^2 [241, 302, 353], but there may be as many as $400-800$ glands/cm^2 on the face and scalp [353]. They are somewhat potato-shaped with a variable size, ranging from 200 to 2000 μm in diameter [113, 302]. Their secretion is called sebum. It is a semiliquid mixture of triglycerides, fatty acids, waxes, cholesterol and cellular remains that is presumably responsible for the lubrication and protection of skin as well as for the maintenance of a weak acidic pH [294, 302].

2.6.3 Sweat glands

Sweat glands are responsible for one of the most visible skin functions: perspiration. They can be further subdivided into eccrine glands, which secrete water, and apocrine glands, which produce the odorous component of sweat [294]. Eccrine glands are by far the predominant appendageal type in human skin in terms of sheer numbers since there exist two to four million of them distributed over the body surface [113, 241] ($100 - 200/cm^2$ or 0.01% of the total surface [302]). They consist of two continuous components: a duct in the upper part that ends at the skin's surface, and the water secreting site, an underlying coiled ball that is located in the lower dermis or sometimes the hypodermis [241, 302, 319]. Their secretion is a dilute salt solution [302].

The apocrine glands are generally larger (by a factor of ten) structures, located deeper than the eccrine glands and usually paired with hair follicles [142, 302]. They, too, are coiled tubes, limited to specific anatomical regions (armpit and pubic areas) and they are fewer in numbers than the eccrine glands. They are "scent" glands, secreting odor components connected with stress or sexual stimulation [294]. Their straight ducts run parallel with the hair follicle and empty their content in an orifice of the hair follicle located above the associated sebaceous gland [241, 303].

2.7 Dermal vasculature

The skin contains a rich vascular network that provides nutrition for the tissue, regulates temperature and blood pressure, and participates in wound repair and immunological responses [137]. The vessels that exist in the dermis originate from small musculocutaneous arteries that penetrate the subcutaneous fat and enter the reticular region.

The geometrical configuration of the vasculature in the human dermis arguably involves two horizontal plexuses, as suggested by the collective work of Braverman et al. [50, 51, 52, 53, 402]. The lower one is located near the dermal-hypodermal junction and gives rise to arterioles and venules that either connect with the upper plexus or branch into the lateral micronetwork that supplies dermal appendices such as hair bulbs and sweat glands. The second, substantially denser, plexus marks the boundary between the papillary and reticular dermis [137], roughly 1 to 2 mm below the skin surface, and is responsible for providing nutrients that are necessary for the survival of the avascular epidermis. As the first permeable part of the circulation that a skin penetrant meets, it is most important in terms of possible vascular clearance of the penetrant. Even though the physiological reality corresponds to a more randomly distributed microcirculation [313] the concept of two distinct horizontal plexuses appears to be functionally valid.

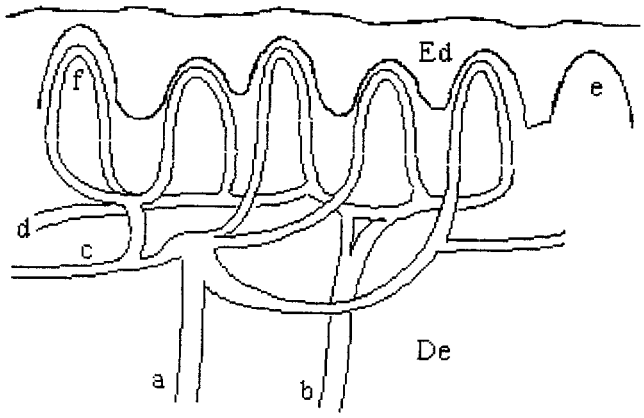

Figure 2.1: Upper dermal microvasculature; Ed epidermis, De dermis, a ascending arteriole, b descending venule, c terminal arteriole, d terminal venule, e dermal papilla, f capillary loop

Studies on the architecture of the upper horizontal plexus show a candelabra-like [313] or better yet an umbrella-like [50] formation (Fig. 2.1). Randomly spaced ascending arterioles divide into four or five branches that constitute the horizontal

part of the network; the terminal arterioles. These in turn lead either directly, or after subdividing once or twice into other vessels (named arterial capillaries), to the smaller, thinner part of the microcirculation, the capillary loop. Capillaries are arguably the only (and surely the most) permeable vessels [86, 252, 255, 307, 405]. The capillary loop takes a hairpin turn, the better part of which is inside the dermal papillae (ridges) at the epidermal-dermal junction. After the loop, venous capillaries join with each other to become postcapillary venules with the descending and grouping happening in the same manner, but not necessarily in the same numbers, by which arterioles ascend and divide. Thus, the handle of the umbrella is the pair arteriole/venule and the umbrella proper is formed by the subsequent continuous branching, which results in a majority of postcapillary vessels. There are approximately $8 - 10$ "umbrellas" per mm^3 of tissue their areas being predominantly arteriolar or venular [50].

The symmetry of the network is partly lost due to alternative routes between the arterial and venular parts named anastomoses [310, 313]. These randomly distributed vessels can be quite numerous (up to 5 / mm^2 [65]) and they may directly connect an arteriole with a venule, or even the arterial part of a capillary with the venular one. However, vascular exchange does not normally happen through them [310]. They can be considered "flow regulators" since they smooth the pulsatile flow through several arterioles of various lengths before it reaches the terminal vessels by diverting blood into multiple peripheral channels [310, 313].

Physiological experiments [149] reveal that apart from the capillary loop there are no sharp distinctions between vessels of different branching order. That explains the confusion in the literature about the definitions of these vessels. The walls of vessels that belong to a different branching order differ structurally. This fact, along with differences in the vessel diameters, has been used to define [310] the various vascular segments.

The following table (Table 2.3) reports the internal and external diameters of the various vessels of the papillary plexus.

Diameter (μm)	External	Endothelial	Wall thickness
Horizontal dermal plexus			
Terminal arteriole with elastin	$17-26$	$7.5-12$	$1-3.5$
Terminal arteriole without elastin[a]	$10-15$	$7.5-12$	$1-3.5$
Arterial capillary	$10-12$	$4-6$	$2-3$
Venous capillary	$10-12$	$4-6$	$2-3$
Postcapillary venule	$18-35$	$10-15$	$3.5-5$

Table 2.3: Vascular vessels diameters [52]; [a] the gradual disappearance of elastic fibers signals the beginning of the capillary bed.

2.7.1 Capillaries

In general, there are three types of capillaries in the human body, continuous, fenestrated and discontinuous, with the presence of fenestrae and/or large open gaps being the distinctive feature [33, 235]. Continuous capillaries, especially the ones in skin and skeletal muscle, are the least permeable [235, 271]. Other organs having continuous capillaries include the cardiac muscle, brain, and lungs [33, 52, 235, 253]. Fenestrae are small circular openings, "membrane-bounded circular discontinuities in the body of an endothelial cell [253]. They have been connected with increased capillary exchange [52, 149], and they can be found in the renal glomeruli, pancreas, intestines, endocrine glands, kidney etc. [33, 51, 64, 253]. Discontinuous capillaries allow the passage of erythrocytes in and out of the systemic circulation through their large gaps; they can be found in the liver and in the lymphatic organs [33].

A capillary can be considered as a bent cylinder with its venular part being slightly wider [65] both internally (lumen diameter) and externally (outside diameter) (Table 2.4). Other studies [74] yielded a luminal diameter of 5.4 ± 0.1 for the foot and 4.4 ± 0.2 for the hand. Measurements of the length of the papillary loop range

Diameter (μm)	Lumen	Endothelial	External	Wall thickness
Ascending limb (extrapapillary)	≈ 2 [149][a] $5-7.5$ [313]	$5-7.5$ [52] ≈ 5 [149]	$8-12$ [52] ≈ 7 [149] $8-12$ [313]	$1-2$ [52]
Intrapapillary loop	$3.5-6$ [313]	$3.5-6$ [52]	$7.5-10$ [52] $7.5-10$ [313]	$0.24-1.5$ [52]
Descending limb (extrapapillary)	≈ 3 [149] $6-10$ [313]	$6-10$ [52] ≈ 7 [149]	$10-17$ [52] ≈ 12 [149] $10-17$ [313]	$1.5-3.5$ [52]

Table 2.4: Capillary segments diameters; [a] values extracted from a graph.

from 150 to 500 μm [52, 310, 402].

The capillary bed in the papillary dermis resembles a more or less periodic structure where capillaries are perpendicular to the surface of the skin [52, 313] but "slight twisting and slanting is not uncommon" [313]. There is usually one capillary per papilla [51, 52, 65, 137, 313] and their surface density is by various accounts ~ 50 [74], or 50 [297], or 60 to 70 [313] capillaries per mm^2 of skin surface. One capillary loop supplies $0.04-0.27$ mm^2 of skin surface, and the average distance between loops is $50-100$ μm [313].

The structure of the capillary wall differs considerably from the other parts of the microcirculation. Internally, the capillary consists of a single layer of elongated endothelial cells [33] and it is devoid of smooth muscle cells and elastic fibers. Instead there is usually a single cell (pericyte) with circumferential arms that encircle the endothelial tube [51, 402] (Fig. 2.2). The basement membrane material that composes the external vascular wall is homogeneous for the most part but becomes multilayered at the extrapapillary descending portion [52, 149, 402]. In a transverse section there are normally two or three endothelial cells [313] resembling "lightly fried eggs rolled over to form a tube" [310]. The cells are attenuated [52, 253] with their cell wall being 0.2 to 0.7 μm [52] or ~ 0.25 μm [253] thick in regions where the nucleus is absent.

At the apex of the loop the cells are extremely flattened and can be as thin as 10 to 40 nm [50, 52].

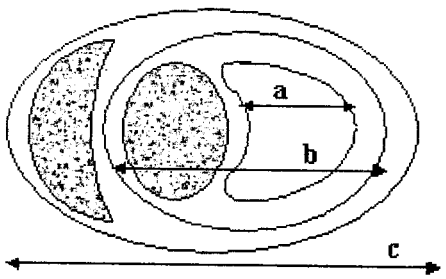

Figure 2.2: Capillary cross section; a lumen, b endothelial, c external

There are two specific structural characteristics of the capillary wall that require attention because they have been linked with the high capillary permeability. These are the plasmalemmal vesicles (Sec. 6.2.5) and the intercellular junctions (Sec. 6.2.1). The former are small spherical vesicles in the cytoplasm of the endothelial cells that appear either individually, or as parts of a chain of fused vesicles. They usually have one of their sides opened to either the blood or tissue front. The maximum density of these vesicles has been observed in the capillary endothelium [253]. Recently other structures have been suggested to contribute in transendothelial transport as well [33]. As far as intercellular junctions are concerned, they progressively became synonymous with the interendothelial clefts of slit-pore theory [235, 263, 371] even though physiology does not necessarily agree with pore equivalency [253].

2.7.2 Rat/mouse capillary parameters

Due to the inability to obtain necessary physiological/transport details by studies on human subjects, extensive experiments have been performed on various animals such as cats, dogs, rats, rabbits, pigs and monkeys, even though there exist interspecies differences in general [232] and circulatory [22] physiology or in capillary permeability [271]. Be that as it may, rats/mice have been commonly used in microcirculation/capillary physiology experiments [22, 29, 148, 155, 167, 220, 288, 309, 356]. Table 2.5 summarizes selected capillary parameters:

Property(units)	Subject[a]/area	Value	Source
Diameter(μm)	(hr/hr)/ear	5.7 ± 1.3	[22]
	Wistar / pad	$4 - 11$	[155]
	(hr/hr) / ear	4.8 ± 0.2	[220]
	Wistar / hindlimb	$\sim 4.8^b$	[309]
Length (μm)	(hr/hr) / ear	161 ± 5	[220]
Functional density[c](cm^{-1})	(hr/hr)/ear	243 ± 16.1^d	[22]
	Wistar / hindlimb	108.9 ± 3.3	[309]
	(hr/hr) /ear	74.5 ± 3.7	[379]
Functional volume[e] (ml/100g)	Wistar/hindquarters[f]	0.375 ± 0.065	[167]
Surface density(# /mm^2)	WKY/back	9.2 ± 2	[288]
Surface fraction[g]	WKY/back	$0.064 \pm 0.01\%$	[288]
Erythrocyte velocity (mm/s)	(hr/hr)/ear	0.06 ± 0.03	[22]
	Wistar / hindlimb	$0.1 - 1.8$	[309]
Blood velocity (μm/s)	(hr/hr) / ear	192 ± 5	[220]
Blood flow velocity (pl/s^{-1})	WKY / auricle	$2.8 - 3.5$	[148]
	(hr/hr) / ear	3.6 ± 0.3	[220]
	Wistar / hindlimb	$\sim 15^b$	[309]

Table 2.5: Rat capillary parameters; [a] type of rat/mouse; [b]value extracted from a graph [c] total length of perfused capillaries per unit area; [d] hair follicles' capillaries probably included; [e]volume of capillaries that allow exchange across them per unit weight; [f] includes muscle and fat besides skin; [g] area of capillaries per area of tissue.

2.7.3 Blood

Blood is a non-Newtonian fluid, a suspension of particles in a complex aqueous continuous phase. Its non-cellular part, called plasma, is a protein suspension that has been

known to behave as Newtonian fluid [343]. It is comprised from 91% water and 7% proteins of which 55% albumins, 38% globulins and 7% fibrinogen. The most common cells that plasma carries (97%) are red blood cells (RBCs), or erythrocytes. Their volume fraction in blood is called hematocrit and is normally $42 - 45\%$ [75]. There are $4.5 - 6\ 10^6$ RBCs / mm^3 blood. On the average there are $4 - 6$ l blood/person out of which $52 - 62\%$ is plasma and $38 - 48\%$ cells. Blood is $3 - 5$ times more viscous than water and has a pH equal to $7.35 - 7.45$ [75, 321]. Its average velocity is $0.68 - 3.87$ mm/sec in arterioles, $0.23 - 1.48$ mm/sec in capillaries and $0.32 - 1.21$ mm/sec in venules. Other researchers measured 0.65 ± 0.3 mm/sec for capillaries at an average skin temperature of $30.4 \pm 2.3°C$ [313].

2.7.4 Thermoregulation / capillary recruitment

Skin blood flow plays a vital role in the thermoregulation process that is responsible for maintaining normal body temperatures. Under extreme conditions of hyperthermia/exercise, skin blood flow can reach 6 to 8 l/min (60 % of cardiac output), while with exposure to extremely cold environments, it can be practically 0, thus minimizing heat transfer to the environment [67]. Under resting conditions and in thermoneutral environments the flow is approximately 250 ml/min [67]. Several factors influence the thermoregulatory response of skin. These factors include acclimation, exercise, fat percentage, total skin surface area and mass, clothing, individuality [145].

It is a well known fact that the skin's nutritional needs could be satisfied with far less than the available microcirculation. At any given time, the numbers of existing and perfused capillaries differ considerably. It seems that skin has a reserve of capillaries that can be used if needed. Recent studies on the human foot [195] suggest that there are 37.1 capillaries/mm^2, out of which 18.1 capillaries/mm^2 or 54.2 % are perfused. Similar studies in skeletal muscle [328] indicate that there are

52.6 capillaries/mm^2 out of which 38.8 capillaries/mm^2 are perfused.

Part I

Macroscopic Transport Studies

Chapter 3

A Whole-Skin, Transient Diffusion Model

3.1 Introduction

This chapter develops a skin transport model that improves upon existing models in several ways. It addresses transport in every skin layer unlike the common approach of including only the epidermis and the portion of the dermis that lies above the capillary plexus. Thus, the model is suitable for quantifying subsurface concentration levels [215, 298] for a wide class of agents designed to have a local (non-systemic) effect, for instance to treat dermal infections/diseases [126, 199, 352] and burn wounds [77], or to induce local anesthesia [4, 325]. It is also particularly suitable for drugs that are not completely cleared by the upper dermal vasculature. This may occur for a variety of reasons such as the nature of the drug [215, 233], co-administration of vasoconstrictive agents [35, 47, 237, 338], or environmental/pathological conditions [119, 302]. On the other hand, the model is capable of predicting undesirable topical or systemic concentrations [6] that follow the application of, or exposure to, a plethora of substances such as pesticides [114], insect repellents [110], fragrances [124], toxins and viruses [70, 71]. The real power of the model lies in the fact that it treats the processes of diffusion/dispersion and clearance

in the same way that these processes occur *in vivo* - as spatially distributed phenomena, the nature and intensity of which depends heavily on depth. This treatment is more realistic than that offered by pharmacokinetic models that lump these processes in well-mixed layers or compartments [46, 78, 80, 88, 135, 136, 212, 239, 242, 282, 283, 292, 320, 329, 337, 339, 364, 365, 376, 380, 394], or models that assume an artificial, perfect-clearance boundary condition at a certain depth within the dermis [20, 38, 73, 111, 135, 136, 138, 144, 169, 185, 186, 189, 190, 216, 323, 329, 364, 366, 367]. For this reason, it also has the potential for better prediction of rates of transdermal drug levels to the systemic circulation.

The analysis to follow addresses the general case of transient one-dimensional penetration from a finite dose. Thus, it is formulated in terms of independent variables z (vertical distance, taken as zero at the skin surface and negative below) and t (time following drug application). Penetration from an effectively infinite dose (providing a constant concentration at the surface) or steady state penetration represent special cases to which the model can be applied, serving as checks on the analysis. Although the focus of the present work is on deeper layers of the skin, the stratum corneum is explicitly accounted for as an interface imbued with a mass transfer resistance reflecting its barrier properties. Clearance through the vasculature is considered to be present in both the dermis and the hypodermis. It is a known fact that most of the clearance occurs in the upper capillary plexus [86, 252, 255, 405], but it is also known that the other parts of the vasculature have an arguably less yet existing permeability that may potentially be important for the fraction of the drug that "escapes" the capillary plexus and continues to diffuse in deeper layers [307].

3.2 Model formulation

3.2.1 Governing equations

Fig. 3.1 shows the simplified representation of structure and the notation used to describe the three layers of skin considered. They are distinguished by subscripts "ed" (epidermis), "de" (dermis) and "hd" (hypodermis) affixed to solute concentration variables C as well as to all physicochemical properties. Key among these properties is the effective diffusion/dispersion coefficient. For the epidermis this coefficient ($D_{\rm ed}$) quantifies molecular diffusion through the heterogeneous microstructure, whereas for the dermis and hypodermis ($D_{\rm de}$, $D_{\rm hd}$) it is likely to reflect some additional effects of convective dispersion due to blood flow through the microvasculature. Vascular clearance (effective disappearance of drug into the systemic circulation) in these latter tissue layers is characterized in terms of volume-average clearance rate coefficients ($k_{\rm de}$, $k_{\rm hd}$) having dimensions of reciprocal time. The diffusion/dispersion and clearance coefficients are all in principle z-dependent because of variations in the number density of capillaries with depth. Each layer is also characterized by a partition coefficient $K_{\rm a/w}$ (a = "ed", "de" or "hd") reflecting drug solubility therein relative to aqueous solutions ("w" for water).

Within this framework, the equations that describe the one-dimensional, transient dispersion-clearance process are:

$$\frac{\partial C_{\rm ed}}{\partial t} = D_{\rm ed}\frac{\partial^2 C_{\rm ed}}{\partial z^2}, \qquad t>0, \quad -h_{\rm ed}<z<0, \tag{3.1}$$

$$\frac{\partial C_{\rm de}}{\partial t} = \frac{\partial}{\partial z}\left(D_{\rm de}\frac{\partial C_{\rm de}}{\partial z}\right) - k_{\rm de}C_{\rm de}, \qquad t>0, \quad -h_{\rm de}<z<-h_{\rm ed}, \tag{3.2}$$

$$\frac{\partial C_{\rm hd}}{\partial t} = \frac{\partial}{\partial z}\left(D_{\rm hd}\frac{\partial C_{\rm hd}}{\partial z}\right) - k_{\rm hd}C_{\rm hd}, \qquad t>0, \quad -h_{\rm hd}<z<-h_{\rm de}. \tag{3.3}$$

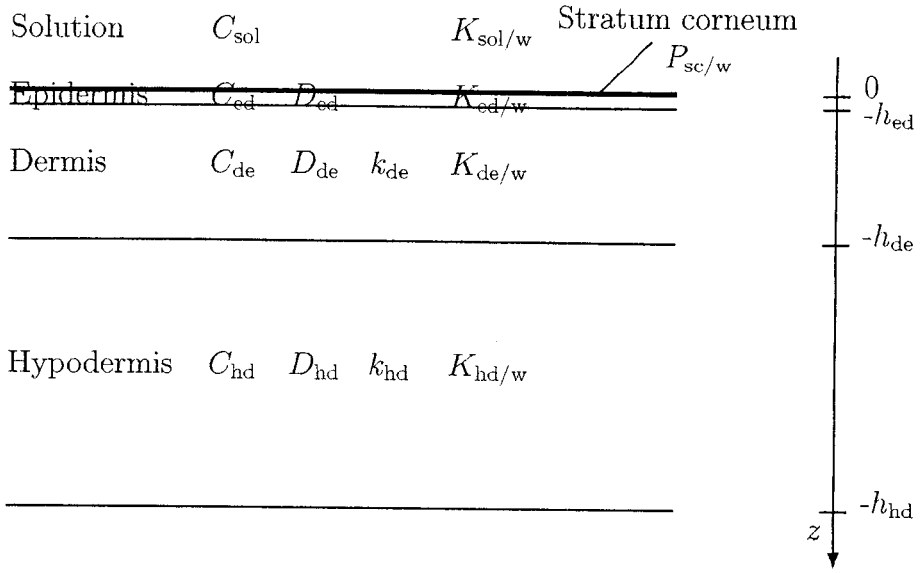

Figure 3.1: Definition sketch for the skin transport model

In Eq. (3.1) it is tacitly assumed that D_{ed} is uniform, but in the deeper tissue layers spatial variations are allowed for in the corresponding dispersivities D_{de} and D_{hd} .

The PDEs in each tissue layer are coupled through the boundary conditions that impose the requirements of a partitioning equilibrium and continuity of flux at the interfaces between them :

$$D_{ed}\left(\frac{\partial C_{ed}}{\partial z}\right) = P_{sc/w}\left(\frac{C_{sol}}{K_{sol/w}} - \frac{C_{ed}}{K_{ed/w}}\right), \quad z = 0, \tag{3.4}$$

$$D_{ed}\left(\frac{\partial C_{ed}}{\partial z}\right) = D_{de}\left(\frac{\partial C_{de}}{\partial z}\right), \quad z = -h_{ed}, \tag{3.5}$$

$$\frac{C_{ed}}{K_{ed/w}} = \frac{C_{de}}{K_{de/w}}, \quad z = -h_{ed}, \tag{3.6}$$

$$D_{de}\left(\frac{\partial C_{de}}{\partial z}\right) = D_{hd}\left(\frac{\partial C_{hd}}{\partial z}\right), \quad z = -h_{de}, \tag{3.7}$$

$$\frac{C_{hd}}{K_{hd/w}} = \frac{C_{de}}{K_{de/w}}, \quad z = -h_{de}, \tag{3.8}$$

$$C_{hd} = 0, \quad z = -h_{hd}. \tag{3.9}$$

Eqs. (3.5) and (3.6) apply to the epidermal-dermal junction, and Eqs. (3.7) and (3.8) to the dermal-hypodermal junction. Eq. (3.4) couples the donor solution concentration C_{sol} with the epidermal concentration immediately below, between which exists the SC barrier, which enters the model through a permeability coefficient $P_{\mathrm{sc/w}}$. In this treatment, the SC acts as an interface of negligible thickness characterized at all times by its steady state permeability. Thus, lag time within the SC itself is not addressed. Eq. (3.9) expresses the assumption of perfect clearance (or negligible drug concentration) at the bottom of the hypodermis, or else effectively no transport beyond this point.

For an infinite-dose application C_{sol} is simply a constant. The case of a finite dose can be treated through the introduction of an additional equation that describes drug depletion through the donor formulation.

The initial state is one in which the skin is drug-free at the time of application :

$$C_{\mathrm{ed}} = C_{\mathrm{de}} = C_{\mathrm{hd}} = 0, \qquad t = 0. \tag{3.10}$$

3.2.2 Dimensionless formulation

All (vertical) positions and length parameters are made dimensionless using a characteristic length $h_{\mathrm{o}} = 100\ \mu$m (chosen as a round number of the order of magnitude of the thickness of epidermis). Dimensionless quantities are distinguished with a hat ("$\hat{}$") affix. Thus, we work with a dimensionless coordinate and lengths :

$$\hat{z} = z/h_{\mathrm{o}}\ ;\ \ \hat{h}_{\mathrm{a}} = h_{\mathrm{a}}/h_{\mathrm{o}},\ \ \mathrm{a} = \text{“ed”, “de” or “hd”}. \tag{3.11}$$

In-tissue diffusion coefficients are made dimensionless with a characteristic diffusivity $D_{\mathrm{o}} = 10^{-5}$ cm^2/sec (representing the order of magnitude of a small-molecule, liquid-

phase diffusivity). Thus :

$$\hat{D}_{\mathrm{a}} \;=\; D_{\mathrm{a}}/D_{\mathrm{o}}\ ,\ \mathrm{a} \;=\; \text{“ed”, “de” or “hd”}. \tag{3.12}$$

A dimensionless time is defined in terms of the diffusive timescale associated with h_{o} and D_{o} as

$$\hat{t} \;=\; \frac{tD_{\mathrm{o}}}{{h_{\mathrm{o}}}^2}. \tag{3.13}$$

The characteristic values h_{o} and D_{o} also figure in dimensionless versions of clearance rate coefficients and SC permeability coefficient:

$$\hat{k}_{\mathrm{a}} \;=\; k_{\mathrm{a}}h_{\mathrm{o}}/D_{\mathrm{o}}\ ,\ \mathrm{a} \;=\; \text{“de” or “hd”}, \tag{3.14}$$

$$\hat{P}_{\mathrm{sc}} \;=\; (P_{\mathrm{sc/w}}h_{\mathrm{o}})/D_{\mathrm{o}}. \tag{3.15}$$

Dimensionless concentrations are defined by :

$$\hat{C}_{\mathrm{a}} \;=\; C_{\mathrm{a}}/C_{\mathrm{o}}\ ,\ \mathrm{a} \;=\; \text{“ed”, “de” or “hd”}. \tag{3.16}$$

where $C_{\mathrm{o}} = 10^{-6}$ moles/cm^3 represents a typical drug concentration in the donor solution.

For numerical purposes, the dimensionless position coordinate $\hat{z}$ is expressed in terms of a new independent variable ζ as :

$$\hat{z} \;=\; \mathcal{F}(\zeta) \tag{3.17}$$

where the function $\mathcal{F}$ (defined in Sec. 3.2.4 below) allows for selective refinement of the computational mesh with depth. It is designed such that $\zeta \in [0, 1]$, with the

epidermal/dermal and dermal/hypodermal interfaces respectively occuring at $\zeta = 1/3$ and $\zeta = 2/3$.

The resulting dimensionless system of equations is:

$$\frac{\partial \hat{C}_{\rm ed}}{\partial \hat{t}} = \hat{D}_{\rm ed}\left(\frac{1}{\mathcal{F}'(\zeta)}\right)^2\left\{\frac{\partial^2 \hat{C}_{\rm ed}}{\partial \zeta^2} - \frac{\mathcal{F}''(\zeta)}{\mathcal{F}'(\zeta)}\frac{\partial \hat{C}_{\rm ed}}{\partial \zeta}\right\}, \qquad \hat{t} > 0, \quad 0 < \zeta < \frac{1}{3}, \tag{3.18}$$

$$\begin{aligned}\frac{\partial \hat{C}_{\rm de}}{\partial \hat{t}} &= \hat{D}_{\rm de}\left(\frac{1}{\mathcal{F}'(\zeta)}\right)^2\left\{\frac{\partial^2 \hat{C}_{\rm de}}{\partial \zeta^2} - \frac{\mathcal{F}''(\zeta)}{\mathcal{F}'(\zeta)}\frac{\partial \hat{C}_{\rm de}}{\partial \zeta}\right\} + \\ &+ \left(\frac{1}{\mathcal{F}'(\zeta)}\right)^2 \frac{\partial \hat{D}_{\rm de}}{\partial \zeta}\frac{\partial \hat{C}_{\rm de}}{\partial \zeta} - \hat{k}_{\rm de}\hat{C}_{\rm de}, \qquad \hat{t} > 0, \quad \frac{1}{3} < \zeta < \frac{2}{3},\end{aligned} \tag{3.19}$$

$$\begin{aligned}\frac{\partial \hat{C}_{\rm hd}}{\partial \hat{t}} &= \hat{D}_{\rm hd}\left(\frac{1}{\mathcal{F}'(\zeta)}\right)^2\left\{\frac{\partial^2 \hat{C}_{\rm hd}}{\partial \zeta^2} - \frac{\mathcal{F}''(\zeta)}{\mathcal{F}'(\zeta)}\frac{\partial C_{\rm hd}}{\partial \zeta}\right\} + \\ &+ \left(\frac{1}{\mathcal{F}'(\zeta)}\right)^2 \frac{\partial \hat{D}_{\rm hd}}{\partial \zeta}\frac{\partial \hat{C}_{\rm hd}}{\partial \zeta} - \hat{k}_{\rm hd}\hat{C}_{\rm hd}, \qquad \hat{t} > 0, \quad \frac{2}{3} < \zeta < 1,\end{aligned} \tag{3.20}$$

$$\hat{D}_{\rm ed}\left(\frac{\partial \hat{C}_{\rm ed}}{\partial \zeta}\right) = \mathcal{F}'(\zeta)\ \hat{P}_{\rm sc}\left(\frac{\hat{C}_{\rm sol}}{K_{\rm sol/w}} - \frac{\hat{C}_{\rm ed}}{K_{\rm de/w}}\right), \qquad \hat{t} > 0, \qquad \zeta = 0, \tag{3.21}$$

$$\hat{D}_{\rm ed}\left(\frac{\partial \hat{C}_{\rm ed}}{\partial \zeta}\right) = \hat{D}_{\rm de}\left(\frac{\partial \hat{C}_{\rm de}}{\partial \zeta}\right), \qquad \hat{t} > 0, \qquad \zeta = \frac{1}{3}, \tag{3.22}$$

$$\frac{\hat{C}_{\rm ed}}{K_{\rm ed/w}} = \frac{\hat{C}_{\rm de}}{K_{\rm de/w}}, \qquad \hat{t} > 0, \qquad \zeta = \frac{1}{3}, \tag{3.23}$$

$$\hat{D}_{\rm de}\left(\frac{\partial \hat{C}_{\rm de}}{\partial \zeta}\right) = D_{\rm hd}\left(\frac{\partial \hat{C}_{\rm hd}}{\partial \zeta}\right), \qquad \hat{t} > 0, \qquad \zeta = \frac{2}{3}, \tag{3.24}$$

$$\frac{\hat{C}_{\rm de}}{K_{\rm de/w}} = \frac{\hat{C}_{\rm hd}}{K_{\rm hd/w}}, \qquad \hat{t} > 0, \qquad \zeta = \frac{2}{3}, \tag{3.25}$$

$$\hat{C}_{\rm hd} = 0 \text{ or } \frac{\partial \hat{C}_{\rm hd}}{\partial \zeta} = 0 \qquad \hat{t} > 0, \qquad \zeta = 1, \tag{3.26}$$

$$\hat{C}_{\rm ed} = \hat{C}_{\rm de} = \hat{C}_{\rm hd} = 0, \qquad \hat{t} = 0. \tag{3.27}$$

3.2.3 Numerical scheme

The preceeding system of equations is solved numerically by applying a finite-difference formulation for the spatial dimension. This approach is based on replacing the derivatives in Eqs. (3.18) - (3.27) with finite difference approximations thereof. These finite differences, generated through the discretization of the depth variable, describe the change of the concentration occuring over small depth intervals (of thickness h) that are defined by two adjacent discrete points (grid points). These grid points are being denoted with an additional subscript/counter (i) that ranges from 0 to $n_{\rm hd}$ (the number of discrete points until the end of hypodermis). The number of grid points for the epidermis and dermis is $n_{\rm ed}$ and $n_{\rm de}$ respectively. Collectively, these points constitute a depth mesh, the spacing of which is controlled by the mesh function ($\mathcal{F}$), described in the next section. Thus, Eqs. (3.18) - (3.20) are transformed into :

$$\frac{\partial \hat{C}_{\rm ed,i}}{\partial \hat{t}} = \hat{D}_{\rm ed}\left(\frac{1}{\mathcal{F}'(\zeta)}\right)^2\left\{\frac{\hat{C}_{\rm ed,i+1}-2\,\hat{C}_{\rm ed,i}+\hat{C}_{\rm ed,i-1}}{h^2}-\frac{\mathcal{F}''(\zeta)}{\mathcal{F}'(\zeta)}\frac{\hat{C}_{\rm ed,i+1}-\hat{C}_{\rm ed,i-1}}{2\,h}\right\},$$

$$\forall \quad 1<i<n_{\rm ed}-1\,, \tag{3.28}$$

$$\frac{\partial \hat{C}_{\rm de,i}}{\partial \hat{t}} = \hat{D}_{\rm de}\left(\frac{1}{\mathcal{F}'(\zeta)}\right)^2\left\{\frac{\hat{C}_{\rm de,i+1}-2\,\hat{C}_{\rm de,i}+\hat{C}_{\rm de,i-1}}{h^2}-\frac{\mathcal{F}''(\zeta)}{\mathcal{F}'(\zeta)}\frac{\hat{C}_{\rm de,i+1}-\hat{C}_{\rm de,i-1}}{2\,h}\right\}$$

$$+\left(\frac{1}{\mathcal{F}'(\zeta)}\right)^2\frac{\partial \hat{D}_{\rm de}}{\partial \zeta}\left(\frac{\hat{C}_{\rm de,i+1}-\hat{C}_{\rm de,i-1}}{2\,h}\right)-\hat{k}_{\rm de}\hat{C}_{\rm de,i}\,,$$

$$\forall \quad n_{\rm ed}+1<i<n_{\rm de}-1\,, \tag{3.29}$$

$$\frac{\partial \hat{C}_{\rm hd,i}}{\partial \hat{t}} = \hat{D}_{\rm hd}\left(\frac{1}{\mathcal{F}'(\zeta)}\right)^2\left\{\frac{\hat{C}_{\rm hd,i+1}-2\,\hat{C}_{\rm hd,i}+\hat{C}_{\rm hd,i-1}}{h^2}-\frac{\mathcal{F}''(\zeta)}{\mathcal{F}'(\zeta)}\frac{\hat{C}_{\rm hd,i+1}-\hat{C}_{\rm hd,i-1}}{2\,h}\right\}$$

$$+\left(\frac{1}{\mathcal{F}'(\zeta)}\right)^2\frac{\partial \hat{D}_{\rm hd}}{\partial \zeta}\left(\frac{\hat{C}_{\rm hd,i+1}-\hat{C}_{\rm hd,i-1}}{2\,h}\right)-\hat{k}_{\rm hd}\hat{C}_{\rm hd,i}\,,$$

$$\forall \quad n_{\rm de}+1<i<n_{\rm hd}-1\,. \tag{3.30}$$

The boundary conditions are treated somewhat differently. Had the usual upwind finite difference approximation been used, the numerical error for the BCs would have been $O(h)$, whereas it is $O(h^2)$ for the PDEs. This difficulty was overcome by considering Taylor expansions for the concentrations near the grid point at each interface. For the boundary condition that incorporates the SC, the expansions used pertained to the two grid points immediately below the interface:

$$\hat{C}_{\mathrm{de},2} = \hat{C}_{\mathrm{de},0} + (\zeta_2 - \zeta_0)\frac{\partial \hat{C}_{\mathrm{ed},0}}{\partial \zeta} + \frac{1}{2}(\zeta_2 - \zeta_0)^2 \frac{\partial^2 \hat{C}_{\mathrm{ed},0}}{\partial \zeta^2} + \dots , \tag{3.31}$$

$$\hat{C}_{\mathrm{de},1} = \hat{C}_{\mathrm{de},0} + (\zeta_1 - \zeta_0)\frac{\partial \hat{C}_{\mathrm{ed},0}}{\partial \zeta} + \frac{1}{2}(\zeta_1 - \zeta_0)^2 \frac{\partial^2 \hat{C}_{\mathrm{ed},0}}{\partial \zeta^2} + \dots \tag{3.32}$$

By considering a linear combination of these eqautions and by neglecting the higher order terms :

$$\begin{aligned} \hat{C}_{\mathrm{de},2} - 4\hat{C}_{\mathrm{de},1} &= -3C_{\mathrm{de},0} - 2(\zeta_1 - \zeta_0)\frac{\partial \hat{C}_{\mathrm{ed},0}}{\partial \zeta} \Rightarrow \\ \frac{\partial \hat{C}_{\mathrm{ed},0}}{\partial \zeta} &= \frac{-3\hat{C}_{\mathrm{de},0} + 4\hat{C}_{\mathrm{de},1} - \hat{C}_{\mathrm{de},2}}{2(\zeta_1 - \zeta_0)} = \\ &= \frac{-3\hat{C}_{\mathrm{de},0} + 4\hat{C}_{\mathrm{de},1} - \hat{C}_{\mathrm{de},2}}{2h} \end{aligned} \tag{3.33}$$

Since

$$\frac{\partial \hat{C}_{\mathrm{ed},0}}{\partial \zeta} = \mathcal{F}'(0)\frac{\hat{P}_{\mathrm{sc}}}{\hat{D}_{\mathrm{ed}}}\left(\frac{\hat{C}_{\mathrm{sol}}}{K_{\mathrm{sol/w}}} - \frac{\hat{C}_{\mathrm{ed},0}}{K_{\mathrm{de/w}}}\right) \tag{3.34}$$

we then have:

$$\hat{C}_{\mathrm{ed},0} = \frac{2h\mathcal{F}'(0)(\hat{P}_{\mathrm{sc}}\hat{C}_{\mathrm{sol}})/(\hat{D}_{\mathrm{ed}}K_{\mathrm{sol/w}}) - 4\hat{C}_{\mathrm{de},1} + \hat{C}_{\mathrm{de},2}}{2h\mathcal{F}'(0)\hat{P}_{\mathrm{sc}}/(\hat{D}_{\mathrm{ed}}K_{\mathrm{ed/w}}) - 3} \tag{3.35}$$

The same methodology is used for the other boundary conditions where Taylor expansions were considered for four grid points (two below and two above the

respective interfaces). This results in the following equations:

$$\hat{C}_{\mathrm{ed},\mathrm{n_{ed}}} = \frac{\hat{D}_{\mathrm{ed}}\left(4\hat{C}_{\mathrm{ed},\mathrm{n_{ed-1}}} - \hat{C}_{\mathrm{ed},\mathrm{n_{ed-2}}}\right) + \hat{D}_{\mathrm{de}}\left(4\hat{C}_{\mathrm{de},\mathrm{n_{ed+1}}} - \hat{C}_{\mathrm{de},\mathrm{n_{ed+2}}}\right)}{3\left(\hat{D}_{\mathrm{ed}} + \hat{D}_{\mathrm{de}}\dfrac{K_{\mathrm{de/w}}}{K_{\mathrm{ed/w}}}\right)}, \quad (3.36)$$

$$\hat{C}_{\mathrm{de},\mathrm{n_{ed}}} = \frac{\hat{D}_{\mathrm{ed}}\left(4\hat{C}_{\mathrm{ed},\mathrm{n_{ed-1}}} - \hat{C}_{\mathrm{ed},\mathrm{n_{ed-2}}}\right) + \hat{D}_{\mathrm{de}}\left(4\hat{C}_{\mathrm{de},\mathrm{n_{ed+1}}} - \hat{C}_{\mathrm{de},\mathrm{n_{ed+2}}}\right)}{3\left(\hat{D}_{\mathrm{de}} + \hat{D}_{\mathrm{ed}}\dfrac{K_{\mathrm{ed/w}}}{K_{\mathrm{de/w}}}\right)}, \quad (3.37)$$

$$\hat{C}_{\mathrm{de},\mathrm{n_{de}}} = \frac{\hat{D}_{\mathrm{de}}\left(4\hat{C}_{\mathrm{de},\mathrm{n_{de-1}}} - \hat{C}_{\mathrm{de},\mathrm{n_{de-2}}}\right) + \hat{D}_{\mathrm{hd}}\left(4\hat{C}_{\mathrm{hd},\mathrm{n_{de+1}}} - \hat{C}_{\mathrm{hd},\mathrm{n_{de+2}}}\right)}{3\left(\hat{D}_{\mathrm{de}} + \hat{D}_{\mathrm{hd}}\dfrac{K_{\mathrm{hd/w}}}{K_{\mathrm{de/w}}}\right)}, \quad (3.38)$$

$$\hat{C}_{\mathrm{hd},\mathrm{n_{de}}} = \frac{\hat{D}_{\mathrm{de}}\left(4\hat{C}_{\mathrm{de},\mathrm{n_{de-1}}} - \hat{C}_{\mathrm{de},\mathrm{n_{de-2}}}\right) + \hat{D}_{\mathrm{hd}}\left(4\hat{C}_{\mathrm{hd},\mathrm{n_{de+1}}} - \hat{C}_{\mathrm{hd},\mathrm{n_{de+2}}}\right)}{3\left(\hat{D}_{\mathrm{hd}} + \hat{D}_{\mathrm{de}}\dfrac{K_{\mathrm{de/w}}}{K_{\mathrm{hd/w}}}\right)}. \quad (3.39)$$

The model has the flexibility of two options for the boundary condition at the end of hypodermis. The first one is a zero concentration (perfect sink) and the second is zero derivative of the concentration:

$$\hat{C}_{\mathrm{hd},\mathrm{n_{hd}}} = 0 \quad (3.40)$$

$$\hat{C}_{\mathrm{hd},\mathrm{n_{hd}}} = \frac{4\hat{C}_{\mathrm{hd},\mathrm{n_{hd-1}}} - \hat{C}_{\mathrm{hd},\mathrm{n_{hd-2}}}}{3} \quad (3.41)$$

3.2.4 Mesh function

The derivation and the specific properties of the function that was used to generate the mesh for the numerical formulation is shown in Appendix A, while Fig. 3.2 shows, in a qualitative way, how this refined mesh function allows for different concentrations of node points in different regions of the skin (more where the permeant concentration is likely to exhibit rapid spatial variations). The mesh function was found to be :

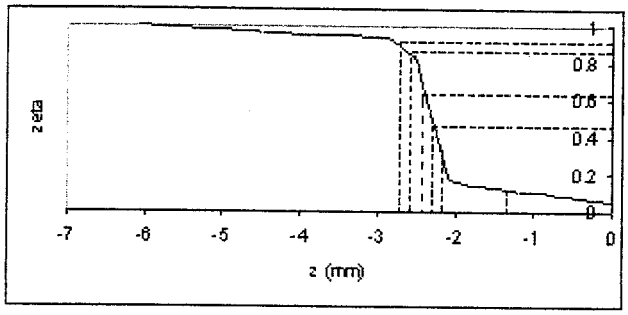

Figure 3.2: The mesh function $\mathcal{F}(\zeta)$. The mesh function generates small intervals for the depths where there is an abrupt change (around the interfaces between the different skin layers) and large intervals for the depths where there is a smooth behavior

$$\begin{aligned}\mathcal{F}(\zeta) &= -0.96\zeta - \frac{58.93}{2}\ln\left\{1+\exp\left[2\left(\frac{\zeta-\zeta_1}{2/60}\right)\right]\right\} - \\ &- \frac{62.27}{2}\ln\left\{1+\exp\left[2\left(\frac{\zeta-\zeta_2}{2/60}\right)\right]\right\} + 2\ 10^{-9}\end{aligned} \tag{3.42}$$

Chapter 4

Application of the Model - Analysis of Experimental Results on Dermal Penetration of Salicylic Acid

4.1 Introduction

The skin transport model described in the previous chapter involves transport, clearance, and partitioning parameters as inputs. Either these parameters must be measured or estimated to make predictions about penetration behavior; or else the model might be used to deduce values of one or more of these dermal parameters by fitting it to measurements of dermal drug distribution. Here we adopt the latter view with reference to a particularly interesting study by P. Singh and M.S. Roberts [336] on the transdermal delivery of salicylic acid in rat skin. While the focus of their work was the comparison between passive and iontophoretic diffusion through skin, they reported a series of valuable results including the percentages of the initial dose found in skin strata *in vivo* after two hours of passive diffusion through epidermis-free rat skin. The usefulness of these results lies in the fact that the experiments were performed a) *in vivo*, i.e., with the microvacular clearance process being present, and b)

after the removal of the stratum corneum and viable epidermis barriers, allowing the mass transfer resistance of the dermis to be measured. Our goal is to use these data to estimate the orders of magnitudes that the effective diffusivity D_{de} and clearance rate coefficient k_{de} in the dermis must have.

We adopt a two-pronged approach to analyzing the experimental situation. A simplified description in terms of steady-state reaction-clearance within the dermis is used to derive rough estimates of D_{de} and k_{de}. Thereafter, a more comprehensive steady state analysis and the full computational model of Chapter 3 are applied to support the preliminary estimates and more particularly, predict the distribution in skin with an intact epidermal barrier. The general scheme by which the model (simple or elaborate) may be used to deduce dermal parameters from data on cutaneous drug distribution is illustrated in Fig. 4.1. By following this methodology, one is able to derive the transport/clearance coefficients by simulating experimental results, and consequently quantitate transport through whole-thickness skin.

Since the experimental data considered salicylic acid, a brief review of this drug is given below, including the binding of salicylic acid to serum proteins, which is potentially important. A discussion of other models in the literature is postponed to the Discussion (Sec. 4.5) in order to provide adequate context to assess them.

4.2 Salicylic acid

Salicylic acid (SA) is a well known topical anti-inflammatory and keratolytic agent used for a variety of skin disorders/diseases such as warts, psoriasis, ichthyosis, and acne [95, 199, 208, 345]. It can be found in over 80 topical preparations [208], and - according to FDA regulations - it can be present in over-the-counter formulations at concentrations below 2 % (w/w) [95]. It's IUPAC name is *ortho*-hydroxybenzoic acid (Fig. 4.2).

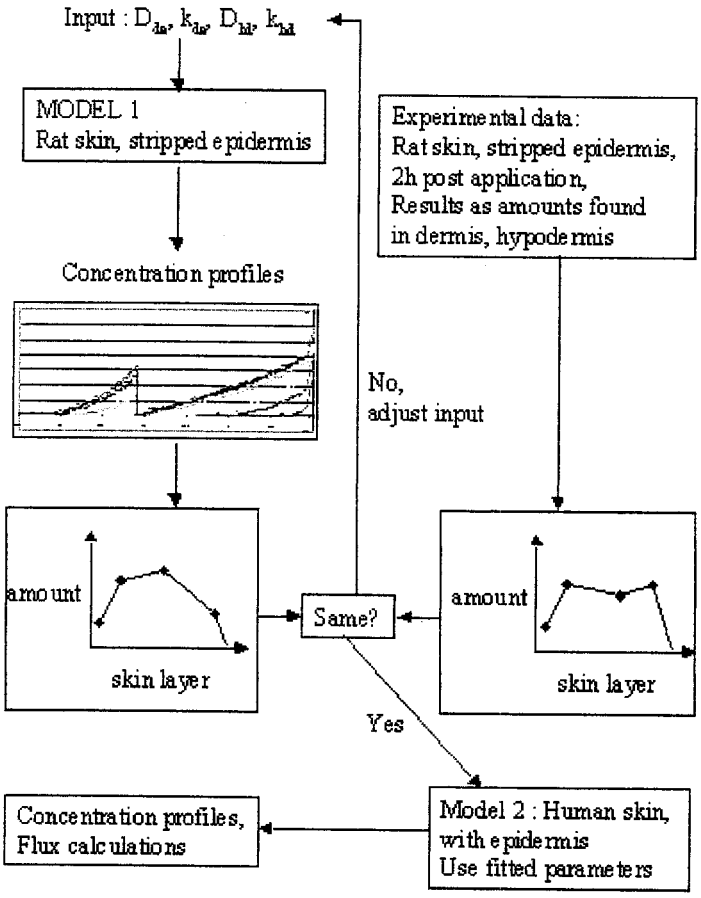

Figure 4.1: Methodology for the skin transport model

Salicylic acid is a small lipophilic molecule that is essentially ionized (to its anion, salicylate (SA^-)) at physiologic pH (7.4). Thus the acid base equilibrium

$$SAH \rightleftharpoons SA^- + H^+ \tag{4.1}$$

is shifted completely to the right. This fact has a profound effect in its partitioning into (solubility in) skin layers [210, 327]. Some of its experimentally determined properties are listed in Table 4.1. The molecular diffusivity of SA, which figures in the subsequent analysis, was determined at 37°C in both water (subscript "w") and octanol (subscript "oct") with the Scheibel equation as described in Reid et al. [287] (Appendix B). The diffusivities are included in the table.

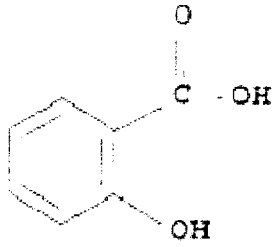

Figure 4.2: Structure of salicylic acid

Property	Value	References
MW (g/mol)	138.12	[248, 334]
pK_a	2.97, 13.9	[248, 334]
Solubility in water (mg/L)	2240[a]	[334]
$Log(K_{oct/w})$[b]	2.21	[201]
$Log(K_{oil/w})$[c]	1	[201]
D_w (cm^2/sec)	$1.15\ 10^{-5}$	[287][d]
D_{oct} (cm^2/sec)	$0.39\ 10^{-5}$	[287][d]

Table 4.1: Properties of salicylic acid; [a] at 25°C; [b] octanol/water partition coefficient; [c] vegetable oil/water partition coefficient; [d] estimated.

4.2.1 Binding of salicylic acid to serum albumin

A key issue in the transdermal delivery of salicylic acid is its documented binding affinity for serum proteins, and most importantly serum albumin [88]. The binding is substantial, and it may potentially alter the pharmacological effect of the drug and its transport and partitioning properties. Therefore, careful review of this phenomenon is pertinent.

Serum albumin is a medium-size protein (MW $\simeq 67,000$ Da [146, 372, 398]) having a blood concentration of $\simeq 50$ g/L [63, 372, 398]. As a result of the plasma leakage from the capillaries [372] that feeds the lymphatic system (see Chap. 2), approximately 60 % of HSA (human serum albumin) is extravascular in the body [63, 146]. The total concentration of HSA in skin is about 40g in a 70 kg man, or

7.7g/kg skin. HSA is the major plasma protein $(50 - 60\%)$ [372] and the major contributor in the normal colloid oncotic pressure $(75 - 80\%)$. It is a highly water soluble protein with a net negative charge at physiologic conditions [179, 372].

Serum albumin possesses a remarkable ability to bind reversibly to both cations and anions. It binds to lipophilic molecules through hydrophobic interactions at its hydrophobic pockets. This protein has been engineered by God or evolution to transport a wide range of endogenous substances such as fatty acids and lipids, hormones, trace metals, enzymes etc. It is safe to assume that if any substantial binding occurs between drugs and serum proteins, it involves serum albumin [63, 179, 372, 398].

Experimental data on the binding of SA (drug) to HSA (protein) are available from a plethora of sources [1, 32, 56, 57, 88, 98, 151, 181, 182, 191, 230, 355, 375, 377]. In some of these studies [1, 32, 56, 181] experimental data from equilibrium dialysis of SA between aqueous buffer and protein solution compartments were fitted with a two-independent-site model of the following form :

$$\frac{C_{\mathrm{b}}}{C_{\mathrm{p}}} = \sum_{\mathrm{i}=1}^{\mathrm{k}} \frac{n_{\mathrm{i}} K_{\mathrm{ai}} C_{\mathrm{u}}}{1 + K_{\mathrm{ai}} C_{\mathrm{u}}} \tag{4.2}$$

with

$C_{\mathrm{b}} \equiv$ bound drug concentration

$C_{\mathrm{p}} \equiv$ protein concentration

$n_{\mathrm{i}} \equiv$ number of binding sites in the ith class of sites

$K_{\mathrm{ai}} \equiv$ association constant for the ith class of sites (M^{-1})

$C_{\mathrm{u}} \equiv$ free (unbound) drug concentration

This Scatchard model accounts for the combination of specific binding in discrete locations on the protein with a high affinity, with specific binding in another class of discrete locations with lower affinities and for greater numbers of ligand molecules.

Another approach seen in the literature [355] involves the distinction of binding to specific sites obeying the law of mass action according to Eq. (4.2), and non-specific, low-affinity binding dominated by an unlimited binding capacity of the drug and obeying partition-like interactions :

$$\frac{C_\mathrm{b}}{C_\mathrm{p}} = \frac{nK_\mathrm{a1}C_\mathrm{u}}{1+K_\mathrm{a1}C_\mathrm{u}} + K_\mathrm{a2}C_\mathrm{u} \tag{4.3}$$

with

$C_\mathrm{b} \equiv$ bound drug concentration

$C_\mathrm{p} \equiv$ protein concentration

$n \equiv$ number of specific binding sites

$K_\mathrm{a1} \equiv$ association constant for specific binding

$K_\mathrm{a2} \equiv$ association constant for non-specific binding (similar to partition coefficient)

$C_\mathrm{u} \equiv$ free (unbound) drug concentration

Thus the second Langmuir-type term in Eq. (4.2) is replaced with a partition-like proportionality. Yet another approach involves a fitting model where the sites of different binding classes are dependent of each other [57]. The actual model used for fitting depends on the form of the data [398].

Table 4.2 contains the aforementioned binding parameters from the literature. There is an obvious and considerable scatter in these data that can be partly explained by different experimental conditions, different kinds of albumins used, different ligand concentrations, and different fitting procedures. Be that as it may, the high-affinity association constants fall in the range from 10^4 to 10^6 M^{-1}, reported to be the typical one for most binding ligands [63]. There seems to exist a general consensus on that the SA - HSA binding exhibits no signs of saturation and that the binding with HSA is extensive [1, 98, 179, 375], and in the order of $\simeq$ 95 % [1, 89, 98, 182]. The low-affinity sites are probably not that important due to the usually low drug dosing levels

that are not high enough to populate these sites [98].

As far as interspecies comparisons are concerned, an experimental study involving 6 different mammals has shown that there are "genuine species differences" [191]. The results of this study indicate that binding of salicylate in rat and dog falls "into a clearly differentiated group having a lower proportion of salicylate bound". They found that only 39 % of salicylate binds to plasma and 34 % specifically to serum albumin extracted from plasma (averages of three measurements with three different salicylic acid concentrations) in rat. Another equilibrium dialysis study with rat plasma [337] (with lower SA concentrations) yielded a 60 % fraction of the drug bound. These results are quite important in the present study since the model was implemented by analyzing rat skin permeability data.

There are also two reported *ex vivo* studies on the impact of SA-serum albumin binding to skin transport. They involve experiments with rats hindlimbs where the circulation was bypassed and a perfusate (containing 4 % bovine serum albumin) instead of blood was allowed to run through the local circulation. The epidermis and hair were removed prior to the solution application. In the first one ([88]) the authors demonstrated that binding results in lower SA tissue levels (and a faster elimination half-life) due to a more effective systemic clearance of the protein-drug complex compared to the clearance of the (unbound) drug when the perfusate was albumin-free. They further suggest a possible binding process of SA extravascularly, although they provide no evidence for it. The second one ([301]) provides a measured unbound fraction of SA with BSA (10 % - they also cite a 10 to 20 % value for human plasma), as well as an estimate (resulting from a compartmental model) for the unbound fraction in tissue (whole hindlimb-12 %). In both of these studies, the authors reference the fact that a single-pass (100% drug-free albumin at every passage) experiment with BSA at flow rates that may induce increased capillary recruitment

Compound	n_1	K_{a1} (M^{-1})	n_2	K_{a2} (M^{-1})	ref.
SA	1.3	13000	30	80[a]	[1]
SA	0.99	45000	3.1	1600	[1][b]
SA	0.95	5650	4.3	443	[32][c]
SA	2.72	10953	51.6	20.7	[32][c,d]
Salicylate		50000			[56][e]
Salicylate		71000		3300	[63][f,g]
Salicylate		220000		1600	[63][f,g]
Salicylate		130000		2900	[63][f,g]
Salicylate		48000000			[98][h]
Salicylate	1	190000	4	16000	[181][i]
SA		40500			[230][j]
SA	2.82	60000	20.36	0	[355][f,k]
SA	1.28	70700			[375][f,l]
Salicylate	4	219000			[375][f,m]
Salicylate	1.04	50000			[375][f,n]
SA	1.55	35800	3.27	43000	[377][o]
SA	1.46	28400	4.09	21000	[377][f]
SA	2.15	12100	4.04	502	[377][f,p]
SA	1.4	28400	4.1	21000	[377][f,p]

Table 4.2: Binding parameters of SA - HSA binding; all values reported were derived from measurements at 37°C, pH 7.4, HSA at 40 g/L and all measurements were fitted to a two-independent site model unless otherwise noted; [a] a very large deviation reported; [b] experiments with bovine serum albumin (BSA); [c] SA $73 - 5839$ μM; [d] experiments with defatted HSA; [e] 25°C, HSA $\simeq$ 2.1 g/L; [f] reported from other sources; [g] no experimental conditions reported; [h] measurements with surface plasmon resonance, 25°C, SA $0.1 - 1000$ μM; [i] pH 7, 20°C, defatted HSA, salicylate $0.035 - 0.116$ mM; [j] defatted BSA 10mg/L, SA $10^{-3} - 10^{-7}$M; [k] 20°C; [l] SA $0.002 - 5$ 10^{-3}M, HSA 0.3%; [m] HSA 0.7%; [n] BSA 4%; [o] SA 2μM; [p] binding in/with serum in general

may produce exaggerated levels of binding.

The values of the binding parameters reported here may be considered as upper limits for the binding that actually occurs in plasma. Serum albumin exists for a variety of reasons, one of which is transporting substances that already exist in the body such as fatty acids. In fact, over 99 % of the fatty acid in the plasma is bound to albumin [24] while studies have shown that fatty acids displace salicylic acid from albumin binding sites in a competitive way [1, 375]. The displacement phenomenon has also been observed during co-administration of SA with other drugs [181].

Besides the competition for the serum albumin binding sites, one must take

into account the fact that most of the values reported stem from *in vitro* experiments that try to simulate the conditions in the plasma. The binding picture in a whole tissue such as skin is probably different. Experiments with postmortem human dermis [218] indicate that HSA may have a tissue concentration as low as $\simeq$ 33 % of that in plasma. Two other independent set of *in vivo* experiments in rat dermis raise that percentage to $\simeq$ 70 % [286, 392], while yet another experimental study (involving the suction blister technique) in human abdominal skin yielded a 46 % tissue-to-plasma albumin concentration ratio [306]. However, one should bear in mind that there is yet no indisputably reliable method for estimating plasma protein concentration levels in the interstitium. A further indication of the smaller extravascular concentration of HSA is its lymph concentration, which is typically 50 % of that in plasma in the skin [19]. Furthermore, it has been demonstrated that not all of the interstitial space is accessible to serum albumin. Albumin is confined to a fraction of the total tissue volume, with that fraction ranging from one to more than two thirds of the total interstitial volume [19, 218, 286, 392].

In view of these considerations, it is logical to assume that the binding process occurs predominantly in the systemic circulation. The immediate effect of such a reality would be a tissue-to-plasma partitioning favoring plasma. Indeed, a noteworthy attempt to model the pharmacokinetics of salicylic acid's permeation yielded a tissue-to-plasma partition coefficient equal to 0.24 for rat dermis (0.22 for hypodermis) [337]. Furthermore, the authors estimate for the unbound fraction of salicylate in the dermis was unity, reinforcing the notion that the binding in tissue is not as important as the binding in plasma. An additional effect would be a more "effective" clearance through the circulation since the drug would be somewhat "trapped" in following the systemic route of the protein. Both of the *ex vivo* studies mentioned earlier ([88, 301]) agree with this conclusion.

Obviously, a detailed model would account for the protein-drug binding in

both tissue and plasma, either explicitly by describing the process in terms of binding reactions and association constants, or implicitly through partition coefficients that embody this phenomenon. However, this would be feasible only if the *in vivo* binding process in the interstitium could be accurately defined and quantitated. Most of the data on the albumin concentration (and, more importantly, pattern of distribution) in the interstitial phase come from *ex vivo* or trauma-inducing *in vivo* experiments with exogenous (and often from different species) albumins. Nevertheless, all these data point in a qualitative way to a reduced binding in tissue. In the absence of accurate pieces of information, and after establishing the conclusion that the binding process is far more intense in plasma than in tissue, one may choose to neglect this process in the interstitium. This translates into treating the skin layers as simple aqueous media as far as partitioning is concerned. Hypodermis must similarly be treated as a medium similar to octanol or another "equivalent" lipophilic medium. The tissue-plasma partitioning favoring plasma will be reflected in our model in the value of the rate coefficients describing clearance in the dermis and the hypodermis.

4.3 Experimental data

4.3.1 Cited transport parameters [336]

Salicylic acid can readily penetrate skin and enter the systemic circulation. There are several experimental studies on the subject [95, 139, 334, 337, 345, 387].

Singh and Roberts used male Wistar rats after removing the hair in their dorsal area. Although they do not explicitly report the thickness of the individual skin layers of the rat, their graphs indicate that the dermis was assumed to be 2 mm thick and the hypodermis 1 mm thick. The experimental conditions were fixed at pH=7.4 in the (aqueous) donor solution and at 37°C external body temperature. The concentration

of the radioactive salicylic acid was 1 mM. After allowing the drug to penetrate tissue for two hours (both passively and iontophoretically - through a donor glass cell affixed to the epidermis), they took a blood sample, sacrificed the animals, and dissected the various tissue layers, going as deep as the muscle. They performed the same *in vivo* experiment by first removing the epidermis with an electrodermatome set at 80 μm. For the *in vitro* experiments, the epidermis was separated from the dermis by the heat method. The samples collected at various times were measured in a liquid scintillation counter.

After 2 hours of transdermal delivery, 34.3 ± 3.68 % of the initial dose was absorbed. Out of this amount, 15.3 ± 3.88 % and 7.13 ± 2.1 % was found in the dermis and in the subcutaneous tissue, respectively. They also found that an additional 4.52 ± 1.25 % of salicylic acid was distributed in deeper tissues such as fascia and muscle. The corresponding permeability coefficients that they calculated for isolated rat dermis were 0.013 ± 0.002 cm/h *in vitro* and 0.23 ± 0.03 *in vivo*, the difference being attributed to the removal of the drug through the dermal vasculature.

4.3.2 Calculated parameters

Simple calculations were performed to extract additional useful parameters from the data reported. The definitive equation for the dermal permeability coefficient is:

$$P_{\mathrm{de/sol}} = \frac{D_{\mathrm{de,mol}}}{h_{\mathrm{de}}} \frac{K_{\mathrm{de/w}}}{K_{\mathrm{sol/w}}} \tag{4.4}$$

Knowing that the donor solution is an aqueous solution ($K_{\mathrm{sol/w}} = 1$), and assuming that the dermis is also effectively an aqueous solution ($K_{\mathrm{de/w}} = 1$) and that it is 2 mm thick ($h_{\mathrm{de}} = 2\mathrm{mm}$), the resulting diffusivity for *in vitro* permeation (using the permeability coefficient reported [336]) is :

$$D_{\mathrm{de,mol}} = 7.22\ 10^{-7} \mathrm{cm}^2/\mathrm{sec} \tag{4.5}$$

Since there is no systemic absorption, this is thought to represent the molecular (no clearance) diffusivity of the dermis.

The concentration of the solution applied was 1 mM and the volume of the solution was 1 ml, while the internal diameter of the donor glass cell used for the experiment was 1.8 cm [299]. Knowing the volume of the donor solution as well as the dimensions of the glass cell, it was determined that the solution was 4 mm thick.

The absolute amounts found in the dermis and the hypodermis, as well as the amount remaining in the solution after 2 hours were calculated (Table 4.3). This was done by dividing the moles reported by the volume of each layer (thickness multiplied by the area defined by the cross section of the glass cell). The rest of the initial amount was assumed to be cleared.

Layer	Amount (10^6 moles/cm^2)
Solution	0.2582
Dermis	0.020623
Hypodermis	0.00961056

Table 4.3: Distribution of salicylic acid. Absolute amounts of initial dosage found in skin strata two hours post-application

Due to the fact that in our model there is a perfect sink at the end of hypodermis, the amounts found in strata deeper than the hypodermis were assumed to be cleared through the circulation. This leads to a slight overestimation of the clearance process. It is a slight overestimation not only because the amount is about 5 %, but also due to the fact that the amounts found in these deeper layers may have been the result of vascular redistribution. Singh and Roberts performed measurements in the contralateral side of the application site. The concentrations found were lower but comparable to the ones found directly below the application site. The explanation that they provided is that the drug was cleared through the dermal capillaries and then redistributed through the deeper layers circulation. The authors took a step

further by suggesting that salicylic can directly penetrate skin only up to a depth of $3-4$ mm, which in our model roughly coincides with the end of the hypodermis.

Even though the experimental results refer to a transient penetration, the disappearance of the initial dose with time, as reported in [336], is "smooth" enough to consider it a quasi-steady state process. This treatment was reinforced later by the model's results for transient delivery (shown in Sec. 4.4.2) suggesting achievement of steady state conditions 30 minutes post-application. Thus, the steady state flux through the dermis is :

$$\text{Flux} \;=\; \text{(amount)/(area)/(time)} \;=\; 1.91\ 10^{-11}\ \text{mole/cm}^2\text{/sec} \qquad (4.6)$$

4.4 Model predictions

4.4.1 Steady state analysis

As mentioned earlier, one of the critical aspects of transdermal transport is the effect of the vascular clearance. One way of quantifying this effect is the comparison of the *in vivo* effective dispersion coefficient with the *in vitro* molecular diffusion coefficient of the dermis. The starting point of this comparison was the simplest one, where only dermis was considered. Steady state conditions and constant dispersion and clearance coefficients (D_{de}, k_{de}) throughout the layer were assumed. Under these assumptions, the analytic solution of Eq. (3.2) describing transport through the dermis is:

$$C_{\text{de}} \;=\; C_{\text{de}}(0)\ \exp\left[\left(\frac{k_{\text{de}}}{D_{\text{de}}}\right)^{1/2} z\right]\ , \qquad (4.7)$$

which is essentially an ideal exponential decay of the concentration. The corresponding flux is given by:

$$\text{Flux} \;=\; C_{\text{sol}}\ \frac{K_{\text{de/w}}}{K_{\text{sol/w}}}\ \sqrt{k_{\text{de}} D_{\text{de}}}\ , \qquad (4.8)$$

and the amount found in the dermis (assuming it to be a semi-infinite region) is:

$$\text{Amount}_{\text{de}} = A\int_0^{-\infty} \exp\left[\sqrt{\frac{k_{\text{de}}}{D_{\text{de}}}}z\right] C_{\text{sol}}\frac{K_{\text{de/w}}}{K_{\text{sol/w}}}dz \tag{4.9}$$

where A is the area of the site. Eq. (4.7) is based on the assumption that the dermis is a semi-infinite region, since it is, on the average, 2mm thick and most of the permeant is cleared within the first few hundred microns. Fitting the data of Singh and Roberts using the latter two equations yielded the following values for the dermal clearance and dispersion coefficients :

$$D_{\text{de}} = 8.9043\ 10^{-7}\ \text{cm}^2/\text{sec} \tag{4.10}$$

$$k_{\text{de}} = 9.079\ 10^{-4}\ \text{sec}^{-1} \tag{4.11}$$

Keeping in mind that the *in vitro* molecular diffusivity was found to be $D_{\text{de,mol}} = 7.2\ 10^{-7}\ \text{cm}^2/\text{sec}$, a first conclusion is that the apparent diffusivity in vascularized skin is greater than the molecular diffusivity, but not much greater.

The exclusion of hypodermis from the calculations might have affected the results on the dermal transport parameters. The next step was to include the subcutaneous tissue in the fitting process. The concentration in this layer is given by:

$$C_{\text{hd}}(z) = C_{\text{de}}(-h_{\text{de}})\frac{K_{\text{hd/w}}}{K_{\text{de/w}}}\exp\left[\sqrt{\frac{k_{\text{hd}}}{D_{\text{hd}}}}(z+h_{\text{de}})\right] , \tag{4.12}$$

in which the prefactor reflects the partitioning equilibrium at the dermal-hypodermal junction. Since there was only one experimental result for hypodermis (amount in layer) and there were three additional parameters to be fitted (the partition coefficient $K_{\text{hd/w}}$, the hypodermal dispersivity D_{hd}, and the hypodermal clearance coefficient k_{hd}), educated guesses about the value of the two of them had to be made. The third equation used in fitting the experimental data was the one giving the amount

of salicylic acid in the hypodermis:

$$\text{Amount}_{\text{hd}} = A\int_{-h_{\text{de}}}^{-\infty} \exp\left[\sqrt{\frac{k_{\text{hd}}}{D_{\text{hd}}}}(z+h_{\text{de}})\right] C_{\text{de}}(-h_{\text{de}})\frac{K_{\text{hd/w}}}{K_{\text{de/w}}} d(z+h_{\text{de}}) \quad (4.13)$$

The equations for the system of dermis and hypodermis were solved for two different cases of hypodermal solubility. The subcutaneous tissue is composed mainly of adipocytes, fat containing cells (Chap. 2), and octanol is known to mimic fat with respect to its transport properties [201]. Therefore, the hypodermal partition coefficient was taken equal to the octanol-water partition coefficient of salicylic acid ($K_{\text{oct/w}} = 162.18$). Although backed with a physical argument, this assumption meant that there would be a huge concentration "jump" at the dermal-hypodermal interface equal to this parameter. The fitting process gave an unrealistically low value for the hypodermal dispersion coefficient but it yielded practically the same dermal coefficients that were found for the isolated dermis.

The same procedure was repeated with the partition coefficient chosen to be $0.3K_{\text{oct/w}}$. This is a more logical value, taking into consideration that 20 % of hypodermis is water. Having not enough data on the subcutaneous layer the ratio $k_{\text{hd}}/D_{\text{hd}}$ was restricted to vary less than an order of magnitude from the ratio $k_{\text{de}}/D_{\text{de}}$. The resulting parameters were:

$$D_{\text{hd}} = 9.3\ 10^{-9}\ \text{cm}^2/\text{sec} \quad (4.14)$$

$$k_{\text{hd}} = 3.32\ 10^{-6}\ \text{sec}^{-1} \quad (4.15)$$

These values are very low and subject to considerable uncertainty. The main finding of this procedure is that the dermal parameter values appeared to be very insensitive to the presence of hypodermis. This leads to the important conclusion that the dermal transport and clearance coefficients can be extracted by studying the isolated dermis. The attempt to include hypodermis suggests that the data analyzed cannot support characterization of this layer. However, the amount of salicylic acid found

in the hypodermis suggests a very large partition coefficient between dermis and hypodermis for this substance.

The preceding simple analytical model generated depth-concentration profiles for the values of the transport parameters from the fitting process. These profiles are shown in Fig. 4.3.

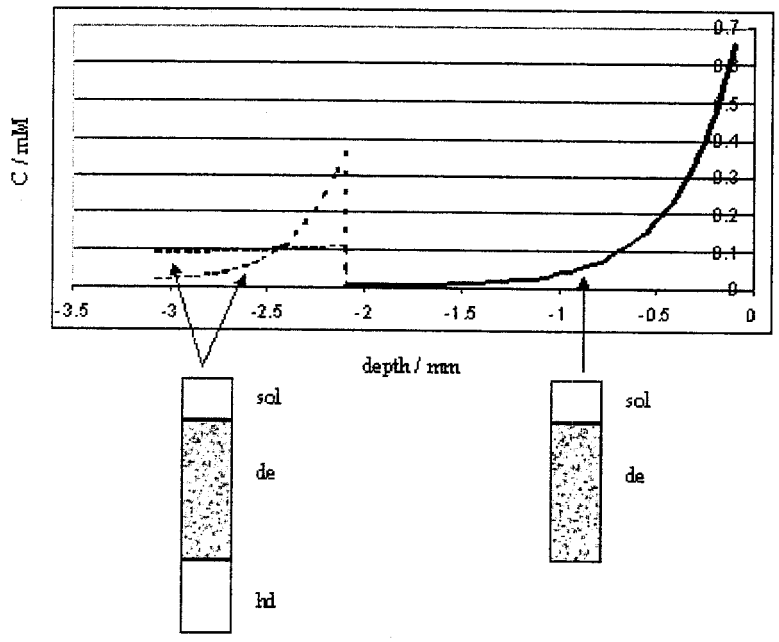

Figure 4.3: Steady state depth-concentration profiles for salicylic acid permeation in an epidermis-free skin. The solid line refers to the isolated dermis (exponential decay). The two dashed lines correspond to the two different assumptions on the hypodermal solubility properties ($K_{\mathrm{hd/w}} = K_{\mathrm{oct/w}}$ and $K_{\mathrm{hd/w}} = 0.3\ K_{\mathrm{oct/w}}$).

The concentration profiles for the two different partition coefficients coincide over the region of the dermis, since the dermal parameters were found to be essentially the same in all cases. They also coincide with the ideal exponential decay, representing the dermis as a semi-infinite tissue layer, indicating that this idealistic model is not far from reality. The profile corresponding to $K_{\mathrm{hd/w}} = 0.3K_{\mathrm{oct/w}}$ has a lower "starting point" in the hypodermal region. Since the area under the curve (amount in hypodermis) was fixed, the result was a virtually absent clearance, i.e.

a very low clearance coefficient. On the other hand the $K_{\mathrm{hd/w}} = K_{\mathrm{oct/w}}$ scenario predicts a concentration below the dermal-hypodermal junction which is larger by a factor of 162.18 than the concentration above the junction, something that is very probably more extreme than the actual concentration jumb.

The following step, after the characterization of the transport properties of the dermis, was to include the stratum corneum and the viable epidermis in the calculations. The SC permeability coefficient was assumed to be given by established formulae in the literature [172] accounting for both lipid and polar pathways:

$$P_{\mathrm{sc/w}} = P_{\mathrm{lip}} + P_{\mathrm{pol}} \tag{4.16}$$

$$P_{\mathrm{pol}} = \left(5\ 10^{-6}\right)\sqrt{\frac{300}{MW}} \tag{4.17}$$

$$\log P_{\mathrm{lip}} = \log K_{\mathrm{oct/w}} - \frac{0.018}{2.303}\,MW - 2.87 \tag{4.18}$$

with the MW being the molecular weight of the solute. Since the formulae correspond to human skin, the permeability coefficient for rat skin was taken to be 10 times as much. It is generally known that the permeability of rat skin is greater than its human counterpart; thus this valid rule-of-thumb estimate was used [170]. It was found to be:

$$P_{\mathrm{sc/w}} = 5.0622\ 10^{-5}\ \mathrm{cm/sec} \tag{4.19}$$

The viable epidermis was regarded as an aqueous-solution/layer of 100μm thickness with an epidermis/water partition coefficient $K_{\mathrm{ed/w}}$= 1 for salicylic acid. The molecular diffusivity of SA in epidermis was assumed to be 5 % of its diffusivity in water (Table 4.1). This value stemmed from the fact that the dermal molecular diffusivity of SA (Eq. (4.5)) is $\simeq$ 6% of the diffusivity in water. The diffusivity in epidermis was taken as approximately the same. The results are shown in Fig. 4.4. The concentration profile for the permeation of isolated dermis was also included for comparison.

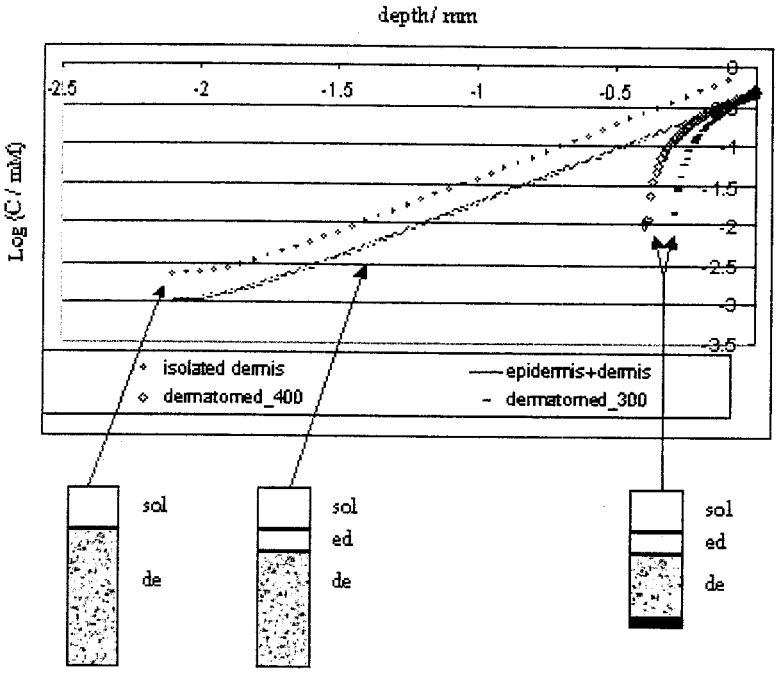

Figure 4.4: Steady state depth-concentration profiles for salicylic acid permeation in intact and dermatomed skin.

By comparing the profiles for the permeation through isolated dermis, and dermis with epidermis, it is obvious that the presence of epidermis results in an additional mass transfer resistance, and consequently to lower concentrations as expected. The two profiles denoted in the graph as "dermatomed - 300" and "dermatomed - 400" correspond to the prediction of the popular approach that assumes perfect clearance of the drug through the dermal capillaries. An analytic solution to the diffusion problem was derived for this approach by imposing a perfect-sink boundary condition at 300 and 400 μm below the skin's surface respectively (Appendix C). The results are very enlighting about what can be predicted by following this simplified model. The prediction of the steady state flux (initial slope of the curves) is quite good since it coincides with the flux predicted from the whole skin model. However, the local concentration levels predicted are dramatically different.

4.4.2 Transient analysis

The main conclusion of the steady state analysis was that the dermal parameters can be determined from an isolated dermis model. The next level of sophistication was to study the transient transport through the isolated, epidermis-free dermis, and to quantify the dermal dispersivity and clearance coefficient under non-steady state conditions. The system of equations describing transport through skin had to be supplemented with an additional equation describing the depletion of the drug in the donor formulation. Since the SC is assumed to offer no drug hold up, one is able to equate the flux going into skin (epidermis) to the flux going out of the solution. By assuming that the thickness of the solution ($h_{\rm sol}$) remains constant, this equation is:

$$\begin{aligned} D_{\rm ed}\left.\frac{\partial C_{\rm ed}}{\partial z}\right|_0 &= \frac{d(Ah_{sol}C_{\rm sol})/dt}{A} \Rightarrow \\ \frac{dC_{\rm sol}}{dt} &= \left(\frac{1}{h_{\rm sol}}\right) D_{\rm ed}\left.\frac{\partial C_{\rm ed}}{\partial z}\right|_0 \qquad (4.20) \\ \text{with } A &\equiv \text{area of application} \\ \text{and } \left.\frac{\partial C_{\rm ed}}{\partial z}\right|_0 &\equiv \text{epidermal concentration} \\ & \qquad \text{gradient just below SC} \end{aligned}$$

The system of equations was solved with simultaneous fitting of the solution concentration and of the amount found in dermis to the two-hour values reported by Singh and Roberts. Initially the solution was considered well-stirred (infinite diffusivity) but the solution exhibited numerical instability. The donor solution layer was then assumed to have an extremely large yet finite diffusivity ($D_{\rm sol} = 10^6$ cm^2/sec). That way the numerical problems were overcome and the solution remained effectively well-stirred. The coefficients obtained for the dermis are:

$$D_{\rm de} = 7.75109\ 10^{-7}\ \text{cm}^2/\text{sec} \qquad (4.21)$$

$$k_{de} = 6.80711\ 10^{-4}\ \text{sec}^{-1} \tag{4.22}$$

Comparison with the analogous results from the steady-state analysis shows that a steady-state approach can provide quite accurate values of the coefficients. More importantly, the value of the dispersivity from both the transient and steady state analysis is almost equal to the molecular diffusivity obtained from *in vitro* measurements. This means that although vascular clearance has a dramatic effect on the amount of the drug transversing the dermis, it does not alter the transport of the non-cleared amount through the layer. The effective dispersivity remains essentially constant.

The values of the transport and clearance coefficients were inserted in the transient model describing transport in the solution and isolated dermis, and concentration profiles for various times were generated (Fig. 4.5). It was assumed that the thickness of the donor solution remained constant throughout the experiment.

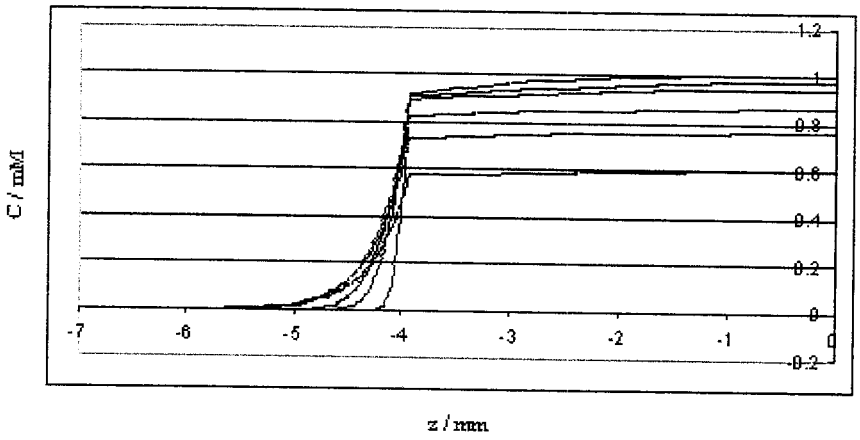

Figure 4.5: Transient depth-concentration profiles for salicylic acid permeation of solution in contact with isolated dermis. Time values are 1, 5, 10, 30, 60 and 120 min in descending line order. Solution is 4 mm thick and dermis is 2 mm thick.

As it can be seen in the graph, it takes about 10 min for salicylic acid to reach the physical end of the dermis, and steady state conditions are effectively achieved

30 min post-application. The almost constant concentration in the solution is an indication that the well-stirred restriction was maintained.

These results were validated by several ways, one of which was to ascertain conservation of mass by calculating the amounts of drug in the solution and in the skin, as well as the amount cleared, and the sum of all these quantities. This treatment offered further insight on the transport/clearance interplay (Fig. 4.6).

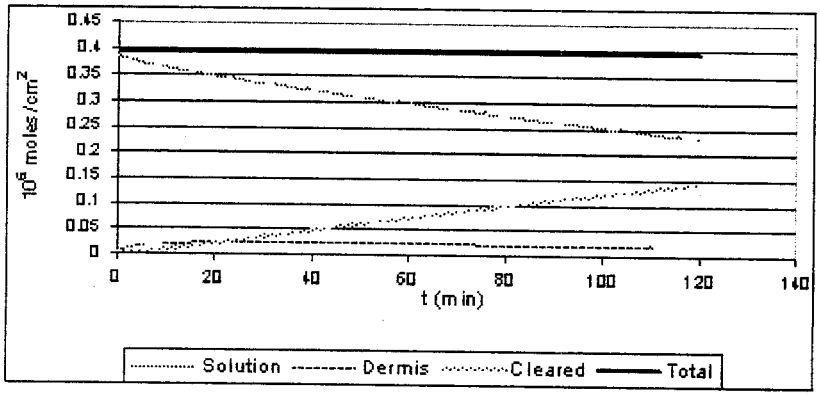

Figure 4.6: Mass conservation calculation for the transient permeation of salicylic acid in isolated dermis

Once again, the dermal transport/clearance coefficients obtained by the fitting process of the experimental results were utilized in order to obtain results for intact skin. The parameters used for the SC and viable epidermis were the ones described earlier, and once again hypodermis was not included since the experimental data could not support its characterization. For this set of results it was assumed that the solution concentration is constant (infinite dose case) and equal to the one that Singh and Roberts reported after two hours of permeation ($C_{\text{sol}} = 0.657$ mM). The resulting concentration profiles are shown in Fig. 4.7. The starting depth-point for these profiles is the point just below the SC. Keeping in mind the value of the concentration in the donor formulation, it is evident that the presence of SC results in a considerable concentration decrease that is very steep during the first minutes

of permeation. Under steady state conditions the concentration gradient imposed by the SC is considerable less, yet important.

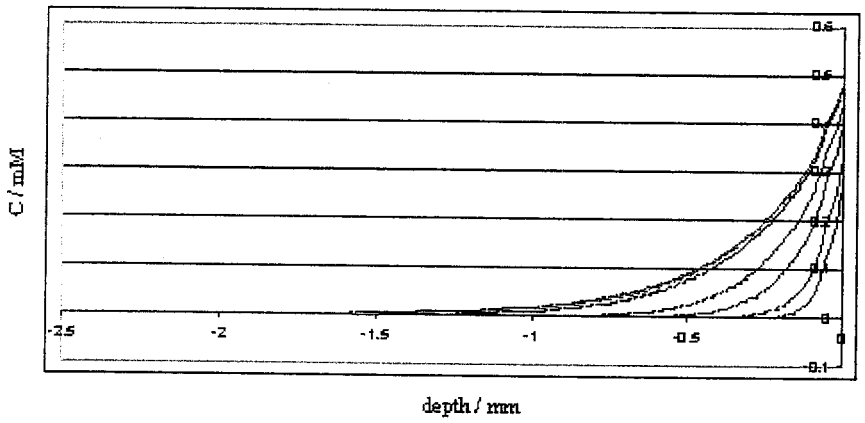

Figure 4.7: Non-steady state depth-concentration profiles of the permeation of salicylic acid in intact skin. Profiles correspond in ascending order to 1, 2, 5, 10, 30, 60, and 120 min after application of the solution. The profiles for 60 and 120 min of permeation coincide (indicating that steady state conditions have effectively been achieved after $\simeq$ 1 hr).

The time needed for the achievement of steady state condition is more clearly visualized through the calculation of the non-steady state flux that enters skin at various times (Fig. 4.8). The flux was calculated according to Eq. (4.23):

$$\text{Flux} \;=\; P_{\text{sc/w}}\,(C_{\text{sol}} - C_{\text{ed}}|_{z=0}) \tag{4.23}$$

It takes approximately 30 to 40 minutes post-application to reach the steady flux which was calculated to be:

$$\text{Steady state flux} \;=\; 9\ 10^{-5}\mu\text{moles / cm}^2\text{ / sec} \tag{4.24}$$

4.5 Discussion

Several valuable conclusions may be drawn from the preceding analysis. The results of the model pertaining to the steady state permeation of salicylic acid through whole-thickness skin indicate that the concentration profile follows an exponential decay pattern with depth, and it can therefore be described in a simple way, through Eq. (4.7).

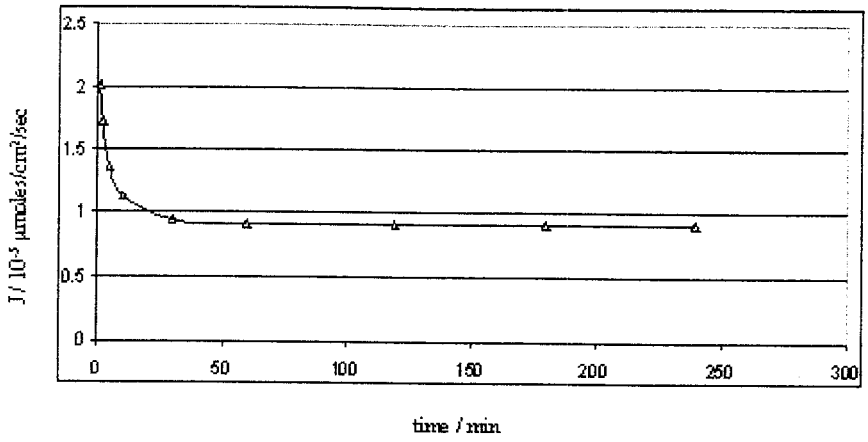

Figure 4.8: Time dependence of flux for the permeation of salicylic acid in intact skin.

This finding, which is in accordance with previous, similar results [133], may have more general implications. Independent experimental reports [37, 133, 221, 233, 322] show depth-concentration profiles that closely resemble exponential decays for the transdermal penetration of a variety of drugs. Certainly, it would be presumptuous to state that this pattern is a universal feature of skin's permeation. However, these results make pertinent a more thorough investigation of the subject, both by applying the model to other skin permeating substances, and by gathering further published experimental studies.

Another point that may be made addresses the impact of the clearance process on the transport properties of dermis. It has been hypothesized [233] that the local dermal vasculature creates a convective force which drags down the non-cleared fraction of the permeating substance. Our results on the values of dermal dispersivity (clearance process present) and dermal molecular diffusivity (clearance process absent) show that transport through the interstitial space is enhanced due to the existence of the microcirculation, but only slightly. Thus, even though clearance has a profound effect on the deep-tissue distribution of a permeant, it appears to influence minimally the diffusion of a drug while it is unabsorbed substance. Con-

tinuing the discussion on the effect of clearance upon drug permeation/distribution, we should also point out the consequences of the extensive SA binding to serum albumin. Based on the literature that was reviewed in Sec. 4.2.1, the assumption of non-substantial binding occuring extravascularly appears valid. A noteworthy analysis of results pertaining to SA permeation [337] agrees with this assumption. The same analysis stresses the importance of binding inside the blood phase (resulting in a blood-dermis partition coefficient equal to four), while another report [88] pinpoints the effect of protein binding to a facilitated, more extensive clearance of SA through the dermal vasculature. In the context of the skin transport model, this phenomenon is shown in the values of the calculated clearance coefficients, i.e., the value of the dermal clearance coefficient for a drug similar to SA which does not bind appreciably to protein would be smaller.

Furthermore, our analysis on the impact of the presence of the subcutaneous fat to transport through dermal tissue directs us to the significant conclusion that dermis can be theoretically characterized as an isolated entity, at least for salicylic acid. This conclusion is reinforced by experimental studies [336] indicating a limited penetration of SA in deeper tissue. As far as the characterization of hypodermis is concerned, our attempts were not conclusive, largely due to the lack of experimental data. Educated guesses had to be made for more than one transport parameter of the hypodermis, which is by far the least studied skin layer. A recent communication [300], raised uncertainty about the estimates of the dermal-hypodermal partition coefficient. A very interesting recent experimental study [279] on the hypodermis - plasma partition coefficients of several drugs, revealed that the "traditional" treatment of subcutaneous fat as an octanol solution may not the best choice. The authors suggest that the partitioning behavior of hypodermis is better characterized by a vegetable oil / water partition coefficient. In our analysis of SA permeation, this would translate in a dermal-hypodermal partition coefficient equal to ten, a figure substan-

tially lower than the ones used in the calculations. This alternative path is backed up by experimental data, and it will be investigated, in the future.

The comparison of a whole-skin model, such as ours, with a model that adapts the assumption of a perfect clearance occuring at the upper dermis is also very enlighting. It was shown that this simple approach is adequate in assessing the steady state transdermal flux of a permeating substance. Nevertheless, this perfect clearance model fails in capturing the essence of the spatially distributed clearance process and the deep-tissue penetration physics in general. Therefore, this model is limited to the description of drugs that actually are completely cleared through the dermal capillaries. Although this constitutes the majority of drugs [325], the fact that perfect clearance may not occur due to blood flow variations [35, 47, 119, 237, 302, 338], or the nature of the drug [215, 233], must not be overlooked. The perfect clearance approach is also inadequate in describing permeation of drugs that are designed to have a local, non-systemic effect [4, 126, 199, 325, 352].

Finally, it is of value to briefly mention a few noteworthy modeling attempts and to discuss how they compare with our model. Gupta et al. [133], reported a distributed transport model that implements an equation for the dermis very similar to Eq. (4.7). This equation, after rearranging the terms, is:

$$C_{\mathrm{de}} = (C_{\mathrm{de}}(0) - C_b)\ \exp\left[-\left(\frac{paq}{D_{\mathrm{de}}(pa+q)}\right)^{1/2} z\right] + C_b \qquad (4.25)$$

with C_b is the drug concentration in the perfusing blood, p is the capillary permeability coefficient, a is the surface area of the capillaries per unit tissue volume, and q is the capillary blood flow rate per unit tissue volume. Although Eqs. (4.7) and (4.25) are not the same, due to different assumptions and levels of detail, they do share a significant common feature, i.e., the log-linear decline of concentration with depth. The authors compared the predictive power of their model with a simple, linear one

that does not account for the distributed nature of the capillaries, and reached the conclusion that the exponential decay better describes dermal penetration. They also cite similar results reported for the intestinal capillaries, further solidifying the view that perfused tissues cannot be described without explicitly accounting for the nature of the clearance process. Twizell [370] considered transient diffusion through skin with a non-perfect clearance at the upper dermis, while the problem was solved with a numerical scheme that employed a division of the solution in its transient and steady state parts. However, he considered skin to consist of only one homogeneous layer (ranging from the surface to a point just above the dermal capillaries) and he kept the concentration fixed at the skin-capillary boundary. Kubota and Maibach [188] stressed the importance of the viable layers underlying stratum corneum by considering a three-layer diffusion model (SC, viable epidermis, and dermis). They attacked the problem by considering the phenomenological nature of diffusion, and thus by applying a random-walk method of solution. Although they presented the system of equations for the case of perfusional capillary resistance, their results pertained to the case where there is perfect clearance at the upper part of the dermis. It is also worth mentioning that they compared the multi-layer model with a single layer (SC) model. They found that the latter underestimates parameters such as the half-life of the drug and the lag time following initial application. Okamoto et al. [246] included the additional complication of a finite dose in their model. They, too, considered an additional well-stirred solution/layer of finite volume applied at the SC surface, while the epidermis and upper dermis were treated as a single layer. They solved the partial differential equations with Laplace transforms, and performed an analysis based on the mean transit time of the drug. However, their model assumes perfect clearance through the dermal capillaries. Anissimov and Roberts [16, 17] studied the transient diffusion through skin, during both an infinite and finite dose application. Stratum corneum was regarded as a membrane, while the viable epidermis and

superficial dermis was assumed to be an unstirred aqueous layer characterized by a pseudo-steady state permeability coefficient. Thus, they avoided the more realistic, and more complex, problem with coupled PDEs for each layer. They also recognized the possibility of a finite clearance, by lumping together the clearance process with diffusion below the dermal microvasculature, thus they did not consider transport in deeper tissue layers. The model was solved in the Laplace domain, and the authors reported a series of parametric studies. However commendable, this model is unable to describe whole-skin permeation, while the lumping of the clearance process [17] resulted in a linear steady state depth-concentration profile that does not predict the *in vivo* reality as well as the exponential model.

Part II

Microscopic Transport Studies

Chapter 5

A Microscopic Model for the Dermal Tissue Transport Properties

5.1 Introduction

The extravascular dermal tissue is a complex, heterogeneous composite, comprising distinctly different substructures (Sec. 2.4). Earlier researchers [76, 230, 325, 360, 390] have debated that transport of a tissue-penetrating substance might be restricted/altered due to physical and/or chemical interactions between the substance and the various elements that are present in the dermal interstitium. Even though under normal conditions dermis is $60-70\%$ water [125], measurements and estimates of its transport properties indicate that its representation simply as an aqueous layer does not suffice in capturing critical dermal characteristics [87, 339, 384, 390].

The first steps toward the construction of a dermal tissue model are presented in this chapter. The dermal interstitial space is considered as a periodic, composite structure, with the skeleton of the dermis, constituted by collagen and elastin, being represented in a physiologically accurate way. Furthermore, the differences between the papillary and reticular dermis are accounted for. Preliminary calculations, com-

plimentary to the model, show the effect that these fibrillar structures have on the diffusion of a permeating substance. Although the model is not complete, the framework upon which the subsequent calculations may be based, is given. These future calculations are discussed later in this chapter.

5.2 Physiological parameters from the literature

Several useful conclusions stem from the cited information about the dermal collagen in Sec. 2.4.1. By examining the distances between the collagen fibrils [270], and the fibers thereof arranged in a bundle ($O(0.1)$ μm for the latter) [231, 368], it is reasonable to consider the spaces between the fibrils inaccessible to a diffusing substance. The same may not hold for diffusion between the fibers since a small molecule, say glucose which has a hydrodynamic radius of 3.6 $\mathring{\text{A}}$ [7], may readily penetrate the bundles from a strictly steric point of view. However, as a first approximation, the bundles will also be regarded impermeable. In addition, the excellent scanning (SEM) and transmission (TEM) electron microscope micrographs of Montagna et al. [231], reveal that the fibers that constitute the bundles are highly ($\simeq$ periodically) organized. Furthermore, the density of the bundles appears to be more or less the same throughout the papillary compartment, and this is also true for the reticular part. The same micrographs [231] confirm the conclusion that the orientation of the bundles is roughly parallel to the skin's surface [115, 241]. These studies also indicate that there are distinct differences between the papillary and the reticular dermis. The bundles are larger in the reticular region [137] (average diameter 25 μm [115], 10 μm in the papillary layer [49]). The percentage of the total weight of the dry dermis that can be attributed to collagen appears to be the same for both sublayers ($\simeq$ 70%, [125]). However, the water content of the wet dermis is $\simeq$ 60% in the reticular part and $\simeq$ 70% in the papillary part [125].

Studies of the network of elastin fibers in the dermis reveal a continuous, randomly oriented network [231] of thin (diameter $\simeq$ 2 μm, [378]), rigid fibers that are thicker in the reticular dermis. The volume ($\simeq$ 2%) and cross-sectional area ($\simeq$ 5.4%) that they occupy in the dermis, in terms of percentages of the total, are far less than the respective figures for collagen [373].

5.3 Geometric formulation

Both the collagen and elastin networks are assumed to be periodic in all three dimensions. Thus, we may deduce their impact on the diffusion of a permeant by focusing on a representative cubic unit cell. It is further assumed that there is no bias in the orientation of the fibers. Thus both unit cells will encompass three identical fibers, of collagen or elastin, perpendicular to one another. However, a preferred orientation could easily be included by reducing or increasing the number of fibers that are oriented along one or more directions of the unit cell. Since there are substantial differences in the properties of the networks in the papillary and reticular layer, two different cells are considered. After the construction of the collagen and elastin cells, they are superimposed in order to yield the final version of the composite structure. These networks are assumed to be impermeable, and the rest of the unit cell is assumed to be occupied by a homogeneous, aqueous solution. The properties of this solution, i.e., viscosity, may be chosen in such a way that it simulates the transport characteristics of the true, inhomogeneous, extrafibrillar material of the dermis. The actual dimensions of the unit cells are derived by matching the aforementioned physiological parameters.

5.3.1 Papillary dermis

It is known that collagen occupies 70% of the dry dermal volume, and that the wet dermis consists of 70% water. Thus, the volume occupied by collagen in the wet dermis is 0.7 0.3 = 0.21. This fraction of the unit cell's (of dimensions $a_{col,pap}$) volume must equal the sum of the volume of the three cylindrical fibers (of average diameter $d_{col,pap} = 10$ μm) that are included in the unit cell. Thus:

$$0.21\ a^3_{col,pap} = 3\pi \left(\frac{d_{col,pap}}{2}\right)^2 a_{col,pap} \Rightarrow$$

$$a_{col,pap} = 33.5\ \mu\text{m}. \tag{5.1}$$

For simplicity, the dimension $a_{col,pap}$ might be rounded up to 30 μm (Fig. 5.1). The

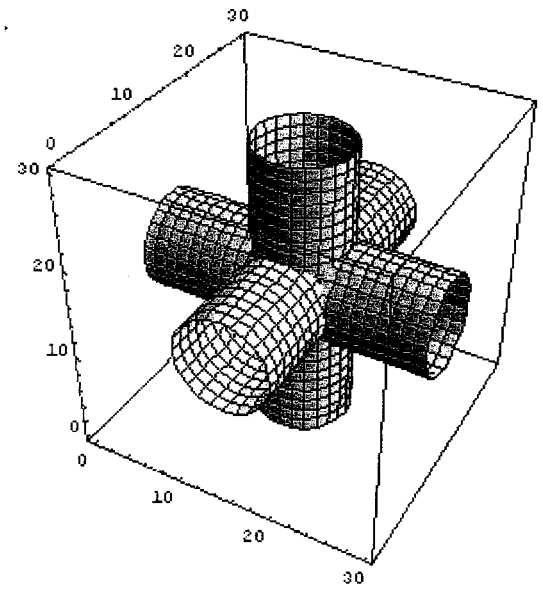

Figure 5.1: Dermal collagen unit cell for the papillary layer. Dimensions in μm.

dry volume that the elastin fibers occupy in the dry papillary layer is 0.75%. Thus the occupied volume in fresh dermis is 0.0075 0.3 = 0.00225. The average diameter for a papillary, elastin fiber is $d_{el,pap} = 0.8$ μm, and the dimension $a_{el,pap}$ of the elastin

unit cell (Fig. 5.2) is given by :

$$0.00225\ a^3_{\text{el,pap}} = 3\pi \left(\frac{\text{d}_{\text{el,pap}}}{2}\right)^2 \text{d}_{\text{el,pap}} \Rightarrow$$

$$\text{a}_{\text{el,pap}} = 25.88\ \mu\text{m} \simeq 30\ \mu\text{m}. \tag{5.2}$$

Thus, for the papillary layer, the dimensions of the two unit cells are approximately

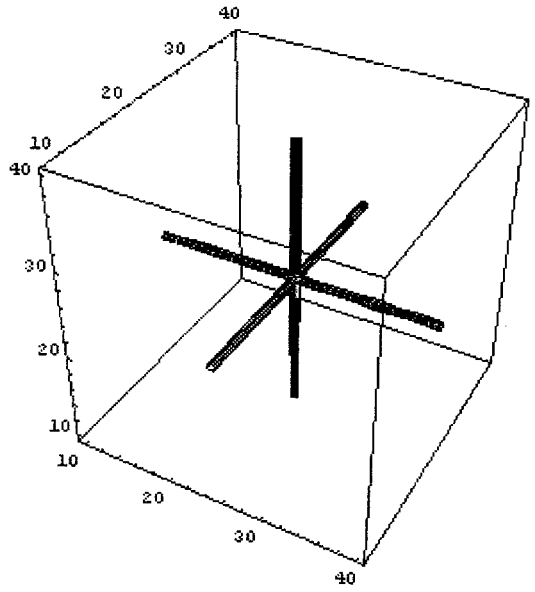

Figure 5.2: Dermal elastin unit cell for the papillary layer. Dimensions in μm.

the same, i.e, there are three collagen and three elastin fiber segments per cell. The composite dermal cell that includes both fibrillar networks is shown in Fig. 5.3. The elastin fibers were shifted so that they do not overlap with the collagen fibers.

5.3.2 Reticular dermis

By following the exact same methodology, it was found that the respective unit cells of collagen (average fiber diameter $\text{d}_{\text{col,ret}} = 25\ \mu\text{m}$) and elastin (average fiber diameter $\text{d}_{\text{el,ret}} = 1.8\ \mu\text{m}$), in the reticular layer have dimensions (Fig. 5.4) $\text{a}_{\text{col,ret}} = 72.52\ \mu\text{m}$ and (Fig. 5.5) $\text{a}_{\text{el,ret}} = 31.9\ \mu\text{m}$, respectively. In the interest of working with round numbers they are taken to be $\text{a}_{\text{col,ret}} = 70\ \mu\text{m}$ and $\text{a}_{\text{el,ret}} = 35\ \mu\text{m}$. The final unit

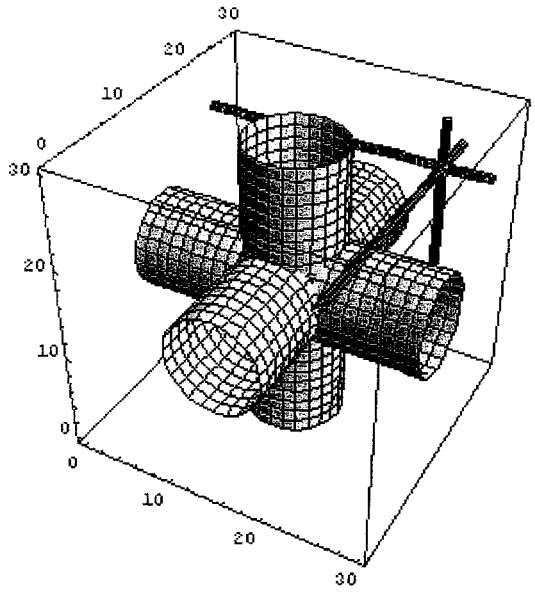

Figure 5.3: Dermal-composite unit cell for the papillary layer. Dimensions in μm.

cell is presented in Fig. 5.6. It comprises one collagen cell and eight elastin cells.

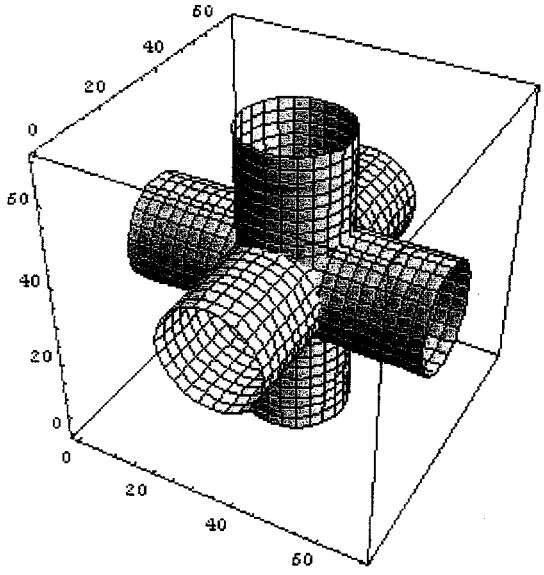

Figure 5.4: Dermal collagen unit cell for the reticular layer. Dimensions in μm.

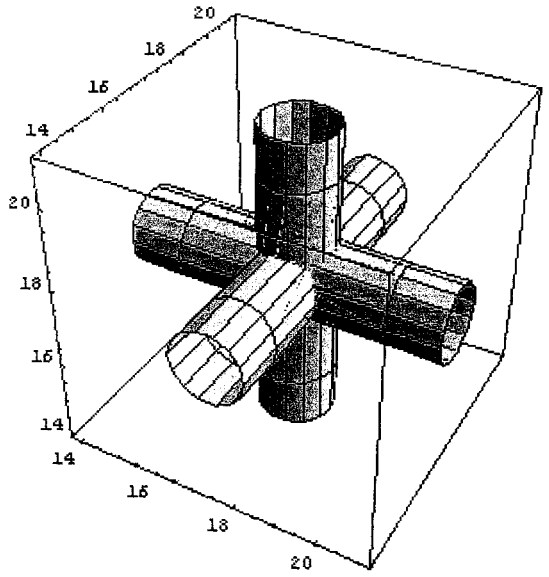

Figure 5.5: Dermal elastin unit cell for the reticular layer. Dimensions in μm.

5.4 Preliminary calculations on the restricted diffusion of a permeating substance

The problem of hindered diffusion through a fibrous medium has been researched extensively [72, 160, 244, 267, 268, 269, 396] since it is encountered in many practical applications, such as gel chromatography and electrophoresis, drug delivery, pulp bleaching etc. [72, 160]. Three formulae [72, 160, 244] that give the effective diffusivity of a fibrous medium were picked from the literature in order to assess the impact of the fibrillar dermis on transdermal diffusion, and to check the validity of our model when this is complete. Ogston et al. [244] studied the interactions between a hard-sphere solute and long, negligibly thin, chains of a cross-linked polymer in a solution. By taking a phenomenological approach that considers diffusion as an eventual chain of random steps, the authors arrived at the following expression:

$$\frac{D_{\text{eff}}}{D_\infty} = \exp\left[-\left(1+\frac{r_{\text{sol}}}{r_{\text{fib}}}\right)\sqrt{\phi}\right]. \tag{5.3}$$

where D_{eff} is the effective diffusivity of the medium, D_∞ is the diffusivity of the bulk solution, r_{sol} and r_{fib} are the radii of solute and fiber, respectively, and ϕ is

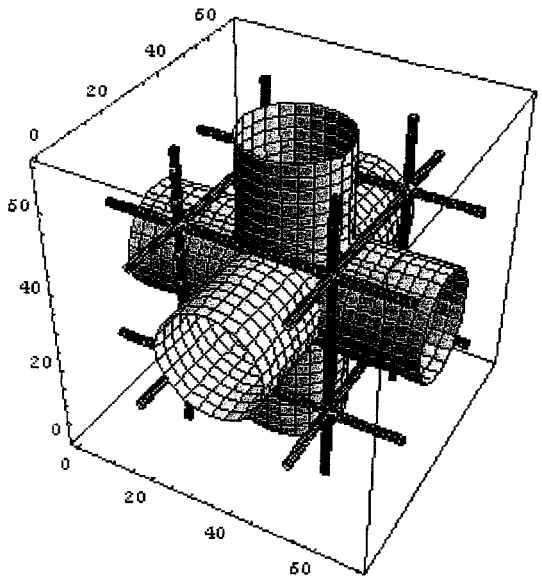

Figure 5.6: Dermal-composite unit cell for the reticular layer. Dimensions in μm.

the volume fraction of the fibers. Johnson et al. [160] took an effective medium approach. They argued that the steric and hydrodynamic effects of the fibers on transport are independent, and furthermore that their combined result may be derived by multiplying these effects. By using Brinkman's equation for the hydrodynamic part and a fitted exponential function for the steric part they concluded to Eq. (5.4).

$$\frac{D_{\text{eff}}}{D_\infty} = \left[1 + \frac{r_{\text{sol}}}{\sqrt{k}} + \frac{r_{\text{sol}}^2}{3k}\right]^{-1} \exp\left[-0.84\left(1 + \frac{r_{\text{sol}}}{r_{\text{fib}}}\right)^2 \phi^{1.09}\right]. \tag{5.4}$$

with k being the hydraulic permeability of the medium. Finally, Clague and Phillips [72] followed the same separation of hydrodynamic and steric hindrances. They calculated the interactions for a spherical solute in a randomly oriented fiber network, suspended in a liquid. Although the authors do not explicitly state the parameters for their fitted exponential, Amsden [7] analyzed their data and derived values of the parameters producing the formula:

$$\frac{D_{\text{eff}}}{D_\infty} = \frac{1}{\left[1 + \frac{2}{3}\left(1 + \frac{r_{\text{sol}}}{r_{\text{fib}}}\right)^2 \phi\right]} \exp\left(-\pi \phi^{0.174 \ln(59.6 r_{\text{fib}}/r_{\text{sol}})}\right). \tag{5.5}$$

We applied initially Eqs. (5.3 - 5.5) to the elastin network. The resulting effective diffusivity ($D_{\text{eff,el}}$) was subsequently assumed to represent the bulk diffusivity of the medium surrounding the collagen fibers in calculating the final effective diffusivity (D_{eff}). The (bulk) diffusivity of the solute in the extrafibrillar dermis was calculated with Einstein's equation:

$$D_{\infty} = 10^{17} \frac{k_{\text{B}}T}{6\pi\mu r_{\text{sol}}} \text{cm}^2/\text{sec.} \tag{5.6}$$

where the Boltzmann's constant is $k_{\text{B}} = 1.38\ 10^{-23}$ J/K, and the temperature $T = 310.15$ K. The viscosity was assumed to be twice the viscosity of water at this temperature. The hydrodynamic radius of a prototypical small solute was taken as $r_{\text{sol}} = 3$ Å. Thus:

$$D_{\infty} = 5.422\ 10^{-6} \text{cm}^2/\text{sec.} \tag{5.7}$$

The rest of the (average) parameters are shown in Table 5.1. The results for this specific set of values yielded by Eqs. (5.3 - 5.5) are shown in Table 5.2. These results indicate that the steric and hydrodynamic hindrance imposed by the fibers is not very large; the effective diffusivity of the composite is 50% to 80% of the diffusivity of a bulk solution with viscosity twice as that of water. This translates into a diffusivity 25% to 40% of the diffusivity in bulk water.

	Fiber radius (μm)	Fiber volume fraction (%)	Hydraulic permeability
Collagen	5	0.25	$3.92\ 10^{-11}$
Elastin	1	0.02	$3.01\ 10^{-11}$

Table 5.1: Parameters of the fibrillar dermis. The hydraulic permeabilities of the elastin and collagen fibrous media were calculated with an established formula in the literature ($k = 0.31\ (r_{\text{fib}}^2)\ (\phi^{-1.17})$) [156].

	D_{eff} (cm^2/sec)		D_{eff}/D_∞
Equation	Elastin	Elastin and collagen	
Ogston et al. [244]	$4.73\ 10^{-6}$	$2.87\ 10^{-6}$	0.53
Johnson et al. [160]	$5.38\ 10^{-6}$	$4.47\ 10^{-6}$	0.82
Clague and Phillips [72]	$5.37\ 10^{-6}$	$4.11\ 10^{-7}$	0.76

Table 5.2: Effective diffusivity of dermis (D_{eff}/D_∞) measured in cm^2/sec.

5.5 Discussion

The preceding analysis will be continued with a refined approach to the tissue that surrounds the fiber networks. Although, the assumption of an aqueous solution having "effective" transport properties is a good first approximation, it has to be determined whether the extrafibrillar dermis should be considered as a homogeneous, or a two-phase material. Uncertainties surrounding the *in vivo* physiological and functional reality of the dermis, became apparent at more than one point in this work (Secs. 2.4.3, 6.3, 6.6). Furthermore, the possibility of a permeant binding to collagen must be investigated, and perhaps included in the model. It has been demonstrated experimentally, for chromium and ferric ions [325] that the dermis may act as a reservoir for ions that can bind to collagen. The aforementioned additions may alter the results reported in Sec. 5.4. These results indicate a significant but not major diffusive restriction due to the collagen and elastin networks. It was expected that the impact on diffusion would be greater.

In our subsequent work, we will try to follow the steps of several excellent approaches on the transport through fibrous heterogeneous, or generally composite, materials [27, 284, 317, 318, 381, 388]. The remarkable review of Batchelor [27] offers a unified theory, according to which physically unrelated processes occurring in heterogeneous media, have the same mathematical structure and therefore may be attacked with the same method of solution. This theory, makes conceivable the application of the dermal model to other areas of application, i.e. it became apparent

that a strikingly similar problem deals involves stress analysis of spacecraft bodies, parts of which are made from composite materials enclosing microfibers.

Chapter 6

Topics in Capillary Clearance

6.1 Introduction

This chapter provides the theoretical background upon which the development of the capillary exchange model (Chap. 7) was based. The microvascular clearance process is the end result of three consecutive steps, namely transport through the pericapillary interstitium, permeation of the capillary wall, and convective clearance through blood flow. Key elements of these steps are presented here with emphasis on the transport behavior of the capillary wall and the surrounding tissue. Furthermore, selected experimental results that help estimate their transport parameters are reported. This chapter also includes a comprehensive comparative review of other capillary exchange models.

6.2 Capillary permeability

Ink has not been spared on the topic of capillary permeability. Numerous investigators have attempted to theoretically predict or experimentally quantify material exchange across the blood-tissue barrier. A couple of *a priori* remarks that may be made are that transport is almost entirely caused by physical driving forces such as concentration and pressure gradients (passive transport) [103, 228, 291, 405], and

that the mechanisms by which small solutes and macromolecules are exchanged are quite different [226, 256]. The following brief review intends to sketch the conceptual framework of this very active area of research and provide selected experimental findings. Excellent and far more extensive reviews exist in the literature [86, 91, 252, 256]. Emphasis is given on small (non-macromolecular) solutes and their transport through skin or other organs' continuous capillaries that most probably [86, 235, 250, 252] have permeability characteristics similar to those of dermal capillaries. The reader should bear in mind that the relevant literature deals almost exclusively with the transport of substances from blood to tissue. However, the passiveness of the exchange process makes the subsequent analysis applicable to the opposite scenario where substances enter the bloodstream from the interstitial space, such as in the case of percutaneous absorption.

6.2.1 Transport pathways

Several routes have been identified in the capillary wall structure as pathways available for exchange. Depending on their nature, size, and lipophilicity, solutes may prefer one or more of them. These pathways include [59, 86, 91, 226, 291]:

- Interendothelial cell junctions. They structurally resemble pores or slits filled with the aqueous extracellular phase. For some of the researchers who try to reconcile the capillary's structure with its functionality, they have become synonymous with the small or large pores of capillary pore theory. They appear to be the preferred, if not the only, pathway for the passage of hydrophilic solutes, and they are also important for small lipophilic solutes.

- Endothelial cells. Traversing the whole thickness cell involves crossing plasma membranes and the cells' cytoplasm. Surprisingly, the nature of these barriers does not restrict this route to lipophilic solutes; water, despite its hydrophilic

nature, readily permeates cell membranes .

- Endothelial cell's membranes. Instead of directly penetrating the endothelial cell, lipophilic molecules may diffuse laterally only within the cell membrane in the lipid phase along the length of interendothelial junctions or vesicles.

- Endothelial cell vesicles. The existence of vesicles on the endothelial wall has been directly connected with their permeability. Most of these circular-like structures have their tissue or blood side open, which results in a ridge-like formation that increases the endothelial surface available for penetration and reduces the transendothelial diffusion path. They can shuttle back and forth (along with their contents) between the cell surfaces (transcytosis) and they often exchange contents with each other or fuse together to form transient channels. Proteins are assumed to be transported this way but there is still doubt about their significance in transport. Mind-settling quantifying studies are lacking.

- Fenestrae (meaning windows in German). As was mentioned earlier (Chap. 2), these discontinuities in the endothelial cell are not found in the horizontal plexuses of skin capillaries.

6.2.2 Transport processes

There is some controversy in the literature about the relative significance of diffusion and convection through the microvasculature. Molecular passive diffusion is the only mechanism by which solutes proceed through cell membranes and is considered to be the main mechanism for small solutes and nutrients such as glucose and oxygen crossing the capillary barrier in general [103]. This has been assumed specifically for hydrophilic molecules smaller than inulin [252], and generally for small molecules, either hydrophilic or lipophilic [86, 91]. Studies in myocardial capillaries have confirmed that small hydrophilic solutes diffuse through the aqua-filled pores [235], while theo-

retical calculations [265] indicate that for tissues other than liver diffusion dominates even for albumin. Generally, it has been stated that for most non-macromolecular solutes convective transport is negligible [86].

Transluminal filtration is the transport of fluid across the capillary wall due to the hydrostatic pressure gradient [252, 254]. The hydrostatic pressure in the capillary is larger than the pressure in the tissue, thus a tendency for an outward convective flow appears. This varying hydrostatic pressure gradient is closely coupled with an opposing osmotic pressure gradient and through this coupling convection occurs. Due to this volumetric flow, the solvent (plasma) "drags" part of a blood-contained solute, resulting in a solute convective flux that may be coupled with the diffusive one.

Ernest Starling is the man who defined, more than a hundred years ago, the forces underlying the convective microcirculatory exchange. In his classic work [350] he first proved the possibility of fluid reabsorption (in a small percentage of the different kinds of connective tissues that exist in the body) from blood vessels by performing experiments in whole body parts (dog limbs). He then argued that the osmotic pressure which the proteins in plasma exert is small but nevertheless comparable with the capillary hydrostatic pressure. Hence, it creates a tension for reabsorption that opposes filtration. The famous Starling's hypothesis followed : "...there must be a balance between the hydrostatic pressure of the blood in the capillaries and the osmotic attraction of the blood for the surrounding fluids" [350]. As it is correctly pointed out by Michel in his excellent review [227], the general notion that Starling suggested a conceptually "convenient" filtration from the arterial end of a capillary and an accompanying reabsorption at the venular end is a misconception. In fact Starling was skeptical about reabsorption in general : "...we have as yet no sufficient evidence that such fluids are absorbed by the blood vessels" [350].

A comprehensive study [227] of the complex phenomena involved indicates

that in tissues such as skin or muscle the only prolonged convective transport is a low level filtration, matched by an equivalent flow of lymph that prevents the formation of edema by sustaining a constant interstitial volume [180, 359]. Reabsorption from the tissue to the circulation is possible and may occur but only as a transient phenomenon. The contradiction to the preceeding observation that arises from the observed large "global" pressure differences might be relaxed by considering "local" variations of the hydrostatic pressure in the capillary and of the capillary permeability. Further calculations [227] reconcile the experimental data with a low filtration rate that occurs mostly through the interendothelial clefts where convection is in fact locally dominating. Another theoretical study [265] strongly suggests that reabsorption in tissues other than liver is minimal and that lymphatic flow arises predominantly from one-way filtration. Filtration is very high in tissues where it is functionally imperative such as the glomerulus [254] and the small intestine [359] but it has been found to be minimal in resting mammalian muscle [307, 359] and the same may be argued for skin. Even in the case of the transcapillary transport of macromolecules, a phenomenon that has been associated closely with filtration, there is some controversy about the predominant exchange mechanism. There are supporters of convective or vesicle transport [226] while there are even results indicating that the main mechanism responsible for the exchange of proteins such as albumin is diffusion [252].

Osmosis is a still incompletely understood [131, 150] phenomenon observed in membranes that restrict passage through them. Whenever miscible solutions of different concentration are separated by a barrier that is permeable to the solvent and partially or completely impermeable to the solute, a convective flux of the solvent occurs from the less concentrated to the more concentrated solution. Although this flux seemingly contradicts Fick's law, since its direction is towards the more concentrated phase, it can be explained in terms of equilibrium thermodynamics [102]. At chemical equilibrium between separate phases each substance should have an equal

value of its chemical potential in all phases between which this substance can freely pass. Only the solvent (plasma) can freely pass through the capillary while its solutes (serum proteins for the most part, as well as other macromolecules) are restricted. The system will try to approach chemical equilibrium by a flow from the phase with the bigger solvent mole fraction (smaller solute concentration) to the phase with the smaller solvent mole fraction (bigger solute concentration). Thus the osmotic flow contradicts filtration and is of vital importance for the restraining of the fluid components of blood inside the capillary [226].

Even though there is no actual hydraulic pressure, the driving force for osmosis is represented as a difference in osmotic pressure ($\Delta\pi$). Osmotic pressure may be regarded as a thermodynamic property of the solution like its freezing point [102]. If even a small fraction of the solute can permeate the barrier (in which case it is named "leaky" membrane) then this driving force is less and it has to be corrected by the osmotic reflection coefficient (Sec. 6.2.3).

The fluid flux J_{v} is thus the sum of the fluxes induced by the hydrostatic pressure differential (ΔP) and by the osmotic pressure differential ($\Delta\pi$), whereas the solute flux (J_{s}) is the sum of the diffusive flux and the flux resulting from the drag induced by the solvent [13, 252, 291]:

$$J_{\mathrm{v}} = L_{\mathrm{p}} S(\Delta P - \sum_{\mathrm{i}}^{\mathrm{k}} \sigma_{d,\mathrm{i}} \Delta\pi_{\mathrm{i}}) \tag{6.1}$$

$$J_{\mathrm{s}} = P_{\mathrm{cap/w}} S\Delta C + (1-\sigma_f) C_{\mathrm{av}} J_{\mathrm{v}} \tag{6.2}$$

The summation in the osmotic term indicates that if more than one restricted solutes are present their osmotic contributions need be added. Naturally, the major contributors in this term are the plasma proteins being large (thus severely restricted) and present in substantial concentrations. The term C_{av}, under certain conditions, represents the arithmetic mean of the concentrations on the two sides of the capillary. The

previous formalism is the most widely used and it is known as the Kedem-Katchalsky equations. These equations stem from non-equilibrium thermodynamics with phenomenological equations relating the occuring flows and forces in a membrane system. Their detailed derivation along with the underlying assumptions (e.g. dilute solution, ideal solution) can be found in a variety of sources [91, 93, 174]. Emphasis should be given to the fact that in the process of this derivation the use of Onsager's reciprocal relation provides additional relationships/restrictions between the phenomenological coefficients, combinations of which are the transport coefficients that appear in the equations. For example, in the general formalism C_{av} is the thermodynamic mean concentration and not the arithmetic one while the membrane permeability $P_{\mathrm{cap/w}}$ is concentration dependent.

A misconception associated with the Kedem-Katchalsky equations is that the two terms resulting in solute flow represent the diffusive and convective flow respectively. However these processes appear to be independent of each other, whereas in reality they are not. This lead to large errors in the analysis of ultrafiltration experiments where the second term of the equation was used to identify the convective part of solute flux [91]. In order to tackle this problem, another phenomenological approach was put forward where points just inside the membrane were taken into account. This approach, as described by Curry [91], yields the following equation for the "true" diffusive and convective components of solute flux :

$$\frac{J_{\mathrm{s}}}{S} = P_{\mathrm{cap/w}}(C_1 - C_2)\left\{\frac{\mathrm{Pe}}{\exp(\mathrm{Pe}) - 1}\right\} + (1 - \sigma_f)C_1\frac{J_{\mathrm{v}}}{S} \tag{6.3}$$

where Pe is the Peclet number and C_1 , C_2 are the concentrations just inside at outside of the membrane. When $\mathrm{Pe} \to 0$ then it reduces to the Kedem-Katchalsky equation. This description is more sound. However its derivation requires even more assumptions about the thermodynamic system in question. If one is interested only in the total solute flux across the capillary and not its components then the first

set of equations is a very good approximation [91]. The definitions of the transport coefficients used in these formulations follows.

6.2.3 Transport coefficients

The transport coefficients commonly used to quantify material exchange across the capillary wall may be categorized as diffusive, hydrodynamically convective, and osmotically convective in nature [13, 91, 225, 228, 247, 252, 256]:

- The (diffusional) permeability coefficient ($P_{\mathrm{cap/w}}$, cm/s) is solute-specific and is defined as the solute flow (J_{s}) (or flux for the physiologists) per unit area (A) per unit concentration difference (ΔC), under negligible volume flow conditions ($J_{\mathrm{v}} = 0$):

$$P_{\mathrm{cap/w}} = \left(\frac{J_{\mathrm{s}}}{A\Delta C}\right)_{J_{\mathrm{v}}=0} \tag{6.4}$$

- The hydraulic permeability (L_{p}, cm/s/mmHg)(*a.k.a.* hydraulic conductivity or filtration coefficient) is defined as the fluid (volumetric) flow through a unit area of the capillary wall per unit difference in hydrostatic pressure (ΔP) across the wall, under a negligible osmotic pressure differential ($\Delta\pi = 0$):

$$L_{\mathrm{p}} = \left(\frac{J_{\mathrm{v}}}{A\Delta P}\right)_{\Delta\pi=0} \tag{6.5}$$

  The reflection coefficient in general compares the ability of a solute to penetrate a barrier with that of the solvent. There are two types of coefficients used, depending on the driving force.

- The solvent drag reflection coefficient (σ_f, dimensionless) (*a.k.a.* ultrafiltration coefficient) is the fraction of the solute "reflected" (rejected) at the capillary wall

during ultrafiltration (as the solvent "drags" the solute through the barrier) in the absence of a concentration difference:

$$\sigma_f = \left(1 - \frac{J_s}{J_v C}\right)_{\Delta C=0} , \tag{6.6}$$

where C is an average intracapillary concentration.

- The osmotic reflection coefficient (σ_d, dimensionless) represents the fraction of the total osmotic pressure that the solute can exert across the wall and thus oppose filtration:

$$\sigma_d = \left(\frac{\Delta P}{\Delta \pi}\right)_{J_v=0} \tag{6.7}$$

This coefficient is independent of the filtration rate and depends on the properties of the wall and the size of the solute molecule. It ranges from 0 to 1, the former value describing a freely permeable capillary and the latter describing an ideal semipermeable barrier (no solute passage). It has been stated that if the membrane is homogeneous in nature and if the solvent resembles an ideal dilute solution, the two reflection coefficients (σ_f, σ_d) equal each other [247, 252].

Apart from the coefficients above, the product of the capillary permeability with the capillary exchange surface ($P_{\mathrm{cap/w}}\mathrm{S}$) is widely used since it is more easily deduced from experimental measurements. This product is named capillary diffusion capacity [85]. The analogous product of the hydraulic permeability with the exchange surface ($L_{\mathrm{p}}\mathrm{S}$) is called hydraulic conductance or capillary filtration coefficient (CFC).

6.2.4 Experimental data

The two main paths of experimental research involve whole-organ and single-capillary studies [85, 127]. In almost all of their variations, a single solute or a mixture of solutes

is introduced into the perfusate of either the entire organ or a specific capillary, and changes in the tissue or in the perfusate composition are monitored during passage [86]. Both approaches can provide only crude information and may be considered supplemental to each other. One should bear in mind that the transport coefficients reported are not direct, bullet-proof measurements, they are merely estimates. Apart from the obvious possibility of misrepresentation of the actual (*in vivo*) processes in intact subjects due to the nature of the experiments [103, 211], the extraction of these coefficients from directly measured quantities involves important assumptions about, and even modeling of, the capillary architecture and population, their true (perfused) exchange surface area, the actual concentration gradient across their wall etc.

Data on skin capillary permeability are scarce. Most of the available data refer to organs such as skeletal muscle, heart, lung, brain, mesentery, and in "combinations" of organs (animal hindlimbs, human forearms etc.). Values reported about skeletal muscle depend heavily of whether it is on a relaxed or exercised state [85, 103, 252]. Numerous studies have shown that brain capillaries are a specialized form that can be considered a category of their own [252, 256]. The lung, heart and mesentery capillaries have quite different architecture as well as flow and surrounding tissue characteristics [256]. One might consider heart as the next best thing in the absence of substantial skin data even though there are differences such as the half intercapillary distance [86, 250] that reflect to a greater total exchange surface area.

The following tables contain selected values of the transport coefficients from the literature. Even though there are values of the exchange surface area in various organs, values of the diffusional and hydraulic permeability were not extracted from the reported products $P_{\mathrm{cap/w}}\mathrm{S}$ and $L_{\mathrm{p}}\mathrm{S}$ since in almost all cases they were obtained from different animals and with different techniques.

After reviewing a plethora of experimental data for various solutes, species, and

$P_{cap/w}$(x 10^5 cm/sec)	Subject	Organ	Solute	Source
0.56[a]	rabbit	skin	Co-B12[b]	[251]
0.88[a]	rabbit	skin	Cr-EDTA[c]	[250]
9.3	rat	testis	Cr-EDTA	[61]
4.3	rat	testis	Co-B12	[61]
22	frog	mesentery	antipyrine	[91]
38	frog	mesentery	aminopyrine	[91]
1.24[d]	dog	heart	sucrose	[252][e]
0.36	dog	heart	inulin	[252][e]
1.08	dog	heart	Cr-EDTA	[252][e]

Table 6.1: Capillary (diffusional) permeability coefficient; [a] assumed total capillary exchange surface area 70 cm^2/g tissue (same as resting skeletal muscle), [b]vitamin, [c] Cr-ethylene-diamine-tetra-acetate, [d] average of three independent measurements, [e] reported from other source.

$P_{cap/w}$S(ml/min/g tissue)	Subject	Organ	Solute	Source
0.023	rabbit	skin	Co-B12	[251]
0.037	rabbit	skin	Cr-EDTA	[250]
0.037 ± 0.001	rat	hindquarters	B12	[140]
0.0701 ± 0.0063	rat	hindquarters	Cr-EDTA	[293]
$1.8 - 3.5$	rat	heart	MIBG[a]	[101]
2.23 ± 0.24	rat	testis	Na	[61]
15	rat	heart	quinidine	[235]
1.06	rabbit	heart	Cr-EDTA	[61][b]
5.35	rat	heart	Cr-EDTA	[61][b]
$0.68 * 10^{-4}$[c]	rat	skin	albumin	[226][b]

Table 6.2: Capillary diffusion capacity; [a] metaiodobenzylguanidine, [b] reported from other source, [c] average of two values.

organs, two major researchers of the field [86] concluded that the capillary permeability is $\sim 10^{-5}$ cm/s for organs other than brain. The data shown above agree with this conclusion for small- to medium-size hydrophilic molecules that most likely use the interendothelial clefts for their passage. It appears to be a valid order-of-magnitude estimate for such molecules traversing the dermal capillaries of human skin. As for small lipophilic solutes, it is reasonable to assume that they mostly choose a path through the endothelial cells. Most likely, the two-lipid-bilayer cell membrane does not constitute a significant permeability barrier, and it has been postulated that the

S(cm^2/g tissue)	Subject	Organ	Source
93.9 ± 5.9	human	sk. muscle (foot)	[74]
83.8 ± 5.4	human	sk. muscle (hand)	[74]
575	rat	heart	[86][a]
560	dog	heart	[291][a]
500		heart	[256][a]
600	rat	heart	[61][a]
70	rat	sk. muscle	[61][a]
27	rat	testis	[61][a]
100	human		[86][b]

Table 6.3: Capillary (inter-organ) exchange surface area; [a] reported from other source, [b] average value assumed for the whole human body.

L_pS (ml/min/mmHg/100ml tissue)	Subject	Organ	Source
~ 0.03	animal	skin	[211][a]
0.05	human	forearm (resting)[b]	[211]
$0.004 - 0.009$[c]	human	forearm (resting)	[211][a]

Table 6.4: Capillary filtration coefficient; [a] reported from other sources, [b] 70 % muscle, 30 % fat and skin, [c] range of five independent measurements.

clearance mechanism in that case is blood flow limited [171].

As far as macromolecules are concerned, experiments in rats with albumin as the test solute showed that its permeability in different organs differs 10-fold. The lowest was found in skin and muscle [271] with the heart/skin permeability ratio being 5 : 1. The range for most of the *in vivo* capillary permeability estimates for a macromolecule like serum albumin is $0.5\ 10^{-8} - 5\ 10^{-8}$ [226].

The data above indicate that $O(100)$ cm^2/g is a reasonable approximation for the capillary exchange surface area of skin. However, one must not forget the problems associated with the heterogeneity of the capillary distribution and capillary recruitment (Sec. 2.7.4). This figure should be regarded as an order-of-magnitude estimate of the average capillary density.

There are also direct values of the hydraulic permeability reported. These

σ_d	Subject	Organ	Solute	Source
0.066	rat	hindquarters	glucose	[293]
0.083	rat	hindquarters	sucrose	[293]
0.05	rat	hindquarters	urea	[293]
0.054	rat	hindquarters	NaCl	[293]
0.15	rat	hindquarters	B12	[293]
0.39	rat	hindquarters	inulin	[293]
0.87	rat	hindquarters	albumin	[293]
0.1^a	rabbit	heart	urea	[252][b]
~ 0.2	rabbit	heart	sucrose	[252][b]
$\sim 0.43^c$	rabbit	heart	inulin	[252][b]

Table 6.5: Osmotic reflection coefficients; [a] average of three independent measurements, [b] reported from other source, [c] average of five independent measurements.

are (after readjusting the units) : 1.15 10^{-7} cm/s/mmHg (heart, [291]) and 10^{-7} cm/s/mm Hg (rat skeletal muscle, average of three, reported from other source, [103]). Generally, lower L_{p} values are correlated with the continuous type capillary while higher values are associated with the fenestrated type [103]. Also, a theoretical result approximately applicable to non-liver tissue in the body predicts that the drag coefficient (σ_f) for albumin is 0.9 [265].

Even though the above data may be considered as estimates of the transport coefficients obtained by experiments on diverse organs with different techniques, one is tempted to compare them in order to draw conclusions about the quantitative importance of diffusion versus convection in skin capillaries.

A simple inspection reveals that the two measured values of the hydraulic permeability in heart and skeletal muscle are $O(10^{-7})$ cm/s/mmHg [103, 291] while the diffusional capillary permeability is $O(10^{-5})$ cm/s or greater in a variety of organs as shown in Table 1. In keeping that at normal tissue hydration states a total (hydrostatic and osmotic) pressure gradient of $O(1)$ mmHg is expected [358], and that the concentration terms (C_{av} and ΔC) will be of the same order of magnitude, one may

conclude by inspecting Eq. (6.2) that the diffusional (first) term will be greater than the convective (second) one.

Furthermore, one might attempt to input some relatively compatible data from various sources into Eq. (6.2). For a relatively small- to medium-size molecule such as vitamin B12 (MW 1354) one has $P_{\mathrm{cap/w}}S = 2.3\ 10^{-2}$ ml/min/g of rabbit skin [251] while a value of 0.03 ml/min/mmHg/100ml of animal skin tissue has been reported for $L_{\mathrm{p}}S$ [211]. Assuming that skin tissue has an average density of 1 g/cm^3 it is $L_{\mathrm{p}}S = 3\ 10^{-4}$ ml/min/mmHg/g. The drag coefficient for B12 may be taken to be equal to the osmotic reflection coefficient in rat hindquarters ($\sigma_f = 0.15$) and the total osmotic pressure gradient may be considered to be the result of a single (albumin) species in serum. The mean osmotic pressure in plasma is 24 mmHg, and measurements at different points of mammalian capillaries performed by Landis showed that an average hydrostatic capillary pressure of 21 is a reasonable assumption [227]. Osmotic pressure in skin interstitium is $\sim$ 10 mmHg while its hydrostatic pressure may be assumed to equal to the one measured in subcutaneous tissue (-2 mmHg) [227]. Assuming that that B12 is introduced in the vicinity of the capillary bed with a constant concentration of 0.01 μmol/cm^3 and that its concentration is negligible inside the capillary, the total solute flow calculated by Eq. (6.2) is: $J_{\mathrm{s}} = 2.3\ 10^{-4} + 1.38\ 10^{-5}$ μmol/min/g tissue. By assuming further that diffusion and convection occur independently of each other, the first term representing the diffusional flow is an order of magnitude greater than the second representing convection.

6.2.5 Permeability gradient

The concept of a permeability gradient along the capillary, and possibly along its proceeding and preceeding vessels, has been put forward by various researchers. There are solid geometrical, structural, and experimental arguments that support this con-

cept.

There is extensive evidence [52, 65, 149, 313] that the descending (venular) part of the capillary loop is wider than the ascending one both internally and externally. The capillary surface available for exchange is thus greater.

Apart from the geometry of the capillary loop, there is also structural evidence of a higher permeability at the venular segment. The descending limb characteristics change steeply at the border where the loop exits the papilla. The basement membrane becomes multilayered in contrast to the homogeneous one observed in the ascending and the intrapapillary portion [50, 52, 149], something that might reflect differences in permeability [149, 313]. Furthermore, the population of the plasmalemmal vesicles is higher on the capillary endothelial cells (900 vesicles / μm^2 compared to 200 vesicles / μm^2 in arterioles) with the maximum being observed in the venular (descending) segments of the capillary (1200 vesicles / μm^2). The distribution of the temporary transendothelial channels that they often form is 60% in the descending segment, 30% in the rest of the capillary loop, and the rest in the arterioles and venules [253].

Experiments performed with dyes and transversing proteins showed that the amount that leaks from the circulation to tissue increases progressively along the microvessels and is maximum at the venular end of the capillary [86, 252, 307, 313]. In a very influential study [307] an invariable to blood flow changes gradient along the whole microcirculatory path (arterioles-capillaries-postcapillary venules) was visualized in skeletal muscle with dyes of different diffusibility. According to these findings, the gradient first becomes effective along the arterioles. It then trends almost vertically upward with the transition to the capillaries, where it keeps mounting steeply until the transition to the venules. From there on, permeability declines gradually. The authors suggested a functional explanation for this gradient. They hypothesized

that the gradient's existence offsets the progressive loss of the blood-carried nutrients, the result being an even serving of the surrounding tissue. They did stress, however, that by incorporating the vast available exchange surface area of the capillaries into the picture, one may conclude that capillaries are the predominant exchange vessels. Measurements of the hydraulic permeability at different positions along the capillary length of rat intestinal muscle revealed a steep gradient that increased from the arterial to the venular end [127]. The same observation was made in frog mesentery capillaries where L_p increased nearly an order of magnitude greater [225].

Even though the existence of a capillary permeability gradient may be considered established, substantial quantitative information is lacking about the permeability "distribution" along the length of a capillary. An assumption of a constant "average" permeability may be regarded as a valid choice.

6.3 Transport through the pericapillary interstitium

While it is safe to consider diffusion, due to the lack of substantial bulk flow, as the dominant transport mechanism in the whole skin, the same does not hold true in the vicinity of the capillary bed in papillary dermis. The existing filtration out of the capillary and the documented localized connection of the filtrate with the initial lymphatics of the dermis indicate that convection through the interstitium and its importance with respect to diffusion needs to be examined.

As the understanding of the *in vivo* interstitial architecture became clearer over the years, the modeling of the extravascular space advanced. Initially, the interstitium was regarded as a well-stirred, fluid-filled compartment [162]. The next step was to consider it as a homogeneous porous medium [9, 116] with the low-Reynolds number fluid flow in the pores obeying Darcy's law :

$$v = -K_t \nabla P \tag{6.8}$$

where v is the velocity vector, P is the tissue hydrostatic pressure, and K_t is the hydrodynamic conductivity of the tissue. On the same path, Salathe [315] stated that interstitium is a two-phase system (with a paucity of interstitial fluid under normal conditions), the fluid being distributed in thin layers of less than 1 μm in thickness, thus justifying the porous medium approach.

The realization of the ground substance's significance in transport triggered new theories. In an eye-opening work, Day [97] used an enzyme that degrades hyaluronic acid and observed flow through connective tissue (fascia) membranes of mice. He demonstrated that the resistance to flow cannot be attributed only to cells and collagen, and he postulated the existence of another permanent structure between the collagen fibers that acts as a macromolecular sieve. He also documented that the degradation of hyaluronic acid leads to a largely increased flow rate. Further experiments with ground substance components illustrated their entanglement in physiologic concentrations and the severe restriction of transport through them [76]. Ogston et al. [244] provided a theoretical basis by interpreting experimental data in terms of diffusion through a uniform random distribution of long molecular fibers. Furthermore, Levick [202] argued through calculations that the extremely high resistivity to flow could be explained by the combined effects of collagen, glygosaminoglycans and proteoglycan core proteins (Chap. 2). It has also been experimentally documented that not all of the extravascular dermal space is accessible to traversing substances. This statement holds true especially for macromolecules such as albumin (volume excluded as high as two thirds of the total) [19, 218, 286, 392]. It stems from the general principle of volume exclusion, which simply states that two objects cannot occupy the same space at the same time. Another reason for exclusion might be the overall negative charge of the extracellular matrix, which may result in electrostatic repulsion of charged polyanions such as albumin [86].

In view of these findings and of other experiments showing injected dyes being transported through the pericapillary interstitium, both rapidly in fine filaments and slowly in a uniform spreading, Wiederhielm [390] put forward the two-phase theory. According to this, there is a three-dimensional mesh work (colloid-rich, gel-like) of glycosaminoglycan complexes and of the basement membrane that excludes bulk flow and transport of proteins. Smaller molecules may diffuse through it at a reduced rate. There is also a continuous free-fluid phase that connects the capillary with the initial lymphatics, which may take the form of vesicles/pathways through which bulk flow occurs at rates higher than diffusion. Silberberg [332] went even further arguing that the fluid channels between the heterogeneously distributed ground substance "should be looked upon as established facts" not only on the basis of experiments but also because it makes the filling of the lymphatics mechanism much more understandable.

In another important modeling attempt [384], the authors refer to the growing experimental support of a two-phase structure for interstitium and consider it to consist of two compartments/phases. Material enters from the blood capillary into only the "free phase" which they regard to be small under normal conditions (having a volume fraction of 0.1 in their calculations). The material exits this compartment through the lymphatics while there is restricted diffusion of the solutes between the gel phase and the free phase. The two compartments are considered well mixed except in the blood-lymph direction in the free-phase compartment. The fitting of plasma-lymph transport data to this model suggested that the interstitial space shows some characteristics of a chromatographic column, with the larger molecules equilibrating in tissue faster than the smaller ones due to their confinement in the fluid phase.

To further complicate things, experimental data and modeling thereof show that part of skin's hyaluronan (25 %), which is arguably the most important barrier to convective flow in interstitium, is drained into lymph [19]. This puts the whole concept

of a static ground substance in question. Moreover, in an excellent review [19] the authors cite experimental findings about the *in vivo* architecture of tissue and about plasma-to-lymph passage time variations that show "a remarkably high degree of inhomogeneity in the interstitium", which contradicts the two clearly-defined-phases model.

6.4 Capillary blood flow pattern

The specifications of blood flow in the capillary plexus were not extensively reviewed since this was not required by the level of detail of the capillary exchange model on this particular aspect. However, it is worthwhile to briefly discuss this issue in addition to the information provided in Chap. 2. Capillary flow may be described as an intermittent, irregular flow of a non-Newtonian fluid (blood) through semi-deformable bent tubes (capillaries) whose dimensions are comparable with the dimensions of the cells carried by plasma (resulting in a piston-like effect). The flow is not pulsatile under normal conditions, but the changes in blood flow are abrupt and substantial, mostly due to the transient "plugging" of the loops by cells [313]. A factor inducing blood flow changes in a given capillary loop is also the existence of anastomoses (shunt pathways) which offer alternative routes to blood; it is believed that they regulate flow so that the pressure in the capillary bed is homogeneous besides the fact that it receives blood from many different arterial segments [313].

Detailed modeling analyses are available from a variety of sources [68, 129, 207, 343, 344]. Most of the models deal with particle (two-phase) creeping flow. Plasma is considered to be a Newtonian fluid that flows between deformable, biconcave, axisymmetric disks (erythrocytes) traveling across the capillary in single file. Less detailed descriptions of capillary flow [96, 180] assume that blood comprises only plasma and that the flow follows Poiseuille's law, a law first derived to describe the

flow in small-diameter tubes. Since in our model blood flow enters only through the blood velocity, it is assumed that the flow is piston-like (plug flow). Thus, the velocity is the same at every point of any capillary cross-section. The value of the velocity for a given cross-section may be regarded as the average of the respective Poiseuillian (parabolic) velocity.

6.5 Review of capillary exchange models

Krogh [183, 184] set the foundations for capillary network modeling. He performed experiments in mammalian muscle and observed that capillaries "are distributed with conspicuous regularity among the muscle fibers." This lead him to what was later known as the Krogh cylinder: Capillaries are assumed to be straight, parallel, identical cylinders that are evenly spaced. Consequently, if one isolates a polygonal tissue surface that surrounds a capillary and that is placed midway from the adjacent capillaries, then this surface will be symmetric. Due to this symmetry, no concentration gradient exists across the surface and there is no net flux; the surface acts as if it were impermeable. It thus suffices to concentrate on a single capillary and its surrounding tissue (unit cell) that can be thought of approximately as a cylinder, and expand the results to the whole organ or body by using the capillary density. Many of the subsequent modeling approaches are extensions of Krogh's work [26, 192, 205, 278, 304, 362, 393].

During the 1960s and early 1970s, many different, more complex alternatives surfaced, almost exclusively dealing with oxygen transport across capillaries. These include a spherical unit cell with the capillary network being a uniform surface layer of well stirred blood [62], parallel "Krogh surfaces" with countercurrent flow that supply cone-like [105], or more general curvilinear [289] regions instead of cylinders, a rectangular capillary mesh which shapes the edges of a rectangular tissue volume

[223], a geometrically symmetric unit cell with asymmetric inlets/outlets of blood (random branching without including the branches in the unit cell) [130] and a pair of capillaries where one acts as a source and the other as a sink [154]. These models are more extensively described in the very good reviews of Fletcher [118] and Popel [274].

Other noteworthy capillary models have also been published: Johnson and Wilson [162] assumed that the exchange is barrier-limited and took the axial tissue diffusivity to be infinite, allowing for rapid equilibration and thus resulting in a uniform tissue concentration. Bassingthwaighighte et al. [26] developed a more generic Krogh cylinder for heart capillaries. The interstitial tissue was considered to be anisotropic, the blood flow was time-dependent and axial diffusion was allowed in the capillary while the capillary permeability varied with length. Chang [66] came up with a steady state model that lies between the "capillary network" and "wall permeability" approaches. He used pore theory to get transport coefficients such as capillary permeability and hydraulic conductivity, and he calculated the volume (with Starling hypothesis [350]) and solute fluxes across the capillary through mass balances for plasma, proteins, solute and hematocrit. Hsu & Secomb [153] included capillary interactions by studying the steady state oxygen transport/consumption in an arbitrary network of microvessels in a big cuboidal tissue volume . Assuming zero flux across the cell boundaries, they represented the capillary as a collection of unit sources distributed on the surface of the capillary wall and solved with a Green's function method for simple geometries. Kuo et al. [192] examined the effects of radial diffusion in the tissue by using an extension of Krogh's cylinder that had permeable unit cell walls and an infinite sink beyond these walls. They established a criterion defining the conditions under which the tissue that surrounds a given capillary can be thought of as infinite. Landahl [196] used two previously reported models - one with uniform tissue concentration [162] and another in which no axial mixing in the

tissue was allowed - and derived approximate, yet analytical solutions. Levitt [204] departed from the rest by examining an approximately random network with respect to a central capillary. He assumed infinite capillary permeability, strong interactions with neighboring capillaries, and weak interactions with the ones further away. The originality of the model lay in the unit cell boundary condition where "complicated variations in concentration in the region of the neighboring capillaries can be replaced by a uniform average concentration which has a time variation similar to the average of the whole tissue region." Titcombe and Ward [362] studied steady state oxygen transport in skeletal muscle. They regarded a 2D arbitrarily-shaped slice of muscle that included a number of capillaries of arbitrary cross sections as their unit cell, then examined diffusion, facilitated diffusion and consumption. Their model, too, implements the Krogh assumption of impermeable cell walls. They used a spatially distributed effective tissue diffusivity (Gaussian distribution) and arrived at an asymptotic solution of the problem through perturbation theory, while criticizing the point-sink solutions as inaccurate. Weiss & Roberts [386] constructed a fundamentally different, stochastic model. They considered a random capillary network and derived equations about the density functions that reflect the random transit times of a molecule that can or cannot diffuse across the capillary wall. Their model included protein binding and quasi-steady capillary exchange. Using experimental results for the transport of lidocaine in the rat hindlimb, they concluded that most of the solutes' dispersion is due to mixing by the capillary network and that the effective tissue diffusivity is very small, probably due to protein binding.

The following tables give the distinctive features of 25 vascular exchange models in a comparative way. Some general remarks that can be made are:

- Blank spaces correspond to either a non-applicable or an unspecified assumption.
- All the models except one ([26]) have assumed steady blood flow, either piston-

like or parabolic in nature.

- Most models have solute enter in the unit cell through blood (capillaries considered sources, not sinks).
- Many of the non-steady state models have some kind of a quasi-steady state assumption, with the most popular one being a quasi-steady exchange due to a very thin capillary wall.
- Some models consider plasma to be the only constituent of blood.
- Models [108], [285] and [399] are compartmental.
- Most of the models assume that the concentration of a solute and/or the flux of a solvent is constant around the perimeter of a given capillary cross section.
- Some of the models either refer to, or have used parameters of specific species / organs / solutes: [26] (cat-rat)/heart, [66] (rat-dog)/(muscle-mesentery-glomerulus), [108] rat/(many organs)/gadoteridol, [117] rat/kidney/sucrose, [141] dog/lung/urea, [153] O_2, [162] mammalian/heart/sucrose, [203] rabbit/knee, [205] muscle-liver, [285] rat/(muscle-skin)/albumin, [304] lung/tracer, [362] skeletal muscle/O_2 , [386] rat/(skin-muscle-fat) /lidocaine, [391] man/bladder/mitomycin C, [393] dog/bone/tracer, [399] man/protein.

6.5.1 "Capillary wall" models

Apart from the aforementioned capillary network modeling attempts, there has been substantial scientific research that has exclusively focused on the microscopic permeability properties of the capillary wall [3, 12, 41, 92, 107, 109, 121, 122, 123, 163, 255, 263, 264, 369, 371, 385]. These "capillary wall" models examine transport between and/or through the capillary endothelial cells in order to determine one or more

Model	[18]	[26]	[25]	[66]	[108]	[117]	[128]	[141]	[153]	[162]	[192]	[196]	[203]
Steady state	X	X	X	√	X	X	X	X	√	X	X	X	√
Spatial dimensions	2	2	2	1		1	1	2	3	1	1	1	2
Single cap.model	√	√	√	√			√	√	X	√	√	√	√
Cap. interactions		X	X	X			X	X	√	X	X		X
Filtration	√	X	X	√	√	√	X	X	X	X	√	X	√
Well mixed blood	X	√	√	√	√		√	√	√	√	√		
Axial diff. in cap.	X	√	√	X			X	X	X	X	X	X	X
Homog. tissue	√	X	√	√	√	X	√	√	√	√	√	√	√
Tissue distr. vol.	X	√	√	X	X	√	X	X	X	√	X	√	√
Tissue Convection	√	X	X	X		√	X	X	X		X		√
Lymph flow	√	X	X	X	X	√	X	X	X	X	X	X	X
Protein binding	X	X	X	X	X	X	X	X	X	X	X	X	X
Consumption	X	X	√	X	X	X	X	X	√	X	X	X	X
Backdiffusion	X	X	√	X	X	X	√	X	X		X		X
Cell 0 flux BC		√	√			√		√	√		X		√
Straight capillary	√	√	√	√			√	√	X	√	√	√	√
Const. cap. length	X	√	√	√			√		X	√	√	√	√
Const. cap. radius	X	√	√	√			√		√	√	√	√	√
Constant PS	√	X	√	√	√		√	√		√	√		X

Table 6.6: Comparison of capillary exchange models A

of the capillary diffusional and/or convective transport coefficients. In a way, they represent attempts to reconcile the qualitative ultrastructure with the quantitative function [225] (Sec. 6.2). Even though the level of detail is far greater than that in the present work, these models attack the same problem from a different perspective. A brief review is useful in understanding the processes that go on in a blood-tissue exchange unit.

One can distinguish two fundamentally different approaches to the problem; pore theory and fiber matrix theory. Pappenheimer et al. [255] set the foundations for the former by postulating a resemblance between the microvascular barrier and an artificial porous membrane "pierced with numerous ultramicroscopic openings". Thus, identical water-filled circular cylindrical pores that allow diffusive and convective (filtration) passage of molecules between a well-mixed plasma and a well-mixed tissue were hypothesized, and the (equivalent) pore radius was picked in order to make the theory compatible with experimental permeability measurements. Kedem & Katchalsky [175] substantially improved the theory by introducing a less idealized barrier that was characterized with an additional (reflection) coefficient, as this was

Model	[204]	[205]	[274]	[278]	[285]	[304]	[?]	[362]	[386]	[391]	[393]	[399]
Steady state	X	X	√	X	X	X	√	√	X	√	X	X
Spatial dimensions	2	1	3	1		1	2	2	1	1	1	
Single cap.model	X	√	√	√		√	√	X	X		√	
Cap. interactions	√	X	√	X		X		√	√		X	
Filtration	X	X	X	X	√	X	√	X	X	X	X	√
Well mixed blood	X	√	√	√	√	X	√		√		√	√
Axial diff. in cap.	X	X	X	√		X	X		X		X	
Homogeneous tissue	√	√	X	√	√	X	√	X	X	√	X	√
Tissue distr.vol.	X	X	X	√	√	√	X	X	√	X	√	√
Tissue Convection	X	X	X	X	√	X	√	X	X	X	X	
Lymph flow	X	X	X	X	√	X	X	X	X	X	X	√
Protein binding	X	X	√	√	X	X	X	√	√	X	X	X
Consumption	X	X	√	√	X	X	X	√	X	X	X	X
Backdiffusion	X	X	X	√	X	X	X	X	X		√	X
Cell 0 flux BC	X	√	√	√		√	√	√	√		√	
Straight capillary	X	√	√	√		√	√	√			√	
Const. cap. length	√	√	√	√		√	√				√	
Const. cap. radius	√	√	√	√		X	X	X			√	
Constant PS	∞	√		X	√	√	X	X			√	√

Table 6.7: Comparison of capillary exchange models B

defined by Staverman [351]. More recent models advanced by considering pores of two [48, 290] or multiple [41] different radii, or to even have a continuous distribution of their radii instead of discrete values [163]. Others regarded pores to be the interendothelial clefts and modeled them as rectangular, constricted ducts with [122, 123, 385] or without [263, 371] a fiber matrix area inside them.

An alternative fiber matrix theory suggests that the capillary exchange takes place in a region consisting of a random array of cylindrical fibers surrounded by water [252], this region being either inside or between the endothelial cells [92]. Though more mathematically cumbersome, this method gained interest, due largely to the inability of pore theory to reproduce a wide range of experimental results and in certain cases because it represented more accurately the physiological reality [107, 109].

Besides the capillary-specific "wall models", one can also turn to the vast literature on membrane permeability in order to comprehend vascular exchange on a microscopic level since a "membrane is any barrier separating two bulk phases which is permeable to one species in the bulk phases and which also distinguishes between

the several species by their respective rates of transport through that barrier" [131]. Various researchers have analyzed different parts of the issue, such as steric exclusion [14, 243, 244, 346], hydrodynamics [54, 94, 156, 206], osmosis [150], electrostatic interactions [39, 161] etc. The interested reader is directed to the good reviews of Amsden [7] and Deen [99]

6.6 Discussion

The complex nature of the capillary exchange process in the dermis is obviously not completely defined. However, the collection of experimental and theoretical work cited here allows for important aspects of this process to be clarified. The framework upon which the capillary model of the next chapter was built becomes apparent by summarizing the preceeding passages.

The permeation of the capillary wall can be considered as a passive process depending on gradients of physical forces [103, 228, 291, 405], while it has been established that small and large molecules choose distinctly different paths both in the interstitium and through the capillary barrier [226, 256, 384, 390]. These different paths are part of the critical problem of the significance of convective transport (filtration - reabsorption - lymph removal) with respect to diffusion. It can be argued that in a tissue such as skin there is only a low-level filtration and an even lower (if any) reabsorption of fluid from tissue to blood [227, 265, 307, 359], with the filtrate being removed (at approximately the same rate by which it is produced [180, 359]) through the lymphatics. Diffusion is thus expected to be the dominant transport process for small molecules that do not bind appreciably to serum proteins [86, 91, 103, 252]. The situation is quite different for macromolecules or strongly bound substances since they will follow the route taken by serum proteins during their transcapillary passage, a passage of which the filtration - lymph removal is a major constituent [180, 326, 359].

In terms of modeling these phenomena, maximum accuracy and flexibility is attained with an always present diffusion and a selectively present convection (both in tissue and across the capillary wall) that can be "switched on and off" depending on the penetrating substance.

The *in vivo* tissue nature around the microcirculation is an incompletely understood piece of the puzzle. A valid first-approximation would be the porous medium approach (Darcy's law) [9, 116] (Chap. 5), even though reality is much more complex [19, 390], with the effective transport parameters encompassing this complexity in an averaging way. In fact, all transport parameters used in the modeling attempt can be nothing else but average values reflecting the fact that there are large fluctuations/deviations from "normal" behavior. This holds true for the perfused capillary density, blood velocity, diffusivity (in a very heterogeneous tissue), capillary permeability etc. On the same path of thinking, blood flow may be considered as a steady flow of since we are only interested in the average clearance rate to deeper, non-exchanging, blood vessels.

The review of the capillary exchange models revealed some remarkable attempts of the authors to grasp the *in vivo* reality and process it in a solvable mathematical format. However, Tables 6.6 and 6.7 indicate that most of these models assume a straight capillary tube with no interactions with adjacent capillaries. Thus, they fail to represent the physiological, three-dimensional, reality of the capillary loop with an ascending and a descending limb, interacting with other capillaries and thus altering the concentration profiles in the surrounding interstitial space. The importance of representing accurately the capillary geometry has been demonstrated by comparisons between the tissue concentration profiles generated by a loop model (for the renal medulla) and by a straight cylinder model [382]. The importance of the loop was evident to other researchers that modeled straight capillaries with countercurrent

flow. However this involved pairs of independent capillaries that had no connection with each other in terms of the concentration in blood. Moreover, the reduction of the dimensions of the problem may lead to erroneous results, as was demonstrated by another three-dimensional model of straight capillary tubes [31].

Chapter 7

A Geometrical Model of Dermal Capillary Exchange

7.1 Introduction

This chapter develops a capillary exchange model that is a substantial departure from Krogh's cylinder archetype [183], and its subsequent modified versions [26, 192, 205, 278, 304, 362, 393]. The three-dimensional, bent-cylinder geometry of the capillaries is accurately represented and mass transfer interactions among capillaries are explicitly accounted for through the imposition of periodic boundary conditions. The model considers both diffusive and convective transport mechanisms (the latter due to capillary leakage and the subsequently formed channels to lymphatic capillaries, Sec. 6.3). Partitioning phenomena both in the blood stream and in the interstitium, which depend on factors such as volume exclusion and binding to serum proteins, are incorporated in principle in the model through the use of the appropriate values of partition coefficients.

The model has the capability of predicting steady state concentration profiles in the interstitial microenvironment of the capillary plexus and variations in blood concentrations along the capillary loop. Thus, it is suitable to explore the topical pharmacological effect of a penetrating drug [215, 325]. It will be shown later in this

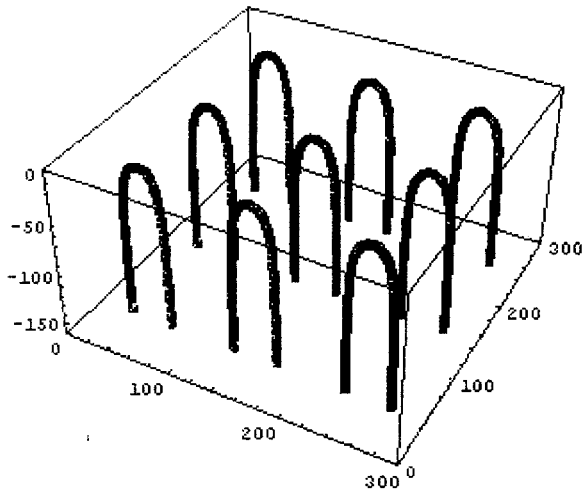

Figure 7.1: Doubly periodic capillary array. Dimensions in μ m

chapter that the model can also be readily utilized in conjuction with the simple, macroscopic, whole-skin approach (Chaps. 3 and 4) to predict the rate of microvascular clearance of a given permeating substance. The significance of such a predictive ability spans the fields of transdermal delivery [178, 341], sunscreens [34], prevention of chemical exposure [6, 219, 272], and protection from biological warfare [70, 71].

The capillary network and the surrounding dermal tissue are thought of as an infinite, two-dimensional, array of identical parallelepipedal unit cells (Fig. 7.1). Each unit cell includes a single capillary and the surrounding interstitium. The preceeding and proceeding parts of the vasculature are assumed to have a negligible permeability (i.e. to be non-exchanging vessels) that supply (arterioles) and accept (venules) the blood flow of the capillary. The steady state transport processes which a skin-penetrating substance undergoes in the interstitium are diffusion and convection generated by filtration. Material is assumed to be exchanged through the capillary wall by both diffusion and filtration at a constant rate, while the model has the ability of predicting possible diffusive reabsorption of substances from the tissue to blood. The blood flow is idealized as a plug flow which diminishes along the capillary loop

due to filtrative losses.

Through the following calculations plasma and interstitial concentration profiles are acquired. The dermal concentration is calculated through a slender body theory formulation. The corresponding equations are coupled with the equations derived from a mass balance that predicts the blood concentration inside the capillary. The model also predicts rates of clearances through the capillaries and changes of transdermal fluxes due to the clearance process.

7.2 Model formulation

7.2.1 Transport through the interstitium

The depth dimension (z) is considered infinite. There is a steady flux of material at $z \to +\infty$: $\frac{\partial C_{\mathrm{de}}(x,y,+\infty)}{\partial z} \to \alpha'$. As the material diffuses downwards it encounters the capillary plexus in a region that, as is demonstrated later, can be thought of as an absorbing zone. A certain amount of the material is absorbed into the capillary loops, in the blood stream, where it is convected from the capillary loop to the next, non-permeable parts of the microvasculature. The material remaining in the extravascular tissue continues to transverse the interstitial space (both by diffusion and convection due to filtration) with a different yet steady flux. The convective transport is characterized by a steady average "seepage" velocity $\vec{U}_{\mathrm{sp}}$. It is logical to assume that this velocity will have its maximum value just outside the capillary wall. It is also logical to assume that as $z \to -\infty$ the convective part of this flux would tend to be zero since it is a localized phenomenon in the space between the vascular and lymphatic capillaries. Thus, it would be $\frac{\partial C_{\mathrm{de}}(x,y,-\infty)}{\partial z} \to \alpha$, which means that the concentration will depend linearly on z : $C_{\mathrm{de}}(x,y,z) \simeq \alpha z + \beta$ asymptotically as $z \to -\infty$. A special case arises when the capillary network is absorbing the material

at the rate at which the material is supplied. In this situation, the flux below the capillary plexus ($z \to -\infty$) would be zero and the respective concentration would be constant.

Since the capillary array is considered periodic in the dimensions parallel to the skin's surface (x and y), periodic conditions apply at the boundaries of each unit cell ($0 : l_x$ and $0 : l_y$). These conditions reflect an equality of concentrations and fluxes on the two sides of the imaginary boundary that separates two adjacent unit cells. Due to the symmetry/periodicity of the problem, a net convective flux from one unit cell to another cannot exist, i.e. the streamlines that describe the fluid's motion are expected to "bend" as they approach the boundary. Thus the boundary conditions involve only diffusive fluxes. The complete mathematical formulation is :

$$\vec{\nabla} \cdot \left\{ -D_{\mathrm{de}} \vec{\nabla} C_{\mathrm{de}}(x,y,z) + \vec{U}_{\mathrm{sp}} C_{\mathrm{de}}(x,y,z) \right\} = 0 \qquad x \in (0,l_x)\,,\ y \in (0,l_y)\,,\ z \in (-\infty,\infty) \tag{7.1}$$

$$C_{\mathrm{de}}(0,y,z) = C_{\mathrm{de}}(l_x,y,z) \qquad y \in (0,l_y)\,,\ z \in (-\infty,\infty) \tag{7.2}$$

$$\frac{\partial C_{\mathrm{de}}(0,y,z)}{\partial x} = \frac{\partial C_{\mathrm{de}}(l_x,y,z)}{\partial x} \qquad y \in (0,l_y)\,,\ z \in (-\infty,\infty) \tag{7.3}$$

$$C_{\mathrm{de}}(x,0,z) = C_{\mathrm{de}}(x,l_y,z) \qquad x \in (0,l_x)\,, \qquad z \in (-\infty,\infty) \tag{7.4}$$

$$\frac{\partial C_{\mathrm{de}}(x,0,z)}{\partial y} = \frac{\partial C_{\mathrm{de}}(x,l_y,z)}{\partial y} \qquad x \in (0,l_x)\,, \qquad z \in (-\infty,\infty) \tag{7.5}$$

$$C_{\mathrm{de}}(x,y,z) \to \alpha z + \beta \qquad x \in (0,l_x)\,,\ y \in (0,l_y)\,,\ z \to -\infty \tag{7.6}$$

$$\frac{\partial C_{\mathrm{de}}(x,y,+\infty)}{\partial z} \to \alpha' \qquad x \in (0,l_x)\,,\ y \in (0,l_y)\,,\ z \to \infty \tag{7.7}$$

7.2.2 Transcapillary flux

We assume that the (homogeneous) capillary wall/membrane is of (constant) thickness h. Its side in contact with blood is denoted by i while its side in contact with the surrounding dermal tissue is denoted by k (Fig. 7.2). The partitioning equilibria

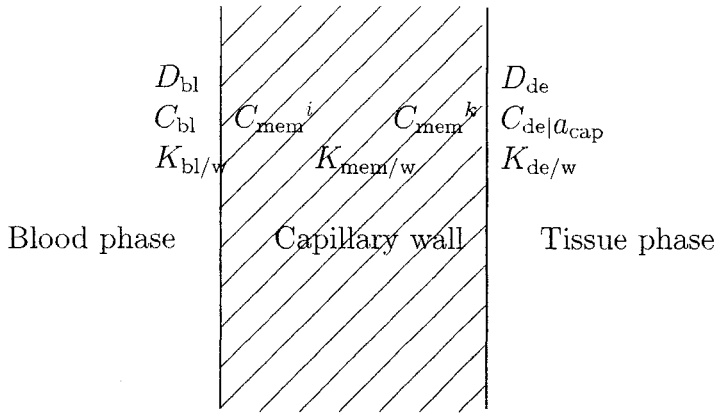

Figure 7.2: Definition sketch for the capillary membrane

between points just inside and outside of the membrane are expressed by the relations:

$$\frac{C_{mem}{}^{i}}{K_{mem/w}} = \frac{C_{bl}}{K_{bl/w}}, \tag{7.8}$$

$$\frac{C_{mem}{}^{k}}{K_{mem/w}} = \frac{C_{de|a_{cap}}}{K_{de/w}}, \tag{7.9}$$

where $K_{mem/w}$, $K_{bl/w}$, and $K_{de/w}$ are the partition coefficients of the solute in the capillary wall, blood and interstitial dermis, respectively, referred to bulk aqueous solution. The term $C_{de|a_{cap}}$ represents the dermal tissue concentration at the capillary (of radius a_{cap}) wall. Since the blood is considered to be well mixed over the capillary cross section, an analogous distinction is not necessary for the blood phase.

The total transcapillary flux (J_{cap}) is the sum of the diffusive flux and convective fluxes between the blood and tissue phases. By adopting the convention that it is positive in the direction from blood to tissue:

$$J_{cap} = D_{mem}\frac{C_{mem}{}^{i} - C_{mem}{}^{k}}{h} + U_{mem}\frac{C_{mem}{}^{i} + C_{mem}{}^{k}}{2} \tag{7.10}$$

where D_{mem} is the diffusion coefficient of the solute in the capillary membrane and

U_{mem} is the volume-averaged outward radial velocity through the capillary membrane. By applying the partitioning equations the preceeding expression becomes:

$$\begin{aligned} J_{\text{cap}} &= \frac{D_{\text{mem}}}{h}\left(\frac{C_{\text{bl}}}{K_{\text{bl/w}}}K_{\text{mem/w}} - \frac{C_{\text{de}|a_{\text{cap}}}}{K_{\text{de/w}}}K_{\text{mem/w}}\right) \\ &+ \frac{U_{\text{mem}}}{2}\left(\frac{C_{\text{bl}}}{K_{\text{bl/w}}}K_{\text{mem/w}} + \frac{C_{\text{de}|a_{\text{cap}}}}{K_{\text{de/w}}}K_{\text{mem/w}}\right) \Rightarrow \\ J_{\text{cap}} &= P_{\text{cap/w}}\left(\frac{C_{\text{bl}}}{K_{\text{bl/w}}} - \frac{C_{\text{de}|a_{\text{cap}}}}{K_{\text{de/w}}}\right) + \frac{U_{\text{mem}}K_{\text{mem/w}}}{2}\left(\frac{C_{\text{bl}}}{K_{\text{bl/w}}} + \frac{C_{\text{de}|a_{\text{cap}}}}{K_{\text{de/w}}}\right) \end{aligned} \quad (7.11)$$

with the (diffusive) capillary permeability coefficient being defined as:

$$P_{\text{cap/w}} = \frac{D_{\text{mem}}K_{\text{mem/w}}}{h} \quad (7.12)$$

This flux should be equal to the flux normal to the capillary wall that enters the tissue:

$$J_{\text{cap}} = (-D_{\text{de}}\vec{\nabla}C_{\text{de}|a_{\text{cap}}} + \vec{U}_{\text{sp}|a_{\text{cap}}}C_{\text{de}|a_{\text{cap}}}) \bullet \vec{n}_{\text{wall}} \quad (7.13)$$

where $\vec{n}_{\text{wall}}$ is the normal to the capillary surface outward unit vector and $\bullet$ symbolizes the dot product. It is assumed that in the vicinity of the capillary wall the seepage velocity ($\vec{U}_{\text{sp}|a_{\text{cap}}}$) will only have an (outward) radial component. Thus, the product $\vec{U}_{\text{sp}|a_{\text{cap}}} \bullet \vec{n}_{\text{wall}}$ will equal the magnitude of $\vec{U}_{\text{sp}|a_{\text{cap}}}$:

$$\begin{aligned} P_{\text{cap/w}}\left(\frac{C_{\text{bl}}}{K_{\text{bl/w}}} - \frac{C_{\text{de}|a_{\text{cap}}}}{K_{\text{de/w}}}\right) + \frac{U_{\text{mem}}K_{\text{mem/w}}}{2}\left(\frac{C_{\text{bl}}}{K_{\text{bl/w}}} + \frac{C_{\text{de}|a_{\text{cap}}}}{K_{\text{de/w}}}\right) &= \\ (-D_{\text{de}}\vec{\nabla}C_{\text{de}|a_{\text{cap}}}) \bullet \vec{n}_{\text{wall}} + U_{\text{sp}|a_{\text{cap}}}C_{\text{de}|a_{\text{cap}}} & \end{aligned} \quad (7.14)$$

Due to the asymmetry of the problem, the value of the dermal concentration on the capillary surface depends on the angle (θ) that determines the location of a particular point on the capillary wall perimeter. A representative concentration is

obtained through averaging over the perimeter of the capillary wall:

$$\int_0^{2\pi}\left[P_{\mathrm{cap/w}}\left(\frac{C_{\mathrm{bl}}}{K_{\mathrm{bl/w}}}-\frac{C_{\mathrm{de}|a_{\mathrm{cap}}}}{K_{\mathrm{de/w}}}\right)+\frac{U_{\mathrm{mem}}K_{\mathrm{mem/w}}}{2}\left(\frac{C_{\mathrm{bl}}}{K_{\mathrm{bl/w}}}+\frac{C_{\mathrm{de}|a_{\mathrm{cap}}}}{K_{\mathrm{de/w}}}\right)\right]d\theta \;=$$

$$\int_0^{2\pi}\left[(-D_{\mathrm{de}}\vec{\nabla}C_{\mathrm{de}|a_{\mathrm{cap}}})\bullet\vec{n}_{\mathrm{wall}}+U_{\mathrm{sp}|a_{\mathrm{cap}}}C_{\mathrm{de}|a_{\mathrm{cap}}}\right]d\theta \;\Rightarrow$$

$$P_{\mathrm{cap/w}}\left[\frac{C_{\mathrm{bl}}}{K_{\mathrm{bl/w}}}-\frac{\langle C_{\mathrm{de}|a_{\mathrm{cap}}}\rangle}{K_{\mathrm{de/w}}}\right]+\frac{U_{\mathrm{mem}}K_{\mathrm{mem/w}}}{2}\left[\frac{C_{\mathrm{bl}}}{K_{\mathrm{bl/w}}}+\frac{\langle C_{\mathrm{de}|a_{\mathrm{cap}}}\rangle}{K_{\mathrm{de/w}}}\right] \;=$$

$$-D_{\mathrm{de}}\langle\vec{\nabla}C_{\mathrm{de}|a_{\mathrm{cap}}}\bullet\vec{n}_{\mathrm{wall}}\rangle+U_{\mathrm{sp}|a_{\mathrm{cap}}}\langle C_{\mathrm{de}|a_{\mathrm{cap}}}\rangle \qquad (7.15)$$

with $\langle\rangle$ denoting the average around the capillary perimeter at a given position along its axis. The seepage velocity $U_{\mathrm{sp}|a_{\mathrm{cap}}}$ is by definition an averaged quantity and therefore does not have to be included in the averaging. Since U_{mem} and $U_{\mathrm{sp}|a_{\mathrm{cap}}}$ are the volume-averaged velocities inside the capillary wall and just outside the capillary wall, they have to be equal to each other:

$$U_{\mathrm{mem}} \;=\; U_{\mathrm{sp}|a_{\mathrm{cap}}} \qquad (7.16)$$

In the previous calculations and throughout this chapter, parameters such as the diffusional capillary permeability and the capillary radius are assumed to be constant along the capillary length. However, the model could easily be extended to treat the case of a varying radius and/or permeability.

7.2.3 Mass and volume balances inside the capillary

It is assumed that there is plug flow inside the capillary, with the blood velocity being reduced as blood flows through the capillary due to the bulk losses of filtration. Diffusion in blood is considered to be negligible with respect to convection. Consider a slice of the capillary (Fig. 7.3) being a straight cylinder of small length (dt). Blood is considered incompressible, so that a volume balance on this slice results in a

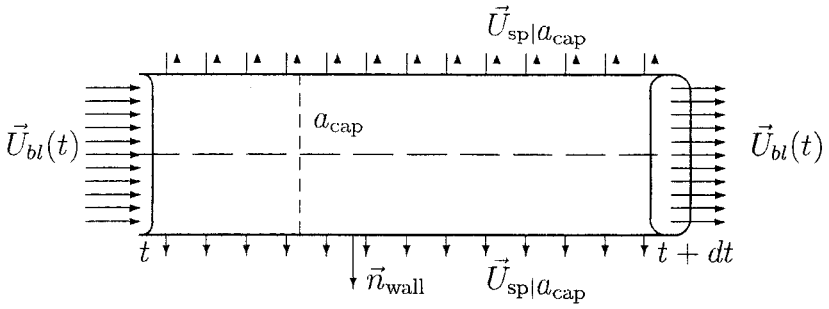

Figure 7.3: Definition sketch of a capillary slice

relationship between the (average) blood velocity (U_{bl}) and the (average) "filtration" velocity ($U_{\mathrm{sp}|a_{\mathrm{cap}}}$) by which blood leaks from the capillary:

$$\begin{aligned}
\pi {a_{\mathrm{cap}}}^2 U_{\mathrm{bl}|t} &= 2\pi a_{\mathrm{cap}} dt U_{\mathrm{sp}|a_{\mathrm{cap}}} + \pi {a_{\mathrm{cap}}}^2 U_{\mathrm{bl}|t+dt} \Rightarrow \\
\frac{dU_{\mathrm{bl}}}{dt} &= -\frac{2\pi a_{\mathrm{cap}} U_{\mathrm{sp}|a_{\mathrm{cap}}}}{\pi {a_{\mathrm{cap}}}^2} \Rightarrow \\
\frac{dU_{\mathrm{bl}}}{dt} &= -\frac{2U_{\mathrm{sp}|a_{\mathrm{cap}}}}{a_{\mathrm{cap}}} \qquad (7.17)
\end{aligned}$$

The net flux (diffusive - convective) of solute entering through the perimeter is $-J_{cap}$ thus the mass balance in this slice (with t being the length coordinate) is:

$$\begin{aligned}
\pi {a_{\mathrm{cap}}}^2 U_{\mathrm{bl}} C_{\mathrm{bl}|t} + \left[2\pi a_{\mathrm{cap}}(t + dt - t)\right](-J_{cap}) &= \pi {a_{\mathrm{cap}}}^2 U_{\mathrm{bl}} C_{\mathrm{bl}|t+dt} \Rightarrow \\
\pi {a_{\mathrm{cap}}}^2 U_{\mathrm{bl}} (C_{\mathrm{bl}|t+dt} - C_{\mathrm{bl}|t}) &= 2\pi a_{\mathrm{cap}}(dt)(-J_{cap}) \overset{dt\ll}{\Rightarrow} \\
\pi {a_{\mathrm{cap}}}^2 U_{\mathrm{bl}} \frac{dC_{\mathrm{bl}}}{dt} &= 2\pi a_{\mathrm{cap}}(-J_{cap}) \Rightarrow \\
\frac{a_{\mathrm{cap}} U_{\mathrm{bl}}}{2} \frac{dC_{\mathrm{bl}}}{dt} &= (-J_{cap}) \Rightarrow
\end{aligned}$$

$$\frac{a_{\mathrm{cap}} U_{\mathrm{bl}}}{2} \frac{dC_{\mathrm{bl}}}{dt} = P_{\mathrm{cap/w}} \left(\frac{\langle C_{\mathrm{de}|a_{\mathrm{cap}}} \rangle}{K_{\mathrm{de/w}}} - \frac{C_{\mathrm{bl}}}{K_{\mathrm{bl/w}}} \right)$$

$$- \frac{U_{\mathrm{sp}|a_{\mathrm{cap}}} K_{\mathrm{mem/w}}}{2} \left(\frac{\langle C_{\mathrm{de}|a_{\mathrm{cap}}} \rangle}{K_{\mathrm{de/w}}} + \frac{C_{\mathrm{bl}}}{K_{\mathrm{bl/w}}} \right) \tag{7.18}$$

$$\text{and} \quad \frac{a_{\mathrm{cap}} U_{\mathrm{bl}}}{2} \frac{dC_{\mathrm{bl}}}{dt} = D_{\mathrm{de}} \langle \vec{\nabla} C_{\mathrm{de}|a_{\mathrm{cap}}} \bullet \vec{n}_{\mathrm{wall}} \rangle - U_{\mathrm{sp}|a_{\mathrm{cap}}} \langle C_{\mathrm{de}|a_{\mathrm{cap}}} \rangle \tag{7.19}$$

Eqs. (7.1 - 7.7) and (7.17 - 7.19) provide the foundation for a solvable mathematical analysis.

7.2.4 Dimensionless formulation

All length figures become dimensionless with a characteristic length $L = 100$ μm (chosen as a round number having an order of magnitude between those of the capillary length and of the capillary radius). Once again, the dimensionless quantities are denoted with a ("$\hat{}$") affix. The dimensionless coordinates and capillary radius are thus

$$\hat{x} = x/L \; ; \; \hat{y} = y/L \; ; \; \hat{z} = z/L \; ; \quad \hat{a}_{\mathrm{cap}} = a_{\mathrm{cap}}/L \tag{7.20}$$

The dermal tissue diffusion coefficient is made dimensionless with a characteristic diffusivity of $D_{\mathrm{o}} = 10^{-7}$ cm^2/sec, stemming for the value obtained from the skin transport model for dermal penetration of salicylic acid (Chap. 4). Thus :

$$\hat{D}_{\mathrm{de}} = D_{\mathrm{de}}/D_{\mathrm{o}} \tag{7.21}$$

Blood velocity is made dimensionless with $U_{\mathrm{o}} = 0.01$ cm/sec which is the order of magnitude of a typically reported velocity of capillary blood flow [129]:

$$\hat{U}_{\mathrm{bl}} = U_{\mathrm{bl}}/U_{\mathrm{o}} \tag{7.22}$$

Finally, dimensionless concentrations are defined by:

$$\hat{C}_{\mathrm{a}} = C_{\mathrm{a}}/C_{\mathrm{o}} \quad , \quad \mathrm{a} = \text{"de" or "bl"} \tag{7.23}$$

where $C_o = 10^{-6}$ μmoles/cm^3 depicts a typical drug concentration in a transdermal application. The resulting dimensionless equations are :

- Interstitium

  By defining the vector $\vec{u}_{sp}$ as the unit vector pointing in the direction of $\vec{U}_{sp}$ Eq. (7.1) becomes:

$$\begin{aligned} \frac{1}{L}\hat{\vec{\nabla}} \cdot \left\{ -\hat{D}_{de} D_o \frac{1}{L}\hat{\vec{\nabla}} \left(\hat{C}_{de} C_o \right) + \vec{u}_{sp} U_{sp} \left(\hat{C}_{de} C_o \right) \right\} &= 0 \Rightarrow \\ \hat{\vec{\nabla}} \cdot \left\{ -\hat{D}_{de} \hat{\vec{\nabla}} \hat{C}_{de} + \frac{U_{sp} L}{D_o} \vec{u}_{sp} \hat{C}_{de} \right\} &= 0 \end{aligned} \tag{7.24}$$

  Also, by introducing a Peclet number for interstitial transport

$$Pe_{int} = \frac{U_{sp} L}{D_o}, \tag{7.25}$$

  the transport equation becomes:

$$\hat{\vec{\nabla}} \cdot \left\{ -\hat{D}_{de} \hat{\vec{\nabla}} \hat{C}_{de} + Pe_{int} \vec{u}_{sp} \hat{C}_{de} \right\} = 0 \tag{7.26}$$

  The corresponding dimensionless boundary conditions (Eqs. (7.2 - 7.7)) are:

$$\hat{C}_{de}(0, \hat{y}, \hat{z}) = \hat{C}_{de}(\hat{l_x}, \hat{y}, \hat{z}) \tag{7.27}$$

$$\frac{\partial \hat{C}_{de}(0, \hat{y}, \hat{z})}{\partial \hat{x}} = \frac{\partial \hat{C}_{de}(\hat{l_x}, \hat{y}, \hat{z})}{\partial \hat{x}} \tag{7.28}$$

$$\hat{C}_{de}(\hat{x}, 0, \hat{z}) = \hat{C}_{de}(\hat{x}, \hat{l_y}, \hat{z}) \tag{7.29}$$

$$\frac{\partial \hat{C}_{de}(\hat{x}, 0, \hat{z})}{\partial \hat{y}} = \frac{\partial C_{de}(\hat{x}, \hat{l_y}, \hat{z})}{\partial \hat{y}} \tag{7.30}$$

$$\hat{C}_{de}(\hat{x}, \hat{y}, z) \rightarrow (\alpha L \hat{z} + \beta)/C_o \rightarrow \hat{\alpha}\hat{z} + \hat{\beta}, \text{ as } z \rightarrow -\infty \tag{7.31}$$

$$\frac{\partial \hat{C}_{de}(\hat{x}, \hat{y}, z)}{\partial \hat{z}} \rightarrow \frac{L}{C_o}\gamma \rightarrow \hat{\gamma}, \text{ as } z \rightarrow \infty \tag{7.32}$$

- Capillary - tissue boundary

  Eq. (7.15) becomes:

$$P_{\mathrm{cap/w}}\left[\frac{\hat{C}_{\mathrm{bl}}C_{\mathrm{o}}}{K_{\mathrm{bl/w}}}-\frac{\langle\left(\hat{C}_{\mathrm{de}}C_{\mathrm{o}}\right)_{|a_{\mathrm{cap}}}\rangle}{K_{\mathrm{de/w}}}\right]+\frac{U_{\mathrm{sp}|a_{\mathrm{cap}}}K_{\mathrm{mem/w}}}{2}\left[\frac{\hat{C}_{\mathrm{bl}}C_{\mathrm{o}}}{K_{\mathrm{bl/w}}}+\frac{\langle\left(\hat{C}_{\mathrm{de}}C_{\mathrm{o}}\right)_{|a_{\mathrm{cap}}}\rangle}{K_{\mathrm{de/w}}}\right] =$$

$$-\hat{D}_{\mathrm{de}}D_{\mathrm{o}}\langle\frac{1}{L}\hat{\vec{\nabla}}\left(\hat{C}_{\mathrm{de}}C_{\mathrm{o}}\right)_{|a_{\mathrm{cap}}}\bullet\vec{n}_{\mathrm{wall}}\rangle+U_{\mathrm{sp}|a_{\mathrm{cap}}}\langle\left(\hat{C}_{\mathrm{de}}C_{\mathrm{o}}\right)_{|a_{\mathrm{cap}}}\rangle \Rightarrow$$

$$\frac{P_{\mathrm{cap/w}}L}{D_{\mathrm{o}}}\left[\frac{\hat{C}_{\mathrm{bl}}}{K_{\mathrm{bl/w}}}-\frac{\langle\hat{C}_{\mathrm{de}|a_{\mathrm{cap}}}\rangle}{K_{\mathrm{de/w}}}\right]+\frac{U_{\mathrm{sp}|a_{\mathrm{cap}}}L}{D_{\mathrm{o}}}\frac{K_{\mathrm{mem/w}}}{2}\left[\frac{\hat{C}_{\mathrm{bl}}}{K_{\mathrm{bl/w}}}+\frac{\langle\hat{C}_{\mathrm{de}|a_{\mathrm{cap}}}\rangle}{K_{\mathrm{de/w}}}\right] =$$

$$-\hat{D}_{\mathrm{de}}\langle\hat{\vec{\nabla}}\hat{C}_{\mathrm{de}|a_{\mathrm{cap}}}\bullet\vec{n}_{\mathrm{wall}}\rangle+\frac{U_{\mathrm{sp}|a_{\mathrm{cap}}}L}{D_{\mathrm{o}}}\langle\hat{C}_{\mathrm{de}|a_{\mathrm{cap}}}\rangle \quad (7.33)$$

  By introducing the dimensionless capillary permeability coefficient

$$\hat{P}_{\mathrm{cap}} = \frac{P_{\mathrm{cap/w}}L}{D_{\mathrm{o}}} \quad (7.34)$$

  this equation becomes:

$$\hat{P}_{\mathrm{cap}}\left[\frac{\hat{C}_{\mathrm{bl}}}{K_{\mathrm{bl/w}}}-\frac{\langle\hat{C}_{\mathrm{de}|a_{\mathrm{cap}}}\rangle}{K_{\mathrm{de/w}}}\right]+Pe_{\mathrm{int}|a_{\mathrm{cap}}}\frac{K_{\mathrm{mem/w}}}{2}\left[\frac{\hat{C}_{\mathrm{bl}}}{K_{\mathrm{bl/w}}}+\frac{\langle\hat{C}_{\mathrm{de}|a_{\mathrm{cap}}}\rangle}{K_{\mathrm{de/w}}}\right] =$$

$$-\hat{D}_{\mathrm{de}}\langle\hat{\vec{\nabla}}\hat{C}_{\mathrm{de}|a_{\mathrm{cap}}}\bullet\vec{n}_{\mathrm{wall}}\rangle+Pe_{\mathrm{int}|a_{\mathrm{cap}}}\langle\hat{C}_{\mathrm{de}|a_{\mathrm{cap}}}\rangle \quad (7.35)$$

- Blood phase

  Here

$$\frac{1}{L}\frac{d(\hat{U}_{\mathrm{bl}}U_{\mathrm{o}})}{d\hat{t}} = -\frac{2\hat{U}_{\mathrm{sp}|a_{\mathrm{cap}}}U_{\mathrm{o}}}{\hat{a}_{\mathrm{cap}}L} \Rightarrow$$

$$\frac{d\hat{U}_{\mathrm{bl}}}{d\hat{t}} = -\frac{2\hat{U}_{\mathrm{sp}|a_{\mathrm{cap}}}}{\hat{a}_{\mathrm{cap}}}, \quad (7.36)$$

so, Eqs. (7.18 - 7.19) become:

$$\frac{a_{\rm cap}U_{\rm bl}}{2}\frac{1}{L}\frac{d\left(\hat{C}_{\rm bl}C_{\rm o}\right)}{d\hat{t}} =$$

$$P_{\rm cap/w}\left(\frac{\langle\left(\hat{C}_{\rm de}C_{\rm o}\right)_{|a_{\rm cap}}\rangle}{K_{\rm de/w}}\frac{\hat{C}_{\rm bl}C_{\rm o}}{K_{\rm bl/w}}\right) -$$

$$\frac{U_{\rm sp|a_{\rm cap}}K_{\rm mem/w}}{2}\left(\frac{\langle\left(\hat{C}_{\rm de}C_{\rm o}\right)_{|a_{\rm cap}}\rangle}{K_{\rm de/w}}+\frac{\hat{C}_{\rm bl}C_{\rm o}}{K_{\rm bl/w}}\right) =$$

$$\hat{D}_{\rm de}D_{\rm o}\langle\frac{1}{L}\hat{\bar{\nabla}}\left(\hat{C}_{\rm de}C_{\rm o}\right)_{|a_{\rm cap}}\bullet\vec{n}_{\rm wall}\rangle - U_{\rm sp|a_{\rm cap}}\langle\left(\hat{C}_{\rm de}C_{\rm o}\right)_{|a_{\rm cap}}\rangle \Rightarrow$$

$$\begin{aligned}\frac{1}{2}\frac{a_{\rm cap}U_{\rm bl}}{D_{\rm o}}\frac{d\hat{C}_{\rm bl}}{d\hat{t}} &= \frac{P_{\rm cap/w}L}{D_{\rm o}}\left(\frac{\langle\hat{C}_{\rm de|a_{\rm cap}}\rangle}{K_{\rm de/w}}-\frac{\hat{C}_{\rm bl}}{K_{\rm bl/w}}\right)\\ &- \frac{U_{\rm sp|a_{\rm cap}}L}{D_{\rm o}}\frac{K_{\rm mem/w}}{2}\left(\frac{\langle\hat{C}_{\rm de|a_{\rm cap}}\rangle}{K_{\rm de/w}}+\frac{\hat{C}_{\rm bl}}{K_{\rm bl/w}}\right)\\ &= \hat{D}_{\rm de}\langle\hat{\bar{\nabla}}\hat{C}_{\rm de|a_{\rm cap}}\bullet\vec{n}_{\rm wall}\rangle-\frac{U_{\rm sp|a_{\rm cap}}L}{D_{\rm o}}\langle\hat{C}_{\rm de|a_{\rm cap}}\rangle\end{aligned}$$

Ultimately,

$$\begin{aligned}Pe_{\rm bl}\frac{d\hat{C}_{\rm bl}}{d\hat{t}} &= 2\hat{P}_{\rm cap}\left(\frac{\langle\hat{C}_{\rm de|a_{\rm cap}}\rangle}{K_{\rm de/w}}-\frac{\hat{C}_{\rm bl}}{K_{\rm bl/w}}\right)\\ &- Pe_{\rm int|a_{\rm cap}}K_{\rm mem/w}\left(\frac{\langle\hat{C}_{\rm de|a_{\rm cap}}\rangle}{K_{\rm de/w}}+\frac{\hat{C}_{\rm bl}}{K_{\rm bl/w}}\right) \qquad (7.37)\end{aligned}$$

$$Pe_{\rm bl}\frac{d\hat{C}_{\rm bl}}{d\hat{t}} = 2\hat{D}_{\rm de}\langle\hat{\bar{\nabla}}\hat{C}_{\rm de|a_{\rm cap}}\bullet\vec{n}_{\rm wall}\rangle - 2Pe_{\rm int|a_{\rm cap}}\langle\hat{C}_{\rm de|a_{\rm cap}}\rangle \qquad (7.38)$$

Here $Pe_{\rm bl}$ is yet another Peclet number, based on the blood flow velocity.

$$Pe_{\rm bl} = \frac{a_{\rm cap}U_{\rm bl}}{D_{\rm o}} \qquad (7.39)$$

The dimensionless groups that arise in the system of Eqs. (7.26 - 7.32), (7.35 - 7.38) are the two Peclet numbers ($Pe_{\rm int}$, $Pe_{\rm bl}$) and the diffusional capillary permeability ($\hat{P}_{\rm cap}$). The value of the interstitial Peclet number on the capillary wall ($Pe_{{\rm int}|a_{\rm cap}}$) can be thought of as the maximum value that $Pe_{\rm int}$ can obtain. These magnitudes offer valuable insights on the importance of diffusive and convective transport.

7.2.5 Capillary centerline / surface

Representations of the capillary centerline and the capillary surface are developed in parametric form. Three different parametric equations (where σ is the name of the parameter varying along the curve) were considered for the centerline. It is most convenient for the consequent derivations to place the apex of the capillary centerline at the dimensional point $(l_x/2, l_y/2, 0)$.

$$x = l_x/2 + a\tanh(\sigma), \quad y = l_y/2, \quad z = -h_o\sigma^2 \tag{7.40}$$

$$x = l_x/2 + a\tanh(\sigma), \quad y = l_y/2, \quad z = -\left[(\cosh(\sigma/\sigma_o) - 1\right] \tag{7.41}$$

$$x = l_x/2 + \sigma, \quad y = l_y/2, \quad z = -\left[\tan(\sigma\sqrt{\pi}/2\lambda_o)\right]^2 \tag{7.42}$$

where a, h_o, σ_o, λ_o are parameters defining the actual size and geometry of a single capillary.

With the computer reconstructed image of a capillary network by Braverman [50] as a guide, the distance between the asymptotes of the two capillary legs was taken to be $\simeq 40\mu$m, while the vertical distance over which the arch extends was taken to be $\simeq 50\mu$m. These geometric criteria are met in all three cases when $a = 20$, $h_o = 20$, $\sigma_o = 0.4$ and $\lambda_o = 11.2$. The centerlines derived from these three parametric representations are shown in Fig. 7.4. The first one was chosen as the most realistic. The interval $-2.738613 \leq \sigma \leq 2.738613$ defines a capillary loop $\simeq 300\mu$m long.

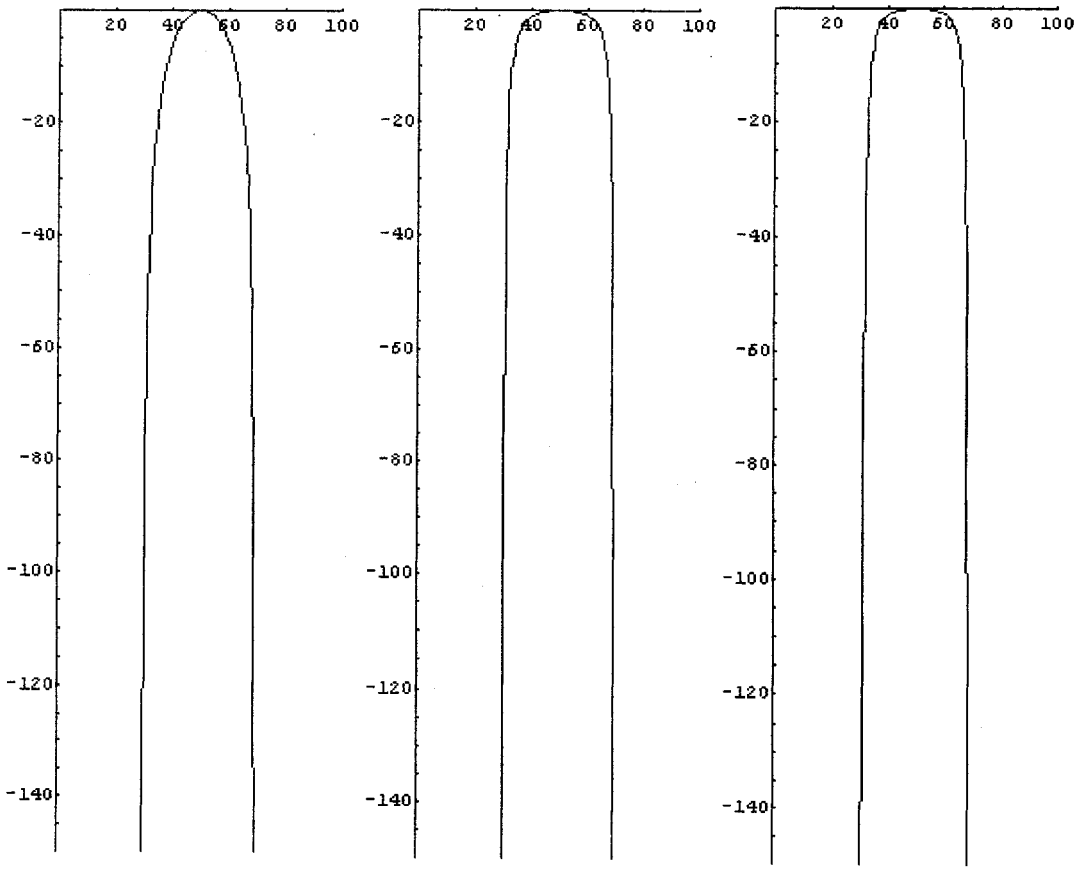

Figure 7.4: Capillary centerline candidates. Dimensions in μ m

In order to define a corresponding representation of the capillary wall, we build on the centerline equation, and introduce three unit vectors are needed, the one tangential to the centerline ($\vec{n_t}$), the one normal to it ($\vec{n_n}$) and the corresponding binormal vector ($\vec{n_b}$). Since the centerline lies in the xz plane one can write:

$$\vec{n_t} = A(\sigma)\vec{e_x} + B(\sigma)\vec{e_z} \tag{7.43}$$

$$\vec{n_n} = C(\sigma)\vec{e_x} + D(\sigma)\vec{e_z} \tag{7.44}$$

$$\vec{n_b} = E(\sigma)\vec{e_y} \tag{7.45}$$

$\vec{n_b}$ has only a y component since it is perpendicular to the xz plane ($\vec{n_b} = \vec{n_t} \times \vec{n_n}$).

These components of these vectors were found to be (Appendix D):

$$A(\sigma) = \frac{a/\cosh^2(\sigma)}{\sqrt{a^2/\cosh^4(\sigma) + 4h_o^2\sigma^2}} \tag{7.46}$$

$$B(\sigma) = \frac{-2h_o\sigma}{\sqrt{a^2/\cosh^4(\sigma) + 4h_o^2\sigma^2}} \tag{7.47}$$

$$C_+(\sigma) = -\sqrt{\frac{1}{1+[A(\sigma)/B(\sigma)]^2}} \tag{7.48}$$

$$C_-(\sigma) = +\sqrt{\frac{1}{1+[A(\sigma)/B(\sigma)]^2}} \tag{7.49}$$

$$D(\sigma) = -\sqrt{1-\frac{1}{1+[A(\sigma)/B(\sigma)]^2}} \tag{7.50}$$

$$E_+(\sigma) = [C_+(\sigma)B(\sigma) - D(\sigma)A(\sigma)]\vec{e_y} \tag{7.51}$$

$$E_-(\sigma) = [C_-(\sigma)B(\sigma) - D(\sigma)A(\sigma)]\vec{e_y} \tag{7.52}$$

with $E_+(\sigma)$, $C_+(\sigma)$ applicable for $0 \leq \sigma \leq +\infty$ and $E_-(\sigma)$, $C_-(\sigma)$ for $-\infty \leq \sigma \leq 0$

The parametric equations that define the capillary surface (for a constant capillary radius of $3\mu m$, Fig. 7.5) are:

$$x = l_x/2 + a\tanh(\sigma) + 3C_\pm(\sigma)\cos(u) \tag{7.53}$$

$$y = l_y/2 + 3E_\pm(\sigma)\sin(u) \tag{7.54}$$

$$z = -h_o\sigma^2 + 3D(\sigma)\cos(u) \tag{7.55}$$

with $u \in [-\pi, \pi]$ defining position around the circumference of the capillary.

7.2.6 Perturbation analysis

Based on the information gathered about the relative significance of convection and diffusion (Sec. 6.2.2 & 6.2.4), one may state that convection may or may not be

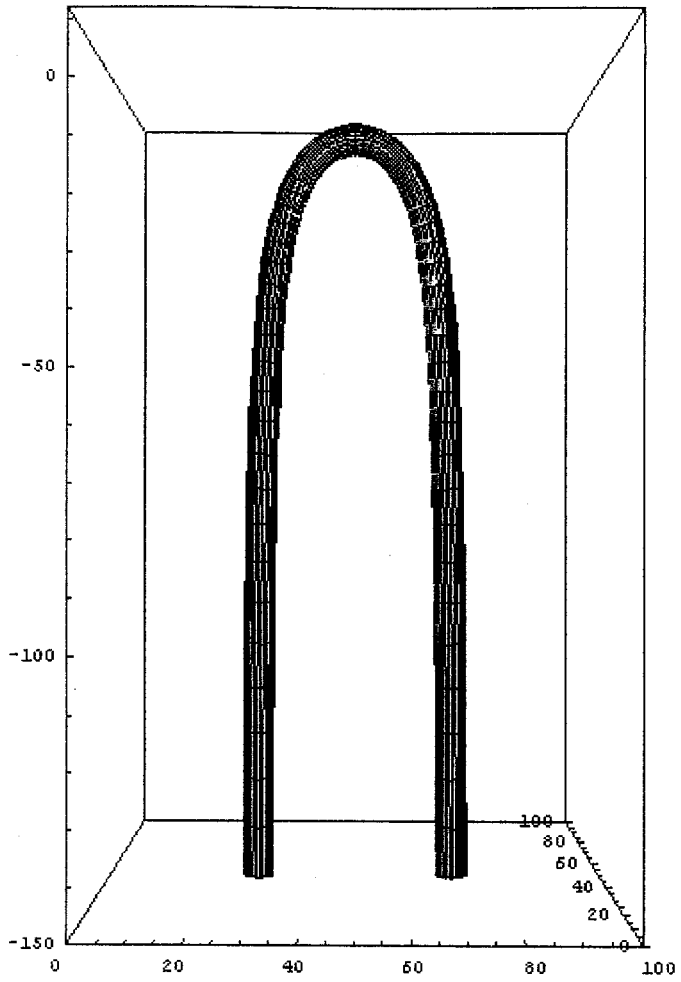

Figure 7.5: Capillary surface. Dimensions in μm

important depending on the properties of the skin-penetrating substance, such as size, lipophilicity, affinity to bind to serum proteins etc. The total disregard of the existing fluid channels that carry the leaked serum from the vascular to the lymphatic capillaries might lead to erroneous results for say, compounds that bind strongly to human serum albumin. Thus, convective transport is treated as a perturbation that can be added to the diffusive transport, if necessary. Mathematically, this was realized through a perturbation analysis. A small-impact convection translates into a small Peclet number :

$$Pe_{\text{int}} = \varepsilon f_{\text{int}}(\tilde{x}) \text{ with } \varepsilon \ll 1 \tag{7.56}$$

The strategy of a regular perturbation analysis [100] involves obtaining the solution of the problem for $\varepsilon = 0$ and then acknowledging the fact that $\varepsilon \neq 0$ by adding correction terms to the solution. Although it is an approximate solution, it is a useful approach. Furthermore, one can control the level of accuracy by choosing the appropriate number of correction terms. For example, Eq. (7.26) may be restated as:

$$\hat{\vec{\nabla}} \cdot \left\{ -\hat{D}_{\mathrm{de}} \hat{\vec{\nabla}} \hat{C}_{\mathrm{de}} + \varepsilon \; f_{\mathrm{int}}(\tilde{x}) \; \vec{u}_{\mathrm{sp}} \hat{C}_{\mathrm{de}} \right\} \;=\; 0 \tag{7.57}$$

A power series is used to express the dependence of $\hat{C}_{\mathrm{de}}$ to ε:

$$\begin{aligned} \hat{C}_{\mathrm{de}} \;&=\; \sum_{n=0}^{\infty} \left\{ \hat{C}_n \varepsilon^n \right\} \\ &=\; \hat{C}_0 + \varepsilon \hat{C}_1 + \varepsilon^2 \hat{C}_2 + \ldots \end{aligned} \tag{7.58}$$

Substituting this function in Eq. (7.57) yields:

$$\begin{aligned} \hat{\vec{\nabla}} \left\{ -\hat{D}_{\mathrm{de}} \hat{\vec{\nabla}} \left\{ \hat{C}_0 + \varepsilon \hat{C}_1 + \varepsilon^2 \hat{C}_2 + \ldots \right\} \right. \;&+ \\ \left. \varepsilon f_{\mathrm{int}}(\tilde{x}) \vec{u}_{\mathrm{sp}} \left\{ \hat{C}_0 + \varepsilon \hat{C}_1 + \varepsilon^2 \hat{C}_2 + \ldots \right\} \right\} \;&=\; 0 \Rightarrow \\ \varepsilon^0 \left\{ -\hat{D}_{\mathrm{de}} \hat{\nabla}^2 \hat{C}_0 \right\} + \varepsilon^1 \left\{ -\hat{D}_{\mathrm{de}} \hat{\nabla}^2 \hat{C}_1 + \hat{\vec{\nabla}} \left[f_{\mathrm{int}}(\tilde{x}) \vec{u}_{\mathrm{sp}} \hat{C}_0 \right] \right\} \;&+ \\ \varepsilon^2 \left\{ -\hat{D}_{\mathrm{de}} \hat{\nabla}^2 \hat{C}_2 + \hat{\vec{\nabla}} \left[f_{\mathrm{int}}(\tilde{x}) \vec{u}_{\mathrm{sp}} \hat{C}_1 \right] \right\} + O\left(\varepsilon^3\right) \;&=\; 0 \end{aligned} \tag{7.59}$$

with $O\left(\varepsilon^3\right)$ including all the higher order terms. This equation generates a sequence of equations that can be solved consecutively. The first approximation is to consider only the $O(1)$ terms (first bracket in equation) and obtain a solution for C_0. This is equivalent to making the assumption that there is no filtration or convection through the interstitium since $Pe_{\mathrm{int}} = 0$. This solution is accurate to within an error of $O(\varepsilon)$ imposed by the neglected terms. The second approximation is to include the $O(\varepsilon)$

terms (by solving the equation in the second bracket). The $O(1)$ terms have already been satisfied and thus by adding the two obtained solutions, one has solution with an error of $O(\varepsilon^2)$, and so on.

7.3 First approximation - negligible convection

7.3.1 System of equations

By setting $Pe_{\text{int}} = 0$, or better yet by setting the maximum value of the Peclet number $Pe_{\text{int}|a_{\text{cap}}}$ equal to zero, one is effectively considering diffusion as the only transport process occuring in the interstitium and through the capillary wall. The only convective process is the blood flow inside the capillary. This may be considered a good approximation for small to medium - size substances that do not bind very extensively to plasma proteins. The equations describing the system are:

- Interstitial phase

$$-\hat{D}_{\text{de}}\hat{\nabla}^2\hat{C}_{\text{de}} = 0 \tag{7.60}$$

$$\hat{C}_{\text{de}}(0,\hat{y},\hat{z}) = \hat{C}_{\text{de}}(\hat{l_x},\hat{y},\hat{z}) \tag{7.61}$$

$$\frac{\partial\hat{C}_{\text{de}}(0,\hat{y},\hat{z})}{\partial\hat{x}} = \frac{\partial\hat{C}_{\text{de}}(\hat{l_x},\hat{y},\hat{z})}{\partial\hat{x}} \tag{7.62}$$

$$\hat{C}_{\text{de}}(\hat{x},0,\hat{z}) = \hat{C}_{\text{de}}(\hat{x},\hat{l_y},\hat{z}) \tag{7.63}$$

$$\frac{\partial\hat{C}_{\text{de}}(\hat{x},0,\hat{z})}{\partial\hat{y}} = \frac{\partial C_{\text{de}}(\hat{x},\hat{l_y},\hat{z})}{\partial\hat{y}} \tag{7.64}$$

$$\hat{C}_{\text{de}}(\hat{x},\hat{y},z) \rightarrow \hat{\alpha}\hat{z}+\hat{\beta}\ \text{, as } z\rightarrow-\infty \tag{7.65}$$

$$\frac{\partial\hat{C}_{\text{de}}(\hat{x},\hat{y},z)}{\partial\hat{z}} \rightarrow \hat{\gamma}\ \text{, as } z\rightarrow\infty \tag{7.66}$$

- Blood phase

$$\frac{d\hat{U}_{\mathrm{bl}}}{d\hat{t}} = 0 \tag{7.67}$$

$$Pe_{\mathrm{bl}}\frac{d\hat{C}_{\mathrm{bl}}}{d\hat{t}} = 2\hat{P}_{\mathrm{cap}}\left(\frac{\langle\hat{C}_{\mathrm{de}|a_{\mathrm{cap}}}\rangle}{K_{\mathrm{de/w}}} - \frac{\hat{C}_{\mathrm{bl}}}{K_{\mathrm{bl/w}}}\right) \tag{7.68}$$

$$Pe_{\mathrm{bl}}\frac{d\hat{C}_{\mathrm{bl}}}{d\hat{t}} = 2\hat{D}_{\mathrm{de}}\langle\hat{\bar{\nabla}}\hat{C}_{\mathrm{de}|a_{\mathrm{cap}}} \bullet \vec{n}_{\mathrm{wall}}\rangle \tag{7.69}$$

7.3.2 Capillary centerline discretization

The capillary centerline is descritized into many straight segments for the subsequent application of numerical methods. There are various possible ways of doing this:

1. Segments of same elevation
2. Chords of same length
3. Arcs of same length

The last method is the most attractive, as it is the simplest to implement. The parametric equations for the centerline are:

$$x = l_x/2 + a\tanh(\sigma), \qquad y = l_y/2, \qquad z = -h_o\sigma^2 \tag{7.70}$$

$$\hat{x} = \left[l_x/2a\tanh(\sigma)\right]/L, \quad \hat{y} = (l_y/2)/L, \quad \hat{z} = -h_o\sigma^2/L \tag{7.71}$$

where $a = 20\mu$m, $h_o = 20\mu$m, $L = 100\mu$m. Varying σ as $-2.738613 \leq \sigma \leq 2.738613$ suffices to produce a realistic capillary length of $O(300)\mu$m.

The centerline is broken into $2N_{max}$ segments ($N_{max} = 10$) corresponding to evenly spaced values of σ. The endpoints of each segment are defined by applying discrete values of σ in the parametric equations. This produces arcs with length $\sigma_{i+1} - \sigma_i = 0.2738613$.

Consider the respective chords of these arc segments. The (dimensionless) length of the ith segment is:

$$\hat{l} = \sqrt{(\hat{x}_{i+1} - \hat{x}_i)^2 + (\hat{y}_{i+1} - \hat{y}_i)^2 + (\hat{z}_{i+1} - \hat{z}_i)^2} \tag{7.72}$$

A new variable $\hat{t}$ is defined that is the "arc length" of the curve that is comprised from these chords. The values of $\hat{t}$ at the junctions between chords are defined by a list (array) of values representing the accumulated length of the chords in either direction.

- $t(0) = 0$ at the peak of the capillary,
- $t(1) = \sqrt{(\hat{x}_1 - \hat{x}_0)^2 + (\hat{y}_1 - \hat{y}_0)^2 + (\hat{z}_1 - \hat{z}_0)^2}$,
- $t(2) = t(1) + \sqrt{(\hat{x}_2 - \hat{x}_1)^2 + (\hat{y}_2 - \hat{y}_1)^2 + (\hat{z}_2 - \hat{z}_1)^2}$

  etc for positive x coordinates,
- $t(-2) = t(-1) - \sqrt{(\hat{x}_{-2} - \hat{x}_{-1})^2 + (\hat{y}_{-2} - \hat{y}_{-1})^2 + (\hat{z}_{-2} - \hat{z}_{-1})^2}$

  for negative x coordinates.

The coordinate values of each segment's endpoints in dimensional and dimensionless form are listed in Table 7.1.

7.3.3 Slender body theory formulation

The elegant slender body theory is used to solve the preceding formulation. This theory has been mainly developed for, and applied to, problems involving Stokes flow [28, 83, 214, 198, 361]. Other applications pertain to shear flow [84] and diffusion [21, 153, 240]. According to Batchelor [28], "The basic idea in slender body theory for Stokes flow is that the disturbance motion due to the presence of the body is approximately the same as that due to a suitably chosen line distribution of Stokeslets".

σ	N	$x(\mu\text{m})$	$y(\mu\text{m})$	$z(\mu\text{m})$	$t(\mu\text{m})$	$\hat{x}$	$\hat{y}$	$\hat{z}$	$\hat{t}$
-2.739	-10	30.167	50	-150	-157.223	0.302	0.5	-1.5	-1.572
-2.465	-9	30.287	50	-121.5	-128.723	0.303	0.5	-1.215	-1.287
-2.191	-8	30.494	50	-96	-103.222	0.305	0.5	-0.96	-1.032
-1.917	-7	30.847	50	-73.5	-80.72	0.309	0.5	-0.735	-0.807
-1.643	-6	31.442	50	-54	-61.211	0.314	0.5	-0.54	-0.612
-1.369	-5	32.429	50	-37.5	-44.681	0.324	0.5	-0.375	-0.447
-1.095	-4	34.023	50	-24	-31.087	0.340	0.5	-0.24	-0.311
-0.822	-3	36.481	50	-13.5	-20.303	0.365	0.5	-0.135	-0.203
-0.548	-2	40.024	50	-6	-12.009	0.4	0.5	-0.06	-0.12
-0.274	-1	44.656	50	-1.5	-5.551	0.447	0.5	-0.015	-0.056
0	0	50	50	0	0	0.5	0.5	0	0
0.274	1	55.344	50	-1.5	5.551	0.553	0.5	-0.015	0.056
0.548	2	59.976	50	-6	12.009	0.6	0.5	-0.06	0.12
0.822	3	63.519	50	-13.5	20.303	0.635	0.5	-0.135	0.203
1.095	4	65.977	50	-24	31.087	0.66	0.5	-0.24	0.311
1.369	5	67.571	50	-37.5	44.681	0.676	0.5	-0.375	0.447
1.643	6	68.558	50	-54	61.211	0.686	0.5	-0.54	0.612
1.917	7	69.153	50	-73.5	80.72	0.692	0.5	-0.735	0.807
2.191	8	69.506	50	-96	103.222	0.695	0.5	-0.96	1.032
2.465	9	69.713	50	-121.5	128.723	0.697	0.5	-1.215	1.287
2.739	10	69.834	50	-150	157.223	0.698	0.5	-1.5	1.572

Table 7.1: Dimensional and dimensionless coordinates of the discrete segments of the capillary centerline.

The same applies here. The solution for the dermal concentration field is expressed as a line distribution of point sinks located on the capillary centerline. The first step is to acquire a doubly periodic Green's function, the solution for the problem where one point source of unit strength is located at an arbitrary point (x_o, y_o, z_o) inside the unit cell. The point source at each point of the capillary centerline is weighted with a corresponding source density strength, which is generally negative reflecting the fact that the capillary is a sink of solute (i.e. absorbing solute). The source density strength (P) is a measure of how strongly it absorbs material and is measured in moles/cm/sec. The next step is to sum these individual-sink solutions by integrating along the capillary centerline, the distribution of the source density

being unknown.

This integral, according to slender body theory, corresponds to the "disturbance" concentration, the perturbation to a "background" linear distribution representing 1-D diffusion in the $-z$ direction (caused by a constant flux supply from above) caused by the existence of the capillary network. The "disturbance" concentration must be added to the "background" concentration, the one that it would have been in the abscence of the capillaries. This "background" linear dependence is chosen to be the same as the one that specifies the concentration asymptotically as $z \to -\infty$. Thus, the concentration at any point (x, y, z) in the unit cell is given by :

$$C_{\text{de}}(x, y, z) = \alpha z + \beta + \int_c P(t) G\left[x, y, z, x_o(t), y_o(t), z_o(t)\right] dl \qquad (7.73)$$

where $P(t)$ is the unknown source density strength, c stands for the capillary centerline, dl is the infinitesimal element of length along it, and t is an arc length variable that is derived from the discretization of the capillary centerline into a finite number of straight segments.

Assuming that $P(t)$ is piecewise constant (i.e. constant over each straight capillary segment), one can factor the source density for each segment out of the integral and write:

$$C_{\text{de}} = \alpha z + \beta + \sum_{-N_{max}}^{N_{max}} P_i(t) \int_{c_i} G\left[x, y, z, x_o(t), y_o(t), z_o(t)\right] \left(\frac{dl}{dt}\right) dt \qquad (7.74)$$

where c_i refers to the center of the ith cylinder. The discrete values of t reported in Table 7.1 are the limits of the integration in Eq. (7.74) for each segment, the length of which is $t_{i+1} - t_i$.

7.3.4 Doubly periodic Green's function

The Green's function (concentration field representing a point source $G(\tilde{x}, \tilde{x_o})$) is the building block for the solution for $C_{\rm de}$. The present calculation pertains to the case where the rate of absorption from the capillary equals the rate of supply. This means that the concentration as $z \to -\infty$ does not vary linearly with depth, but rather is constant.

The lateral dimensions of the unit cell are l_x and l_y chosen to be $l_x = l_y = 100\mu$m (yielding a realistic average capillary density of $O(100)/\mu\text{m}^2$). G is governed by an equation describing steady state diffusion with a unit sink at a point $\tilde{x_o}$:

$$D_{\rm de}\nabla^2 G + \delta(\vec{x} - \vec{x_o})\dot{m} = 0 \tag{7.75}$$

where

$$\delta(\vec{x} - \vec{x_o}) = \delta(x - x_o)\delta(y - y_o)\delta(z - z_o) \tag{7.76}$$

and $\dot{m}$ is the rate of moles (moles/sec) at which the sink is absorbing solute. By making the equation dimensionless (the dimensionless variables and characteristic values have been previously defined) one has:

$$D_{\rm de}\frac{\hat{\nabla}^2}{L^2}\hat{G}C_{\rm o} = -\dot{m}\frac{\delta(\hat{\vec{x}} - \hat{\vec{x_o}})}{L^3} \tag{7.77}$$

$$\hat{\nabla}^2\hat{G} = -\frac{\dot{m}}{D_{\rm de}LC_{\rm o}}\delta(\hat{\vec{x}} - \hat{\vec{x_o}}) \tag{7.78}$$

We define $\dot{m}$ such that

$$\frac{\dot{m}}{D_{\rm de}LC_{\rm o}} = 1 \tag{7.79}$$

$$C_{\rm o} = \frac{\dot{m}}{D_{\rm de}L}. \tag{7.80}$$

then

$$\hat{\nabla}^2\hat{G} = -\delta(\hat{\vec{x}} - \hat{\vec{x_o}}) \tag{7.81}$$

The Green's function for an isolated point source is given by the well known formula

$$\hat{G}(\hat{\vec{x}}, \hat{\vec{x_o}}) = \frac{1}{4\pi|\hat{\vec{x}} - \hat{\vec{x_o}}|} \tag{7.82}$$

which satisfies

$$\hat{\nabla}^2 \hat{G}(\hat{\vec{x}}, \hat{\vec{x_o}}) = -\delta(\hat{\vec{x}} - \hat{\vec{x_o}}) \tag{7.83}$$

In the present case one has to obtain a 2D periodic Green's function, a function that will be the solution for the case where there are periodic point sinks, one in each capillary cell. The steady state problem that needs to be solved is as follows (in which all variables are dimensionless, the affix "$\hat{}$" now being dropped):

$$\nabla^2 G(x,y,z) = -\delta(x-x_o)(y-y_o)(z-z_o) \qquad x \in (0,l_x)\,,\ y \in (0,l_y)\,,\ z \in (-\infty,\infty) \tag{7.84}$$

$$G(0,y,z) = G(l_x,y,z) \qquad y \in (0,l_y)\,,\ z \in (-\infty,\infty) \tag{7.85}$$

$$\frac{\partial G(0,y,z)}{\partial x} = \frac{\partial G(l_x,y,z)}{\partial x} \qquad y \in (0,l_y)\,,\ z \in (-\infty,\infty) \tag{7.86}$$

$$G(x,0,z) = G(0,l_y,z) \qquad x \in (0,l_x)\,, \qquad z \in (-\infty,\infty) \tag{7.87}$$

$$\frac{\partial G(x,0,z)}{\partial y} = \frac{\partial G(0,l_y,z)}{\partial y} \qquad x \in (0,l_x)\,, \qquad z \in (-\infty,\infty) \tag{7.88}$$

$$\frac{\partial G(x,y,z)}{\partial z} \to 0 \qquad x \in (0,l_x)\,,\ y \in (0,l_y)\,,\ z \to -\infty \tag{7.89}$$

$$\frac{\partial G(x,y,z)}{\partial z} = \frac{1}{l_x l_y} \qquad x \in (0,l_x)\,,\ y \in (0,l_y)\,,\ z \to \infty \tag{7.90}$$

The slope at $+\infty$ must be $\frac{1}{l_x l_y}$ because the flux away at $+\infty$ must balance the unit flux coming out from the point source.

The problem involves an inhomogeneous PDE with inhomogeneous boundary conditions in three dimensions. It was solved with the method of separation of variables (Appendix E), and its solution for the two semi-infinite regions $z \prec z_o$ and $z \succ z_o$ is given by

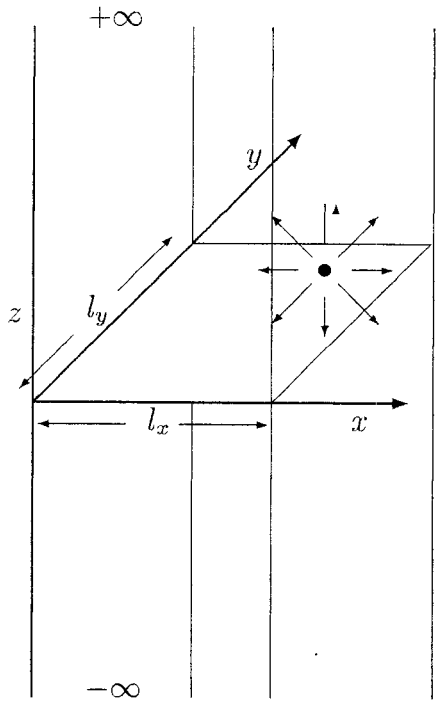

Figure 7.6: Definition sketch for Green's function formulation

- $z \prec z_o$

$$
\begin{aligned}
G &= 0 + \frac{1}{2\pi l_x} \sum_{m=1}^{\infty} \frac{1}{m} \cos\left(\frac{2\pi m(y-y_o)}{l_y}\right) \exp\left[\frac{2\pi m}{l_y}(z-z_o)\right] \\
&+ \frac{1}{2\pi l_y} \sum_{n=1}^{\infty} \frac{1}{n} \cos\left(\frac{2\pi n(x-x_o)}{l_x}\right) \exp\left[\frac{2\pi n}{l_x}(z-z_o)\right] \\
&- \frac{4}{l_x l_y} \sum_{n=1}^{\infty} \sum_{m=1}^{\infty} \left[\cos\left(\frac{2\pi n(x-x_o)}{l_x}\right) \cos\left(\frac{2\pi m(y-y_o)}{l_y}\right)\right] \\
&\left\{ - \frac{\exp\left[\sqrt{\left(\frac{2n\pi}{l_x}\right)^2 + \left(\frac{2m\pi}{l_y}\right)^2}(z-z_o)\right]}{2\sqrt{\left(\frac{2n\pi}{l_x}\right)^2 + \left(\frac{2m\pi}{l_y}\right)^2}} \right\}
\end{aligned}
\tag{7.91}
$$

- $z \succ z_o$

$$
G = -(z-z_o) + \frac{1}{2\pi l_x} \sum_{m=1}^{\infty} \frac{1}{m} \cos\left(\frac{2\pi m(y-y_o)}{l_y}\right) \exp\left[-\frac{2\pi m}{l_y}(z-z_o)\right]
$$

$$
\begin{aligned}
&+ \frac{1}{2\pi l_y}\sum_{n=1}^{\infty}\frac{1}{n}\cos\left(\frac{2\pi n(x-x_o)}{l_x}\right)\exp\left[-\frac{2\pi n}{l_x}(z-z_o)\right] \\
&- \frac{4}{l_x l_y}\sum_{n=1}^{\infty}\sum_{m=1}^{\infty}\left[\cos\left(\frac{2\pi n(x-x_o)}{l_x}\right)\cos\left(\frac{2\pi m(y-y_o)}{l_y}\right)\right] \\
&\left\{-\frac{\exp\left[-\sqrt{\left(\frac{2n\pi}{l_x}\right)^2+\left(\frac{2m\pi}{l_y}\right)^2}(z-z_o)\right]}{2\sqrt{\left(\frac{2n\pi}{l_x}\right)^2+\left(\frac{2m\pi}{l_y}\right)^2}}\right\}
\end{aligned}
\tag{7.92}
$$

The obtained solution involves a double series that converges very slowly as $z \to z_o$, for examble $11,757$ terms are needed for the solution on the plane $z - z_o = 0.001$ in order to have an error less than 10^{-10}. Thus, one needs to implement a procedure that will make the series converge more rapidly. There are a variety of methods that have been used for this purpose [132, 152, 166, 209, 217, 330, 340, 342]. Some of them were named after their inventors such as Kummer's transform, Shanks transform, Levin transform. In many of these methods, one has to "extract" the singularity, the cause of slow convergence, from the series for the Green's function.

This general type of thing is done here. We write

$$
f(x,y,z,x_o,y_o,z_o) = G - \frac{1}{4\pi\sqrt{(x-x_o)^2+(y-y_o)^2+(z-z_o)^2}} \tag{7.93}
$$

The formulae giving G were used to get values of G (and therefore f) at the points $(x,y,z) = (x_o, y_o, z_o + 0.01)$, $(x,y,z) = (x_o, y_o, z_o - 0.01)$, ...,. Values of f at $z = z_o$ were obtained by extrapolation of the value at $z = z_o \pm 0.01$ and $z_o \pm 0.02$. These were fitted with a convenient formula representing f close to the singular point (x_o, y_o, z_o). For example, the approximation for f with $(x_o, y_o, z_o) \equiv (l_x/2, l_y/2, 0)$ is:

$$
\begin{aligned}
f(x,y,z,x_o,y_o,z_o) \simeq\ & -0.31037316607682 + 0.35934349472441(x-x_o)^2 \\
&+ 0.35934349472441(y-y_o)^2 - 0.5(z-z_o)
\end{aligned}
$$

$$- \quad 0.71880194952219(z - z_o)^2 \tag{7.94}$$

Our overall scheme for computing G is to write

$$G = \frac{1}{4\pi\sqrt{(x-x_o)^2+(y-y_o)^2+(z-z_o)^2}} + f(x, y, z, x_o, y_o, z_o) \tag{7.95}$$

f is computed as the difference in Eq. (7.93) with G summed according to Eqs. (7.91 - 7.92) if $\vec{x}$ is far away from $\vec{x_o}$. It is computed with Eq. (7.95) if $\vec{x}$ is close to $\vec{x_o}$. Various tests were performed on the Green's function in order to establish the correctness and accuracy of the solution (Appendix F).

7.3.5 Integration of Green's function

Now we return to the affix "$\hat{}$" for the dimensionless variables. According to slender body theory, the (dimensionless) concentration $\hat{C}_{\text{de}}$ at an arbitrary point $(\hat{x}, \hat{y}, \hat{z})$ is equal to the concentration that it would have been if the capillary did not exist $(\hat{\alpha}\hat{z} + \hat{\beta})$ plus the "disturbance" caused by the presence of the capillary segment. After the discretization, this disturbance is equal to the sum of the "disturbances" generated by each discrete segment. Since sources are concerned, their "strengths", quantified through the source densities $\hat{P}_i$, will be negative.

$$\hat{C}_{\text{de}} = \hat{\alpha}\hat{z} + \hat{\beta} + \sum_{i=-N_{max}}^{N_{max}} \hat{P}_i \int_{\hat{t}_i}^{\hat{t}_{i+1}} \hat{G}\left[\hat{x}, \hat{y}, \hat{z}, \hat{x}_o(\hat{t}), \hat{y}_o(\hat{t}), \hat{z}_o(\hat{t})\right] d\hat{t} \tag{7.96}$$

To carry out these integrations, one has to formulate the coordinates of the point sources $(\hat{x}_o, \hat{y}_o, \hat{z}_o)$ in terms of the integration variable t, which represents the accumulated arc length of the curve that is comprising the consecutive straight segments of the centerline. This is given by the linera relation:

$$\vec{x}_o = \vec{x}_i + (\vec{x}_{i+1} - \vec{x}_i)\frac{t - t_i}{t_{i+1} - t_i} \tag{7.97}$$

This equation provides the x_o, y_o, z_o coordinates of a sink point in terms of the t variable.

Integration of Green's function is carried out by integrating separately each of it's two parts:

$$\hat{G} = \frac{1}{4\pi\sqrt{(\hat{x}-\hat{x}_o)^2+(\hat{y}-\hat{y}_o)^2+(\hat{z}-\hat{z}_o)^2}} + f(\hat{x},\hat{y},\hat{z},\hat{x}_o,\hat{y}_o,\hat{z}_o) \quad (7.98)$$

The first term is integrated analytically. For this reason, a general formula for the respective integral has been derived (Appendix G). Batchelor [28] derived a similar analytical formula for the integral $1/|\vec{x}-\vec{x_o}|$ for the case where the slender body had an irregular cross section and its length was far greater than the distance between the body and the point at which the concentration was calculated. The definite integral of the function $\frac{1}{\sqrt{(\hat{x}-\hat{x}_o)^2+(\hat{y}-\hat{y}_o)^2+(\hat{z}-\hat{z}_o)^2}}$ over an arbitrary length h is:

$$\begin{aligned} I &= \int_{-\frac{h}{2}}^{\frac{h}{2}} \frac{1}{\sqrt{(\hat{x}-\hat{x}_o)^2+(\hat{y}-\hat{y}_o)^2+(\hat{z}-\hat{z}_o)^2}} \\ &= \ln\left(\sqrt{1+\left(\frac{h/2-x_1}{r}\right)^2}+\frac{h/2-x_1}{r}\right) \\ &- \ln\left(\sqrt{1+\left(\frac{-h/2-x_1}{r}\right)^2}+\frac{-h/2-x_1}{r}\right) \end{aligned} \quad (7.99)$$

For each capillary centerline segment, this length given by $h = t_{i+1} - t_i$, while r and x_1 are parameters defined in the local geometry (Appendix G). Batchelor's corresponding formula [28] for a slender body with a constant cross section is:

$$I = 2\log(h) + 2\log\left[\frac{\sqrt{1-\left(\frac{2x_1}{h}\right)^2}}{r}\right] \quad (7.100)$$

which applies to the limit $\frac{2r}{h} \ll 1$. Indeed, the results of Eq. (7.99) and Eq. (7.100) agree up to four decimals when $\frac{2r}{h} = 0.01$ and up to one decimal when $\frac{2r}{h} = 0.5$.

The second part of the Green's function (f) is integrated numerically using Simpson's rule. For that part, every segment is divided into 10 subsegments. The coordinates of the endpoints of each subsegment are calculated according to Eq. (7.97). These values are used for the calculation of the f function from Eq. (7.94).

7.3.6 Line-thin capillary loop

The whole formulation up to this point was put to the test by assuming that the strength density ($P(t)$) is constant and equal to -1. Although this source distribution is not generally compatible with the equation of transcapillary flux to dermal flux from the capillary wall, it does illustrate the general character of absorption and concentration profiles.

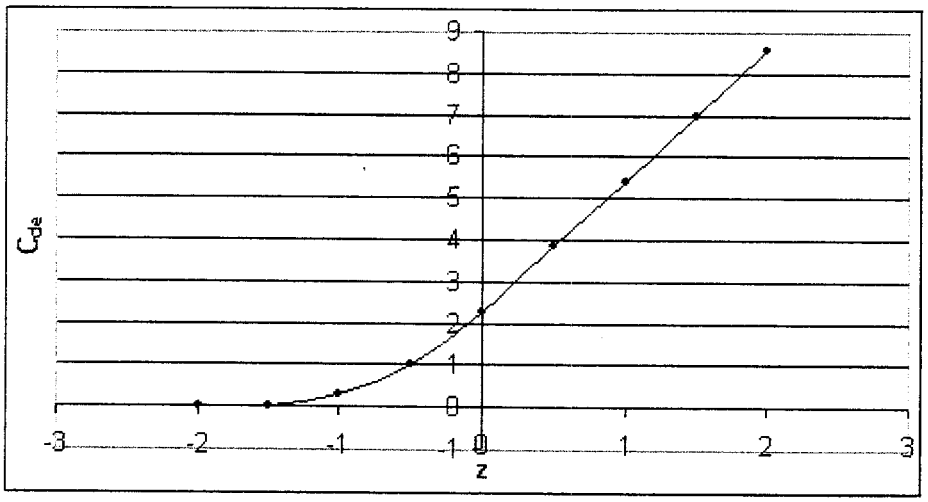

Figure 7.7: Depth concentration profile for constant strength density $P(t) = -1$ of the point sinks. Fixed coordinates: $x = 0.2$, $y = 0.3$. C_{de} in μmoles/cm^3, z in 100 μm. Capillary extending from $z = 0$ to $z = -1.5$

Eq. (7.96) was used to calculate the steady state dermal concentration along

a depth line transversing the unit cell (Fig. 7.7), and on two xy planes of the unit cell (Fig. 7.8). The depth concentration profile is linear at positive (pre-capillary) z values. The clearance of material through the point sinks (that extend in depths from 0 to -1.5) is nearly complete for the specific parameters used. The two planar plots illustrate absorption in another way. At $z = 0.3$, a plane above the capillary array, the concentration field is slightly to moderately distorted. A well is beginning to form indicating that material is most strongly absorbed at the center of the plane, as expected. At $z = -1$, deep inside the capillary array, the dimensionless concentration $\hat{C}_{\mathrm{de}}$ has been substantially decreased to approximately an order of magnitude less than its value at the $z = 0.3$ plane. The two point sinks of this plane (corresponding to absorption by the two capillary legs) may now be clearly seen.

7.3.7 Perimeter-averaged concentration and derivative thereof

The asymmetry of the problem makes the dermal concentration at the capillary surface vary along the perimeter. The representative value of the concentration is derived by averaging over the perimeter for a given capillary cross section. The goal at hand is to calculate the concentration at points along the perimeter of a capillary's cross section and then take the average around the perimeter, denoted by angle brackets $<>$ as before:

$$\begin{aligned}
\langle \hat{C}_{\mathrm{de}|a_{\mathrm{cap}}} \rangle &= \langle \hat{\alpha}\hat{z} + \hat{\beta} \rangle + \langle \sum_{i=-N_{max}}^{N_{max}} \hat{P}_i \int_{\hat{t}_i}^{\hat{t}_{i+1}} \hat{G}\left[\hat{x}, \hat{y}, \hat{z}, \hat{x}_o(\hat{t}), \hat{y}_o(\hat{t}), \hat{z}_o(\hat{t})\right] d\hat{t} \rangle \\
&= \langle \hat{\alpha}\hat{z} + \hat{\beta} \rangle + \sum_{i=-N_{max}}^{N_{max}} \hat{P}_i \langle \int_{\hat{t}_i}^{\hat{t}_{i+1}} \hat{G}\left[\hat{x}, \hat{y}, \hat{z}, \hat{x}_o(\hat{t}), \hat{y}_o(\hat{t}), \hat{z}_o(\hat{t})\right] d\hat{t} \rangle \\
&= \langle \hat{\alpha}\hat{z} + \hat{\beta} \rangle + \sum_{i=-N_{max}}^{N_{max}} \hat{P}_i \left[\langle \int_{\hat{t}_i}^{\hat{t}_{i+1}} f(\hat{x}, \hat{y}, \hat{z}, \hat{x}_o(\hat{t}), \hat{y}_o(\hat{t}), \hat{z}_o(\hat{t})) d\hat{t} \rangle \right.
\end{aligned}$$

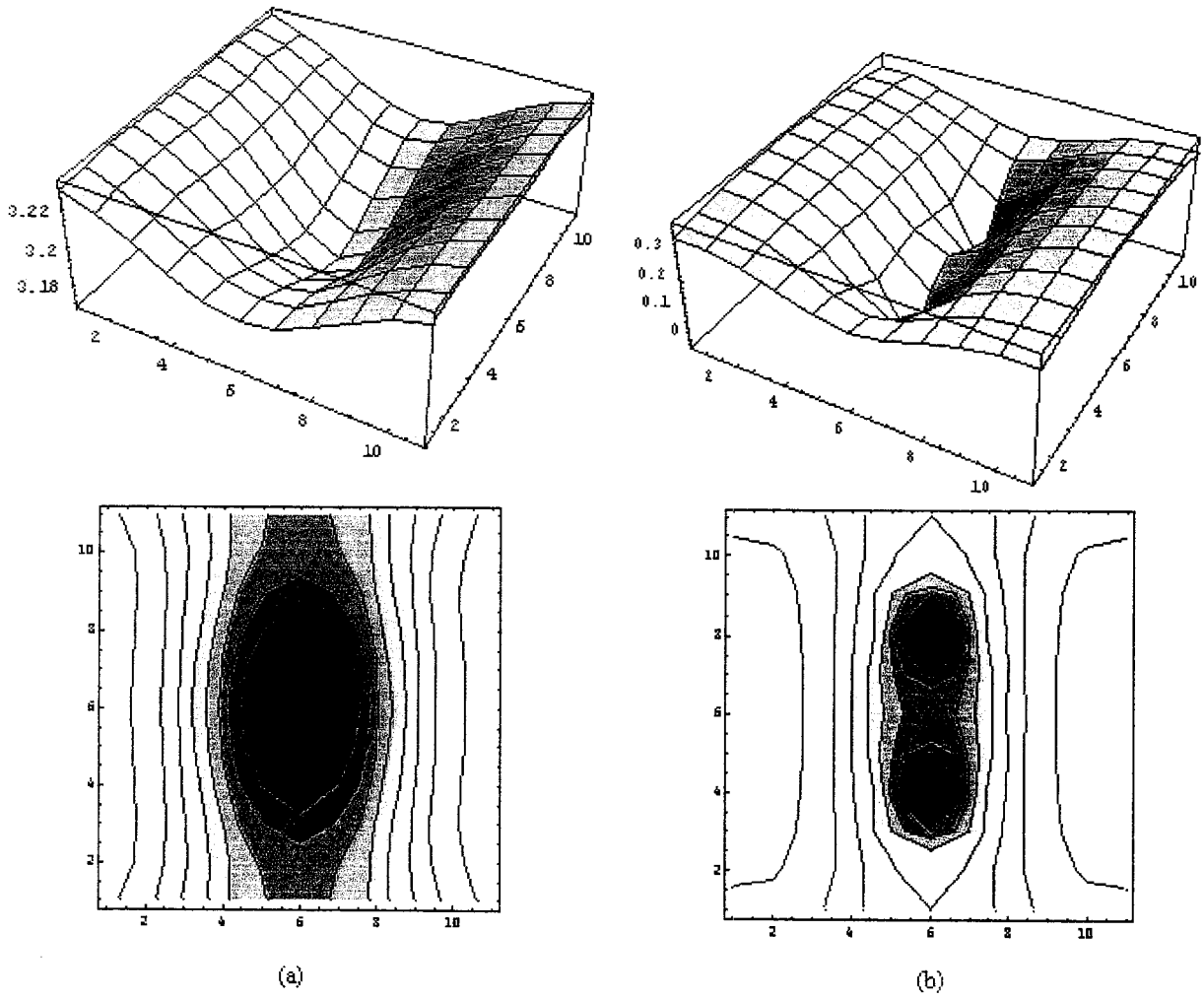

Figure 7.8: Concentration contour profiles for constant strength density $P(t) = -1$ of the point sinks. (a) plane $z = 0.3$, (b) plane $z = -1$. Dimensionless variables. In the contour plots, concentration decreases with darkness of color.

$$+ \quad \langle \int_{\hat{t}_i}^{\hat{t}_{i+1}} \frac{1}{4\pi\sqrt{(\hat{x}-\hat{x}_o(\hat{t}))^2+(\hat{y}-\hat{y}_o(\hat{t}))^2+(\hat{z}-\hat{z}_o(\hat{t}))^2}} d\hat{t} \rangle \Bigg] \quad (7.101)$$

The two parts of Green's function are treated differently. The analytical integral of $1/4/\pi/|\underline{x}-\underline{x_o}|$ over a straight segment of length h and center $\underline{x_o}$ evaluated at an arbitrary point $\underline{x}$ is calculated following the methodology described previously (Sec. 7.3.5). Assuming that this point is a point on the perimeter of a given capillary cross section, one has to evaluate this integral at different points on the perimeter. For this purpose, the local geometry involving a certain capillary segment and a cross section of another capillary segment is considered without any loss of generality (Appendix H). Through this local geometry, the arguments of the integral r, x_1, h are determined for the case where $\underline{x}$ is an arbitrary point on the perimeter of an arbitrary cross section of the capillary. Subsequently, the integral is calculated for a number of points on this perimeter. We define the location of $\underline{x}$ as:

$$\underline{x} = \underline{x_c} + a_{\text{cap}}(\vec{n}_n \cos\phi + \vec{n}_b \sin\phi) \ , \quad (7.102)$$

where $\vec{n}_n$ and $\vec{n}_b$ are the unit normal and bimodal vectors of the capillary centerline as defined previously, $\underline{x_c} = \underline{x_c}(t)$ is the center of the cross section. By varying ϕ from 0 to 2π one goes once around the perimeter and the average $< \ldots >$ corresponds to $(1/2\pi)\int_0^{2\pi} \ldots d\phi$. The integration is carried out numerically with equal weights on points around the perimeter.

For the other (singular) part of Green's function, we consider the Taylor expansion of the function f near the center point of the cross section at which the perimeter average must be calculated:

$$f(\underline{x}) \quad = \quad f(\underline{x_c}) + (\underline{x}-\underline{x_c})\vec{\nabla} f(\underline{x_c}) + \frac{1}{2}(\underline{x}-\underline{x_c})^2 \vec{\nabla}\vec{\nabla} f(\underline{x_c}) + \ldots \quad (7.103)$$

stemming from Eq. (7.102):

$$\begin{aligned} \underline{x} &= \underline{x_c} + a_{\text{cap}}(\vec{n}_n \cos\phi + \vec{n}_b \sin\phi) \Rightarrow \\ \underline{x} - \underline{x_c} &= a_{\text{cap}}(\vec{n}_n \cos\phi + \vec{n}_b \sin\phi) \Rightarrow \qquad (7.104) \\ (\underline{x} - \underline{x_c})^2 &= {a_{\text{cap}}}^2(\vec{n}_n \cos\phi + \vec{n}_b \sin\phi)^2 \qquad (7.105) \end{aligned}$$

It is evident from Eq. (7.104) that if one allows $\underline{x} - \underline{x_c}$ to vary with ϕ from 0 to 2π and then takes the average, the value is 0 when averaged around the capillary perimeter. Thus, the first-order-derivative term of the series is 0. If the second and higher order terms are neglected, the final result (to within an error of $O(\varepsilon = \frac{{a_{\text{cap}}}^2}{L^2})$) is that the perimeter-averaged value of the integral (over a straight segment $[-h/2, h/2]$) of f for a given cross section, is the value of the integral of f calculated at the center of this cross section:

$$\langle \int_{-h/2}^{h/2} f(\underline{x})dt \rangle = \int_{-h/2}^{h/2} f(\underline{x_c})dt \qquad (7.106)$$

In this way, the perimeter-averaged dermal concentration at any axial distance along the capillary wall may now be calculated through Eq. (7.101). In the governing equations, the quantity $\langle \vec{\hat{\nabla}} \hat{C}_{\text{de}|a_{\text{cap}}} \bullet \vec{n}_{\text{wall}} \rangle$ also arises. It is the gradient of the concentration, calculated at a point on the capillary perimeter, dot-multiplied by the unit normal vector at the capillary wall and averaged over the perimeter of the particular cross section:

$$\begin{aligned} \langle \vec{\hat{\nabla}} \hat{C}_{\text{de}|a_{\text{cap}}} \bullet \vec{n}_{\text{wall}} \rangle &= \langle \Big\{ \vec{\hat{\nabla}} \left(\hat{\alpha}\hat{z} + \hat{\beta} \right) \\ &+ \sum_{i=-N_{max}}^{N_{max}} \hat{P}_i \left[\vec{\hat{\nabla}} \int_{\hat{t}_i}^{\hat{t}_{i+1}} f(\hat{x}, \hat{y}, \hat{z}, \hat{x}_o(\hat{t}), \hat{y}_o(\hat{t}), \hat{z}_o(\hat{t}))d\hat{t} \right. \\ &+ \left. \vec{\hat{\nabla}} \int_{\hat{t}_i}^{\hat{t}_{i+1}} \frac{1}{4\pi\sqrt{(\hat{x} - \hat{x}_o(\hat{t}))^2 + (\hat{y} - \hat{y}_o(\hat{t}))^2 + (\hat{z} - \hat{z}_o(\hat{t}))^2}} d\hat{t} \right] \Big\} \end{aligned}$$

$$\bullet \ \vec{n}_{\text{wall}}\rangle \tag{7.107}$$

Since the scalar product is commutative and distributive:

$$\begin{aligned}
\langle\vec{\hat{\nabla}}\hat{C}_{\text{de}|a_{\text{cap}}} \bullet \vec{n}_{\text{wall}}\rangle &= \langle\vec{n}_{\text{wall}} \bullet \vec{\hat{\nabla}}\left(\hat{\alpha}\hat{z}+\hat{\beta}\right)\rangle \\
&+ \sum_{i=-N_{max}}^{N_{max}} \hat{P}_i\langle\vec{n}_{\text{wall}} \bullet \vec{\hat{\nabla}}\int_{\hat{t}_i}^{\hat{t}_{i+1}} f(\hat{x},\hat{y},\hat{z},\hat{x}_o(\hat{t}),\hat{y}_o(\hat{t}),\hat{z}_o(\hat{t}))d\hat{t}\rangle \\
&+ \sum_{i=-N_{max}}^{N_{max}} \hat{P}_i\langle\vec{n}_{\text{wall}} \\
&\bullet \ \vec{\hat{\nabla}}\int_{\hat{t}_i}^{\hat{t}_{i+1}} \frac{1}{4\pi\sqrt{(\hat{x}-\hat{x}_o(\hat{t}))^2+(\hat{y}-\hat{y}_o(\hat{t}))^2+(\hat{z}-\hat{z}_o(\hat{t}))^2}}d\hat{t}\rangle
\end{aligned} \tag{7.108}$$

The first term reduces to $\langle\hat{\alpha}\vec{n}_{\text{wall}}\rangle$ and since $\vec{n}_{\text{wall}} = \vec{n}_n\cos\phi + \vec{n}_b\sin\phi$, its average around the perimeter value is 0. The second term may be rewritten as:

$$\sum_{i=-N_{max}}^{N_{max}} \hat{P}_i\int_{\hat{t}_i}^{\hat{t}_{i+1}}\langle\vec{n}_{\text{wall}} \bullet \vec{\hat{\nabla}}f(\hat{x},\hat{y},\hat{z},\hat{x}_o(\hat{t}),\hat{y}_o(\hat{t}),\hat{z}_o(\hat{t}))\rangle d\hat{t} \tag{7.109}$$

where the order of integration has been changed, i.e., we consider first the averaging over the perimeter and second the integration over the centerline segment. Consideration of the Taylor expansion of $\vec{\hat{\nabla}}f$ leads to:

$$\sum_{i=-N_{max}}^{N_{max}} \hat{P}_i\int_{\hat{t}_i}^{\hat{t}_{i+1}}\langle\vec{n}_{\text{wall}} \bullet \left[\vec{\hat{\nabla}}f(\underline{x_c}) + (\underline{x}-\underline{x_c})\vec{\hat{\nabla}}\left(\vec{\hat{\nabla}}f(\underline{x_c})+...\right)\right]\rangle d\hat{t} \ =$$

$$\sum_{i=-N_{max}}^{N_{max}} \hat{P}_i\int_{\hat{t}_i}^{\hat{t}_{i+1}}\langle\left[\vec{n}_{\text{wall}} \bullet \vec{\hat{\nabla}}f(\underline{x_c}) + (\underline{x}-\underline{x_c})\ \vec{n}_{\text{wall}} \bullet \vec{\hat{\nabla}}\left(\vec{\hat{\nabla}}f(\underline{x_c})+...\right)\right]\rangle d\hat{t} \tag{7.110}$$

to within an error of $O(\varepsilon = \frac{{a_{\text{cap}}}^2}{L^3})$

The function f (Eq. (7.94)) is a smooth well-behaved function and its gradient will be another smooth function. The term $\vec{\hat{\nabla}}f(\underline{x_c})$ will be some constant value, for

any point $\underline{x_c}$ examined. The perimeter-average of $\vec{n}_{\text{wall}} \bullet \vec{\hat{\nabla}} f(\underline{x_c})$ will then again be 0 since the outward unit normal vector $\vec{n}_{\text{wall}}$ cancels itself out. The average of the term $(\underline{x} - \underline{x_c})\vec{n}_{\text{wall}} \bullet \vec{\hat{\nabla}} \left(\vec{\hat{\nabla}} f(\underline{x_c}) \right)$ may be neglected on the rationale that was implemented earlier (Eq. (7.104)). Thus, the second term of Eq. (7.108) may be neglected altogether with the imposement of a very small error.

For the calculation of the third term, two additional unit vectors are defined. $\vec{i}_\varsigma$ is defined by points $\underline{x_1}$ and $\underline{x_2}$ with direction towards $\underline{x_2}$, and $\vec{i}_\rho$ is defined by points $\underline{x}$ and $\underline{x_a}$ with direction towards $\underline{x_a}$ (the points defined in the definition sketch in Appendix H. The gradient of the integral is then:

$$\vec{\hat{\nabla}} I = \vec{i}_\varsigma \frac{\partial I}{\partial x_1} + \vec{i}_\rho \frac{\partial I}{\partial r} \tag{7.111}$$

where x_1 and r are the arguments of the integral. The partial derivatives of the integral with respect to x_1 and r are:

$$\begin{aligned} \frac{\partial I}{\partial x_1} &= -\frac{r}{r^2 + (h/2 - x_1)^2} \sqrt{1 + \left(\frac{h/2 - x_1}{r} \right)^2} \\ &+ \frac{r}{r^2 + (-h/2 - x_1)^2} \sqrt{1 + \left(\frac{-h/2 - x_1}{r} \right)^2} \end{aligned} \tag{7.112}$$

$$\begin{aligned} \frac{\partial I}{\partial r} &= -\frac{h/2 - x_1}{r^2 + (h/2 - x_1)^2} \sqrt{1 + \left(\frac{h/2 - x_1}{r} \right)^2} \\ &+ \frac{-h/2 - x_1}{r^2 + (-h/2 - x_1)^2} \sqrt{1 + \left(\frac{-h/2 - x_1}{r} \right)^2} \end{aligned} \tag{7.113}$$

Thus

$$\vec{n}_{\text{wall}} \cdot \left(\vec{i}_\varsigma \frac{\vartheta I}{\vartheta x_1} + \vec{i}_\rho \frac{\vartheta I}{\vartheta r} \right) = \vec{n}_{\text{wall}} \cdot \vec{i}_\varsigma \frac{\vartheta I}{\vartheta x_1} + \vec{n}_{\text{wall}} \cdot \vec{i}_\rho \frac{\vartheta I}{\vartheta r}$$

may now be constructed. Its perimeter-averaged value is calculated by again varying ϕ and taking the mean of the corresponding values.

7.3.8 Linear system of equations for the value P_i of the source line density

The unknown quantities in the governing equations are the blood concentration at any given point along the capillary and the sink density strength of every discrete segment of the centerline. The first step towards solving the problem is to use Eq. (7.68) in order to express the blood concentration in terms of the sink density strengths. This expression will take the place of C_{bl} in the right hand side of Eq. (7.68) which will in turn be equated to the right hand side of Eq. (7.69) yielding a solvable linear system of equations where the sink density strength array is the only unknown. It is:

$$\begin{aligned} Pe_{\mathrm{bl}}\frac{d\hat{C}_{\mathrm{bl}}}{d\hat{t}} &= 2\hat{P}_{\mathrm{cap}}\left(\frac{\langle\hat{C}_{\mathrm{de}|a_{\mathrm{cap}}}\rangle}{K_{\mathrm{de/w}}}-\frac{\hat{C}_{\mathrm{bl}}}{K_{\mathrm{bl/w}}}\right)\Rightarrow \\ \frac{d\hat{C}_{\mathrm{bl}}}{d\hat{t}} &= \frac{2}{Pe_{\mathrm{bl}}}\frac{\hat{P}_{\mathrm{cap}}}{K_{\mathrm{de/w}}}\langle\hat{C}_{\mathrm{de}|a_{\mathrm{cap}}}\rangle-\frac{2}{Pe_{\mathrm{bl}}}\frac{\hat{P}_{\mathrm{cap}}}{K_{\mathrm{bl/w}}}\hat{C}_{\mathrm{bl}}\Rightarrow \\ \frac{d\hat{C}_{\mathrm{bl}}}{d\hat{t}} &= -k_1\hat{C}_{\mathrm{bl}}+k_2\langle\hat{C}_{\mathrm{de}|a_{\mathrm{cap}}}\rangle \end{aligned} \tag{7.114}$$

where:

$$k_1 = \frac{2\hat{P}_{\mathrm{cap}}}{Pe_{\mathrm{bl}}K_{\mathrm{bl/w}}} \tag{7.115}$$

$$k_2 = \frac{2\hat{P}_{\mathrm{cap}}}{Pe_{\mathrm{bl}}K_{\mathrm{de/w}}} \tag{7.116}$$

The solution of Eq. (7.114) is:

$$\exp(k_1\hat{t})\frac{d\hat{C}_{\mathrm{bl}}}{d\hat{t}}+\exp(k_1\hat{t})k_1\hat{C}_{\mathrm{bl}} = \exp(k_1\hat{t})k_2\langle\hat{C}_{\mathrm{de}|a_{\mathrm{cap}}}\rangle\Rightarrow$$

$$\frac{d}{d\hat{t}}\left[\exp(k_1\hat{t})\hat{C}_{\rm bl}\right] = k_2\exp(k_1\hat{t})\langle\hat{C}_{\rm de|a_{cap}}\rangle \Rightarrow$$

$$\int_{\hat{t}_o}^{\hat{t}}\frac{d}{d\hat{t}}\left[\exp(k_1\hat{t})\hat{C}_{\rm bl}\right]d\hat{t} = \int_{\hat{t}_o}^{\hat{t}} k_2\exp(k_1\hat{t}')\langle\hat{C}_{\rm de|a_{cap}}\rangle d\hat{t}' \Rightarrow$$

$$\exp(k_1\hat{t})\hat{C}_{\rm bl}(\hat{t}) = \exp(k_1\hat{t}_o)\hat{C}_{\rm bl}(\hat{t}_o) + \int_{\hat{t}_o}^{\hat{t}} k_2\exp(k_1\hat{t}')\langle\hat{C}_{\rm de|a_{cap}}\rangle d\hat{t}' \Rightarrow$$

$$\hat{C}_{\rm bl}(\hat{t}) = \exp\left[k_1(\hat{t}_o-\hat{t})\right]\hat{C}_{\rm bl}(\hat{t}_o) + k_2\exp(-k_1\hat{t}')\int_{\hat{t}_o}^{\hat{t}}\exp(k_1\hat{t})\langle\hat{C}_{\rm de|a_{cap}}\rangle d\hat{t}' \qquad (7.117)$$

By choosing $\hat{t}_o$ to be the first permeable part of the capillary that blood enters into, $\hat{C}_{\rm bl}(\hat{t}_o) = 0$. Thus the equation becomes:

$$\hat{C}_{\rm bl}(\hat{t}) = k_2\exp(-k_1\hat{t})\int_{\hat{t}_o}^{\hat{t}}\exp(k_1\hat{t}')\langle\hat{C}_{\rm de|a_{cap}}\rangle d\hat{t}' \qquad (7.118)$$

where $\hat{t}'$ is a new dummy variable of integration. It represents the total arc length between the starting point $\hat{t}_o$ and $\hat{t}$, which is the point at which the blood concentration is calculated. Equating the right hand sides of Eq. (7.68) and Eq. (7.69) (with the use of Eqs. (7.101), (7.108), and (7.118)) yields:

$$2\hat{D}_{\rm de}\sum_{i=-N_{max}}^{N_{max}}\hat{P}_i\langle\vec{n}_{\rm wall}\bullet\vec{\hat{\nabla}}\int_{\hat{t}_i}^{\hat{t}_{i+1}}\frac{1}{4\pi\sqrt{(\hat{x}-\hat{x}_o(\hat{t}))^2+(\hat{y}-\hat{y}_o(\hat{t}))^2+(\hat{z}-\hat{z}_o(\hat{t}))^2}}d\hat{t}\rangle =$$

$$\frac{2\hat{P}_{\rm cap}}{K_{\rm de/w}}\left\{\sum_{i=-N_{max}}^{N_{max}}\hat{P}_i\langle\int_{\hat{t}_i}^{\hat{t}_{i+1}}\frac{1}{4\pi\sqrt{(\hat{x}-\hat{x}_o(\hat{t}))^2+(\hat{y}-\hat{y}_o(\hat{t}))^2+(\hat{z}-\hat{z}_o(\hat{t}))^2}}d\hat{t}\rangle + \right.$$

$$\sum_{i=-N_{max}}^{N_{max}}\hat{P}_i\int_{\hat{t}_i}^{\hat{t}_{i+1}} f(\hat{x}_c,\hat{y}_c,\hat{z}_c,\hat{x}_o(\hat{t}),\hat{y}_o(\hat{t}),\hat{z}_o(\hat{t})) +$$

$$\left.\langle\hat{\alpha}\hat{z}+\hat{\beta}\rangle\right\} -$$

$$\frac{2\hat{P}_{\rm cap}}{K_{\rm bl/w}}k_2\left\{\sum_{i=-N_{max}}^{N_{max}}\hat{P}_i\exp(-k_1\hat{t})\int_{\hat{t}_o}^{\hat{t}}\left[\exp(k_1\hat{t}')\right.\right.$$

$$\langle \int_{\hat{t}_i}^{\hat{t}_{i+1}} \frac{1}{4\pi\sqrt{(\hat{x}'-\hat{x}_o(\hat{t}))^2+(\hat{y}'-\hat{y}_o(\hat{t}))^2+(\hat{z}'-\hat{z}_o(\hat{t}))^2}} d\hat{t}\rangle d\hat{t}' \Bigg] \; -$$

$$\sum_{i=-N_{max}}^{N_{max}} \hat{P}_i \exp(-k_1\hat{t}) \int_{\hat{t}_o}^{\hat{t}} \left\{ \exp(k_1\hat{t}') \int_{\hat{t}_i}^{\hat{t}_{i+1}} f(\hat{x}'_c, \hat{y}'_c, \hat{z}'_c, \hat{x}_o(\hat{t}), \hat{y}_o(\hat{t}), \hat{z}_o(\hat{t})) d\hat{t}' \right\} \; -$$

$$\exp(-k_1\hat{t}) \int_{\hat{t}_o}^{\hat{t}} \exp(k_1\hat{t}') \langle \hat{\alpha}\hat{z}' + \hat{\beta} \rangle d\hat{t}' \Bigg\} \qquad (7.119)$$

A new summation is defined to better describe the integration with respect to the new variable ($\hat{t}'$). The terms that include the integration with this variable are broken into two parts. The first term ($\sum_1^m \int_{\hat{t}_{m-1}}^{\hat{t}_m} ...$) encompasses the integration over all the segments prior to the segment at which the blood concentration would be calculated . The second part ($\int_{\hat{t}_m}^{\hat{t}} ...$) is the integration over the segment in question. After rearranging the terms and by defining:

$$k_3 = \frac{\hat{P}_{\text{cap}}}{K_{\text{de/w}}\hat{D}_{\text{de}}} \qquad (7.120)$$

$$k_4 = \frac{\hat{P}_{\text{cap}}}{K_{\text{bl/w}}\hat{D}_{\text{de}}} k_2 \qquad (7.121)$$

Eq. (7.119) becomes:

$$\left[\sum_{i=-N_{max}}^{N_{max}} \hat{P}_i \langle \vec{n}_{\text{wall}} \bullet \vec{\hat{\nabla}} \int_{\hat{t}_i}^{\hat{t}_{i+1}} \frac{1}{4\pi\sqrt{(\hat{x}-\hat{x}_o(\hat{t}))^2+(\hat{y}-\hat{y}_o(\hat{t}))^2+(\hat{z}-\hat{z}_o(\hat{t}))^2}} d\hat{t} \rangle \right] \; -$$

$$\left[k_3 \sum_{i=-N_{max}}^{N_{max}} \hat{P}_i \langle \int_{\hat{t}_i}^{\hat{t}_{i+1}} \frac{1}{4\pi\sqrt{(\hat{x}-\hat{x}_o(\hat{t}))^2+(\hat{y}-\hat{y}_o(\hat{t}))^2+(\hat{z}-\hat{z}_o(\hat{t}))^2}} d\hat{t} \rangle \right] \; -$$

$$\left[k_3 \sum_{i=-N_{max}}^{N_{max}} \hat{P}_i \int_{\hat{t}_i}^{\hat{t}_{i+1}} f(\hat{x}_c, \hat{y}_c, \hat{z}_c, \hat{x}_o(\hat{t}), \hat{y}_o(\hat{t}), \hat{z}_o(\hat{t})) \right] \; +$$

$$\left[k_4 \sum_{i=-N_{max}}^{N_{max}} \hat{P}_i \exp(-k_1\hat{t}) \sum_1^m \int_{\hat{t}_{m-1}}^{\hat{t}_m} \left\{ \exp(k_1\hat{t}') \right.$$

$$\langle \int_{\hat{t}_i}^{\hat{t}_{i+1}} \frac{1}{4\pi\sqrt{(\hat{x}' - \hat{x}_o(\hat{t}))^2 + (\hat{y}' - \hat{y}_o(\hat{t}))^2 + (\hat{z}' - \hat{z}_o(\hat{t}))^2}} d\hat{t} \rangle d\hat{t}' \Big\} \Big] \quad +$$

$$\Big[k_4 \sum_{i=-N_{max}}^{N_{max}} \hat{P}_i \exp(-k_1 \hat{t}) \int_{\hat{t}_m}^{\hat{t}} \Big\{ \exp(k_1 \hat{t}')$$

$$\langle \int_{\hat{t}_i}^{\hat{t}_{i+1}} \frac{1}{4\pi\sqrt{(\hat{x}' - \hat{x}_o(\hat{t}))^2 + (\hat{y}' - \hat{y}_o(\hat{t}))^2 + (\hat{z}' - \hat{z}_o(\hat{t}))^2}} d\hat{t} \rangle d\hat{t}' \Big\} \Big] \quad +$$

$$\Big[k_4 \sum_{i=-N_{max}}^{N_{max}} \hat{P}_i \exp(-k_1 \hat{t}) \sum_{1}^{m} \int_{\hat{t}_{m-1}}^{\hat{t}_m} \Big\{ \exp(k_1 \hat{t}') \int_{\hat{t}_i}^{\hat{t}_{i+1}} f(\hat{x}'_c, \hat{y}'_c, \hat{z}'_c, \hat{x}_o(\hat{t}), \hat{y}_o(\hat{t}), \hat{z}_o(\hat{t})) d\hat{t}' \Big\} \Big] \quad +$$

$$\Big[k_4 \sum_{i=-N_{max}}^{N_{max}} \hat{P}_i \exp(-k_1 \hat{t}) \int_{\hat{t}_m}^{\hat{t}} \Big\{ \exp(k_1 \hat{t}') \int_{\hat{t}_i}^{\hat{t}_{i+1}} f(\hat{x}'_c, \hat{y}'_c, \hat{z}'_c, \hat{x}_o(\hat{t}), \hat{y}_o(\hat{t}), \hat{z}_o(\hat{t})) d\hat{t}' \Big\} \Big] \quad =$$

$$\Big[k_3 \langle \hat{\alpha}\hat{z} + \hat{\beta} \rangle \Big] \quad -$$

$$\Big[k_4 \exp(-k_1 \hat{t}) \sum_{1}^{m} \int_{\hat{t}_{m-1}}^{\hat{t}_m} \exp(k_1 \hat{t}') \langle \hat{\alpha}\hat{z}' + \hat{\beta} \rangle d\hat{t}' \Big] \quad -$$

$$\Big[k_4 \exp(-k_1 \hat{t}) \int_{\hat{t}_m}^{\hat{t}} \exp(k_1 \hat{t}') \langle \hat{\alpha}\hat{z}' + \hat{\beta} \rangle d\hat{t}' \Big] \quad (7.122)$$

Finally, by factoring out the sink density strength array one has:

$$\sum_{i=-N_{max}}^{N_{max}} \hat{P}_i \Big\{ \langle \vec{n}_{\text{wall}} \bullet \hat{\vec{\nabla}} \int_{\hat{t}_i}^{\hat{t}_{i+1}} \frac{1}{4\pi\sqrt{(\hat{x} - \hat{x}_o(\hat{t}))^2 + (\hat{y} - \hat{y}_o(\hat{t}))^2 + (\hat{z} - \hat{z}_o(\hat{t}))^2}} d\hat{t} \rangle \quad -$$

$$k_3 \langle \int_{\hat{t}_i}^{\hat{t}_{i+1}} \frac{1}{4\pi\sqrt{(\hat{x} - \hat{x}_o(\hat{t}))^2 + (\hat{y} - \hat{y}_o(\hat{t}))^2 + (\hat{z} - \hat{z}_o(\hat{t}))^2}} d\hat{t} \rangle \quad -$$

$$k_3 \int_{\hat{t}_i}^{\hat{t}_{i+1}} f(\hat{x}_c, \hat{y}_c, \hat{z}_c, \hat{x}_o(\hat{t}), \hat{y}_o(\hat{t}), \hat{z}_o(\hat{t})) \quad +$$

$$k_4 \exp(-k_1 \hat{t}) \sum_{1}^{m} \int_{\hat{t}_{m-1}}^{\hat{t}_m} \Big[\exp(k_1 \hat{t}')$$

$$\langle \int_{\hat{t}_i}^{\hat{t}_{i+1}} \frac{1}{4\pi\sqrt{(\hat{x}' - \hat{x}_o(\hat{t}))^2 + (\hat{y}' - \hat{y}_o(\hat{t}))^2 + (\hat{z}' - \hat{z}_o(\hat{t}))^2}} d\hat{t} \rangle d\hat{t}' \Big] \quad +$$

$$k_4 \exp(-k_1\hat{t}) \int_{\hat{t}_m}^{\hat{t}} \Big[\exp(k_1\hat{t}')$$

$$\langle \int_{\hat{t}_i}^{\hat{t}_{i+1}} \frac{1}{4\pi\sqrt{(\hat{x}' - \hat{x}_o(\hat{t}))^2 + (\hat{y}' - \hat{y}_o(\hat{t}))^2 + (\hat{z}' - \hat{z}_o(\hat{t}))^2}} d\hat{t} \rangle d\hat{t}' \Big] \quad +$$

$$k_4 \exp(-k_1\hat{t}) \sum_1^m \int_{\hat{t}_{m-1}}^{\hat{t}_m} \exp(k_1\hat{t}') \int_{\hat{t}_i}^{\hat{t}_{i+1}} f(\hat{x}'_c, \hat{y}'_c, \hat{z}'_c, \hat{x}_o(\hat{t}), \hat{y}_o(\hat{t}), \hat{z}_o(\hat{t})) d\hat{t}' \quad +$$

$$k_4 \exp(-k_1\hat{t}) \int_{\hat{t}_m}^{\hat{t}} \exp(k_1\hat{t}') \int_{\hat{t}_i}^{\hat{t}_{i+1}} f(\hat{x}'_c, \hat{y}'_c, \hat{z}'_c, \hat{x}_o(\hat{t}), \hat{y}_o(\hat{t}), \hat{z}_o(\hat{t})) d\hat{t}' \quad =$$

$$\Big[k_3 \langle \hat{\alpha}\hat{z} + \hat{\beta} \rangle\Big] \quad -$$

$$\Big[k_4 \exp(-k_1\hat{t}) \sum_1^m \int_{\hat{t}_{m-1}}^{\hat{t}_m} \exp(k_1\hat{t}') \langle \hat{\alpha}\hat{z}' + \hat{\beta} \rangle d\hat{t}'\Big] \quad -$$

$$\Big[k_4 \exp(-k_1\hat{t}) \int_{\hat{t}_m}^{\hat{t}} \exp(k_1\hat{t}') \langle \hat{\alpha}\hat{z}' + \hat{\beta} \rangle d\hat{t}'\Big] \qquad (7.123)$$

By applying Eq. (7.123) to the midpoint of each capillary segment, a linear system of equations of the form $AP(t) = B$ is formed where the only unknowns are the source densities of each segment P_i. Since the capillary has been discretized in 20 segments the linear system is comprised from 20 equations with 20 unknowns. The calculations were performed with original Fortran codes.

7.3.9 Blood and tissue concentrations calculation

Once the sink density strength array has been determined, the interstitial concentration in every point inside the unit cell can be readily calculated through the use of Eq. (7.74). Similarly the concentration in the blood along the capillary loop is found through Eq. (7.118), which in a more explicit form (by substituting $\langle \hat{C}_{\mathrm{de}|a_{\mathrm{cap}}} \rangle$) is:

$$\hat{C}_{\mathrm{bl}}(\hat{t}') = k_2 \exp(-k_1\hat{t}) \Big\{ \sum_1^m \int_{\hat{t}_{m-1}}^{\hat{t}_m} \exp(k_1\hat{t}') \langle \hat{\alpha}\hat{z}' + \hat{\beta} \rangle d\hat{t}' \quad +$$

$$\int_{\hat{t}_m}^{\hat{t}'} \exp(k_1\hat{t}')\langle\hat{\alpha}\hat{z}' + \hat{\beta}\rangle d\hat{t}' \quad +$$

$$\sum_{1}^{m} \int_{\hat{t}_{m-1}}^{\hat{t}_m} \Big[\exp(k_1\hat{t}')$$

$$\langle \int_{\hat{t}_i}^{\hat{t}_{i+1}} \frac{1}{4\pi\sqrt{(\hat{x}' - \hat{x}_o(\hat{t}))^2 + (\hat{y}' - \hat{y}_o(\hat{t}))^2 + (\hat{z}' - \hat{z}_o(\hat{t}))^2}} d\hat{t}\rangle d\hat{t}' \Big] \quad +$$

$$\int_{\hat{t}_m}^{\hat{t}'} \Big[\exp(k_1\hat{t}')$$

$$\langle \int_{\hat{t}_i}^{\hat{t}_{i+1}} \frac{1}{4\pi\sqrt{(\hat{x}' - \hat{x}_o(\hat{t}))^2 + (\hat{y}' - \hat{y}_o(\hat{t}))^2 + (\hat{z}' - \hat{z}_o(\hat{t}))^2}} d\hat{t}\rangle d\hat{t}' \Big] \quad +$$

$$\sum_{1}^{m} \int_{\hat{t}_{m-1}}^{\hat{t}_m} \exp(k_1\hat{t}') \int_{\hat{t}_i}^{\hat{t}_{i+1}} f(\hat{x}'_c, \hat{y}'_c, \hat{z}'_c, \hat{x}_o(\hat{t}), \hat{y}_o(\hat{t}), \hat{z}_o(\hat{t}))d\hat{t}' \quad +$$

$$\int_{\hat{t}_m}^{\hat{t}'} \exp(k_1\hat{t}') \int_{\hat{t}_i}^{\hat{t}_{i+1}} f(\hat{x}'_c, \hat{y}'_c, \hat{z}'_c, \hat{x}_o(\hat{t}), \hat{y}_o(\hat{t}), \hat{z}_o(\hat{t}))d\hat{t}' \qquad (7.124)$$

7.4 Results

7.4.1 Analysis with parameter values from the literature

The performance of the model was initially validated by using capillary parameters gathered from the literature (Sec. 2.7.1 & 6.2.4). The model drug used for the calculations was once again salycilic acid (Sec. 4.2). The molecular diffusivity of the substance in the dermis was determined from the skin transport model (Sec. 4.4). It was initially assumed that the partition coefficient of SA in the dermis is equal to 1 and the same was assumed for partitioning in the blood phase. Although this is probably a very good assumption for the dermis (Sec. 4.2.1, [300]), it might not be such a good one for the blood. The extensive binding of SA to serum albumin (Sec. 4.2.1) will favor partitioning to the blood phase. A blood/water partition coefficient

($K_{bl/w}$) equal to 4 might be a better representation of reality [300, 337]. However, the main goal of this study was to demonstrate the predictive power of the model. The model can be utilized for a wide range of skin-penetrating substances, thus the results obtained for the chosen specific drug were produced for illustrative purposes. In any case, the magnitude of the error introduced by the choice of the blood/water partition coefficient ($K_{bl/w}$) is discussed later (Sec. 7.7). The values of the parameters used are shown in Table 7.2.

Model drug	Salicylic acid
Diffusivity in dermis (D_{de})	7.2 10^{-7} cm^2/sec
Blood/water partition coefficient ($K_{bl/w}$)	1
Dermis/water partition coefficient ($K_{de/w}$)	1

Table 7.2: Model drug parameters for the capillary exchange model

The parameters associated with the capillary loop itself are shown in Table 7.3. The capillary permeability was the parameter with the most uncertainty, especially since salicylic acid is a small lipophilic molecule that will probably have a substantial permeability (Sec.6.2.4). Be that as it may, the value chosen was the best educated guess at the time. The values of the sink density strength of the discrete

Radius (a_{cap})	3 μm
Length (L)	300 μm
Density	100 cap./mm^2
Permeability ($P_{cap/w}$)	10^{-5} cm/sec
Blood velocity (U_{bl})	0.01 cm/sec

Table 7.3: Capillary loop parameters for the capillary exchange model

capillary segments offer valuable insight since they illustrate the pattern by which the penetrating molecule is absorbed (Fig. 7.9). The left part of this graph corresponds to the arterial leg of the loop while the right (positive x coordinate) corresponds to the venular part. The more negative the value of the density the stronger a given segment absorbs material. The minimum density value (strongest absorption) is ob-

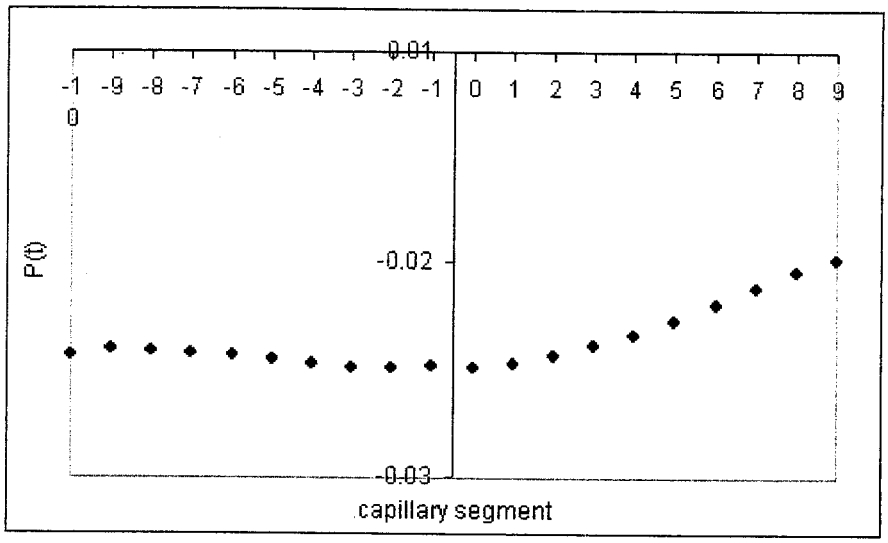

Figure 7.9: Sink density strength of the discrete capillary segments. Sink density measured in 10^{-7} μmol/cm/sec.

served at the apex of the loop. The weakest absorption is observed at the end of the venular leg, likely for two reasons. The first is location. It is the deepest permeable part; thus the concentration around it is expected to be less than that around more superficial parts. The second is blood concentration. As blood enters the loop at the arterial end, it starts picking up material and the concentration difference across the capillary wall starts to become less, its least value at the end of the venular leg where blood concentration is expected to be maximum. That is the same reason why the beginning of the arterial leg absorbs more strongly even though it is at the same depth. Blood there is drug-free and the concentration difference is larger, driving permeation through the capillary wall. The next graph (Fig. 7.10) is a depth concentration profile moving vertically near the capillary loop. The straight line depicts the aforementioned "background" concentration (Sec. 7.3.3) the concentration that would have existed, if the capillaries and the concomitant clearance process did not exist. It was chosen so the concentration would be 1 μM at the depth of the apex and that it would become 0 at the dermal-hypodermal junction. The second line cor-

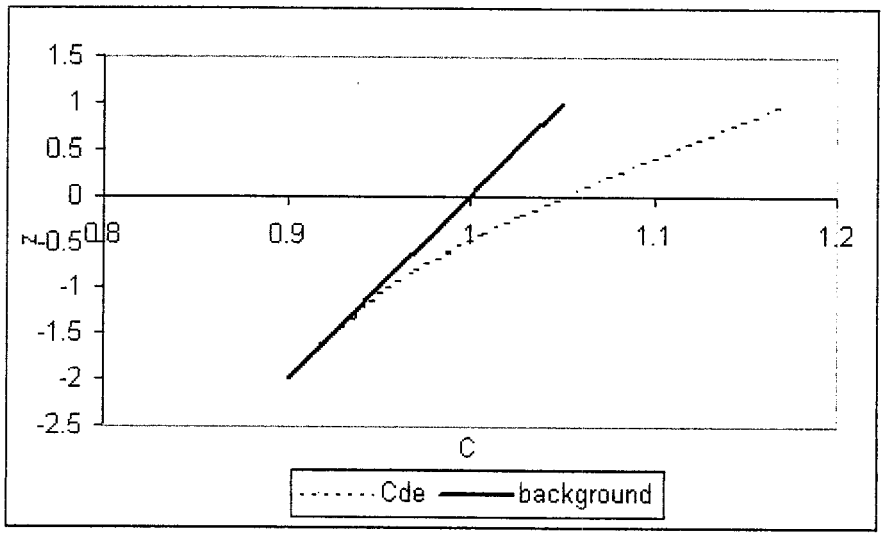

Figure 7.10: Depth concentration profile. Capillary loop extends from $z = 0$ to $z = -1.5$ (150 μm), concentration measured in μmoles/cm^3

responds to the model's prediction. It was generated with the additional restriction that the model yield the same concentration profile in below the capillary loop.

The impact that the clearance process has is the "bending" of the concentration profile. The predictive usefulness of this calculation becomes apparent if one considers the straight "background" profile as being the result of an *in vitro* steady-state experiment. Implementing this result, the model can effectively predict how much one would have to increase the flux from the donor formulation in order to have the same concentration levels at the deeper dermis *in vivo*. In the present case one would have to increase the flux 145 %. This value can be considered very low given the common knowledge of the strength of the clearance process in reality, something that increased our scepticism about the chosen parameter values. A more clear picture of the local concentration profile around the capillary is shown in Fig. 7.11. It is a planar profile corresponding to a depth level at 100 μm deeper than the capillary apex. The pattern of absorption is evident. The concentration in the blood along the

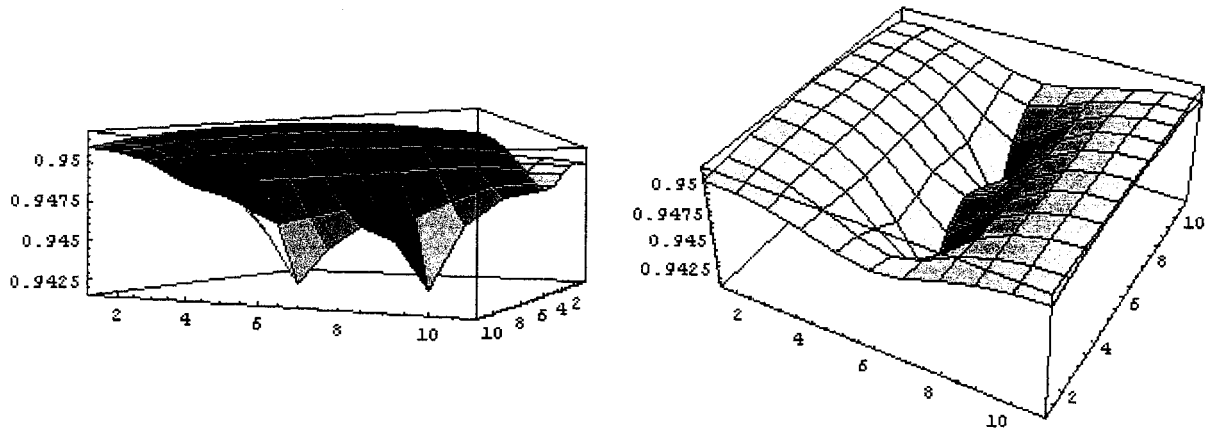

Figure 7.11: Depth planar $(x - y)$ concentration profile. The plane is located 100 μm below the apex of the capillary. x and y dimensions in 10 μm, concentration measured in μmoles/cm^3.

capillary loop is shown in Fig. 7.12. Apparently, there are no blood flow limitations, blood is picking up material steadily, in an unsaturated way. The clearance rate was calculated by multiplying the blood concentration at the end of the venular leg (assumed to be the last permeable part) with the cross section of the capillary, the blood velocity, and with the capillary density. It was found to be:

$$Cl \;=\; 4.9\ 10^{-8} \mu\text{moles/sec/mm}^2\text{skin}$$

7.4.2 Parametric study - effect of blood flow rate

The possibility of blood flow limitations/alterations on capillary clearance was investigated next. As described earlier (Sec. 2.7.4), blood flow in the capillaries may vary widely for a variety of reasons such as pathologic conditions, thermoregulation, vasoconstrictive drugs, etc. Thus, a parametric study was performed with varying the blood flow rate 4-fold and keeping every other parameter (Tables 7.2 and 7.3) the

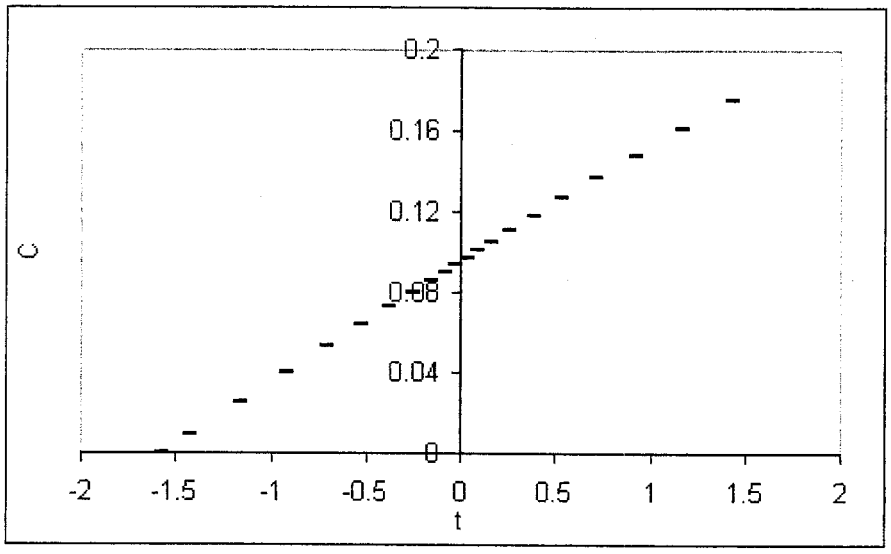

Figure 7.12: Blood concentration profile; t is the arc length variable along the capillary loop, concentration measured in μmoles/cm^3.

same. The results are presented in the same manner as in Sec. 7.4.1, and the same explanations of the nature of the results and the assumptions under which they were derived applies. The pattern of absorption along the capillary loop is quite revealing as far as the physics of the clearance process are concerned (Fig. 7.13). For relatively "normal" blood velocities ($U_{bl} = 0.1$ and 0.01 cm/sec) the sink density strength array is of the same form as before with the strongest absorption at the apex and the weakest absorption at the end of the venular leg. At blood velocity $U_{bl} = 0.001$ cm/sec the flow limitations are obvious. Blood flow is too slow, the drug concentration in the blood becomes too big too soon, the concentration gradient across the capillary wall is diminished and thus absorption is greatly reduced. At $U_{bl} = 0.0001$ cm/sec the limitations are profound, blood simply cannot accommodate the drug, and absorption is minimal.

The depth concentration profiles illustrate the same phenomenon (Fig. 7.14). At $U_{bl} = 0.0001$ cm/sec the effect of clearance is just a 7 % increase of the flux as

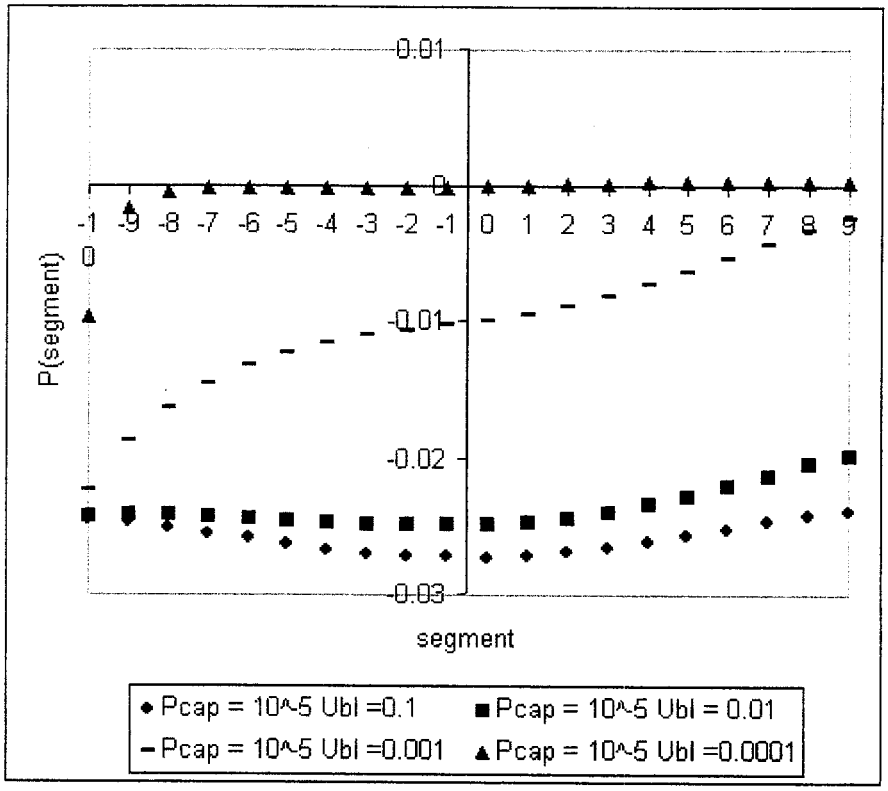

Figure 7.13: Linear sink density - Effect of blood flow rate. Sink density measured in 10^{-7} μmol/cm/sec.

shown in table 7.4. Another conclusion from the clearance rates and flux increases reported in Table 7.4 is that the clearance effect is generally low no matter what the blood velocity is. This says that the value for the capillary permeability is low (possibly uncharacteristically low).

Blood velocity (cm/sec)	0.0001	0.001	0.01	0.1
Clearance rate (10^{-8} μmoles/sec/mm^2 skin)	0.3	2.4	4.9	11
SS flux increase due to clearance (%)	6.9	69	145	158

Table 7.4: Clearance rates and flux increases with blood flow variation. The values were derived following the methodology described in Sec. 7.4.1.

The blood concentration profiles show the saturation effect even more clearly (Fig. 7.15). There is a plateau value in the case where $U_{bl} = 0.0001$ cm/sec after which absorption in the capillary practically does not occur. For the case where $U_{bl} = 0.001$

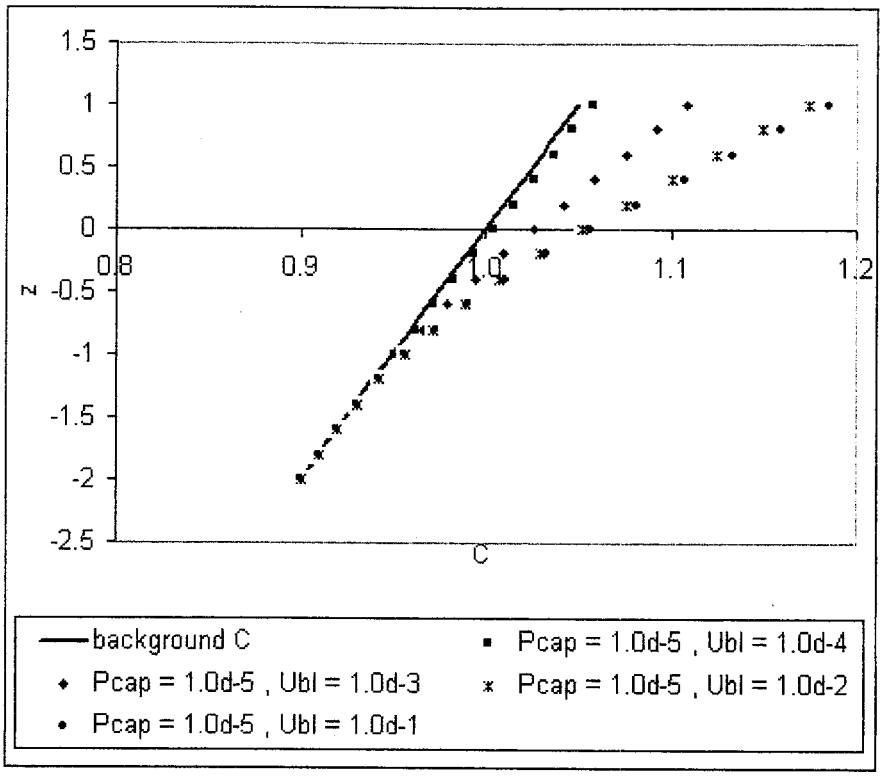

Figure 7.14: Depth concentration profile - Effect of blood flow rate

cm/sec the slight curvature indicates that this value may be the threshold below which flow limitations are manifested for this particular set of parameters.

7.4.3 Parametric study - effect of capillary permeability

It became evident from the previous results that the capillary permeability value of 10^{-5} cm/sec reported in the literature for hydrophilic molecules might be too low for salicylic acid. Thus, the capillary permeability was increased with all the other parameters (including the blood velocity which was fixed at 0.1 cm/sec) kept unchanged.

The respective sink density strength profiles (Fig. 7.16) reveal that capillary permeability is the dominant factor in terms of the amount cleared through the cap-

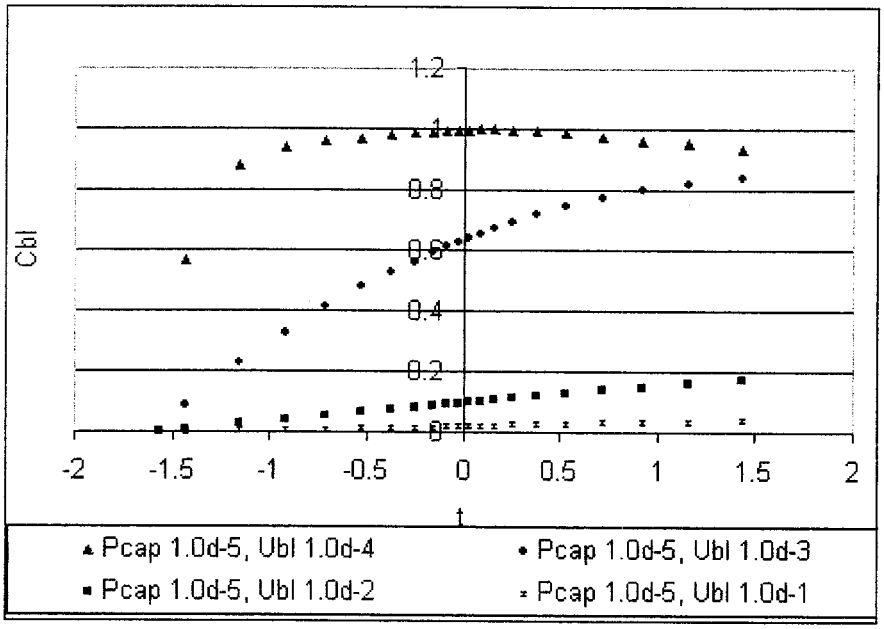

Figure 7.15: Blood concentration profile - Effect of blood flow rate

illaries. An increase of the permeability ($P_{\text{cap/w}} = 10^{-4}$ cm/sec) by an order of magnitude leads to an increase of the sink strength by an order of magnitude. The increase of the absorptive strength increases by two additional orders of magnitude with $P_{\text{cap/w}} = 10^{-3}$ cm/sec.

Another feature of the physics of the clearance process that can be seen from this graph is the possibility of reabsorption of the drug from the blood phase to the tissue phase. At $P_{\text{cap/w}} = 10^{-3}$ cm/sec positive values of the sink density strength were obtained for the last segments of the venular leg. This means that these segments are behaving as sources of material and not as sinks. The possibility of visualizing a diffusive analogue of what Starling [350] had hypothesized a century ago was very intriguing. This possibility became clearer in a subsequent set of results.

The quantitative importance of the capillary permeability is also demonstrated with the depth concentration profiles (Fig. 7.17) and the respective clearance rates

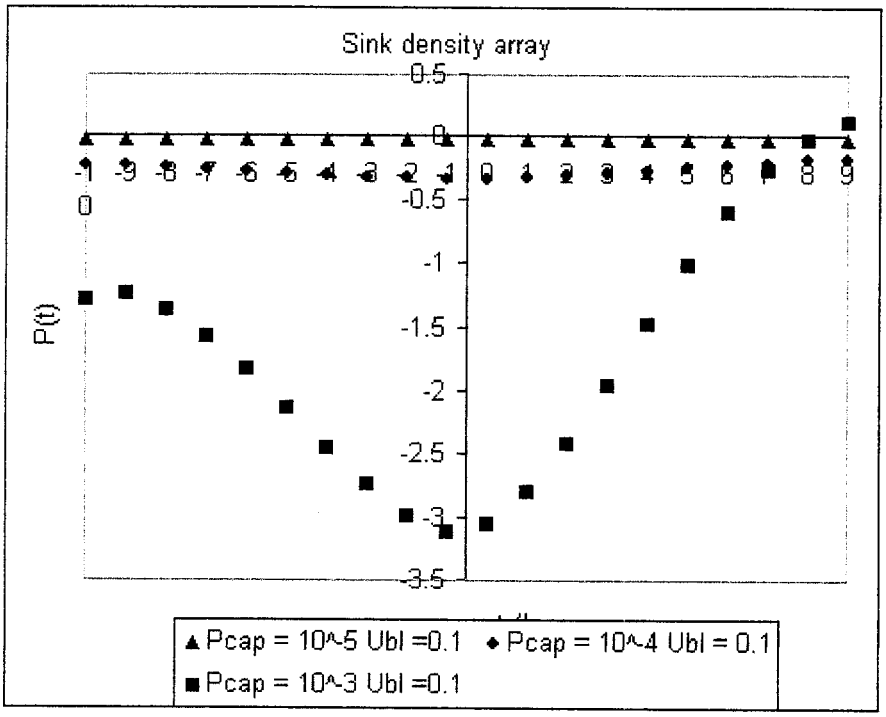

Figure 7.16: Sink density strength of the discrete capillary segments with varying capillary permeability (A). Sink density measured in 10^{-7} μmol/cm/sec.

(Table 7.5). The effect of clearance when $P_{\text{cap/w}} = 10^{-3}$ cm/sec is a flux 92 times greater than the "*in vitro*" flux and a clearance rate which is 21 times greater than the one when $P_{\text{cap/w}} = 10^{-5}$ cm/sec.

Capillary permeability (cm/sec)	10^{-5}	10^{-4}	10^{-3}
Clearance rate (10^{-8} μmoles/sec/mm^2 skin)	11	49	237
SS flux increase due to clearance (%)	158	1573	9261

Table 7.5: Clearance rates and flux increases with capillary permeability variation. The values were derived following the methodology described in Sec. 7.4.1.

The blood concentration profiles (Fig. 7.18) indicate that when $P_{\text{cap/w}} = 10^{-3}$ cm/sec blood flow limitations are present, something that explains the reabsorption to tissue at the end of the loop. This is because the concentration levels in the loop ap-

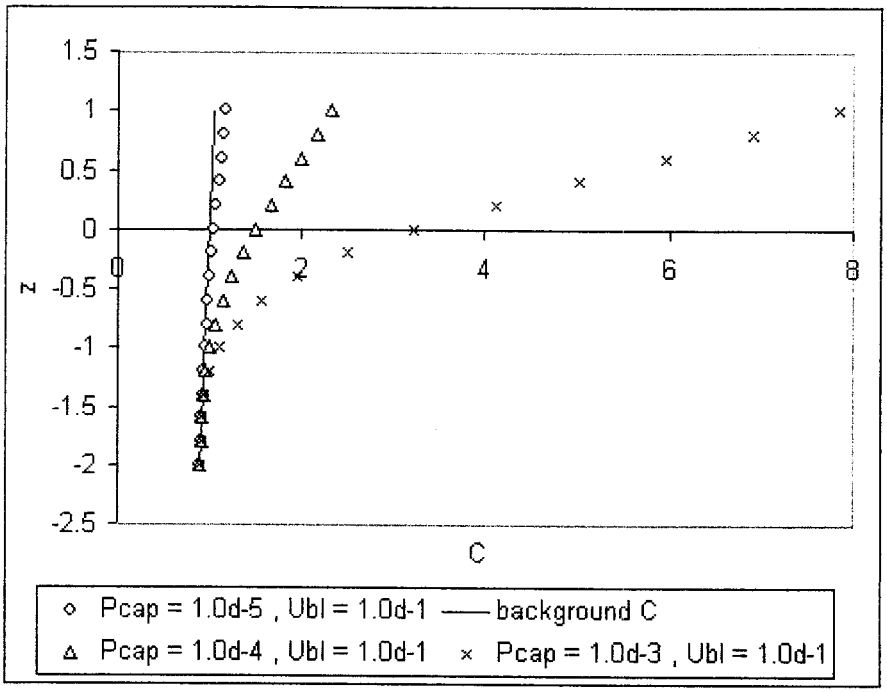

Figure 7.17: Depth concentration profile - Effect of capillary permeability

proach the value 1 μmole/cm^3 which is the (infinite-dose) steady concentration in the tissue at the depth where the apex of the capillary is located, thus the concentration gradient that causes clearance is diminished.

In order to investigate further possible blood flow limitations, yet another parametric study was performed. The capillary permeability was varied in the same manner as before with the blood velocity reduced to 0.01 cm/sec. The pattern of absorption for these cases (Fig. 7.19) that for a "high" capillary permeability, blood flow limitations may occur even when blood velocity has a "normal" value. The reabsorption phenomenon is even more profound. It appears much earlier, at almost the beginning of the venular leg and the value of the sink density strengths indicate that it is much more intense.

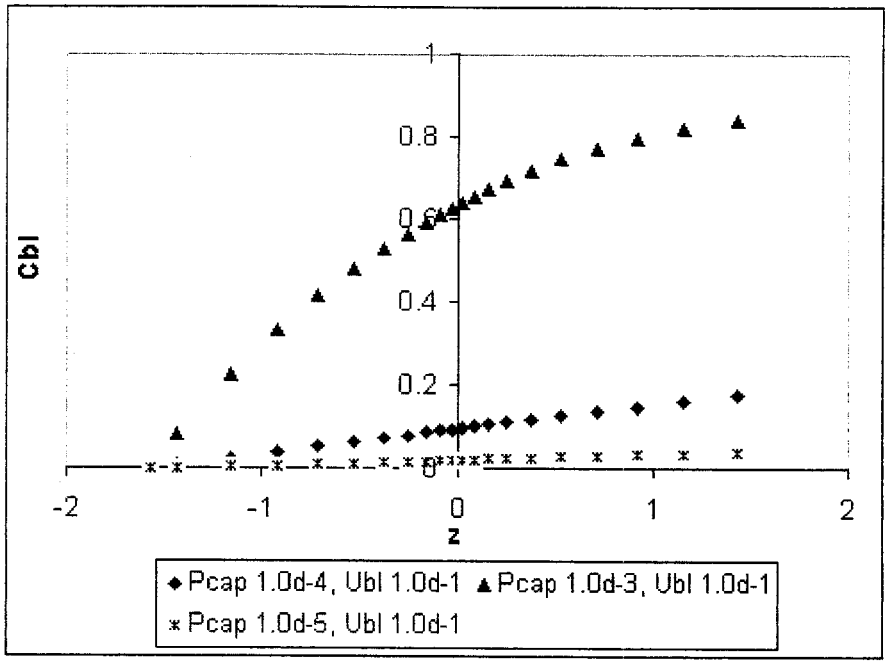

Figure 7.18: Blood concentration profile - Effect of capillary permeability

7.5 Macroscopic approach - homogeneous absorbing capillary zone

The capillary exchange model may also be embedded in the simple whole-skin transport approach (Chaps. 3 nad 4) in order to provide useful macroscopic insights on the skin transport and clearance processes. This approach is illustrated in Fig. 7.20 and it is based on the simplifying replacement of the capillaries with a finite-depth, homogeneously-absorbing, zone in the papillary dermis. The absorption of material in this zone is characterized by a first order rate constant (k_{de}). It is assumed that above the zone the drug is transported with steady state diffusion; when it reaches the absorbing zone, that has different transport properties than the rest of the skin, a certain amount will be cleared/absorbed and the rest will continue to traverse the dermis by a steady new flux. This simple model can be easily adjusted so that it produces the same clearance pattern as the more elaborate capillary model. Thus, the

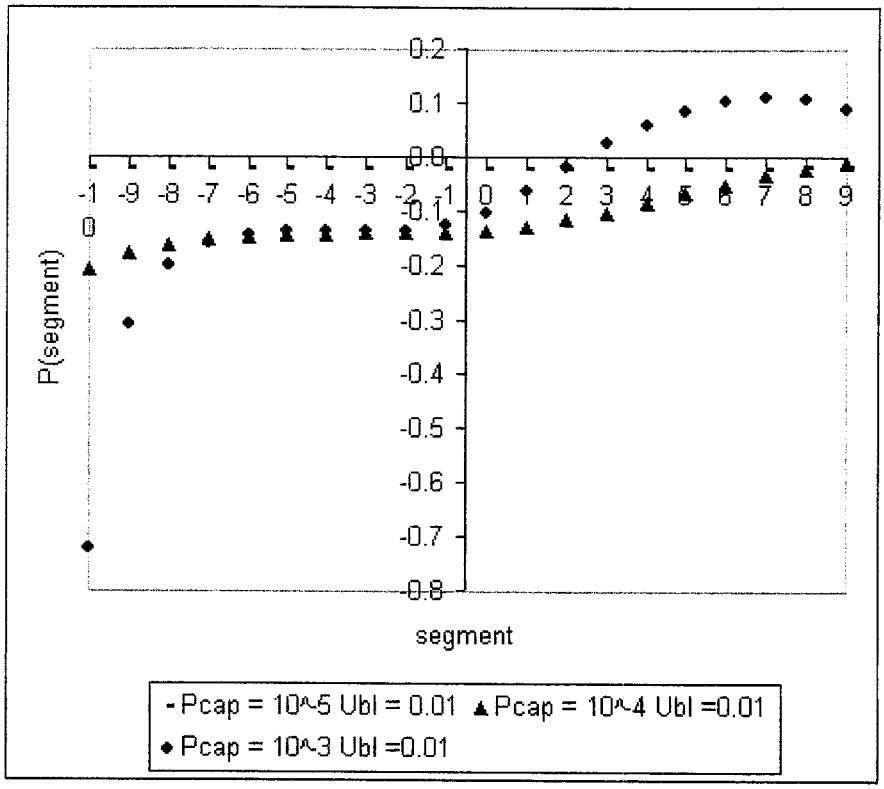

Figure 7.19: Sink density strength of the discrete capillary segments with varying capillary permeability (B). Sink density measured in 10^{-7} μmol/cm/sec.

clearance process may be characterized accurately by a simple, fictional, yet accurate 1-D representation of the capillary array.

Transport in each of the dermal zones defined in Fig. 7.20 is described by the following equations:

$$D_{\mathrm{de}}\frac{d^2C_{\mathrm{de}}}{dz^2} = 0, \quad z_1 < z < +\infty \tag{7.125}$$

$$D^*_{\mathrm{de}}\frac{d^2C_{\mathrm{de}}}{dz^2} - k_{\mathrm{de}}C_{\mathrm{de}} = 0, \quad z_2 < z < z_1 \tag{7.126}$$

$$D_{\mathrm{de}}\frac{d^2C_{\mathrm{de}}}{dz^2} = 0, \quad -\infty < z < z_2 \tag{7.127}$$

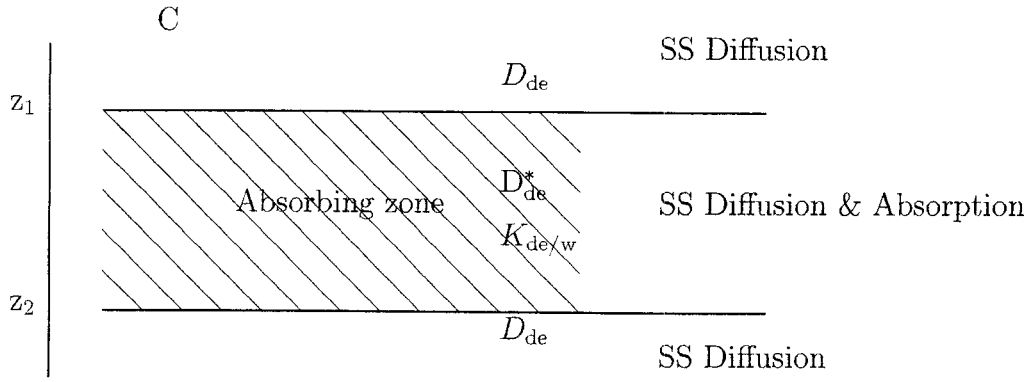

Figure 7.20: Definition sketch for the homogeneous absorbing capillary zone.

The solution of the constant-coefficient, ordinary differential Eq. (7.126) is:

$$C_{de} = C_1 \exp(\sqrt{\frac{k_{de}}{D_{de}}} z) + C_2 \exp(-\sqrt{\frac{k_{de}}{D_{de}}} z) \tag{7.128}$$

and thus:

$$\frac{dC_{de}}{dz} = C_1 \sqrt{\frac{k_{de}}{D_{de}}} \exp(\sqrt{\frac{k_{de}}{D_{de}}} z) - C_2 \sqrt{\frac{k_{de}}{D_{de}}} \exp(-\sqrt{\frac{k_{de}}{D_{de}}} z) \tag{7.129}$$

Since steady state transport is considered, and by defining the fluxes that enter the absorbing zone at $z = z_1$ and exit the absorbing zone at $z = z_2$ as a' and a respectively, one has:

$$-D^*_{de} \left. \frac{dC_{de}}{dz} \right|_{z_1} = a' \tag{7.130}$$

$$-D^*_{de} \left. \frac{dC_{de}}{dz} \right|_{z_2} = a \tag{7.131}$$

$$C_{de}|_{z_1} = a' z_1 + b' \tag{7.132}$$

$$C_{de}|_{z_2} = a z_2 + b \tag{7.133}$$

By substituting Eqs. (7.128) and (7.129) in Eqs. (7.130 - 7.133), the following system of equations arises:

$$a' = -D^*_{\rm de}\left\{C_1\sqrt{\frac{k_{\rm de}}{D_{\rm de}}}\exp(\sqrt{\frac{k_{\rm de}}{D_{\rm de}}}z_1) - C_2\sqrt{\frac{k_{\rm de}}{D_{\rm de}}}\exp(-\sqrt{\frac{k_{\rm de}}{D_{\rm de}}}z_1)\right\} \quad (7.134)$$

$$a = -D^*_{\rm de}\left\{C_1\sqrt{\frac{k_{\rm de}}{D_{\rm de}}}\exp(\sqrt{\frac{k_{\rm de}}{D_{\rm de}}}z_2) - C_2\sqrt{\frac{k_{\rm de}}{D_{\rm de}}}\exp(-\sqrt{\frac{k_{\rm de}}{D_{\rm de}}}z_2)\right\} \quad (7.135)$$

$$a'z_1 + b' = C_1\exp(\sqrt{\frac{k_{\rm de}}{D_{\rm de}}}z_1) + C_2\exp(-\sqrt{\frac{k_{\rm de}}{D_{\rm de}}}z_1) \quad (7.136)$$

$$az_2 + b = C_1\exp(\sqrt{\frac{k_{\rm de}}{D_{\rm de}}}z_2) + C_2\exp(-\sqrt{\frac{k_{\rm de}}{D_{\rm de}}}z_2) \quad (7.137)$$

This system has 4 equations and 6 unknowns (a', a, b', b, C_1, and C_2). If one fixes two of the unknowns, say, the steady state concentration profile below the absorbing zone (unknowns a and b), then the system may be readily solved for the rest of the unknowns. This may be done by adjusting (fitting) the zone parameters (depth of the zone $z_1 - z_2$ and strength of absorption $k_{\rm de}$) to the transport/clearance characteristics that the capillary model yields. The starting depth of the absorbing zone may be taken to be the same with the actual starting depth of the capillary plexus in the dermis. Thus, the two parameters (z_2 and $k_{\rm de}$) can be fitted so that the macroscopic model predicts the same amount to be cleared/absorbed and the same concentration at a fixed depth, say, 100 μm above the zone, with the capillary exchange model. Having established the parameters of the absorbing zone, one is then able to study whole-skin transport with the scheme of Fig. 7.20. This is the type of models carried out in Chaps. 3 and 4.

7.6 Second approximation - diffusion and convection

As mentioned earlier, the peri- and intra-capillary convective transport processes may or may not be important depending on the specific substance studied. Inclusion of filtration and interstitial convection increases considerably the complexity of the model. However, following the methodology previously described (Sec. 7.2.6) one is able to "correct" the results obtained with the first approximation (dominant diffusion) by adding the solution of the problem where convection is present. Although final results

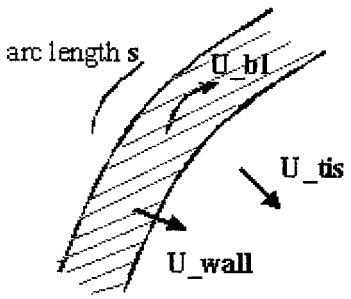

Figure 7.21: Definition sketch for the convective processes in the capillary exchange model.

for this case were not obtained, the framework of the solution was established and the equations to be solved according to the aforementioned methods were derived. A good first approach for the interstitium (Fig. 7.21) is to regard it as a porous medium, obeying Darcy's law. Thus, the average fluid velocity in tissue (the "seepage" velocity in Sec. 7.2.1) would be:

$$u_{\text{tis}} = -K_{\text{tis}} \nabla P_{\text{tis}} \tag{7.138}$$

where P is the interstitial pressure and K_{tis} is the hydrodynamic conductivity of the tissue (Sec. 6.3). Fluid may be considered incompressible, thus the continuity equation is:

$$\nabla u_{\text{tis}} = 0 \tag{7.139}$$

By combining these two equations, the pressure field in the tissue can be determined:

$$\nabla^2 P_{\text{tis}} = 0 \tag{7.140}$$

Mathematically, the problem of determining the interstitial pressure is the same with the problem of defining the tissue concentration field when the diffusive processes are dominant (Eq. (7.60)). Therefore, by using the exact same methodology previously described, one can readily solve Eq. (7.140).

The capillary wall may also be treated as a porous medium obeying Darcy's law, with the pressure-driven convective force being determined by the interplay of hydraulic and osmotic pressures:

$$u_{\text{wall}} = -K_{\text{wall}} \left[P_{\text{bl}} - \Pi_{\text{bl}} - (P_{\text{tis}} - \Pi_{\text{tis}}) \right] \tag{7.141}$$

The blood velocity is connected with the filtration velocity u_{wall} as described by Eq. (7.17):

$$\frac{du_{\text{bl}}}{ds} = -\frac{2u_{\text{wall}}}{a_{\text{cap}}} \tag{7.142}$$

If Pouiseuille's flow is assumed for the blood phase, it will be:

$$\frac{dP_{\text{bl}}}{ds} = -\left(\frac{8\mu}{\pi \rho {a_{\text{cap}}}^4} \right) u_{\text{bl}} = -\chi \, u_{\text{bl}} \tag{7.143}$$

By using Eqs. (7.141), (7.142), and (7.143) a solvable equation for the pressure of blood along the capillary arises:

$$\frac{d^2 P_{\text{bl}}}{ds^2} = \frac{2\chi}{a_{\text{cap}}} \left[P_{\text{bl}} - \Pi_{\text{bl}} - (\langle P_{\text{tis}} \rangle - \Pi_{\text{tis}}) \right] \tag{7.144}$$

where $\langle P_{\text{tis}} \rangle$ is the perimeter-averaged interstitial pressure on the capillary wall that can be determined by following the methodology described at Sec. 7.3.7. After obtaining P_{bl}, Eqs. (7.143) and (7.141) can be used for the determination of u_{bl} and u_{wall}, respectively.

7.7 Discussion

The possibility of a blood-flow limited clearance, as well as the possibility of an alteration of the pharmacological effect of a drug induced by blood flow variations, has received attention theoretically [16, 119, 171, 302, 325]. It has also been demonstrated experimentally [35, 296, 338], yet investigations on this subject are limited. It is also known that skin blood flow may reach extreme upper or lower levels, due to thermoregulation [67]. Through the results of our model, it is argued that blood flow limitations may occur with just a moderate reduction of blood flow in skin, particularly when the permeating substance can penetrate easily the microvascular barrier, i.e., a lipophilic molecule. This is another indication (Sec. 4.5) that the common, perfect-clearance, assumption may not be as universally applicable as previously thought. Certainly, more results on the clearance of several substances are needed in order to establish flow-limiting thresholds. However, first indications reveal that skin blood flow may be a critical, rate-determining variable. These results also establish the permeability of the microvascular barrier as the quantitatively dominant process. The amount of the permeating substance cleared, when there is sufficient blood flow, is very sensitive to the value of $P_{\mathrm{cap/w}}$, and it dramatically increases with an increase of the permeability. The reported in the literature value of $P_{\mathrm{cap/w}} = 10^{-5}$ cm/sec, yielded a very low clearance rate; given the uncertainty surrounding the experiments that gave rise to this value, one can not help thinking that it may be an underestimation of the true, *in vivo*, permeability, even for hydrophilic molecules.

Furthermore, our model is suitable for predicting the administration of drugs targeting the skin itself, or anatomical sites beneath it, without prior entry into the systemic circulation [89, 215, 298, 308]. Its usefulness becomes more apparent with the consideration of an accompanying, whole-skin, macroscopic approach, as described in Sec. 7.5. Within this formalism, the capillary exchange model is used to produce a

single, absorption rate constant that applies to a fictional, yet functionally accurate, homogeneously absorbing zone in the dermis. Thus, the microscopic analysis used in the language of the macroscopic 1-D diffusion/clearance analysis of Chap. 3 and 4.

As for the specific results reported herein for the microvascular clearance of salicylic acid, it is recognized that the effect of its binding to serum proteins in the blood phase may have been underestimated. As described in Sec. 4.2.1, SA binds extensively to serum albumin. It has been shown experimentally [88] that protein binding significantly affects the tissue penetration and distribution of SA. It would therefore be a very good model drug with the inclusion of the convective transport processes, since convection is the preferred transport mechanism for macromolecules. Furthermore, analysis of experimental results [337] yielded a dermis-plasma partition coefficient equal to 0.24 ± 0.04. In our case, this would translate to a blood-water partition coefficient $K_{\mathrm{bl/w}} \simeq 4$. By examining carefully Eqs. (7.115 - 7.116), (7.120 - 7.121), it becomes apparent that only certain terms of Eq. (7.123) are affected by this change. Further examination reveals that these terms become important only when the capillary permeability ($P_{\mathrm{cap/w}}$) is large. Even then, the choice of a larger blood-water partition coefficient would result to a lower value for these terms. Therefore, the error in the reported results may be considered small for most of them, and not so large for the rest of them.

Future steps will certainly include more results for a wide variety of substances with different properties. The important conclusions drawn in this work need be confirmed, while there may be general principles of capillary absorption, that can help categorize the different permeating substances, waiting to be discovered by modeling attempts such as this one. It has also been shown that, besides predicting clearance rates for a wide variety of permeants, the model has the potential of possibly addressing fundamental transport questions. One of these questions is the existence of reabsorption of material from the tissue to the blood phase. The results indicate a

possible diffusive analogue of Starling's hypothesis, and this is surely something worthy of further investigation. The model is somewhat incomplete since, in its current status, it considers diffusive processes to be dominant. This may be considered a good approximation for small molecules that do not bind appreciably with serum proteins, but it is possibly not a good depiction of reality for macromolecules or strong binders. However, the framework for including the well-documented, convective capillary leakage has been set and it is our intention to proceed along this path in the future. A further addition to the model may explicitly include the lymphatic capillary network, either deterministically like the blood capillaries, or stochastically by regarding them as a localized sink at the boundaries of the unit cell. Furthermore, it is recognized that the mathematics of transcapillary diffusion are very similar to the ones describing heat transfer from the blood to tissue. A possible important application of the model to the prediction of the very important thermoregulation process will be examined.

Appendix A

Mesh Function for the Finite Differences Calculation of the Skin Transport Model

The necessary depth mesh for the application of the finite differences scheme was generated with the use of a specialized mesh function. A first, simple, mesh function can be derived by the constriction that all grid points be equally spaced. Thus, the mesh is generated by assigning equally spaced values of the skin's depth to the grid points. Knowing the physiological depth of each skin layer (Chap. 2), the dimensionless depth boundaries for each layer are:

$$\hat{h}_{ed} = -1, \tag{A.1}$$

$$\hat{h}_{de} = -21, \tag{A.2}$$

$$\hat{h}_{hd} = -61, \tag{A.3}$$

$$\text{with } \hat{z} \in [-61, 0]. \tag{A.4}$$

By assigning 20 grid points ($n_{ed} = 20$) for the epidermal layer, the depth intervals (of thickness 1/20 or 5μm in dimensional form) yield 20 ODEs that can be solved with the use of the numerical scheme with an acceptable accuracy. Nevertheless, in order for one to achieve the same accuracy for the other two layers, one would have to

solve 400 ODEs for the dermis and 800 ODEs for the hypodermis. The computational effort of this process would be too big, therefore there is a need for a refined mesh function.

The refined mesh function takes into account the localized nature of transport through skin and clearance through the vasculature. It is intuitively known that the "important" points in skin are the interfaces between layers, where there may be intense partitioning phenomena, and the papillary dermis where most, if not all, of the clearance takes place. It is likely that the rest of the skin offers a smooth, "uneventful", and easily predictable background for transport. Thus, one should direct his attention (and the maximum possible accuracy in the calculations) to certain skin depths. The clearance process is effectively described by the distributed clearance rate constants thus one has to concentrate at the boundaries of each layer. This is done by constructing a mesh with unequal spacing. In mathematical terms, this was achieved by a change of the depth variable:

$$\hat{z} = \mathcal{F}(\zeta), \qquad \zeta \in [0,1]. \tag{A.5}$$

the number of grid points for each layer were chosen to be the same (resulting to 60 ODEs instead of 1200):

$$n_{ed} = 20, \tag{A.6}$$

$$n_{de} = 40, \tag{A.7}$$

$$n_{hd} = 60. \tag{A.8}$$

by matching the values of $\hat{z}$ and $\mathcal{F}(\zeta)$ at the boundaries of each layer, 4 equations/conditions for $\mathcal{F}(\zeta)$ take shape:

$$\text{At } \hat{h} = 0 \qquad \hat{z} = 0, \quad \zeta = \zeta_0, \quad n = 0, \qquad \zeta_0 = \frac{0}{n_{hd}} = 0, \tag{A.9}$$

$$\text{At } \hat{h}_{ed} = -1 \quad \hat{z} = -1, \quad \zeta = \zeta_1, \quad n_{ed} = 20, \quad \zeta_1 = \frac{n_{ed}}{n_{hd}} = \frac{1}{3}, \tag{A.10}$$

$$\text{At } \hat{h}_{de} = -21 \quad \hat{z} = -21, \quad \zeta = \zeta_2, \quad n_{de} = 40, \quad \zeta_2 = \frac{n_{de}}{n_{hd}} = \frac{2}{3}, \tag{A.11}$$

$$\text{At } \hat{h}_{hd} = -61 \quad \hat{z} = -61, \quad \zeta = \zeta_3, \quad n_{hd} = 60, \quad \zeta_0 = \frac{n_{hd}}{n_{hd}} = 1. \tag{A.12}$$

thus,

$$\mathcal{F}(0) = 0, \tag{A.13}$$

$$\mathcal{F}\left(\frac{1}{3}\right) = -1, \tag{A.14}$$

$$\mathcal{F}\left(\frac{2}{3}\right) = -21, \tag{A.15}$$

$$\mathcal{F}(1) = -61. \tag{A.16}$$

The form of the function $\mathcal{F}$ is chosen such that the thickness of the intervals for the finite differences formulation depends on the slope of the function. This slope changes every time we consider a deeper skin layer by adding another term in the mesh function:

$$\hat{z} = \mathcal{F}(\zeta) = e_0\zeta + e_1\mathcal{G}(\zeta - \zeta_1) + e_2\mathcal{G}(\zeta - \zeta_2). \tag{A.17}$$

with e_0, e_1, e_2 being the slopes of the function that are added consecutively each time the depth crosses into another skin layer. $\mathcal{G}$ is another function that determines how the transition from one slope to the next (one skin layer to the next) takes place. For an "ideal", "sudden" transition (Fig. A.1) this function is simply:

$$\mathcal{G}(\mathrm{a}) = \begin{cases} 0 & \text{if a} \leq 0 \\ \mathrm{a} & \text{if a} \succ 0 \end{cases} \tag{A.18}$$

The slopes are calculated by solving consecutively their definitive equations:

$$e_0 = \frac{\hat{z}_1 - \hat{z}_0}{\zeta_1 - \zeta_0} = -3, \tag{A.19}$$

$$e_0 + e_1 = \frac{\hat{z}_2 - \hat{z}_1}{\zeta_2 - \zeta_1} \Rightarrow e_1 = -57, \tag{A.20}$$

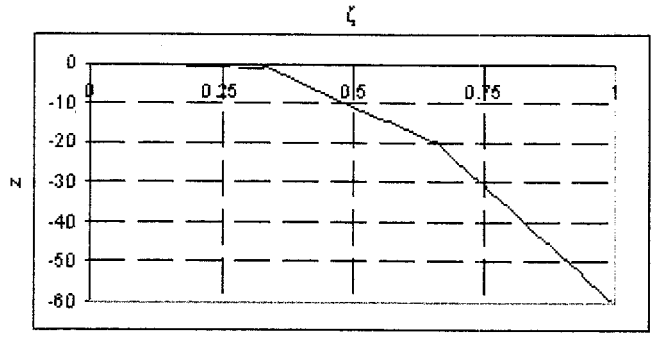

Figure A.1: Ideal transition of the mesh function between skin layers.

$$e_0 + e_1 + e_2 \;=\; \frac{\hat{z}_3 - \hat{z}_2}{\zeta_3 - \zeta_2} \;\Rightarrow\; e_2 = -60. \tag{A.21}$$

thus, the mesh function is:

$$\mathcal{F}(\zeta) \;=\; \begin{cases} -3\zeta & 0 \le \zeta \le \frac{1}{3} \\ -3\zeta - 57(\zeta - \zeta_1) & \frac{1}{3} \le \zeta \le \frac{2}{3} \\ -3\zeta - 57(\zeta - \zeta_1) - 60(\zeta - \zeta_2) & \frac{2}{3} \le \zeta \le 1 \end{cases} \tag{A.22}$$

However, the transition from one skin layer to the next should be a smooth one and thus a more complex $\mathcal{G}$ function has to be employed:

$$\mathcal{G} \;=\; \frac{1}{2}\ln\left(1 + e^{2a}\right). \tag{A.23}$$

by defining $\mathcal{F}$ as:

$$\hat{z} \;=\; \mathcal{F}(\zeta) \;=\; e_0\zeta + e_1\mathcal{G}\left(\frac{\zeta - \zeta_1}{k_1}\right) + e_2\mathcal{G}\left(\frac{\zeta - \zeta_2}{k_2}\right) + C_o \tag{A.24}$$

one is able to control the number of depth intervals around the interfaces that are employed in the transition from one slope to another by controlling the values of k_1 and k_2. The four unknowns (the three slopes and the constant C_o) were determined by solving the system of Eq. (A.13 - A.16) for various k_1 - k_2 combinations (Table A.1).

	e_0	e_1	e_2	C_o
Ideal	-3	-57	60	—
$k_1 = k_2 = 5/60$	2.37	-62	-66	$8.7\ 10^{-4}$
$k_1 = k_2 = 2/60$	-0.96	-58.93	-62.27	$2\ 10^{-9}$
$k_1 = k_2 = 1/60$	-2	-57.95	-61.11	0

Table A.1: Determination of mesh function parameters

Thus, the final version of the mesh function is:

$$\begin{aligned} \mathcal{F}(\zeta) &= -0.96\zeta - \frac{58.93}{2} \ln\left\{1 + \exp\left[2\left(\frac{\zeta - \zeta_1}{2/60}\right)\right]\right\} - \\ &- \frac{62.27}{2} \ln\left\{1 + \exp\left[2\left(\frac{\zeta - \zeta_2}{2/60}\right)\right]\right\} + 2\ 10^{-9} \end{aligned} \tag{A.25}$$

Appendix B

Calculation of the Molecular Diffusivity of Salicylic Acid in Water and Octanol

The molecular diffusivities were calculated with Scheidel's equation (Eq. (B.1), [287] pp. 286).

$$D_{\text{mol}} = 8.2\ 10^{-8}\ \frac{\left[1 + \left(3\ \frac{V_{\text{sol}}}{V_{\text{drug}}}\right)^{2/3}\right]\ T}{\mu_{\text{sol}}\ V_{\text{drug}}^{1/3}}, \tag{B.1}$$

with

$D_{\text{mol}} \equiv$ molecular diffusivity in cm^2/sec,

$V \equiv$ molecular volume in cm^3/gmole,

$T \equiv$ temperature in Kelvin,

$\mu \equiv$ viscocity in cP.

The molecular volumes were calculated with Schroeder's method ([287], pp. 52) and were checked with Lebas method [287]. The value of the molecular volume of water used in the calculations came from the literature (18.7 cm^3/gmole).

$$V_{\text{H}_2\text{O}} = 21\ \text{cm}^3/\text{gmole}, \tag{B.2}$$

$$V_{SA} = 126 \text{ cm}^3/\text{gmole}, \tag{B.3}$$

$$V_{oct} = 189 \text{ cm}^3/\text{gmole}. \tag{B.4}$$

The viscosities of water and octanol at 37°C (skin temperature) were calculated with Eq. (B.5).

$$\mu = \frac{Nh}{V} \exp\left(3.8 \frac{T_b}{T}\right), \tag{B.5}$$

with

$N \equiv$ Avogadro number $6.023\ 10^{23}$ gmole^{-1},

$h \equiv$ Planck number $6.624\ 10^{-27}$ g/cm^2/sec,

$T_b \equiv$ boiling temperature in Kelvin.

They were found to be in agreement with published experimental values:

$$\mu_{H_2O} = 0.695 \text{ cP}, \tag{B.6}$$

$$\mu_{oct} = 4.83 \text{ cP}. \tag{B.7}$$

Finally, the calculated molecular diffusivities of salicylic acid in water and octanol are:

$$D_{mol/H_2O} = 1.15 \text{ cm}^2/\text{sec}, \tag{B.8}$$

$$D_{mol/oct} = 0.39 \text{ cm}^2/\text{sec}. \tag{B.9}$$

Appendix C

Application of the Finite Fourier Transform on Non-Steady State Calculations in Epidermal (or Dermatomed) Skin Transport

The (normalized) equations describing the non-steady state, unidimensional, diffusion through epidermis, assuming absolute clearance at its end, are :

$$\frac{\vartheta C}{\vartheta t} = D_{\mathrm{ed}} \frac{\vartheta^2 C}{\vartheta z^2}, \quad t \succ 0, \quad -1 \prec z \prec 0, \tag{C.1}$$

$$D_{\mathrm{ed}} \frac{\vartheta C}{\vartheta z} = P_{\mathrm{sc/w}} \left(\frac{C_{\mathrm{sol}}}{K_{\mathrm{sol/w}}} - \frac{C}{K_{\mathrm{ed/w}}} \right), \quad t \succ 0, \quad z = 0, \tag{C.2}$$

$$C = 0, \quad t \succ 0, \quad z = -1, \tag{C.3}$$

$$C = 0, \quad t = 0, \quad -1 \prec z \prec 0. \tag{C.4}$$

The same formulation may be applied to the case of dermatomed skin, or fat-free, whole thickness skin with a perfect clearance/removal at a certain depth if one assumes that the transport properties of epidermis and dermis (diffusivities/partition

coefficients) are similar. By setting for simplicity:

$$a = D_{\mathrm{ed}}, \tag{C.5}$$

$$b = \frac{P_{\mathrm{sc/w}}}{D_{\mathrm{ed}} K_{\mathrm{ed/w}}}, \tag{C.6}$$

$$c = \frac{P_{\mathrm{sc/w}} C_{\mathrm{sol}}}{D_{\mathrm{ed}} K_{\mathrm{sol/w}}}. \tag{C.7}$$

the problem is transformed:

$$\frac{\vartheta C}{\vartheta t} = a \frac{\vartheta^2 C}{\vartheta z^2}, \quad t \succ 0, \quad -1 \prec z \prec 0 \tag{C.8}$$

$$\frac{\vartheta C}{\vartheta z} + bC = c, \quad t \succ 0, \quad z = 0 \tag{C.9}$$

$$C = 0, \quad t \succ 0, \quad z = -1 \tag{C.10}$$

$$C = 0, \quad t = 0, \quad -1 \prec z \prec 0 \tag{C.11}$$

For its solution, the finite Fourier transform (FFT) method was followed, as described by Deen [100]. The first step of this method is to find the basis functions (eigenfunctions) of the problem $(\Phi_n(z))$. In order to do so, one must identify the boundary conditions that must be satisfied by $\Phi_n(z)$ by substituting to the homogeneous form of the original boundary conditions, a non-trivial solution of the form $C(z,t) = \Phi_n(z)\ Y(t)$:

$$\begin{aligned} C(-1,t) &= 0 \Rightarrow \\ \Phi_n(-1)\ Y(t) &= 0 \Rightarrow \\ \Phi_n(-1) &= 0 \text{ and} \\ \frac{\vartheta C(0,t)}{\vartheta z} + b\ C(0,t) &= 0 \Rightarrow \\ Y(t)\ \frac{d\Phi_n(0)}{dz} + bY(t)\Phi_n(0) &= 0 \Rightarrow \end{aligned} \tag{C.12}$$

$$\Phi_n'(0) + b\Phi_n(0) = 0. \tag{C.13}$$

thus, the associated eigenvalue problem has one Robin and one Dirichlet condition:

$$\Phi'' = -\lambda^2\Phi, \tag{C.14}$$

$$\Phi(-1) = 0, \tag{C.15}$$

$$\Phi'(0) + b\Phi(0) = 0. \tag{C.16}$$

by exploring the possible values of λ (positive, negative, zero) it is evident that :

- If $\lambda \prec 0$ then the problem has no solution.
- If $\lambda = 0$ then the problem has only the trivial solution :

$$\begin{aligned} \Phi'' &= 0 \Rightarrow \\ \Phi' &= A \Rightarrow \\ \Phi &= Az + B \text{ and} \end{aligned} \tag{C.17}$$

$$\begin{aligned} \Phi(-1) &= 0 \Rightarrow \\ A - B &= 0 \Rightarrow \\ A &= B \text{ and} \end{aligned} \tag{C.18}$$

$$\begin{aligned} \Phi'(0) + b\Phi(0) &= 0 \Rightarrow \\ A + bB &= 0 \Rightarrow \\ A(1+b) &= 0 \Rightarrow \\ A = B &= 0 \end{aligned} \tag{C.19}$$

- If $\lambda \succ 0$ then the problem has a non-trivial solution:

$$\Phi = A\sin(\lambda z) + B\cos(\lambda z) \tag{C.20}$$

$$\Phi' = \lambda A\cos(\lambda z) - \lambda B\sin(\lambda z) \tag{C.21}$$

$$\Phi'(0) + b\Phi(0) = 0 \Rightarrow$$

$$\begin{aligned}
\lambda A + bB &= 0 \Rightarrow \\
B &= -\frac{\lambda}{b} \text{ and} \qquad \text{(C.22)} \\
\Phi(-1) &= 0 \Rightarrow \\
A\sin(-\lambda) + B\cos(-\lambda) &= 0 \Rightarrow \\
-A\sin\lambda + B\cos\lambda &= 0 \Rightarrow \\
-A\sin\lambda - \frac{\lambda}{b}A\cos\lambda &= 0 \Rightarrow \\
-A\left[\sin\lambda + \frac{\lambda}{b}\cos\lambda\right] &= 0 \Rightarrow \\
\sin\lambda &= -\frac{\lambda}{b}\cos\lambda \Rightarrow \\
\tan\lambda &= -\frac{\lambda}{b}. \qquad \text{(C.23)}
\end{aligned}$$

which is the characteristic equation of the problem. Thus, the basis function is :

$$\Phi_n(z) = A_n\left[\sin(\lambda z) - \frac{\lambda}{b}\cos(\lambda z)\right]. \qquad \text{(C.24)}$$

The coefficient A_n is found through the restriction that Φ_n be orthonormal. It has to be :

$$\int_{-1}^{0}\Phi_n(z)\Phi_m(z)w(z)dz = \delta_{nm} = \begin{cases} 0 & \text{if } n \neq m \\ 1 & \text{if } n = m \end{cases} \qquad \text{(C.25)}$$

but the functions are self-adjoint so the condition for orthonormality is :

$$\begin{aligned}
\int_{-1}^{0}\left[\Phi_n\right]^2 dz &= 1 \Rightarrow \\
A_n^2\int_{-1}^{0}\left[\sin(\lambda z) - \frac{\lambda}{b}\cos(\lambda z)\right]^2 dz &= 1 \Rightarrow \\
A_n^2\left\{\int_{-1}^{0}\sin^2(\lambda z)dz + \frac{\lambda^2}{b^2}\int_{-1}^{0}\cos^2(\lambda z)dz - 2\frac{\lambda}{b}\int_{-1}^{0}\sin(\lambda z)\cos(\lambda z)dz\right\} &= 1. \qquad \text{(C.26)}
\end{aligned}$$

The values of the three integrals involved are :

- $$\begin{aligned}\int_{-1}^{0}\sin^2(\lambda z)dz &= \int_{-1}^{0}\left[\frac{1}{2}-\frac{\cos(2\lambda z)}{2}\right]dz \\ &= \frac{1}{2}\int_{-1}^{0}(z)'dz-\frac{1}{2}\frac{1}{2\lambda}\int_{-1}^{0}[\sin(2\lambda z)]'dz \\ &= \frac{1}{2}[0-(-1)]-\frac{1}{4\lambda}[0-\sin(-2\lambda)] \\ &= \frac{1}{2}-\frac{\sin(2\lambda)}{4\lambda} \end{aligned} \tag{C.27}$$

- $$\begin{aligned}\int_{-1}^{0}\cos^2(\lambda z)dz &= \int_{-1}^{0}\left[1-\sin^2(\lambda z)\right]dz \\ &= 1-\frac{1}{2}+\frac{\sin(2\lambda)}{4\lambda} \\ &= \frac{1}{2}+\frac{\sin(2\lambda)}{4\lambda} \end{aligned} \tag{C.28}$$

- $$\begin{aligned}\int_{-1}^{0}\sin(\lambda z)\cos(\lambda z)dz &= \int_{-1}^{0}\left[\frac{\sin(2\lambda z)}{2}\right]dz \\ &= \frac{1}{2}\frac{1}{2\lambda}\int_{-1}^{0}[-\cos(2\lambda z)]'dz \\ &= \frac{1}{4\lambda}[-1-\cos(-2\lambda)] \\ &= \frac{\cos(2\lambda)}{4\lambda}-\frac{1}{4\lambda} \end{aligned} \tag{C.29}$$

thus, Eq. (C.26) becomes :

$$A_n^2\left\{\frac{1}{2}-\frac{\sin(2\lambda)}{4\lambda}+\frac{\lambda^2}{2b^2}+\frac{\lambda\sin(2\lambda)}{4b^2}-\frac{\cos(2\lambda)}{2b}+\frac{1}{2b}\right\} = 1 \Rightarrow$$

$$A_n^2\left\{\frac{2\lambda b^2-b^2\sin(2\lambda)+2\lambda^3+\lambda^2\sin(2\lambda)-2\lambda b\cos(2\lambda)+2\lambda b}{4\lambda b^2}\right\} = 1 \Rightarrow$$

$$A_n^2\left\{\frac{2\lambda\left[\lambda^2+b^2\right]+\sin(2\lambda)\left[\lambda^2-b^2\right]+2\lambda b\left[1-\cos(2\lambda)\right]}{4\lambda b^2}\right\} = 1 \Rightarrow$$

$$A_n^2\left\{\frac{2\lambda\left[\lambda^2+b^2\right]+2\sin\lambda\cos\lambda\left[\lambda^2-b^2\right]+4\lambda b\sin^2\lambda}{4\lambda b^2}\right\} = 1 \Rightarrow$$

$$A_n=\sqrt{\frac{2\lambda b^2}{\lambda\left[\lambda^2+b^2\right]+\sin\lambda\cos\lambda\left[\lambda^2-b^2\right]+2\lambda b\sin^2\lambda}}. \tag{C.30}$$

Having found the z dependence of the solution, one is able to apply the FFT in order to extract the part of the solution that depends on t, namely the $\Theta_n(t)$ function :

$$\frac{\vartheta C}{\vartheta t}-a\frac{\vartheta^2 C}{\vartheta z^2}=0 \longrightarrow \int_{-1}^{0}\Phi_n(z)\left[\frac{\vartheta C}{\vartheta t}-a\frac{\vartheta^2 C}{\vartheta z^2}\right]dz=0. \tag{C.31}$$

The first term becomes :

$$\begin{aligned}\int_{-1}^{0}\Phi_n(z)\frac{\vartheta C}{\vartheta t}dz &= \frac{\vartheta}{\vartheta t}\int_{-1}^{0}\Phi_n(z)C(z,t)dz \\ &= \frac{d\Theta_n(t)}{dt},\end{aligned} \tag{C.32}$$

since by definition:

$$\Theta_n(t) = \int_{-1}^{0}\Phi_n(z)C(z,t)dz. \tag{C.33}$$

The second term is :

$$\begin{aligned}\int_{-1}^{0}\Phi_n(z)-a\frac{\vartheta^2 C}{\vartheta z^2}dz &= -a\left\{\left[\Phi_n(z)\frac{\vartheta C}{\vartheta z}\right]_{-1}^{0}-\int_{-1}^{0}\frac{\vartheta\Phi_n(z)}{\vartheta z}\frac{\vartheta C}{\vartheta z}dz\right\} \\ &= -a\left\{\left[\Phi_n(z)\frac{\vartheta C}{\vartheta z}\right]_{-1}^{0}-\left[C\frac{\vartheta\Phi_n(z)}{\vartheta z}\right]_{-1}^{0}+\int_{-1}^{0}\frac{\vartheta^2\Phi_n(z)}{\vartheta z^2}Cdz\right\}\end{aligned} \tag{C.34}$$

It is known that:

$$\Phi_n = -1 \quad \text{and} \quad C(-1,t) = 0 \tag{C.35}$$

so the equation becomes :

$$\begin{aligned}\int_{-1}^{0}\Phi_n(z)-a\frac{\vartheta^2 C}{\vartheta z^2}dz &= -a\left\{\left(\Phi_n(z)\frac{\vartheta C}{\vartheta z}\right)\Big|_0-\left(\frac{\vartheta\Phi_n(z)}{\vartheta z}C\right)\Big|_0+\int_{-1}^{0}\frac{\vartheta^2\Phi_n(z)}{\vartheta z^2}Cdz\right\}\\ &= -a\left\{\Phi_n(0)\frac{\vartheta C(0,t)}{\vartheta z}-\frac{\vartheta\Phi_n(0)}{\vartheta z}C(0,t)+\int_{-1}^{0}\frac{\vartheta^2\Phi_n(z)}{\vartheta z^2}Cdz\right\} \quad \text{(C.36)}\end{aligned}$$

by inspecting the boundary conditions that Φ_n and C satisfy we get :

$$\frac{\vartheta\Phi_n(0)}{\vartheta z} = -b\Phi_n(0) \text{ and} \quad \text{(C.37)}$$

$$\frac{\vartheta C(0,t)}{\vartheta z}+bC(0,t) = c. \quad \text{(C.38)}$$

It is also true that :

$$\begin{aligned}\frac{\vartheta\Phi_n(z)}{\vartheta z} &= A_n\left[\lambda\cos(\lambda z)+\frac{\lambda^2}{b}\sin(\lambda z)\right]\Rightarrow\\ \frac{\vartheta^2\Phi_n(z)}{\vartheta z^2} &= A_n\left[-\lambda^2\sin(\lambda z)+\frac{\lambda^3}{b}\cos(\lambda z)\right]\Rightarrow\\ &= \lambda^2\Phi_n(z) \quad \text{(C.39)}\end{aligned}$$

thus,

$$\begin{aligned}\int_{-1}^{0}\frac{\vartheta^2\Phi_n(z)}{\vartheta z^2}Cdz &= -\lambda^2\int_{-1}^{0}\Phi_n(z)Cdz\\ &= -\lambda^2\Theta_n(t). \quad \text{(C.40)}\end{aligned}$$

thus, by substituting the second term becomes :

$$\begin{aligned}\int_{-1}^{0}\Phi_n(z)-a\frac{\vartheta^2 C}{\vartheta z^2}dz &= -a\left\{\Phi_n(0)\left[c-bC(0,t)\right]+b\Phi_n(0)C(0,t)-\lambda^2\Theta_n(t)\right\}\\ &= a\lambda^2\Theta_n(t)-ac\Phi_n(0). \quad \text{(C.41)}\end{aligned}$$

Combining the first and second term yields an ODE with $\Theta_n(t)$ as the unknown:

$$\frac{d\Theta_n(t)}{dt}+a\lambda^2\Theta_n(t) = ac\Phi_n(0) \quad \text{(C.42)}$$

and since the initial condition is $C = 0$ then it will be $\Theta_n(0) = 0$. It is :

$$\begin{aligned}
\left[\frac{d\Theta_n(t)}{dt} + a\lambda^2\Theta_n(t)\right]\exp(a\lambda^2 t) &= ac\Phi_n(0)\exp(a\lambda^2 t) \Rightarrow \\
\left[\Theta_n(t)\exp(a\lambda^2 t)\right]' &= ac\Phi_n(0)\exp(a\lambda^2 t) \Rightarrow \\
\int_0^t \left[\Theta_n(t)\exp(a\lambda^2 t)\right]' dt &= ac\Phi_n(0)\int_0^t \exp(a\lambda^2 t)dt \Rightarrow \\
\Theta_n(t)\exp(a\lambda^2 t) - \Theta_n(0)exp(0) &= \frac{ac\Phi_n(0)}{a\lambda^2}\left[\exp(a\lambda^2 t) - 1\right] \Rightarrow \\
\Theta_n(t) &= \frac{c\Phi_n(0)}{\lambda^2}\left[1 - \exp(-a\lambda^2 t)\right]. \qquad \text{(C.43)}
\end{aligned}$$

and since:

$$\Phi_n(0) = A_n\left(-\frac{\lambda}{b}\right) \qquad \text{(C.44)}$$

it will be:

$$\Theta_n(t) = -\frac{c}{b\lambda}A_n\left[1 - \exp(-a\lambda^2 t)\right]. \qquad \text{(C.45)}$$

Finally, the solution of the original problem is :

$$\begin{aligned}
C(z,t) &= \sum_1^\infty \Theta_n(t)\Phi_n(z) \Rightarrow \\
C(z,t) &= \sum_1^\infty -\frac{c}{b\lambda}A_n\left[1 - \exp(-a\lambda^2 t)\right]A_n\left[\sin(\lambda z) - \frac{\lambda}{b}\cos(\lambda z)\right] \Rightarrow \\
C(z,t) &= \sum_1^\infty -\left[\frac{c}{b\lambda}\right]\left[\frac{2\lambda b^2}{\lambda\left[\lambda^2 + b^2\right] + \sin\lambda\cos\lambda\left[\lambda^2 - b^2\right] + 2\lambda b\sin^2\lambda}\right] \\
&\quad \left[1 - \exp(-a\lambda^2 t)\right]\left[\sin(\lambda z) - \frac{\lambda}{b}\cos(\lambda z)\right] \Rightarrow \\
C(z,t) &= -2bc\sum_1^n \frac{\left[1 - \exp(-a\lambda^2 t)\right]\left[\sin(\lambda z) - \frac{\lambda}{b}\cos(\lambda z)\right]}{\lambda\left[\lambda^2 + b^2\right] + \sin\lambda\cos\lambda\left[\lambda^2 - b^2\right] + 2\lambda b\sin^2\lambda}. \qquad \text{(C.46)}
\end{aligned}$$

One can go even further by dividing the solution into its steady state and transient parts:

$$C(z,t) = C_{\rm ss}(z) + C_{\rm trans}(z,t) \Rightarrow \tag{C.47}$$

$$C(z,t) = -2bc\sum_{1}^{n}\frac{\left[\sin(\lambda z) - \frac{\lambda}{b}\cos(\lambda z)\right]}{\lambda\left[\lambda^2+b^2\right] + \sin\lambda\cos\lambda\left[\lambda^2-b^2\right] + 2\lambda b\sin^2\lambda} + 2bc\sum_{1}^{n}\frac{\left[\exp(-a\lambda^2 t)\right]\left[\sin(\lambda z) - \frac{\lambda}{b}\cos(\lambda z)\right]}{\lambda\left[\lambda^2+b^2\right] + \sin\lambda\cos\lambda\left[\lambda^2-b^2\right] + 2\lambda b\sin^2\lambda}. \tag{C.48}$$

with the steady state part being the expansion of a straight line.

Appendix D

Determination of the Unit Vectors that Define the Capillary Surface

In order to define the capillary's surface, three unit vectors are needed : the tangential to the surface vector, the one normal to the surface, and the bimodal vector:

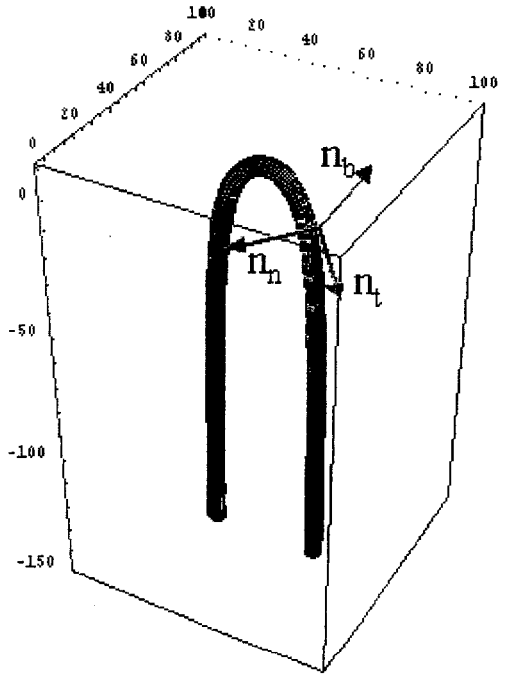

Figure D.1: Definition of the unit vectors that define the capillary surface. Dimensions of axes in μm. Tangential vector n_t, normal vector n_n, and bimodal vector n_b

The changes on the curvature along the capillary wall are not very abrupt, thus we can consider these vectors to be approximately equal to the respective vectors of the capillary's centerline. The tangential to the centerline unit vector will have an x and a z component since the centerline lies to a constant-y plane:

$$\vec{n_t} = A(\sigma)\vec{e_x} + B(\sigma)\vec{e_z}. \tag{D.1}$$

with σ being the parameter that describes the centerline. The definitive equations of the vector are:

$$\vec{n_t} = \vec{t}/|\vec{t}|, \tag{D.2}$$

$$\vec{t} = d\vec{R}(\sigma)/d\sigma = \sum_i (dx_i/d\sigma)\,\vec{e_i}, \tag{D.3}$$

$$|\vec{t}| = \sqrt{\sum_i (x_i)^2}. \tag{D.4}$$

with (Sec. 7.2.5):

$$\begin{aligned} \vec{t} &= [a\tanh(\sigma)]'\vec{e_x} - (h_o\sigma^2)'\vec{e_z} \\ &= a/\cosh^2(\sigma)\vec{e_x} - 2h_o\sigma\vec{e_z}. \end{aligned} \tag{D.5}$$

and:

$$|\vec{t}| = \sqrt{a^2/\cosh^4(\sigma) + 4h_o^2\sigma^2} \tag{D.6}$$

$$\vec{n_t} = \frac{a/\cosh^2(\sigma)\vec{e_x} - 2h_o\sigma\vec{e_z}}{\sqrt{a^2/\cosh^4(\sigma) + 4h_o^2\sigma^2}}. \tag{D.7}$$

thus,

$$A(\sigma) = \frac{a/\cosh^2(\sigma)}{\sqrt{a^2/\cosh^4(\sigma) + 4h_o^2\sigma^2}}, \tag{D.8}$$

$$B(\sigma) = \frac{-2h_o\sigma}{\sqrt{a^2/\cosh^4(\sigma) + 4h_o^2\sigma^2}}. \tag{D.9}$$

The normal vector too will be in a xz plane:

$$\vec{n_{\rm n}} = C(\sigma)\vec{e_{\rm x}} + D(\sigma)\vec{e_{\rm z}}. \tag{D.10}$$

It will have unit magnitude:

$$\sqrt{C(\sigma)^2 + D(\sigma)^2} = 1. \tag{D.11}$$

It will be perpendicular to the tangential vector:

$$\begin{aligned}
\vec{n_{\rm n}} \cdot \vec{n_{\rm t}} &= 0 \Rightarrow \\
[C(\sigma)\vec{e_{\rm x}} + D(\sigma)\vec{e_{\rm z}}] \cdot [A(\sigma)\vec{e_{\rm x}} + B(\sigma)\vec{e_{\rm z}}] &= 0 \Rightarrow \\
C(\sigma)A(\sigma)\vec{e_{\rm x}} \cdot \vec{e_{\rm x}} + C(\sigma)B(\sigma)\vec{e_{\rm x}} \cdot \vec{e_{\rm z}} &+ \\
D(\sigma)A(\sigma)\vec{e_{\rm z}} \cdot \vec{e_{\rm x}} + D(\sigma)B(\sigma)\vec{e_{\rm z}} \cdot \vec{e_{\rm z}} &= 0 \Rightarrow \\
C(\sigma)A(\sigma) + D(\sigma)B(\sigma) &= 0 \Rightarrow \\
D(\sigma) &= -A(\sigma)C(\sigma)/B(\sigma).
\end{aligned} \tag{D.12}$$

and:

$$\begin{aligned}
\sqrt{C(\sigma)^2 + D(\sigma)^2} &= 1 \Rightarrow \\
C(\sigma) &= \pm\sqrt{\frac{1}{1 + [A(\sigma)/B(\sigma)]^2}}, \qquad \text{(D.13)} \\
D(\sigma) &= \pm\sqrt{1 - \frac{1}{1 + [A(\sigma)/B(\sigma)]^2}}. \qquad \text{(D.14)}
\end{aligned}$$

Since the capillary is taken to extend into the $-z$ direction and $\vec{n_{\rm n}}$ is the inward normal vector [281], its $\vec{e_{\rm z}}$ component will always be negative:

$$D(\sigma) = -\sqrt{1 - \frac{1}{1 + [A(\sigma)/B(\sigma)]^2}}. \tag{D.15}$$

Up to this point, there is no apparent restriction for the sign of $C(\sigma)$, other the general one that the combination of the unit vectors must give the capillary cylinder.

The bimodal vector is the cross product of the tangential and normal vectors:

$$\vec{n_{\rm b}} = \vec{n_{\rm t}} \times \vec{n_{\rm n}} = \begin{vmatrix} \vec{e_{\rm x}} & \vec{e_{\rm y}} & \vec{e_{\rm z}} \\ A(\sigma) & 0 & B(\sigma) \\ C(\sigma) & 0 & D(\sigma) \end{vmatrix} = [C(\sigma)B(\sigma) - D(\sigma)A(\sigma)]\vec{e_{\rm y}} \quad = E(\sigma). \tag{D.16}$$

with:

$$\vec{n_{\rm b}} \quad = \quad E(\sigma)\vec{e_{\rm y}}. \tag{D.17}$$

Attempts to produce the capillary surface through the parametric unit vectors were unsuccessful, it was evident that the sign of $C(\sigma)$ does matter. By defining two opposite quantities as:

$$C_{+}(\sigma) \quad = \quad -\sqrt{\frac{1}{1+[A(\sigma)/B(\sigma)]^2}}, \tag{D.18}$$

$$C_{-}(\sigma) \quad = \quad +\sqrt{\frac{1}{1+[A(\sigma)/B(\sigma)]^2}}. \tag{D.19}$$

we get the respective bimodal vectors:

$$E_{+}(\sigma) \quad = \quad [C_{+}(\sigma)B(\sigma) - D(\sigma)A(\sigma)]\vec{e_{\rm y}}, \tag{D.20}$$

$$E_{-}(\sigma) \quad = \quad [C_{-}(\sigma)B(\sigma) - D(\sigma)A(\sigma)]\vec{e_{\rm y}}. \tag{D.21}$$

The pair $E_{+}(\sigma)$, $C_{+}(\sigma)$ is used to produce one "limb" of the capillary ($0 \leq \sigma \leq +\infty$), while the pair $E_{-}(\sigma)$, $C_{-}(\sigma)$ is used for the case where $-\infty \leq \sigma \leq 0$

Appendix E

Solution of the Doubly Periodic Green's Function

The set of the equations for the Green's function formulation is :

$$\nabla^2 G(x,y,z) = -\delta(x-x_o)(y-y_o)(z-z_o),\ 0<x<l_x,\ 0<y<l_y,\ -\infty<z<+\infty, \quad \text{(E.1)}$$

$$G(0,y,z) = G(l_x,y,z),\qquad 0<y<l_y,\ -\infty<z<+\infty, \quad \text{(E.2)}$$

$$\frac{\vartheta G(0,y,z)}{\vartheta x} = \frac{\vartheta G(l_x,y,z)}{\vartheta x},\qquad 0<y<l_y,\ -\infty<z<+\infty, \quad \text{(E.3)}$$

$$G(x,0,z) = G(0,l_y,z),\qquad 0<x<l_x,\qquad -\infty<z<+\infty, \quad \text{(E.4)}$$

$$\frac{\vartheta G(x,0,z)}{\vartheta y} = \frac{\vartheta G(0,l_y,z)}{\vartheta y},\qquad 0<x<l_x,\qquad -\infty<z<+\infty, \quad \text{(E.5)}$$

$$\frac{\vartheta G(x,y,-\infty)}{\vartheta z} = 0,\qquad 0<x<l_x,\ 0<y<l_y, \quad \text{(E.6)}$$

$$\frac{\vartheta G(x,y,+\infty)}{\vartheta z} = l_x l_y,\qquad 0<x<l_x,\ 0<y<l_y. \quad \text{(E.7)}$$

It involves an inhomogeneous PDE in three dimensions with inhomogeneous boundary conditions. Consider temporarily the solution of the homogeneous equation $\nabla G = 0$. Assume that the variables x, y, z in this solution are separable:

$$G(x,y,z) = f(x)g(y)h(z). \quad \text{(E.8)}$$

by substituting the solution in the homogeneous PDE, it is:

$$\begin{aligned} f''(x)g(y)h(z) + f(x)g''(y)h(z) + f(x)g(y)h''(z) &= 0 \overset{:f(x)g(y)h(z)}{\Rightarrow} \\ \frac{f''(x)}{f(x)} + \frac{g''(y)}{g(y)} + \frac{h''(z)}{h(z)} &= 0 \Rightarrow \\ \frac{f''(x)}{f(x)} = -\left[\frac{g''(y)}{g(y)} + \frac{h''(z)}{h(z)}\right] &= -c. \end{aligned} \tag{E.9}$$

The power of the separation of variables method lies in the fact that one is able to isolate the dependence of the problem to each of the three dimensions. Thus, for the x dependence it is:

$$f''(x) + cf(x) = 0, \tag{E.10}$$

$$f(0) = f(l_x), \tag{E.11}$$

$$f'(0) = f'(l_x). \tag{E.12}$$

exploring the possible values of c yields:

- $c < 0 \Rightarrow c = -k^2,\ k > 0$

$$\begin{aligned} f''(x) - k^2 f(x) &= 0 \Rightarrow \\ f(x) &= A\exp(kx) + B\exp(-kx) \Rightarrow \\ f'(x) &= Ak\exp(kx) - Bk\exp(-kx). \end{aligned} \tag{E.13}$$

and with the application of the boundary conditions:

$$\begin{aligned} f(0) &= f(l_x) \Rightarrow \\ A + B &= A\exp(kl_x) + B\exp(-kl_x) \Rightarrow \\ A[1 - \exp(kl_x)] &= B[-1 + \exp(-kl_x)]. \end{aligned} \tag{E.14}$$

and:

$$\begin{aligned} f'(0) &= f'(l_x) \Rightarrow \\ Ak - Bk &= Ak\exp(kl_x) - Bk\exp(-kl_x) \Rightarrow \\ A[1-\exp(kl_x)] &= -B[-1+\exp(-kl_x)] \end{aligned} \tag{E.15}$$

since k and l_x are both greater than zero, the terms inside the brackets can never be zero. Therefore, both BC's are satisfied when both A and B are 0 (trivial solution).

- $c = 0$

$$\begin{aligned} f''(x) &= 0 \Rightarrow \\ f'(x) &= A \Rightarrow \\ f(x) &= Ax + B. \end{aligned} \tag{E.16}$$

application of the boundary condition yields:

$$\begin{aligned} f(0) &= f(l_x) \Rightarrow \\ B &= Al_x + B \Rightarrow \\ Al_x &= 0 \Rightarrow \\ A &= 0. \end{aligned} \tag{E.17}$$

since $A = 0$, $f'(x) = 0 \; \forall \; B$ thus

$$f(x) = B. \tag{E.18}$$

which is a non-trivial solution.

- $c > 0 \Rightarrow c = k^2, \; k > 0$

$$\begin{aligned} f''(x) + k^2 f(x) &= 0 \Rightarrow \\ f(x) &= A\sin(kx) + B\cos(kx) \Rightarrow \\ f'(x) &= Ak\cos(kx) - Bk\sin(kx). \end{aligned} \tag{E.19}$$

Eq. (E.11) becomes:

$$\begin{aligned} f(0) &= f(l_x) \Rightarrow \\ B &= A\sin(kl_x) + B\cos(kl_x) \Rightarrow \\ A\sin(kl_x) &= B\left[1 - \cos(kl_x)\right]. \end{aligned} \tag{E.20}$$

and Eq. (E.12) becomes:

$$\begin{aligned} f'(0) &= f'(l_x) \Rightarrow \\ Ak &= Ak\cos(kl_x) - Bk\sin(kl_x) \Rightarrow \\ A(\cos(kl_x) - 1) &= B\sin(kl_x) \Rightarrow \\ -B\sin(kl_x) &= A\left[1 - \cos(kl_x)\right]. \end{aligned} \tag{E.21}$$

If both $\sin(kl_x)$ and $1 - \cos(kl_x)$ are different than zero, by dividing Eqs. (E.20) and (E.21) we get :

$$\frac{A}{-B} = \frac{B}{A} \Rightarrow A^2 = -B^2, \text{ impossible } \forall\, A, B \in \Re. \tag{E.22}$$

If one of the above is zero and the other is not, then we get the trivial solution $A = B = 0$. However, if both $\sin(kl_x)$ and $1 - \cos(kl_x)$ are equal to zero, then:

$$kl_x = 2n\pi \Rightarrow k = \frac{2n\pi}{l_x} \Rightarrow c = \left(\frac{2n\pi}{l_x}\right)^2. \tag{E.23}$$

This last case gives rise to the solution:

$$f_n(x) = A_n \sin\left(\frac{2n\pi x}{l_x}\right) + B_n \cos\left(\frac{2n\pi x}{l_x}\right). \tag{E.24}$$

by setting $c = 0$ in Eq. (E.24), we have $f_o(x) = B_o$ which is the solution obtained for the case where c was assumed zero. Thus, Eq. (E.24) is a valid solution $\forall\, n \geq 0$.

By following the same procedure for the y dependence of the solution, we have:

$$g''(y) + dg(y) = 0, \tag{E.25}$$

$$g(0) = g(l_y), \tag{E.26}$$

$$g'(0) = g'(l_y). \tag{E.27}$$

since the formulation is the same one with the x dependence, the solution will be the same:

$$g_m(y) = \Gamma_m \sin\left(\frac{2m\pi y}{l_y}\right) + \Delta_m \cos\left(\frac{2m\pi y}{l_y}\right). \tag{E.28}$$

Thus, the solution of the homogeneous PDE has the form:

$$G(x,y,z) = \sum_{n=0}^{\infty}\sum_{m=0}^{\infty}\left[A_n \sin\left(\frac{2n\pi x}{l_x}\right) + B_n \cos\left(\frac{2n\pi x}{l_x}\right)\right]$$
$$\left[\Gamma_m \sin\left(\frac{2m\pi y}{l_y}\right) + \Delta_m \cos\left(\frac{2m\pi y}{l_y}\right)\right] h(z). \tag{E.29}$$

The next step of the solution involves substitution of this solution to the inhomogeneous, initial Eq. (E.1). The components of the left-hand-side (LHS) of the equation (the second derivatives of the Green's function with respect to x, y, and z) are:

$$\frac{\vartheta^2 G(x,y,z)}{\vartheta z^2} = \sum_{n=0}^{\infty}\sum_{m=0}^{\infty} f_n(x) g_m(y) h''(z), \tag{E.30}$$

$$\frac{\vartheta G(x,y,z)}{\vartheta x} = \sum_{n=0}^{\infty}\sum_{m=0}^{\infty}\left[A_n \frac{2n\pi}{l_x}\cos\left(\frac{2n\pi x}{l_x}\right) + B_n\left(-\frac{2n\pi}{l_x}\right)\sin\left(\frac{2n\pi x}{l_x}\right)\right]$$
$$g_m(y) h(z), \tag{E.31}$$

$$\frac{\vartheta^2 G(x,y,z)}{\vartheta x^2} = \sum_{n=0}^{\infty}\sum_{m=0}^{\infty}\left[A_n\left(-\frac{4n^2\pi^2}{l_x^2}\right)\sin\left(\frac{2n\pi x}{l_x}\right) + B_n\left(-\frac{4n^2\pi^2}{l_x^2}\right)\cos\left(\frac{2n\pi x}{l_x}\right)\right]$$
$$g_m(y) h(z), \tag{E.32}$$

$$\frac{\vartheta^2 G(x,y,z)}{\vartheta y^2} = \sum_{n=0}^{\infty}\sum_{m=0}^{\infty} f_n(x)\left[\Gamma_m\left(-\frac{4m^2\pi^2}{l_y^2}\right)\sin\left(\frac{2m\pi y}{l_y}\right) + \Delta_m\left(-\frac{4m^2\pi^2}{l_y^2}\right)\cos(\frac{2m\pi y}{l_y})\right]$$

$h(z)$. (E.33)

In order to obtain the z dependence of the solution ($h(z)$), one has to expand the right-hand-side (RHS) of Eq. (E.1) in terms of a Fourier series and compare this expansion with the LHS. There are four combinations of functions at the LHS: $\sin(\alpha x)\sin(\beta y)$, $\sin(\alpha x)\cos(\beta y)$, $\cos(\alpha x)\sin(\beta y)$, and $\cos(\alpha x)\cos(\beta y)$. The same will emerge in the RHS if the component of the delta function $\delta(x - x_o)$ is expanded in terms of $\sin(\alpha x)$ and $\cos(\alpha x)$, while $\delta(y - y_o)$ is expanded in terms of $\sin(\beta y)$ and $\cos(\beta y)$. In order to calculate the expansion coefficients, special attention must be given to the cases where both or one of n, m are zero.

- For $n \neq 0$ and $m \neq 0$ it is:

$$\begin{aligned}
\delta(x - x_o)\delta(y - y_o) &= \\
\sum_{n=1}^{\infty}\sum_{m=1}^{\infty}\left[K_n \sin\left(\frac{2n\pi x}{l_x}\right) + \Lambda_n \cos\left(\frac{2n\pi x}{l_x}\right)\right]\left[K_m \sin\left(\frac{2m\pi y}{l_y}\right) + \Lambda_m \cos\left(\frac{2m\pi y}{l_y}\right)\right] &= \\
\sum_{n=1}^{\infty}\sum_{m=1}^{\infty} K_n K_m \sin\left(\frac{2n\pi x}{l_x}\right)\sin\left(\frac{2m\pi y}{l_y}\right) + \Lambda_n K_m \cos\left(\frac{2n\pi x}{l_x}\right)\sin\left(\frac{2m\pi y}{l_y}\right) &+ \\
K_n \Lambda_m \sin\left(\frac{2n\pi x}{l_x}\right)\cos\left(\frac{2m\pi y}{l_y}\right) + \Lambda_n \Lambda_m \cos\left(\frac{2n\pi x}{l_x}\right)\cos\left(\frac{2m\pi y}{l_y}\right). & \quad \text{(E.34)}
\end{aligned}$$

with:

$$K_n K_m = \frac{\int_0^{l_x}\int_0^{l_y} \delta(x - x_o)\delta(y - y_o)\sin\left(\frac{2n\pi x}{l_x}\right)\sin\left(\frac{2m\pi y}{l_y}\right) dydx}{\int_0^{l_x}\int_0^{l_y}\left[\sin\left(\frac{2n\pi x}{l_x}\right)\sin\left(\frac{2m\pi y}{l_y}\right)\right]^2 dydx}. \quad \text{(E.35)}$$

The delta function has the property:

$$\int_0^{l} \delta(t - t_o) f(t) dt = f(t_o). \quad \text{(E.36)}$$

thus, the numerator of $K_n K_m$ becomes $\sin\left(\frac{2n\pi x_o}{l_x}\right)\sin\left(\frac{2m\pi y_o}{l_y}\right)$. The components

of the double integral in the denominator are:

$$\int_0^{l_x} \cos^2(\frac{2n\pi x}{l_x})dx = \int_0^{l_x} \left[\frac{1+\cos(\frac{4n\pi x}{l_x})}{2}\right] dx = \frac{l_x}{2} + \frac{1}{2}\int_0^{l_x} \left[\frac{\sin(\frac{4n\pi x}{l_x})}{\frac{4n\pi x}{l_x}}\right] dx$$

$$= \frac{l_x}{2} + \frac{l_x}{8n\pi}[\sin(4n\pi) - \sin(0)] = \frac{l_x}{2}. \quad \text{(E.37)}$$

and

$$\int_0^{l_y} \sin^2(\frac{2n\pi x}{l_x})dx = \int_0^{l_x} \left[\frac{1-\cos(\frac{4n\pi x}{l_x})}{2}\right] dx = \frac{l_x}{2} - \frac{1}{2}\int_0^{l_x} \left[\frac{\sin(\frac{4n\pi x}{l_x})}{\frac{4n\pi x}{l_x}}\right] dx$$

$$= \frac{l_x}{2} - \frac{l_x}{8n\pi}[\sin(4n\pi) - \sin(0)] = \frac{l_x}{2}. \quad \text{(E.38)}$$

and therefore:

$$K_n K_m = \frac{\sin\left(\frac{2n\pi x_o}{l_x}\right)\sin\left(\frac{2m\pi y_o}{l_y}\right)}{\frac{l_x l_y}{4}}. \quad \text{(E.39)}$$

Similarly, the rest of the coefficients of the double series in Eq. (E.34) are:

$$\Lambda_n K_m = \frac{\cos\left(\frac{2n\pi x_o}{l_x}\right)\sin\left(\frac{2m\pi y_o}{l_y}\right)}{\frac{l_x l_y}{4}}, \quad \text{(E.40)}$$

$$K_n \Lambda_m = \frac{\sin\left(\frac{2n\pi x_o}{l_x}\right)\cos\left(\frac{2m\pi y_o}{l_y}\right)}{\frac{l_x l_y}{4}}, \quad \text{(E.41)}$$

$$\Lambda_n \Lambda_m = \frac{\cos\left(\frac{2n\pi x_o}{l_x}\right)\cos\left(\frac{2m\pi y_o}{l_y}\right)}{\frac{l_x l_y}{4}}. \quad \text{(E.42)}$$

- In a similar way, the expansion for $n = 0$ and $m \neq 0$ yields:

$$\delta(x-x_o)\delta(y-y_o) = \sum_{m=1}^{\infty} \Lambda_0 \left[K_m \sin\left(\frac{2m\pi y}{l_y}\right) + \Lambda_m \cos\left(\frac{2m\pi y}{l_y}\right)\right]$$

$$= \sum_{m=1}^{\infty} \Lambda_0 K_m \sin\left(\frac{2m\pi y}{l_y}\right) + \Lambda_0 \Lambda_m \cos\left(\frac{2m\pi y}{l_y}\right) \quad \text{(E.43)}$$

with:

$$\Lambda_0 K_m = \frac{\sin\left(\frac{2m\pi y_o}{l_y}\right)}{\frac{l_x l_y}{2}}, \tag{E.44}$$

$$\Lambda_0 \Lambda_m = \frac{\cos\left(\frac{2m\pi y_o}{l_y}\right)}{\frac{l_x l_y}{2}}. \tag{E.45}$$

- Similarly, for $n \neq 0$ and $m = 0$ it is:

$$\delta(x - x_o)\delta(y - y_o) = \sum_{n=1}^{\infty} \left[K_n \Lambda_0 \sin\left(\frac{2n\pi x}{l_x}\right) + \Lambda_n \Lambda_0 \cos\left(\frac{2n\pi x}{l_x}\right) \right] \tag{E.46}$$

with:

$$K_n \Lambda_0 = \frac{\sin\left(\frac{2n\pi x_o}{l_x}\right)}{\frac{l_x l_y}{2}}, \tag{E.47}$$

$$\Lambda_n \Lambda_0 = \frac{\cos\left(\frac{2n\pi x_o}{l_x}\right)}{\frac{l_x l_y}{2}}. \tag{E.48}$$

- Finally, the expansion of the RHS for $n = 0$ and $m = 0$ is:

$$\delta(x - x_o)\delta(y - y_o) = \Lambda_0 \Lambda_0 = 1. \tag{E.49}$$

The extraction of the z dependence through the comparison of the two sides of the PDE has to follow the same pattern as far as the values of n and m are concerned:

- $n \neq 0$ and $m \neq 0$

$$\begin{aligned} LHS = \sum_{n=1}^{\infty} \sum_{m=1}^{\infty} \Bigg\{ & -A_n \Gamma_m \left(\frac{2n\pi}{l_x}\right)^2 \sin\left(\frac{2n\pi x}{l_x}\right) \sin\left(\frac{2m\pi y}{l_y}\right) \\ & - B_n \Gamma_m \left(\frac{2n\pi}{l_x}\right)^2 \cos\left(\frac{2n\pi x}{l_x}\right) \sin\left(\frac{2m\pi y}{l_y}\right) \\ & - A_n \Delta_m \left(\frac{2n\pi}{l_x}\right)^2 \sin\left(\frac{2n\pi x}{l_x}\right) \cos\left(\frac{2m\pi y}{l_y}\right) \end{aligned}$$

$$
\begin{aligned}
&- B_n\Delta_m\left(\frac{2n\pi}{l_x}\right)^2\cos\left(\frac{2n\pi x}{l_x}\right)\cos\left(\frac{2m\pi y}{l_y}\right)\}\,h(z)\\
&+ \sum_{n=1}^{\infty}\sum_{m=1}^{\infty}\{-A_n\Gamma_m\left(\frac{2m\pi}{l_y}\right)^2\sin\left(\frac{2n\pi x}{l_x}\right)\sin\left(\frac{2m\pi y}{l_y}\right)\\
&- B_n\Gamma_m\left(\frac{2m\pi}{l_y}\right)^2\cos\left(\frac{2n\pi x}{l_x}\right)\sin\left(\frac{2m\pi y}{l_y}\right)\\
&- A_n\Delta_m\left(\frac{2m\pi}{l_y}\right)^2\sin\left(\frac{2n\pi x}{l_x}\right)\cos\left(\frac{2m\pi y}{l_y}\right)\\
&- B_n\Delta_m\left(\frac{2m\pi}{l_y}\right)^2\cos\left(\frac{2n\pi x}{l_x}\right)\cos\left(\frac{2m\pi y}{l_y}\right)\}\,h(z)\\
&+ \sum_{n=1}^{\infty}\sum_{m=1}^{\infty}\left\{A_n\Gamma_m\sin\left(\frac{2n\pi x}{l_x}\right)\sin\left(\frac{2m\pi y}{l_y}\right)\right.\\
&+ B_n\Gamma_m\cos\left(\frac{2n\pi x}{l_x}\right)\sin\left(\frac{2m\pi y}{l_y}\right)\\
&+ A_n\Delta_m\sin\left(\frac{2n\pi x}{l_x}\right)\cos\left(\frac{2m\pi y}{l_y}\right)\\
&+ \left.B_n\Delta_m\cos\left(\frac{2n\pi x}{l_x}\right)\cos\left(\frac{2m\pi y}{l_y}\right)\right\}h''(z). \qquad \text{(E.50)}
\end{aligned}
$$

and:

$$
\begin{aligned}
RHS &= \sum_{n=1}^{\infty}\sum_{m=1}^{\infty}\left\{K_nK_m\sin\left(\frac{2n\pi x}{l_x}\right)\sin\left(\frac{2m\pi y}{l_y}\right)+\Lambda_nK_m\cos\left(\frac{2n\pi x}{l_x}\right)\sin\left(\frac{2m\pi y}{l_y}\right)\right.\\
&+ \left.K_n\Lambda_m\sin\left(\frac{2n\pi x}{l_x}\right)\cos\left(\frac{2m\pi y}{l_y}\right)+\Lambda_n\Lambda_m\cos\left(\frac{2n\pi x}{l_x}\right)\cos\left(\frac{2m\pi y}{l_y}\right)\right\}\\
&\quad[-\delta(z-z_o)]\,. \qquad \text{(E.51)}
\end{aligned}
$$

term by term comparison reveals:

$$K_nK_m = A_n\Gamma_m,\quad \Lambda_nK_m = B_n\Gamma_m,\quad K_n\Lambda_m = A_n\Delta_m,\quad \Lambda_n\Lambda_m = B_n\Delta_m.$$

and:

$$h''(z) - \left\{ \left(\frac{2n\pi}{l_x}\right)^2 + \left(\frac{2m\pi}{l_y}\right)^2 \right\} h(z) \;=\; -\delta(z - z_o). \qquad \text{(E.52)}$$

Substituting the "$K\Lambda$" coefficients in the LHS yields too many arguments, thus one has to simplify. Simple inspection of each of the three terms of the LHS reveals that there are identical arguments present in each one. The LHS may be rewritten as:

$$\sum_{n=1}^{\infty}\sum_{m=1}^{\infty} \left\{ \lambda \left[2\sin\left(\frac{2n\pi x}{l_x}\right)\sin\left(\frac{2n\pi x_o}{l_x}\right)\right]\left[2\sin\left(\frac{2m\pi y}{l_y}\right)\sin\left(\frac{2m\pi y_o}{l_y}\right)\right] \;+\right.$$

$$\lambda \left[2\cos\left(\frac{2n\pi x}{l_x}\right)\cos\left(\frac{2n\pi x_o}{l_x}\right)\right]\left[2\sin\left(\frac{2m\pi y}{l_y}\right)\sin\left(\frac{2m\pi y_o}{l_y}\right)\right] \;+$$

$$\lambda \left[2\sin\left(\frac{2n\pi x}{l_x}\right)\sin\left(\frac{2n\pi x_o}{l_x}\right)\right]\left[2\cos\left(\frac{2m\pi y}{l_y}\right)\cos\left(\frac{2m\pi y_o}{l_y}\right)\right] \;+$$

$$\left.\lambda \left[2\cos\left(\frac{2n\pi x}{l_x}\right)\cos\left(\frac{2n\pi x_o}{l_x}\right)\right]\left[2\cos\left(\frac{2m\pi y}{l_y}\right)\cos\left(\frac{2m\pi y_o}{l_y}\right)\right]\right\}\xi(z). \qquad \text{(E.53)}$$

with λ being $-(\frac{2n\pi}{l_x})^2\frac{1}{l_x l_y}$, $-(\frac{2m\pi}{l_y})^2\frac{1}{l_x l_y}$, or $\frac{1}{l_x l_y}$ and $\xi(z)$ being $h(z)$, $h(z)$, or $h''(z)$ for the first, second, or third terms of the series of the LHS, respectively. Through the identities:

$$\cos(\alpha+\beta) = \sin\alpha\sin\beta - \cos\alpha\cos\beta, \qquad \text{(E.54)}$$

$$\cos(\alpha-\beta) = \sin\alpha\sin\beta + \cos\alpha\cos\beta. \qquad \text{(E.55)}$$

each of the three terms of the LHS becomes:

$$\sum_{n=1}^{\infty}\sum_{m=1}^{\infty} \left\{ \left[\cos\left(\frac{2n\pi(x-x_o)}{l_x}\right) + \cos\left(\frac{2n\pi(x+x_o)}{l_x}\right)\right] \cdot \right.$$

$$\left[\cos\left(\frac{2m\pi(y-y_o)}{l_y}\right) + \cos\left(\frac{2m\pi(y+y_o)}{l_y}\right)\right] \;+$$

$$\left.\left[\cos\left(\frac{2n\pi(x-x_o)}{l_x}\right) - \cos\left(\frac{2n\pi(x+x_o)}{l_x}\right)\right] \cdot \right.$$

$$\left[\cos\left(\frac{2m\pi(y-y_o)}{l_y}\right)+\cos\left(\frac{2m\pi(y+y_o)}{l_y}\right)\right] \quad +$$

$$\left[\cos\left(\frac{2n\pi(x-x_o)}{l_x}\right)+\cos\left(\frac{2n\pi(x+x_o)}{l_x}\right)\right] \quad \cdot$$

$$\left[\cos\left(\frac{2m\pi(y-y_o)}{l_y}\right)-\cos\left(\frac{2m\pi(y+y_o)}{l_y}\right)\right] \quad +$$

$$\left[\cos\left(\frac{2n\pi(x-x_o)}{l_x}\right)-\cos\left(\frac{2n\pi(x+x_o)}{l_x}\right)\right] \quad \cdot$$

$$\left[\cos\left(\frac{2m\pi(y-y_o)}{l_y}\right)-\cos\left(\frac{2m\pi(y+y_o)}{l_y}\right)\right]\Bigg\}\lambda\xi(z) \quad =$$

$$\sum_{n=1}^{\infty}\sum_{m=1}^{\infty}\Bigg\{2\cos\left(\frac{2n\pi(x-x_o)}{l_x}\right)\left[\cos\left(\frac{2m\pi(y-y_o)}{l_y}\right)+\cos\left(\frac{2m\pi(y+y_o)}{l_y}\right)\right] \quad +$$

$$2\cos\left(\frac{2n\pi(x-x_o)}{l_x}\right)\left[\cos\left(\frac{2m\pi(y-y_o)}{l_y}\right)-\cos\left(\frac{2m\pi(y+y_o)}{l_y}\right)\right]\Bigg\}\lambda\xi(z) \quad =$$

$$\sum_{n=1}^{\infty}\sum_{m=1}^{\infty}4\cos\left(\frac{2n\pi(x-x_o)}{l_x}\right)\cos\left(\frac{2m\pi(y-y_o)}{l_y}\right)\lambda\xi(z). \qquad \text{(E.56)}$$

Thus, after substitution of the coefficients, the PDE (for $n \neq 0$ and $m \neq 0$) becomes:

$$\frac{4}{l_x l_y}\Bigg\{\sum_{n=1}^{\infty}\sum_{m=1}^{\infty}\left[-\left(\frac{2n\pi}{l_x}\right)^2\cos\left(\frac{2n\pi(x-x_o)}{l_x}\right)\cos\left(\frac{2m\pi(y-y_o)}{l_y}\right)\right]h(z) \quad +$$

$$\sum_{n=1}^{\infty}\sum_{m=1}^{\infty}\left[-\left(\frac{2m\pi}{l_y}\right)^2\cos\left(\frac{2n\pi(x-x_o)}{l_x}\right)\cos\left(\frac{2m\pi(y-y_o)}{l_y}\right)\right]h(z) \quad +$$

$$\sum_{n=1}^{\infty}\sum_{m=1}^{\infty}\left[\cos\left(\frac{2n\pi(x-x_o)}{l_x}\right)\cos\left(\frac{2m\pi(y-y_o)}{l_y}\right)\right]h''(z)\Bigg\} \quad =$$

$$-\delta(z-z_o). \quad \text{(E.57)}$$

- $n = 0$ and $m \neq 0$

$$LHS \quad = \quad \sum_{m=1}^{\infty}\left[-B_0\Gamma_m\left(\frac{2m\pi}{l_y}\right)^2\sin\left(\frac{2m\pi y}{l_y}\right)-B_0\Delta_m\left(\frac{2m\pi}{l_y}\right)^2\cos\left(\frac{2m\pi y}{l_y}\right)\right]h(z)$$

$$+ \sum_{m=1}^{\infty} \left[B_0 \Gamma_m \sin\left(\frac{2m\pi y}{l_y}\right) + B_0 \Delta_m \cos\left(\frac{2m\pi y}{l_y}\right) \right] h''(z). \tag{E.58}$$

and

$$RHS = \sum_{m=1}^{\infty} \left[\Lambda_0 K_m \sin\left(\frac{2m\pi y}{l_y}\right) + \Lambda_0 \Lambda_m \sin\left(\frac{2m\pi y}{l_y}\right) \right] [-\delta(z - z_o)]. \tag{E.59}$$

Comparison of the two sides of the equation gives:

$$B_0 \Gamma_m = \Lambda_0 K_m, \quad B_0 \Delta_m = \Lambda_0 \Lambda_m. \tag{E.60}$$

and:

$$h''(z) - \left(\frac{2m\pi}{l_y}\right)^2 h(z) = -\delta(z - z_o). \tag{E.61}$$

Substituting the $K\Lambda$ coefficients in the terms of the LHS yields:

$$\sum_{m=1}^{\infty} \mu \left\{ \left[2 \sin\left(\frac{2m\pi y}{l_y}\right) \sin\left(\frac{2m\pi y_o}{l_y}\right) \right] + \left[2 \cos\left(\frac{2m\pi y}{l_y}\right) \cos\left(\frac{2m\pi y_o}{l_y}\right) \right] \right\} v(z). \tag{E.62}$$

with μ being $-(\frac{2m\pi}{l_y})^2 \frac{1}{l_x l_y}$ or $\frac{1}{l_x l_y}$ and $v(z)$ being $h(z)$ or $h''(z)$ for the first and second series terms of the LHS, respectively. Each of the two terms of the LHS becomes:

$$\sum_{m=1}^{\infty} \left\{ \left[\cos\left(\frac{2m\pi(y - y_o)}{l_y}\right) + \cos\left(\frac{2m\pi(y + y_o)}{l_y}\right) \right] + \left[\cos\left(\frac{2m\pi(y - y_o)}{l_y}\right) - \cos\left(\frac{2m\pi(y + y_o)}{l_y}\right) \right] \right\} \mu v(z) =$$

$$\sum_{m=1}^{\infty} 2 \cos\left(\frac{2m\pi(y - y_o)}{l_y}\right) \mu v(z). \tag{E.63}$$

Thus, the PDE (for $n = 0$ and $m \neq 0$) becomes:

$$\frac{2}{l_x l_y}\left\{\sum_{m=1}^{\infty}\left[-\left(\frac{2m\pi}{l_y}\right)^2 \cos\left(\frac{2m\pi(y-y_o)}{l_y}\right)\right] h(z) \quad + \right.$$

$$\left. \sum_{m=1}^{\infty}\left[\cos\left(\frac{2m\pi(y-y_o)}{l_y}\right)\right] h''(z)]\right\} \quad = \quad -\delta(z-z_o). \quad \text{(E.64)}$$

- $n \neq 0$ and $m = 0$

  Following the exact same procedure, the PDE for $m = 0$ is:

$$\frac{2}{l_x l_y}\left\{\sum_{m=1}^{\infty}\left[-\left(\frac{2n\pi}{l_x}\right)^2 \cos\left(\frac{2n\pi(x-x_o)}{l_x}\right)\right] h(z) \quad + \right.$$

$$\left. \sum_{m=1}^{\infty}\left[\cos\left(\frac{2n\pi(x-x_o)}{l_x}\right)\right] h''(z)\right\} \quad = \quad -\delta(z-z_o). \quad \text{(E.65)}$$

- $n = 0$ and $m = 0$

  The equation simply becomes:

$$h''(z) \quad = \quad -\delta(z-z_o). \quad \text{(E.66)}$$

Having found the solution dependence on x and y, we can derive the z dependence by considering that, for the various combinations of the values of n and m, the function $h(z)$ must be a solution of the following problems:

- $n \neq 0$ and $m \neq 0$

$$h''(z) - \left[\left(\frac{2n\pi}{l_x}\right)^2 + \left(\frac{2m\pi}{l_y}\right)^2\right] h(z) \quad = \quad -\delta(z-z_o), \quad \text{(E.67)}$$

$$h'(-\infty) \quad = \quad 0, \quad \text{(E.68)}$$

$$h'(+\infty) \quad = \quad l_x l_y. \quad \text{(E.69)}$$

- $n = 0$ and $m \neq 0$

$$h''(z) - \left(\frac{2m\pi}{l_y}\right)^2 h(z) = -\delta(z - z_o), \tag{E.70}$$

$$h'(-\infty) = 0, \tag{E.71}$$

$$h'(+\infty) = l_x l_y. \tag{E.72}$$

- $n \neq 0$ and $m = 0$

$$h''(z) - \left(\frac{2n\pi}{l_x}\right)^2 h(z) = -\delta(z - z_o), \tag{E.73}$$

$$h'(-\infty) = 0, \tag{E.74}$$

$$h'(+\infty) = l_x l_y. \tag{E.75}$$

- $n = 0$ and $m = 0$

$$h''(z) = -\delta(z - z_o), \tag{E.76}$$

$$h'(-\infty) = 0, \tag{E.77}$$

$$h'(+\infty) = l_x l_y. \tag{E.78}$$

In the first three cases the equation is of the same form; they will be dealt with together. There exists no solution of the problem that is valid over the entire z. Therefore, the problem will be solved in two semi-infinite regions, $z \in (-\infty, z_o)$ and $z \in (z_o, +\infty)$. In both of these regions the delta function is zero, thus the ODE is homogeneous.

- $n \neq 0$ or $m \neq 0$

  The constant-coefficient ODE (Eq. (E.67)) is homogeneous in both of the semi-infinite regions considered since $-\delta(z - z_o) = 0$. The characteristic polynomial

is :

$$\lambda^2 = \begin{cases} (\frac{2n\pi}{l_x})^2 + (\frac{2m\pi}{l_y})^2 & \forall n \neq 0, m \neq 0 \\ (\frac{2n\pi}{l_x})^2 & \forall n \neq 0, m = 0 \\ (\frac{2m\pi}{l_y})^2 & \forall n = 0, m \neq 0 \end{cases} \quad \text{(E.79)}$$

and

$$\lambda_{1,2} = \begin{cases} \pm\sqrt{(\frac{2n\pi}{l_x})^2 + (\frac{2m\pi}{l_y})^2} & \forall n \neq 0, m \neq 0 \\ \pm(\frac{2n\pi}{l_x}) & \forall n \neq 0, m = 0 \\ \pm(\frac{2m\pi}{l_y}) & \forall n = 0, m \neq 0 \end{cases} \quad \text{(E.80)}$$

– If $z < z_o$, then the general solution of Eq. (E.67) is:

$$h(z) = C_1 \exp(\lambda_1 z) + C_2 \exp(-\lambda_1 z), \quad \text{(E.81)}$$

$$h'(z) = C_1\lambda_1 \exp(\lambda_1 z) - C_2\lambda_1 \exp(-\lambda_1 z). \quad \text{(E.82)}$$

with:

$$\begin{aligned} h'(-\infty) = 0 \Rightarrow C_1\lambda_1 0 - C_2\lambda_1(+\infty) &= 0 \Rightarrow \\ C_2 &= 0 \Rightarrow \\ h(z) &= C_1 \exp(\lambda_1 z) \end{aligned} \quad \text{(E.83)}$$

– If $z > z_o$ then again it is:

$$h(z) = C_3 \exp(\lambda_1 z) + C_4 \exp(-\lambda_1 z), \quad \text{(E.84)}$$

$$h'(z) = C_3\lambda_1 \exp(\lambda_1 z) - C_4\lambda_1 \exp(-\lambda_1 z). \quad \text{(E.85)}$$

with:

$$\begin{aligned} h'(+\infty) = l_x l_y \Rightarrow C_3\lambda_1(+\infty) - C_4\lambda_1 &= l_x l_y \Rightarrow \\ C_3 &= 0 \Rightarrow \\ h(z) &= C_4 \exp(-\lambda_1 z) \end{aligned} \quad \text{(E.86)}$$

Thus, $\forall z \neq z_o$, it is:

$$h(z) = \begin{cases} \exp(\lambda_1 z) & z < z_o \\ C_4 \exp(-\lambda_1 z) & z > z_o \end{cases} \quad \text{(E.87)}$$

or in another form:

$$h(z-z_o) = \begin{cases} C_1 \exp(\lambda_1(z-z_o)) & z < z_o \\ C_4 \exp(-\lambda_1(z-z_o)) & z > z_o \end{cases} \quad \text{(E.88)}$$

This solution must be continuous at z_o thus, with ε being a very small number, it must be:

$$\begin{aligned} h\,|_{z_o+\varepsilon} &= h\,|_{z_o-\varepsilon} \Rightarrow \\ C_4 \exp(-\lambda_1(z_o+\varepsilon-z_o)) &= C_1 \exp(\lambda_1(z_o-\varepsilon-z_o)) \Rightarrow \\ C_4 \exp(-\lambda_1\varepsilon) &= C_1 \exp(-\lambda_1\varepsilon) \Rightarrow \\ C_4 &= C_1. \end{aligned} \quad \text{(E.89)}$$

Eq. (E.88) thus becomes:

$$h(z) = C_1 \exp(-\lambda_1|z-z_o|). \quad \text{(E.90)}$$

The ODE at $z = z_o$ is $h'' - \lambda_1^2 h = -\delta(z-z_o)$. This form has to be valid in the "tiny" neighborhood of z_o ($z \in (z_o-\varepsilon, z_o+\varepsilon)$). By integrating the equation in this interval we get:

$$\begin{aligned} \int_{z_o-\varepsilon}^{z_o+\varepsilon} [h'' - \lambda_1^2 h]dz = \int_{z_o-\varepsilon}^{z_o+\varepsilon} -\delta(z-z_o)dz &= -1 \Rightarrow \\ \int_{z_o-\varepsilon}^{z_o+\varepsilon} h''dz - \lambda_1^2 \int_{z_o-\varepsilon}^{z_o+\varepsilon} h dz &= -1 \Rightarrow \\ h'\,|_{z_o-\varepsilon}^{z_o+\varepsilon} - \lambda_1^2 \frac{h^2}{2}\,|_{z_o-\varepsilon}^{z_o+\varepsilon} &= -1. \end{aligned} \quad \text{(E.91)}$$

But h, and therefore $\frac{h^2}{2}$, is bounded, and through the second integral, it is multiplied by a very small number ε. The outcome of this integral, even for the maximum possible value of h, remains a very small, thus negligible number:

$$h'\,|_{z_o+\varepsilon} - h'\,|_{z_o-\varepsilon} \simeq -1 \Rightarrow$$

$$
\begin{aligned}
C_1(-\lambda_1)\exp(-\lambda_1(z_o+\varepsilon-z_o)) &- \\
C_1\lambda_1\exp(\lambda_1(z_o-\varepsilon-z_o)) &\simeq -1 \Rightarrow \\
-2C_1\lambda_1 &\simeq -1 \Rightarrow \\
C_1 &= \frac{1}{2\lambda_1}. \qquad \text{(E.92)}
\end{aligned}
$$

and

$$
h(z) = \frac{1}{2\lambda_1}\exp(-\lambda_1|z-z_o|). \qquad \text{(E.93)}
$$

- $m = n = 0$

  - If $z < z_o$ then:

$$
\begin{aligned}
h''_{00}(z) = 0 \quad &\text{and} \quad h''_{00}(z-z_o) = 0 \Rightarrow \\
h'_{00}(z-z_o) &= C_1 \Rightarrow \\
h_{00}(z-z_o) &= C_1(z-z_o)+C_2. \qquad \text{(E.94)}
\end{aligned}
$$

    with:

$$
\begin{aligned}
h'_{00}(-\infty) &= 0 \Rightarrow \\
C_1 &= 0 \Rightarrow \\
h_{00}(z-z_o) &= C_2 \qquad \text{(E.95)}
\end{aligned}
$$

  - If $z > z_o$ we have again:

$$
\begin{aligned}
h''_{00}(z-z_o) &= 0 \Rightarrow \\
h'_{00}(z-z_o) &= C_3 \Rightarrow \\
h_{00}(z-z_o) &= C_3(z-z_o)+C_4 \qquad \text{(E.96)}
\end{aligned}
$$

    and

$$
\begin{aligned}
h'_{00}(+\infty) &= l_x l_y \Rightarrow \\
C_3 &= l_x l_y \qquad \text{(E.97)}
\end{aligned}
$$

The solution is thus:

$$h_{00}(z-z_o) = \begin{cases} C_2 & z < z_o \\ C_3(z-z_o)+C_4 & z > z_o \end{cases} \tag{E.98}$$

By following the same methodology, we have the restriction that the solution be continuous on z_o:

$$\begin{aligned} h_{00}\,|_{z_o+\varepsilon} &= h_{00}\,|_{z_o-\varepsilon} \Rightarrow \\ C_2 &= C_4. \end{aligned} \tag{E.99}$$

Integration in the neighborhood of z_o yields:

$$\begin{aligned} \int_{z_o-\varepsilon}^{z_o+\varepsilon} h''dz &= -1 \Rightarrow \\ h'\,|_{z_o+\varepsilon} - h'\,|_{z_o-\varepsilon} &= -1 \Rightarrow \\ C_3 - 0 = -1 \Rightarrow C_3 &= -1. \end{aligned} \tag{E.100}$$

and thus the solution becomes:

$$h_{00}(z-z_o) = \begin{cases} C_2 & z < z_o \\ -(z-z_o)+C_2 & z > z_o \end{cases}. \tag{E.101}$$

where C_2 is a "free" constant, i.e., the choice of its value is arbitrary:

$$h_{00}(z-z_o) = \begin{cases} 0 & z < z_o \\ -(z-z_o) & z > z_o \end{cases} \tag{E.102}$$

By combining the parts obtained with the aforementioned, the solution of the original problem (Green's function) is:

$$G(x,y,z;x_o,y_o,z_o) = \sum_{n=0}^{\infty}\sum_{m=0}^{\infty} f_n(x)g_m(y)h(z) \tag{E.103}$$

$$= G_{00} + \sum_{m=1}^{\infty} G_{0m} + \sum_{n=1}^{\infty} G_{n0} + \sum_{n=1}^{\infty}\sum_{m=1}^{\infty} f_n(x)g_m(y)h(z) \tag{E.104}$$

In the two semi-infinite depth regions the solution has the form:

- $z < z_o$

$$
\begin{aligned}
G &= 0 + \frac{1}{2\pi l_x}\sum_{m=1}^{\infty}\frac{1}{m}\cos\left(\frac{2\pi m(y-y_o)}{l_y}\right)\exp\left[\frac{2\pi m}{l_y}(z-z_o)\right] \\
&+ \frac{1}{2\pi l_y}\sum_{n=1}^{\infty}\frac{1}{n}\cos\left(\frac{2\pi n(x-x_o)}{l_x}\right)\exp\left[\frac{2\pi n}{l_x}(z-z_o)\right] \\
&- \frac{4}{l_x l_y}\sum_{n=1}^{\infty}\sum_{m=1}^{\infty}\left[\cos\left(\frac{2\pi n(x-x_o)}{l_x}\right)\cos\left(\frac{2\pi m(y-y_o)}{l_y}\right)\right] \\
&\left\{-\frac{\exp\left[\sqrt{\left(\frac{2n\pi}{l_x}\right)^2+\left(\frac{2m\pi}{l_y}\right)^2}(z-z_o)\right]}{2\sqrt{\left(\frac{2n\pi}{l_x}\right)^2+\left(\frac{2m\pi}{l_y}\right)^2}}\right\}. \qquad \text{(E.105)}
\end{aligned}
$$

- $z > z_o$

$$
\begin{aligned}
G &= -(z-z_o) + \frac{1}{2\pi l_x}\sum_{m=1}^{\infty}\frac{1}{m}\cos\left(\frac{2\pi m(y-y_o)}{l_y}\right)\exp\left[-\frac{2\pi m}{l_y}(z-z_o)\right] \\
&+ \frac{1}{2\pi l_y}\sum_{n=1}^{\infty}\frac{1}{n}\cos\left(\frac{2\pi n(x-x_o)}{l_x}\right)\exp\left[-\frac{2\pi n}{l_x}(z-z_o)\right] \\
&- \frac{4}{l_x l_y}\sum_{n=1}^{\infty}\sum_{m=1}^{\infty}\left[\cos\left(\frac{2\pi n(x-x_o)}{l_x}\right)\cos\left(\frac{2\pi m(y-y_o)}{l_y}\right)\right] \\
&\left\{-\frac{\exp\left[-\sqrt{\left(\frac{2n\pi}{l_x}\right)^2+\left(\frac{2m\pi}{l_y}\right)^2}(z-z_o)\right]}{2\sqrt{\left(\frac{2n\pi}{l_x}\right)^2+\left(\frac{2m\pi}{l_y}\right)^2}}\right\}. \qquad \text{(E.106)}
\end{aligned}
$$

Appendix F

Green's Function Diagnostic Tests

Various terms were performed to ensure that the mathematical solution and the accompanying Fortran code were accurate. The Green's function of this problem must always satisfy the Laplacian. Two random values for the sink coordinates (x_o, y_o, z_o) were chosen and the second derivatives of the Green's function with respect to x (G_{xx}), y (G_{yy}), and z (G_{zz}) were calculated. Their sum, which constitutes the Laplacian, was found to be always zero (Table F.1). Furthermore, whenever the case $x_o = y_o$ arose, it was $G_{xx} = G_{yy}$ as it should be, since the problem is symmetric in the x and y coordinates.

$x_o = 0.4,\ y_o = 0.4,\ z_o = 0.6$						
x	y	z	G_{xx}	G_{yy}	G_{zz}	∇^2
0.01	0.01	0.01	−0.090522	−0.090522	0.181044	0
0.727	0.533	−0.926	−0.000204	0.000285	−0.000081	0
0.2	0.85	0.926	0.09578	−0.700911	0.605834	0
0.5	0.5	−0.4	0.010316	0.010316	−0.020632	0
0.936	0.8	10	0	0	0	0
$x_o = 0.2,\ y_o = 0.3,\ z_o = -0.4$						
0.4	0.6	−0.7	−0.099318	0.532552	−0.433234	0

Table F.1: Green's function diagnostic test. Laplacian satisfaction by Green's function

It should also be $G\,(4\pi|\underline{x}-\underline{x}_o|) \to 1$ as $z \to z_o$. This condition stems from the fact that Green's function should behave like the function $\frac{1}{4\pi|\underline{x}-\underline{x}_o|}$ as the singularity is approached. The product was calculated for values of z approaching $z_o$and the result is presented in Fig. F.1. It is obvious that this condition is satisfied too.

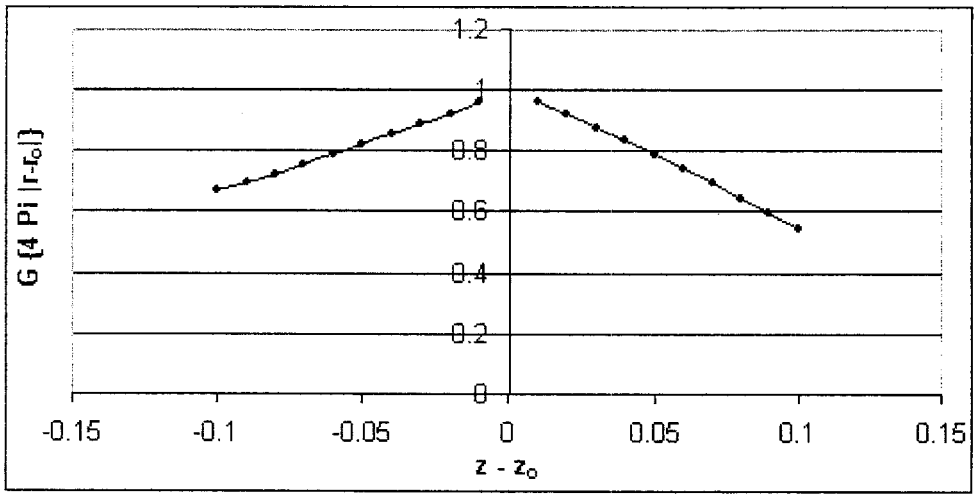

Figure F.1: Green's function diagnostic test. Calculation of the product $G\,(4\pi|\underline{x}-\underline{x}_o|)$

The sum $G - \left(\frac{1}{4\pi|r|}\right)$ should remain bounded $(O(1))$ as $z \to z_o$ (Fig. F.2). That is another indication that G behaves as the function $\left(\frac{1}{4\pi|r|}\right)$ in the vicinity of the singularity.

Finally, the flux through two xy planes, one located above z_o and one below, was calculated. The sum of these two fluxes was -1 counterbalancing the unit sink at z_o. Thus, mass is conserved (Table F.2).

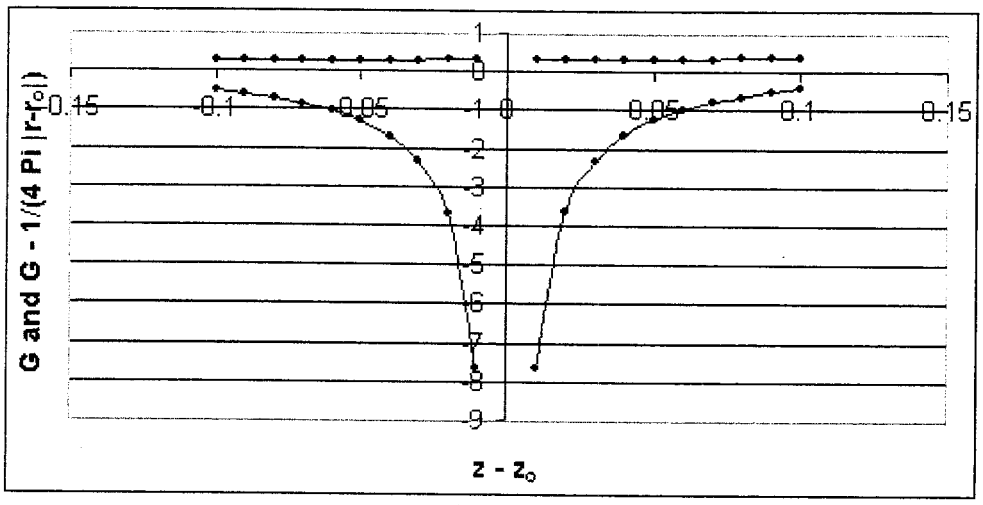

Figure F.2: Green's function diagnostic test. Calculation of the term $G - \left(\frac{1}{4\pi|r|}\right)$. G alone is also included for the same coordinates to illustrate that its behavior is that of $1/(4\pi|r|)$

	Plane 1 ($z = 0$)	Plane 2 ($z = -0.8$)
Subplane 1	-0.279705	0.029705
Subplane 2	-0.244784	-0.005216
Subplane 3	-0.244784	-0.005216
Subplane 4	-0.230727	-0.019273
Total	-1.000000	0.000000

Table F.2: Flux diagnostic calculations for Green's function. Flux calculation on planes above and below the unit sink. The planes were divided into four subplanes to minimize round-off errors. The point sink coordinates were assumed to be $(0.2, 0.3, -0.4)$ while the planes were at elevations $z = 0$ and $z = -0.8$

Appendix G

Calculation of the Definite Integral of $\frac{1}{4\pi\sqrt{(x-x_O)^2+(y-y_O)^2+(z-z_O)^2}}$

Let XYZ be a local coordinate system and (x, y, z) be a random point. Let the X axis coincide with a small, straight by approximation, centerline segment (of length h) with its point of origin being the middle point of the segment (Fig. G.1). A random point-sink situated on the discrete segment of the capillary's centerline will have coordinates $(x_1, 0, 0)$. The projection point of (x, y, z) on the X axis will have the (variable) coordinates $(x', 0, 0)$. The integral required is:

$$\frac{1}{4\pi\vec{r}} = \frac{1}{4\pi}\int_{-\frac{h}{2}}^{\frac{h}{2}} \frac{1}{\sqrt{(x'-x_1)^2+(y-0)^2+(z-0)^2}} = \frac{1}{4\pi}\int_{-\frac{h}{2}}^{\frac{h}{2}} \frac{1}{\sqrt{(x'-x_1)^2+y^2+z^2}}. \quad \text{(G.1)}$$

Since it is evident that $y^2 + z^2 = r^2$, one has to calculate the integral of $\frac{1}{\sqrt{(x'-x_1)^2+r^2}}$.

This calculation is performed with a change of variables, by setting:

$$x' = x_1 + r\tan\omega \quad , \quad \omega \in (-\pi/2, \pi/2). \quad \text{(G.2)}$$

The function $\tan\omega$ is able to sample all possible values without becoming infinite. It is:

$$x_1 - x' = -r\tan\omega \Rightarrow$$

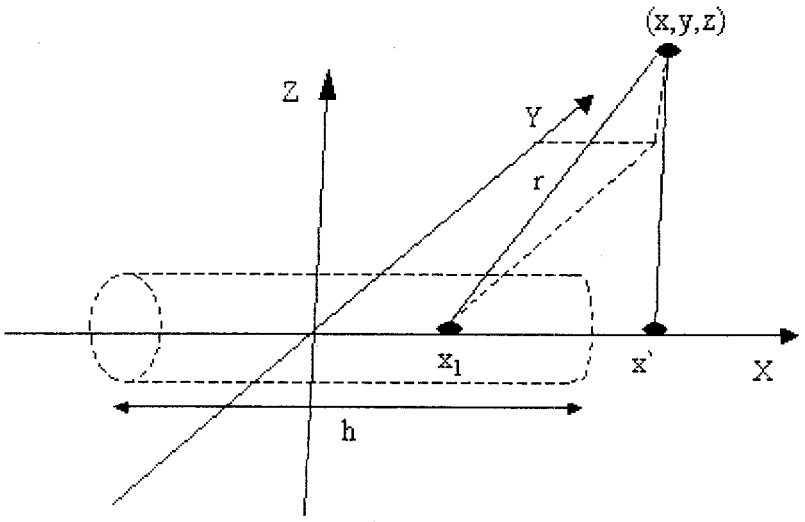

Figure G.1: Definition sketch for the integration of Green's function

$$\begin{aligned}
(x_1 - x')^2 &= r^2 \tan^2 \omega \Rightarrow \\
(x_1 - x')^2 + r^2 &= r^2(1 + \tan^2 \omega) \Rightarrow \\
(x_1 - x')^2 + r^2 &= r^2 \sec^2 \omega \Rightarrow \\
\sqrt{(x_1 - x')^2 + r^2} &= r|\sec \omega| \qquad \text{(G.3)}
\end{aligned}$$

but $\sec\omega > 0,\ \forall\ \omega \in\ (-\pi/2, \pi/2)$, thus $\sqrt{(x_1 - x')^2 + r^2}\ =\ r\sec\omega$ and:

$$\begin{aligned}
dx' &= d(x_1 + r\tan\omega) \Rightarrow \\
dx' &= r d\tan\omega \Rightarrow \\
dx' &= r(\tan\omega)' d\omega \Rightarrow \\
dx' &= r\sec^2\omega d\omega. \qquad \text{(G.4)}
\end{aligned}$$

The indefinite integral in question becomes:

$$\begin{aligned}
I &= \int \frac{dx'}{\sqrt{(x_1 - x')^2 + r^2}} \\
&= \int \frac{r\sec^2\omega d\omega}{r\sec\omega}
\end{aligned}$$

$$= \int \sec\omega d\omega$$

$$= \ln|\sec\omega + \tan\omega|. \tag{G.5}$$

but it is also:

$$\tan\omega = \frac{x' - x_1}{r} \Rightarrow$$

$$\tan^2\omega = \left(\frac{x' - x_1}{r}\right)^2 \Rightarrow$$

$$1 + \tan^2\omega = 1 + \left(\frac{x' - x_1}{r}\right)^2 \Rightarrow$$

$$\sec^2\omega = 1 + \left(\frac{x' - x_1}{r}\right)^2 \Rightarrow$$

$$\sec\omega = \sqrt{1 + \left(\frac{x' - x_1}{r}\right)^2}. \tag{G.6}$$

by changing back to the original variables, we have:

$$I = \int \frac{dx'}{\sqrt{(x_1 - x')^2 + r^2}}$$

$$= \ln\left|\sqrt{1 + \left(\frac{x' - x_1}{r}\right)^2} + \frac{x' - x_1}{r}\right|. \tag{G.7}$$

and since $\sqrt{1 + \left(\frac{x'-x_1}{r}\right)^2} > \frac{x'-x_1}{r}$ and $\sqrt{1 + \left(\frac{x'-x_1}{r}\right)^2} > 0$, it is:

$$I = \ln\left(\sqrt{1 + \left(\frac{x' - x_1}{r}\right)^2} + \frac{x' - x_1}{r}\right)$$

$$= \operatorname{arcsinh}\left(\frac{x' - x_1}{r}\right) \tag{G.8}$$

The corresponding definite integral over an arbitrary length h is thus:

$$\begin{aligned}\int_{-\frac{h}{2}}^{\frac{h}{2}} I \;&=\; \ln\left(\sqrt{1+\left(\frac{h/2-x_1}{r}\right)^2}+\frac{h/2-x_1}{r}\right)- \\ &\quad \ln\left(\sqrt{1+\left(\frac{-h/2-x_1}{r}\right)^2}+\frac{-h/2-x_1}{r}\right) \qquad \text{(G.9)}\end{aligned}$$

The parameters r, x_1 and h depend on the local geometry used. Thus they make Eq. (G.9) applicable in every segment of the capillary loop. They only need to be translated to the "global" coordinate system whenever the formula is being used.

Appendix H

Calculations on the Averaging Over the Capillary Perimeter

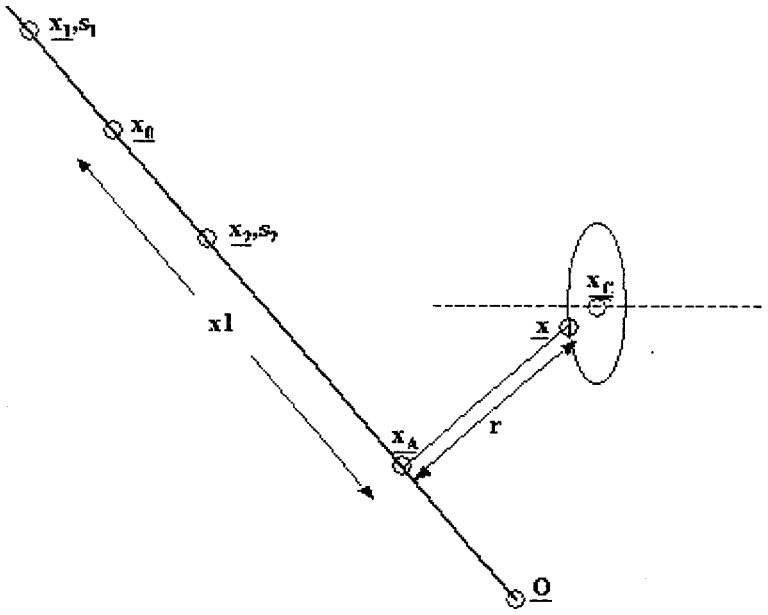

Figure H.1: Definition sketch for the over-the-capillary-perimeter averaging

The input of the present calculation are the coordinates of the center of the cross section in question, the coordinates of the endpoints of the segment carrying the sinks and the cross section (capillary) radius:

$$\underline{x_c} \equiv (x_c, y_c, z_c),$$

$$\underline{x_1} \equiv (x_1, y_1, z_1),$$

$$\underline{x_2} \equiv (x_2, y_2, z_2),$$

a_{cap}.

By defining the local geometry as shown in Fig. H.1, the determination of the arguments included in the integral is possible. The length of the straight segment having the point sinks is:

$$h = \sqrt{(x_2 - x_1)^2 + (y_2 - y_1)^2 + (z_2 - z_1)^2}. \tag{H.1}$$

The center point of the straight segment is:

$$\underline{x_o} \equiv (\frac{x_1 + x_2}{2}, \frac{y_1 + y_2}{2}, \frac{z_1 + z_2}{2}). \tag{H.2}$$

The projection of the random perimeter point $\underline{x}$ on the line that carries the straight segment is point $\underline{x_a}$. Since, $\underline{x_a}$ and $\underline{x_1}$ are on the same, constant - y, plane, it is $y_a = y_1$. Furthermore, points $\underline{x_a}$, $\underline{x_1}$ and $\underline{x_2}$ are on the same line, which lies on the aforementioned , constant - y plane. This line has the form $z = \mu x + \nu$ with:

$$\mu = \frac{z_2 - z_1}{x_2 - x_1}, \tag{H.3}$$

$$\nu = z_1 - \mu x_1. \tag{H.4}$$

Thus, it is:

$$z_a = \mu x_a + \nu. \tag{H.5}$$

The triangle $\underline{x_o x_a x}$ is orthogonal on $\underline{x_a}$. By using the Pythagorium theorem for a given $\underline{x}$, having as knowns $\underline{x_o}$ and two of the three coordinates of $\underline{x_a}$, one is able to derive an equation through which the only unknown coordinate, x_a, is calculated:

$$Ax_a^2 + Bx_a + \Gamma = 0. \tag{H.6}$$

with:

$$A = 1 + \mu^2, \tag{H.7}$$

$$B = 2\mu\nu - (x + x_o) + \mu(z + z_o), \tag{H.8}$$

$$\Gamma = \nu^2 - \nu(z - z_o) + y_a^2 - y_a(y - y_o) + xx_o + yy_o + zz_o, \tag{H.9}$$

This second order equation yields two solutions for x_a. The correct one is the one that corresponds to the smallest r since this is the distance between $\underline{x}$ and $\underline{x_a}$. Having $\underline{x_a}$ defined, the arguments of the integral are:

$$x1 = \sqrt{(x_o - x_a)^2 + (y_o - y_a)^2 + (z_o - z_a)^2}, \tag{H.10}$$

$$r = \sqrt{(x - x_a)^2 + (y - y_a)^2 + (z - z_a)^2}. \tag{H.11}$$

Bibliography

[1] L. Aarons et al., Aspirin binding and the effect of albumin on spontaneous and enzyme-catalyzed hydrolysis. *Journal of Pharmacy and Pharmacology*, **32**, pp. 537–543 (1980).

[2] C. Ackermann, G.L. Flynn, Ether-water partitioning and permeability through nude mouse skin in vitro. I. Urea, thiourea, glycerol and glucose. *International Journal of Pharmaceutics*, **36**, pp. 61–66 (1987).

[3] R.H. Adamson, An extension of the fiber matrix model of vascular permeability. *Microvascular Research*, **42**, pp. 352–356 (1992).

[4] J. Adriani, R. Zepernick, Clinical effectiveness of drugs used for topical anesthesia. *JAMA*, **118**, pp. 711–711 (1964).

[5] W.J. Albery and J. Hadgraft, Percutaneous absorption: in vivo experiments. *Journal of Pharmacy and Pharmacology*, **31**, pp. 140–147 (1979).

[6] S. Amin, S. Freeman, H.I. Maibach, Systemic toxicity in man secondary to percutaneous absorption, pp. 103–125 in *Dermal Absorption and Toxicity Assessment*, Ed. M.S. Roberts, K.A. Walters, Marcel Dekker Inc., New York-Basel-Hong Kong (1998).

[7] B. Amsden, Solute diffusion within hydrogels. Mechanisms and models. *Macromolecules*, **31**, pp. 8382–8395 (1998).

[8] B.G. Amsden and M.F.A. Goosen, Transdermal delivery of peptide and protein drugs: an overview. *AIChE Journal*, **41**, pp. 1972–1997 (1995).

[9] K.N. An, E.P. Salathe, A theory of interstitial fluid motion and its implications for capillary exchange. *Microvascular Research*, **12**, pp. 103–119 (1976).

[10] B.D. Anderson, W.I. Higuchi, P.V. Raykar, Heterogeneity effects on permeability-partition coefficient relationships in human stratum corneum. *Pharmaceutical Research*, **5**, pp. 566–573 (1988).

[11] B.D. Anderson, P.V. Raykar, Solute structure-permeability relationships in human stratum corneum. *Journal of Investigative Dermatology*, **93**, pp. 280–286 (1989).

[12] J.L Anderson, Configurational effect on the reflection coefficient for rigid solutes in capillary pores. *Journal of Theoretical Biology*, **90**, pp. 405–426 (1981).

[13] J.L. Anderson, D.M. Malone, Mechanism of osmotic flow in porous membranes. *Biophysical Journal*, **14**, pp. 957–982 (1974).

[14] J.L. Anderson, J.A. Quinn, Restricted transport in small pores: A model for steric exclusion and hindered particle motion. *Biophysical Journal*, **14**, pp. 130–150 (1974).

[15] W. Andrew, R.H. Behnke, T. Sato, Changes with advancing age in the cell population of human dermis. *Gerontologia*, **10**, pp. 1–19 (1964/65).

[16] Y.G. Anissimov, M.S. Roberts, Diffusion modeling of percutaneous absorption kinetics. 1. Effects of flow rate, receptor sampling rate, and viable epidermal resistance for a constant donor concentration. *Journal of Pharmaceutical Sciences*, **88**, pp. 1201–1209 (1999).

[17] Y.G. Anissimov, M.S. Roberts, Diffusion modeling of percutaneous absorption kinetics. 2. Finite vehicle volume and solvent deposited solids. *Journal of Pharmaceutical Sciences*, **90**, pp. 504–520 (2001).

[18] A. Apelblat, A. Katzir-Katchalsky, A. Silberberg, A mathematical analysis of capillary tissue fluid exchange. *Biorheology*, **11**, pp. 1–49 (1974).

[19] K. Aukland, R.K. Reed, Interstitial-lymphatic mechanisms in the control of extracellular fluid volume. *Physiological Reviews*, **73**, pp. 1–78 (1993).

[20] T.R. Auton et al., A physiologically based mathematical model of dermal absorption in man. *Human & Experimental Toxicology*, **13**, pp. 51–60 (1994).

[21] G. Balgi, D.E. Leckband, J.M. Nitsche, Transport effects on the kinetics of protein-surface binding. *Biophysical Journal*, **68**, pp. 2251–2260 (1995).

[22] J.H. Barker et al., The hairless mouse ear for in vivo studies of skin microcirculation. *Plastic and Reconstructive Surgery*, **83**, pp. 948–959 (1989).

[23] B.W. Barry, Novel mechanisms and devices to enable successful transdermal drug delivery. *European Journal of Pharmaceutical Sciences*, **14**, pp. 101–114 (2001).

[24] E. Barta, S. Sideman, J.B. Bassingthwaighte, Facilitated diffusion and membrane permeation of fatty acid in albumin solutions. *Annals of Biomedical Engineering*, **28**, pp. 331–345 (2000).

[25] J.B. Bassingthwaighte, I.S.J. Chan, C.Y. Wang, Computationally efficient algorithms for convection-permeation-diffusion models for blood tissue exchange. *Annals of Biomedical Engineering*, **20**, pp. 687–725 (1992).

[26] J.B. Bassingthwaighte, T.J. Knopp, J.B. Hazelrig, A concurrent flow model for capillary-tissue exchanges. pp. 60–80 in: *Capillary Permeability, Alfred Benzon Symposium II*, Ed. C. Crone, N.A. Lassen, Academic Press, NY (1970).

[27] G.K. Batchelor, Transport properties of two phase materials with random structure. *Annual Review of Fluid Mechanics*, **6**, pp. 227–255 (1974).

[28] G.K. Batchelor, Slender-body theory for particles of arbitrary cross-section in Stokes flow. *Journal of Fluid Mechanics*, **44**, pp. 419–440 (1970).

[29] S. Batra, K. Rakusan, Capillary length, tortuosity, and spacing in rat myocardium during cardiac cycle. *American Journal of Physiology*, **263**, pp. H1369–H1376 (1992).

[30] L.T. Baxter, R.K. Jain, E. Svenso, Vascular permeability and interstitial diffusion of macromolecules in the hamster cheek pouch. *Microvascular Research*, **34**, pp. 336–348 (1987).

[31] D.A. Beard, J.B. Bassingthwaighte, Advection and diffusion of substances in biological tissues with complex vascular networks. *Annals of Biomedical Engineering*, **28**, pp. 253–268 (2000).

[32] H.L. Behm, G.L. Flynn, J.G. Wagner, Binding of tolmetin and salicylic acid to human serum albumin as a function of temperature. *Biopharmaceutics & Drug Disposition*, **2**, pp. 235–244 (1981).

[33] M. Bendayan, Vascular permeability in blood capillary. *Microscopy Research and Technique*, **57**, pp. 263–268 (2002).

[34] F. Benech-Kieffer et al., Percutaneous absorption of sunscreens in vitro: Interspecies comparison, skin models and reproducibility aspects. *Skin Pharmacology and Applied Skin Physiology*, **13**, pp. 324–335 (2000).

[35] N.L. Benowitz et al., Intravenous nicotine retards transdermal absorption of nicotine: Evidence of blood flow-limited percutaneous absorption. *Clinical Pharmacology & Therapeutics*, **52**, pp. 223–230 (1992).

[36] P.R. Bergstresser, R.J. Pariser, J.R. Taylor, Counting and sizing of epidermal cells in normal human skin. *The Journal of Investigative Dermatology*, **70**, pp. 280–284 (1978).

[37] E. Bernard, J.L. Dubois, J. Wepierre, Importance of sebaceous glands in cutaneous penetration of an antiandrogen: Target effect of liposomes. *Journal of Pharmaceutical Sciences*, **86**, pp. 573–578 (1997).

[38] B. Berner, Pharmacokinetics of transdermal drug delivery. *Journal of Pharmaceutical Sciences*, **74**, pp. 718–721 (1985).

[39] S. Bhattacharjee, A. Sharma, Apolar, polar and electrostatic interactions of spherical particles in cylindrical pores. *Journal of Colloid and Interface Science*, **187**, pp. 83–95 (1997).

[40] M.H. Bickel, The role of adipose tissue in the distribution and storage of drugs. *Progress in Drug Research*, **28**, pp. 273–303 (1984).

[41] L.H. Blake, N.C. Staub, Pulmonary vascular transport in sheep. A mathematical model. *Microvascular Research*, **12**, pp. 197–220 (1976).

[42] I.H. Blank and R.J. Scheuplein, Transport into and within the skin. *British Journal of Dermatology*, **81**, pp. 4–10 (1969).

[43] I.H. Blank, R.J. Scheuplein, D.J. MacFarlane, Mechanism of percutaneous absorption III. The effect of temperature on the transport of non-electrolytes across the skin. *Journal of Investigative Dermatology*, **48**, pp. 79–88 (1967).

[44] K. Bauerova, D. Matušová, Z. Kassai, Chemical enhancers for transdermal drug transport. *European Journal of Drug Metabolism and Pharmacokinetics*, **26**, pp. 85–94 (2001).

[45] H.E. Boddé et al., Visualization of *in vitro* percutaneous penetration of mercuric chloride; transport through intercellular space versus cellular uptake through desmosomes. *Journal of Controlled Release*, **15**, pp. 227–236 (1991).

[46] R.L. Bookout, D.W. Quinn, J.N. McDougal, Parallel dermal subcompartments for modeling chemical absorption. *SAR and QSAR in Environmental Research*, **7**, pp. 259–279 (1997).

[47] P. Boutsiouki, J.P. Thompson, G.F. Clough, Effects of local blood flow on the percutaneous absorption of the organophosphorus compound malathion: a microdialysis study in man. *Archives of Toxicology*, **75**, pp. 321–328 (2001).

[48] R.D.H. Boyd at al., Permeability of lung capillaries to macromolecules in fetal and new-born lambs ans sheep. *Journal of Physiology*, **201**, pp. 567–588 (1969).

[49] M.C. Branchet et al., Morphometric analysis of dermal collagen fibers in normal human skin as a function of age. *Archives of Gerontology and Geriatrics*, **13**, pp. 1–14 (1991).

[50] I.M. Braverman, The cutaneous microcirculation: Ultrastructure and microanatomical organization. *Microcirculation*, **4**, pp. 329-341 (1997).

[51] I.M. Braverman, Anatomy and physiology of the cutaneous microcirculation, pp. 1–22 in *Bioengineering of the Skin: Cutaneous Blood Flow and Erythema*, Ed. E. Berardesca, P. Elsner, H.I. Maibach, CRC Press, Boca Raton (1999).

[52] I.M. Braverman and A. Yen, Ultrastructure of the human dermal microcirculation. II. The capillary loops of the dermal papillae. *Journal of Investigative Dermatology*, **68**, pp. 44-52 (1977).

[53] I.M. Braverman and A. Yen, Ultrastructure of the human dermal microcirculation. III. The vessels in the mid- and lower dermis and subcutaneous fat. *Journal of Investigative Dermatology*, **77**, pp. 297-304 (1981).

[54] H. Brenner, L.J Gaydos, The constrained Brownian movement of spherical particles in cylindrical pores of comparable radius. *Journal of Colloid and Interface Science*, **58**, pp. 312–356 (1977).

[55] R.A. Briggaman, Biochemical composition of the epidermal-dermal junction and other basement membrane. *Journal of Investigative Dermatology*, **78**, pp. 1–6 (1982).

[56] R. Brodersen, B. Honore, F.G. Larsen, Serum albumin - A non-saturable carrier. *Acta Pharmacologica et Toxicologica*, **54**, pp. 129–133 (1984).

[57] R. Brodersen et al., Characterization of binding equilibrium data by a variety of fitted isotherms. *Journal of Biochemistry*, **169**, pp. 487–495 (1987).

[58] P. Buchwald, N. Bodor, A simple, predictive, structure-based skin permeability model. *Journal of Pharmacy and Pharmacology*, **53**, pp. 1087–1098 (2001).

[59] M. Bundgaard, Transport pathways in capillaries - in search of pores. *Annual Reviews in Physiology*, **42**, pp. 325–336 (1980).

[60] R.E. Burgeson, A.M. Christiano, The dermal-epidermal junction. *Current Opinion in Cell Biology*, **9**, pp. 651–658 (1997).

[61] J.C. Bustamante, B.P. Setchell, The permeability of the microvasculature of the perfused rat testis to small hydrophilic substances. *Journal of Andrology*, **21**, pp. 444–451 (2000).

[62] F. Caligara, G. Rooth, Measurement of the oxygen diffusion coefficient in the subcutis of man. *Acta Physiologica Scandinavica*, **53**, pp. 114–127 (1961).

[63] D.C. Carter, J.X. Ho, Structure of serum albumin, *Advances in Protein Chemistry*, **45**, pp. 153–203 (1994).

[64] J.R. Casley-Smith, Endothelial fenestrae in intestinal villi: differences between the arterial and venous end of the capillaries. *Microvascular Research*, **3**, p. 49 (1971).

[65] R.H. Champion, Blood Vessels and Lymphatics of the Skin, pp. 114-123 in: *An Introduction to the Biology of Skin*, Ed. R.H, Champion, T. Gillman, A.J. Rook, R.T. Sims, Blackwell Scientific Publications, Oxford-Edinburgh (1970).

[66] R.L.S. Chang, A model of capillary solutes and fluid exchange. *Chemical Engineering Communications*, **4**, pp. 189–206 (1980).

[67] N. Charkoudian, Skin blood flow in adult human thermoregulation: How it works, when it does not, and why. *Mayo Clinic Proceedings*, **78**, pp. 603–612 (2003).

[68] S. Childress, Aspects of physiological fluid mechanics, pp. 141–163 in *Lectures in Applied Mathematics*, **19** - Mathematical Aspects of Physiology, Ed. F.C. Hoppensteadt, American Mathematical Society, Providence, Rhode Island (1981).

[69] M. Chvapil, pp. 32–33, 83–87 in *Physiology of Connective Tissue*, Butterworths, London (1967).

[70] T.J. Cieslak, G.W. Christofer, M.G. Ottolini, Biological warfare and the skin II: Viruses. *Clinics in Dermatology*, **20**, pp. 355–364 (2002).

[71] T.J. Cieslak, T.B. Talbot, B.H. Hartstein, Biological warfare and the skin I: Bacteria and toxins. *Clinics in Dermatology*, **20**, pp. 346–354 (2002).

[72] D.S. Clague, R.J. Phillips, Hindered diffusion of spherical macromolecules through dilute fibrous media. *Physics of Fluids*, **8**, pp. 1720–1731 (1996).

[73] R.L. Cleek, A.L. Bunge, A new method for estimating dermal absorption from chemical exposure. 1. General approach. *Pharmaceutical Research*, **10**, pp. 497–506 (1993).

[74] G. Clough, A quantitative study of the exchange microvasculature of muscles from the human foot and hand. *International Journal of Microcirculation: Clinical and Experimental*, **6**, pp. 237–243 (1987).

[75] G.R. Cokelet, The Rheology of Human Blood, pp. 63–103 in *Biomechanics, Its Foundations and Objectives*, Ed. Y.C. Fung, N. Perrone, M. Anliker, Prentice-Hall Inc. Englewood Cliffs, NJ (1970).

[76] W.D. Comper, T.C. Laurent, Physiological function of connective tissue polysaccharides. *Physiological Reviews*, **58**, pp. 255–315 (1978).

[77] D.M. Connelly, Silver nitrate. Ideal burn wound therapy? *NY State Journal of Medicine*, **70**, pp. 1642–1644 (1970).

[78] E.R. Cooper, Effect of diffusional lag time on multicompartmental pharmacokinetics for transepidermal infusion. *Journal of Pharmaceutical Sciences*, **68**, pp. 1469–1470 (1979).

[79] E.R. Cooper, Increased skin permeability for lipophilic molecules. *Journal of Pharmaceutical Sciences*, **73**, pp. 1153–1156 (1984).

[80] E.R. Cooper, B. Berner, Finite dose pharmacokinetics of skin penetration. *Journal of Pharmaceutical Sciences*, **74**, pp. 1100–1102 (1985).

[81] G. Cotta-Pereira, F.G. Rodrigo, S. Bittencourt-Sampaio, Oxytalan, elaunin and elastic fibers in the human skin. *The Journal of Investigative Dermatology*, **66**, pp. 143–148 (1976).

[82] T. Cowen, P. Trigg, R.A.J. Eady, Distribution of mast cells in human dermis: development of a mapping technique. *British Journal of Dermatology*, **100**, pp. 635–640 (1979).

[83] R.G. Cox, The motion of long slender bodies in a viscous fluid. Part 1. General theory. *Journal of Fluid Mechanics*, **44**, pp. 791–810 (1970).

[84] R.G. Cox, The motion of long slender bodies in a viscous fluid. Part 2. Shear flow. *Journal of Fluid Mechanics*, **45**, pp. 625–657 (1971).

[85] C. Crone, Permeability of single capillaries compared with results from whole-organ studies. *Acta Physiologica Scandinavica Suppl.*, **463**, pp. 75–80 (1979).

[86] C. Crone, D.G. Levitt, Capillary permeability to small solutes. *Handbook of Physiology. The Cardiovascular System. Microcirculation*, Bethesda, MD: American Physiological Society, sect. 2, **IV**, chapt.10, pp. 411–466 (1984).

[87] S.E. Cross et al., Determination of the effect of lipophilicity on the *in vitro* permeability and tissue characteristics of topically applied solutes in human skin layers. *Journal of Investigative Dermatology*, **120**, pp. 759–764 (2003).

[88] S.E. Cross, Z. Wu, M.S. Roberts, The effect of protein binding on the deep tissue penetration and efflux of dermally applied salicylic acid, lidocaine, and diazepam in the perfused rat hindlimb. *The Journal of Pharmacology and Experimental Therapeutics*, **277**, pp. 366–374 (1996).

[89] S.E. Cross, M.S. Roberts, Targeting local tissues by transdermal application: Understanding drug physicochemical properties that best exploit protein binding and blood flow effects. *Drug Development Research*, **46**, pp. 309–315 (1999).

[90] C. Cullander and R.H. Guy, (D) Routes of delivery: case studies. (6) Transdermal delivery of peptides and proteins. *Advanced Drug Delivery Reviews*, **8**, pp. 291–329 (1992).

[91] F.E. Curry, Mechanics and thermodynamics of transcapillary exchange. *Handbook of Physiology. The Cardiovascular System. Microcirculation*, Bethesda, MD: American Physiological Society, sect. 2, **IV**, chapt.10, pp. 309–374 (1983).

[92] F.E. Curry, C.C. Michel, A fiber matrix model of capillary permeability. *Microvascular Research*, **20**, pp. 96–99 (1980).

[93] P.F. Curran, S.G. Schultz, Transport across membranes: general principles, pp. 1217–1243 in *Handbook of Physiology*, **III**, Marely Press (1968).

[94] M.G. Davidson, W.M. Deen, Hydrodynamic theory for the hindered transport of flexible macromolecules in porous membranes. *Journal of Membrane Science*, **35**, pp. 167–192 (1988).

[95] D.A.P. Davis et al., Percutaneous absorption of salicylic acid after repeated (14-day) in vivo administration to normal, acnegenic or aged human skin. *Journal of Pharmaceutical Sciences*, **86**, pp. 896–899 (1997).

[96] T.H. Dawson, Scaling laws for capillary vessels of mammals at rest and in exercise. *Proceedings of the Royal Society of London B*, **270**, pp. 755–763 (2003).

[97] T.D. Day, The permeability of interstitial connective tissue and the nature of the interfibrillary substance. *Journal of Physiology*, **117**, pp. 1–8 (1952).

[98] Y.S.N. Day, D.G. Myszka, Characterizing a drug's primary binding site on albumin. *Journal of Pharmaceutical Sciences*, **92**, pp. 333–343 (2003).

[99] W.M. Deen, Hindered transport of large molecules in liquid-filled pores. *AIChE Journal*, **33**, pp. 1409–1425 (1987).

[100] W.M. Deen, pp. 132–164 in Analysis of Transport Phenomena, Oxford University Press, New York (1998).

[101] T.R. DeGrado, S. Wang, Transcapillary transport of Metaiodobenzylguanidine (MIBG) in isolated rat heart. *Nuclear Medicine & Biology*, **25**, pp. 455–465 (1998).

[102] K. Denbigh F. R. S. , The Principles of Chemical Equilibrium. **4**th Edition, Cambridge University Press, New York (1981).

[103] J.N. Diana, B.P. Fleming, L.E. Bairnsfather, Correlation of fluid exchange in the microcirculation and macrocirculation. *International Journal of Microcirculation: Clinical and Experimental*, **1**, pp. 393–407 (1982).

[104] L.A. Diaz, Molecular structure of the epidermal extracellular spaces. *International Journal of Dermatology*, **18**, pp. 434–442 (1979).

[105] K. Diemer, Eine verbesserte modellvorstellung zur O_2-versorgung des gehirns. *Naturwissenschaften*, **50**, pp. 617–618 (1963).

[106] W.E. Dressler, Percutaneous absorption of hair dyes, pp. 489–536 in *Dermal Absorption and Toxicity Assessment*, Ed. M.S. Roberts, K.A. Walters, Marcel Dekker Inc., New York-Basel-Hong Kong (1998).

[107] M.C. Drumond, W.M. Deen, Hindered transport of macromolecules through a single row of cylinders: Application to glomerular filtration. *Journal of Biomechanical Engineering - Transactions of the ASME*, **117**, pp. 414–422 (1995).

[108] S.M. Eaton et al., A multi-organ, axially distributed model of capillary permeability for a magnetic resonance imaging contrast agent. *Journal of Pharmaceutical Sciences*, **82**, pp. 531–536 (1993).

[109] A. Edwards, B.S. Daniels, W.M. Deen, Hindered transport of macromolecules in isolated glomeruli .II. Convection and pressure effects in basement membrane. *Biophysical Journal*, **72**, pp. 241–222 (1997).

[110] D.L. Edwards, C.E. Johnson, Insect-repellent-induced toxic encephalopathy in a child. *Clinical Pharmacology*, **6**, pp. 496–498 (1987).

[111] D.A. Edwards and R. Langer, A linear theory of transdermal transport phenomena. *Journal of Pharmaceutical Sciences*, **83**, pp. 1315–1334 (1994).

[112] P.M. Elias and D.S. Friend, The permeability barrier in mammalian epidermis. *Journal of Cell Biology*, **65**, pp. 180–191 (1979).

[113] D.W. Fawcett, pp. 525–558 in *A Textbook of Histology*, 12th Edition, Chapman & Hall, New York - London (1994).

[114] R.J. Feldmann, H.I. Maibach, Percutaneous penetration of some pesticides and herbicides in man. *Toxicology and Applied Pharmacology*, **28**, pp. 126–132 (1974).

[115] A.G. Ferdman, I.V. Yannas, Scattering of light from histologic sections: A new method for the analysis of connective tissue. *The Journal of Investigative Dermatology*, **100**, pp. 710–716 (1993).

[116] G.J. Fleischman, T.W. Secomb, Effect of extravascular pressure gradients on capillary fluid exchange. *Mathematical Biosciences*, **81**, pp. 145–164 (1986).

[117] M.F. Flessner, R.L. Dedrick, J.S. Schultz, A distributed model of peritoneal-plasma transport: theoretical considerations. *American Journal of Physiology*, **246**, pp. R597–R607 (1984).

[118] J.E. Fletcher, Mathematical modeling of the microcirculation. *Mathematical Biosciences*, **38**, pp. 159–202 (1978).

[119] G.L. Flynn and B. Stewart, Percutaneous drug penetration: choosing candidates for transdermal development. *Drug Development Research*, **13**, pp. 169–185 (1988).

[120] B. Forslind, A domain mosaic model of the skin barrier. *Acta Dermatologica e Venereologica (Stockholm)*, **74**, pp. 1–6 (1994).

[121] B.M. Fu, R.H. Adamson, F.E. Curry, Test of a two-pathway model for small-solute exchange across the capillary wall. *American Journal of Physiology*, **274**, pp. H2062–H2073 (1998).

[122] B.M. Fu, F.E. Curry, S. Weinbaum, A diffusion wake model for tracer ultrastructure-permeability studies in microvessels. *American Journal of Physiology*, **269**, pp. H2124–H2140 (1995).

[123] B.M. Fu, S. Weinbaum, R.Y. Tsay, F.E. Curry, A junction-orifice-fiber entrance layer model for capillary permeability: Application to frog mesenteric capillaries. *Journal of Biomechanical Engineering*, **116**, pp. 502–513 (1994).

[124] G.F. Gerberick et al., Understanding fragrance allergy using an exposure-based risk assessment approach. *Contact Dermatitis*, **45**, pp. 333–340 (2001).

[125] T. Gillman, The Dermis, pp. 76–113 in: *An Introduction to the Biology of Skin*, Ed. R.H, Champion, T. Gillman, A.J. Rook, R.T. Sims, Blackwell Scientific Publications, Oxford-Edinburgh (1970).

[126] A. Gonsho et al., Controlled (trans)dermal delivery of an antiviral agent (acyclovir). I : An in vivo animal model for efficacy evaluation in cutaneous HSV - 1 infections. *International Journal of Pharmaceutics*, **65**, pp. 183–194 (1990).

[127] R.W. Gore, P.F. McDonagh, Fluid exchange across single capillaries. *Annual Reviews of Physiology*, **42**, pp. 337-357 (1980).

[128] C.A. Goresky, W.H. Ziegler, G.G. Bach, Capillary exchange modeling. *Circulation Research*, **27**, pp. 739–764 (1970).

[129] J.F. Gross, J. Aroesty, Mathematical models of capillary flow: A critical review. *Biorheology*, **9**, pp. 225–264 (1972).

[130] W. Grunewald, The influence of the three dimensional capillary pattern on the intercapillary oxygen diffusion-a new composed model for comparison of calculated and measured oxygen distribution pp. 5–17 in *Oxygen Supply* (Ed. M. Kessler et al.), Urban & Schwarzenberg, Munchen-Berlin-Wien (1973).

[131] D.C. Guell, H. Brenner, Physical mechanism of membrane osmotic phenomena. *Industrial and Engineering Chemical Research*, **35**, pp. 3004-3014 (1996).

[132] N. Guerin, S. Enoch, G. Tayeb, Combined method for the computation of the doubly periodic Green's function. *Journal of Electromagnetic Waves and Applications*, **15**, pp. 205–221 (2001).

[133] E. Gupta, M.G. Wientjes, J.L.-S. Au, Penetration kinetics of 2'-3'-dideoxyinosine in dermis is described by the distributed model. *Pharmaceutical Research*, **12**, pp. 108–112 (1995).

[134] R.H. Guy, Current status and future prospects of transdermal drug delivery. *Pharmaceutical Research*, **13**, pp. 1765–1769 (1996).

[135] R.H. Guy, J. Hadgraft, Prediction of drug disposition kinetics in skin and plasma following topical administration. *Journal of Pharmaceutical Sciences*, **73**, pp. 883–887 (1984).

[136] R.H. Guy, J. Hadgraft, H.I. Maibach, A pharmacokinetic model for percutaneous absorption. *International Journal of Pharmaceutics*, **11**, pp. 119–129 (1982).

[137] A.R. Haake, K. Holbrook, The Structure and Development of Skin, pp. 70–114 *Dermatology in General Medicine*, Ed. I.M. Freedberg, A.Z. Eisen, K. Wolff,

K.F. Austen, L.A. Goldsmith, S.I. Katz, T.B. Fitzpatrick (Hon), 5th Edition, **I**, McGraw-Hill, New York (1999).

[138] J. Hadgraft, The epidermal reservoir: A theoretical approach. *International Journal of Pharmaceutics*, **2**, pp. 265–274 (1979).

[139] K. Harada et al., In-vitro permeability to salicylic acid of human, rodent, and shed snake skin. *Journal of Pharmacy and Pharmacology*, **45**, pp. 414–418 (1993).

[140] B. Haraldsson, U. Zackrisson, B. Rippe, Calcium dependence of histamine-induced increases in capillary permeability in isolated perfused rat hindquarters. *Acta Physiologica Scandinavica*, **128**, pp. 247–258 (1986).

[141] F.R. Haselton et al., An effective-diffusivity model of pulmonary capillary exchange: General theory, limiting cases and sensitivity analysis. *Mathematical Biosciences*, **70**, pp. 237–263 (1984).

[142] K. Hashimoto, The Apocrine Gland, pp. 1575–1596 in *The Physiology and Pathophysiology of the Skin*, Ed. A. Jarrett, Academic Press, London-New York, **V**(1978).

[143] T. Hatanaka, M. Inuma, K. Sugibayashi, Y. Morimoto, Prediction of skin permeability to drugs. I. Comparison with artificial membrane. *Chemical and Pharmaceutical Bulletin*, **38**, pp. 3452–3459 (1990).

[144] T. Hatanaka, E. Manabe, K. Sugibayashi, Y. Morimoto, An application of the hydrodynamic pore theory to percutaneous absorption of drugs. *Pharmaceutical Research*, **11**, pp. 654–658 (1994).

[145] G. Havenith, Individualized model of human thermoregulation for the simulation of heat stress response. *Journal of Applied Physiology*, **90**, pp. 1943–1954 (2001).

[146] X.M. He, D.C. Carter, Atomic structure and chemistry of human serum albumin. *Nature*, **358**, pp. 209–215 (1992).

[147] M. Heisig et al., Non steady-state descriptions of drug permeation through stratum corneum. I. The biphasic brick-and-mortar model. *Pharmaceutical Research*, **13**, pp. 421–426 (1996).

[148] R.F. Hertel, A. Creutzig, PGE_1 improves blood flow in skin capillaries of conscious rats (WKY and SHR) through their lifetime in different dose ranges. *Progress in Clinical and Biological Research*, **301**, pp. 429–433, (1989).

[149] J.C. Higgins, R.A.J. Eady, Human dermal microvasculature: I. Its segmental differentiation. Light and electron microscopic study. *British Journal of Dermatology*, **104**, pp. 117-129 (1981).

[150] A.E. Hill, Osmotic flow in membrane pores. *International Review of Cytology*, **163**, pp. 1–42 (1995).

[151] J. Hirate et al., Further observations on the disposition characteristics of salicylic acid in analbuminemic rats. *Biopharmaceutics and Drug Disposition*, **10**, pp. 299–309 (1989).

[152] K.V. Horoshenkov, S.N. Chandler-Wilde, Efficient calculation of two-dimensional periodic and waveguide acoustic Green's functions. *The Journal of the Acoustical Society of America*, **111**, pp. 1610–1622 (2002).

[153] R. Hsu, T.W. Secomb, A Green's function model for analysis of oxygen delivery to tissue by microvascular networks. *Mathematical Biosciences*, **96**, pp. 61–78 (1989).

[154] G. Hutten, G. Thews, P. Vaupel, Some special problems concerning the oxygen supply to tissue, as studied by an analogue computer pp. 25–31 in *Oxygen Supply*, (Ed. M. Kessler et al.), University Park Press, Baltimore (1973).

[155] S. Imayama, Scanning and transmission electron microscope study on the terminal blood vessels of the rat skin. *The Journal of Investigative Dermatology*, **76**, pp. 151–157 (1981).

[156] G.W. Jackson, D.F. James, The permeability of fibrous porous media. *The Canadian Journal of Chemical Engineering* **64**, pp. 364–374 (1986).

[157] A. Jarrett, The Epidermis and Its Relations with the Dermis, pp. 3-44 in: *The Physiology and Pathophysiology of the Skin, Vol I:The Epidermis*, Ed. A. Jarrett, Academic Press, London-New York, (1973).

[158] A. Jarrett, The Physical Nature of the Dermis in Living Skin, pp. 873-893 in: *The Physiology and Pathophysiology of the Skin, Vol III:The Dermis and the Dendrocytes*, Ed. A. Jarrett, Academic Press, London-New York, (1974).

[159] A. Jarrett, The Chemistry and Molecular Biology of Collagen, pp. 809-846 in: *The Physiology and Pathophysiology of the Skin, Vol III:The Dermis and the Dendrocytes*, Ed. A. Jarrett, Academic Press, London-New York, (1974).

[160] E.M. Johnson, D.A. Berk, R.K. Jain, W.M. Deen, Hindered diffusion in agarose gels: Test of effective medium model. *Biophysical Journal*, **70**, pp. 1017–1026 (1996).

[161] E.M. Johnson, W.M. Deen, Electrostatic effects on the equilibrium partitioning of spherical colloids in random fibrous media. *Journal of Colloid and Interface Science*, **178**, pp. 749–756 (1996).

[162] J.A. Johnson, T.A. Wilson, A model for capillary exchange. *American Journal of Physiology*, **210**, pp. 1299-1303 (1966).

[163] J.A. Johnson, et al., A distributed pore size model for capillaries. *Microvascular Research*, **10**, pp. 217–219 (1975).

[164] M.E. Johnson, D. Blankstein and R. Langer, Evaluation of solute permeation through the stratum corneum: lateral bilayer diffusion as the primary transport mechanism. *Journal of Pharmaceutical Sciences*, **86**, pp. 1162–1172 (1997).

[165] A. Joshi, J. Raje, Sonicated transdermal drug transport. *Journal of Controlled Release*, **83**, pp. 13–22 (2002).

[166] K. Kambe, Theory of electron diffraction by crystals. *Zeitschrift fur Naturforschung*, **22a**, pp. 422–431 (1967).

[167] A. Kamiya, B. Rippe, B. Folkow, Volume of the capillary exchange vessels measured with a gravimetric method in rat hindquarters. *Microvascular Research*, **17**, pp. 142–157 (1979).

[168] J.R. Kanagy, Sorption of Water by Collagen, pp. 373–391 in *Biophysical Properties if the Skin*, Ed. H.R. Elden, Wiley-Interscience, New York-London-Sydney-Tokyo (1971).

[169] G.B. Kasting, Kinetics of finite dose absorption through skin 1. Vanillylnonanamide. *Journal of Pharmaceutical Sciences*, **90**, pp. 202–212 (2001).

[170] G.B. Kasting, Personal communication, June 2002.

[171] G.B. Kasting, P.J. Robinson, Can we assign an upper limit to skin permeability? *Pharmaceutical Research*, **10**, pp. 930–931 (1993).

[172] G.B. Kasting, R.L. Smith & B.D. Anderson, Chapter 3: Prodrugs for dermal delivery: solubility, molecular size, and functional group effects, pp. 117–161 in *Prodrugs: Topical and Ocular Drug Delivery* (K.B. Sloan, ed.). Marcel Dekker, New York (1992).

[173] G.B. Kasting, R.L. Smith and E.R. Cooper, Effect of lipid solubility and molecular size on percutaneous absorption, pp. 138–153 in *Pharmacology and the Skin*, Ed. B. Shroot, H. Schaefer, Valbonne, Karger, Basel (1987).

[174] A. Katchalsky, P.F. Curran, Membrane Permeability to Nonelectrolytes: Discontinuous Systems, pp. 113–132 in *Nonequilibrium Thermodynamics in Biophysics*, Harvard University Press, Cambridge, Massachusetts (1965).

[175] O. Kedem, A. Katchalsky, Thermodynamic analysis of the permeability of biological membranes to non-electrolytes. *Biochimica et Biophysica Acta*, **27**, pp. 229–246, (1958).

[176] D.R. Keene, K. McDonald, The ultrastructure of the connective tissue matrix of skin and cartilage after high-pressure freezing and freeze-substitution. *The Journal of Histochemistry and Cytochemistry*, **41**, pp. 1141–1153 (1993).

[177] Y.-H. Kim, A.-H. Ghanem, W.L. Higuchi, Model studies of epidermal permeability. *Seminars in Dermatology*, **11**, pp. 145–156 (1992).

[178] V.M. Knepp, J. Hadgraft, R.H. Guy, Transdermal drug delivery: Problems and possibilities. *CRC Critical Reviews in Therapeutic Drug Carrier Systems*, **4**, pp. 13–37 (1987).

[179] J. Koch-Weser, E.M. Sellers, Binding of drugs to serum albumin. *Medical Intelligence*, **294**, pp. 311–316 (1976).

[180] E.K. Kozlova, A.M. Chernysh, T.N. Matteys, Modeling of blood flow as the result of filtration-reabsorption processes in capillaries. *Advances in Physiology Education*, **23**, pp. 32–39 (2000).

[181] U. Kragh-Hansen, Evidence for a large and flexible region of human serum albumin possessing high affinity binding sites for salicylate,warfarin, and other ligands. *Molecular Pharmacology*, **34**, pp. 160–171 (1988).

[182] E. Kramer, J.I. Routh, The binding of salicylic acid and acetylsalicylic acid to human serum albumin. *Clinical Biochemistry*, **6**, pp. 98–105 (1973).

[183] A. Krogh, The number and distribution of capillaries in muscles with calculations of the oxygen pressure head necessary for supplying the tissue. *Journal of Physiology - London*, **52**, pp. 409–415 (1919).

[184] A. Krogh, The supply of oxygen to the tissues and the regulation of the capillary circulation. *Journal of Physiology - London*, **52**, pp. 457–474 (1919).

[185] K. Kubota, Finite dose percutaneous drug absorption: A BASIC program for the solution of the diffusion equation. *Computers and Biomedical Research*, **24**, pp. 196–207 (1991).

[186] K. Kubota, T. Ishizaki, A diffusion-diffusion model for percutaneous absorption. *Journal of Pharmacokinetics and Biopharmaceutics*, **14**, pp. 409–415, (1986).

[187] K. Kubota , H.I. Maibach, A compartment model for percutaneous absorption: Compatibility of lag time and steady state flux with diffusion model. *Journal of Pharmaceutical Sciences*, **81**, pp. 863–865 (1992).

[188] K. Kubota , H.I. Maibach, Significance of viable skin layers in percutaneous permeation and its implication in mathematical models: Theoretical consideration based on parameters for betamethasone 17-valerate. *Journal of Pharmaceutical Sciences*, **83**, pp. 1300–1306 (1994).

[189] K. Kubota, E.H. Twizell, A nonlinear numerical model of percutaneous drug absorption. *Mathematical Biosciences*, **108**, pp. 157–178 (1992).

[190] K. Kubota, T. Yamada, Finite dose percutaneous absorption: Theory and its application to in vitro Timolol permeation. *Journal of Pharmaceutical Sciences*, **79**, pp. 1015–1019 (1990).

[191] J.L. Kucera, F.J. Bullock, The binding of salicylate to plasma protein from several animal species. *Journal of Pharmacy and Pharmacology*, **21**, pp. 293–296 (1969).

[192] Y.M. Kuo, W.A. Gustafson, J.J. Friedman, Radial diffusion effects in a finite extravascular space surrounding a single capillary. *Microvascular Research*, **5**, pp. 148–154 (1973).

[193] R.S. Kurban, J. Bhawan, Histologic changes in skin associated with aging. *Journal of Dermatologic Surgery and Oncology*, **16**, pp. 908–914 (1990).

[194] T. Kurihara-Bergstrom, et al., Percutaneous absorption enhancement of an ionic molecule by ethanol-water systems in human skin. *Pharmaceutical Research*, **7**, pp. 762–766 (1990).

[195] M. Lamah, P.S. Mortimer, J.A. Dormandy, Study of temporal and perfusion physiology of skin capillaries in the dorsum of the foot. *Journal of Vascular Research*, **38**, pp. 59–63 (2001).

[196] H.D. Landahl, Approximate solution for capillary exchange models with and without axial mixing. *Bulletin of Mathematical Biology*, **49**, pp. 719–727 (1987).

[197] R. Lange-Lieckfeldt and G. Lee, Use of a model lipid matrix to demonstrate the dependence of the stratum corneum's barrier properties on its internal geometry. *Journal of Controlled Release*, **20**, pp. 183–194 (1992).

[198] L.G. Leal, The slow motion of slender rod-like particles in a second-order fluid. *Journal of Fluid Mechanics*, **69**, pp. 305–337 (1975).

[199] M. Lebwohl, The role of salicylic acid in the treatment of psoriasis. *International Journal of Dermatology*, **38**, pp. 16–24 (1999).

[200] A.J. Lee, J.R. King, D.A. Barrett, Percutaneous absorption: a multiple pathway model. *Journal of Controlled Release*, **45**, pp. 141–151 (1997).

[201] A. Leo, C. Hansch, D. Elkins, Partition coefficients and their uses. *Chemical Reviews*, **71**, pp. 525–615 (1971).

[202] J.R. Levick, Flow through interstitium and other fibrous matrices. *Quarterly Journal of Experimental Physiology*, **72**, pp. 409–438 (1987).

[203] J.R. Levick, A two-dimensional morphometry-based model of interstitial and transcapillary flow in rabbit synovium. *Experimental Physiology*, **76**, pp. 905–921 (1991).

[204] D.G. Levitt, Theoretical model of capillary exchange incorporating interactions between capillaries. *American Journal of Physiology*, **220**, pp. 250–255 (1971).

[205] D.G. Levitt, Capillary-tissue exchange kinetics: An analysis of the Krogh cylinder model. *Journal of Theoretical Biology*, **34**, pp. 103–124 (1972).

[206] D.G. Levitt, General continuum analysis of transport through pores: (II) Nonuniform pores. *Biophysical Journal*, **15**, pp. 553–563 (1975).

[207] K.L. Lin, L. Lopez, J.D. Hellums, Blood flow in capillaries. *Microvascular Research*, **5**, pp. 7–19 (1973).

[208] A.N. Lin, T. Nakatsui, Salicylic acid revisited. *International Journal of Dermatology*, **37**, pp. 335–342 (1998).

[209] N. Liron Stokes flow due to infinite arrays of stokeslets in three dimensions. *Journal of Engineering Mathematics*, **30**, pp. 267–297 (1996).

[210] T. Loftsson, The effect of ionization on partition coefficients and topical delivery. *Acta Pharmacologica Suecica*, **22**, pp. 209–214 (1985).

[211] J. Lundvall, T. Lanne, Much larger transcapillary hydrodynamic conductivity in skeletal muscle and skin of man than previously believed. *Acta Physiologica Scandinavica*, **136**, pp. 7–16 (1989).

[212] K.D. McCarley, A.L. Bunge, Physiologically relevant two-compartment models for skin. *Journal of Pharmaceutical Sciences*, **89**, pp. 1212–1235 (2000).

[213] J.N. McDougal, J.L. Jurgens-Whitehead, Short-term dermal absorption and penetration of chemicals from aqueous solutions: Theory and experiment. *Risk Analysis*, **21**, pp. 719–726.

[214] M.B. Mackaplow, E.S.G. Shaqfeh, A numerical study of the rheological properties of suspensions of rigid, non-Brownian fibers. *Journal of Fluid Mechanics*, **329**, pp. 155–186 (1996).

[215] S.C. McNeill, R.O. Potts, M.L. Francoeur, Local enhanced topical delivery (LETD) of drugs: Does it trully exist? *Pharmaceutical Research*, **9**, pp. 1422–1427 (1992).

[216] R. Manitz et al., On mathematical modeling of dermal and transdermal drug delivery. *Journal of Pharmaceutical Sciences*, **87**, pp. 873–879 (1998).

[217] S.L. Marshall, A periodic Green's function for calculation of coulombic lattice potentials. *Journal of Physics : Condensed Matter*, **12**, pp. 4575–4601 (2000).

[218] J.M. Mathieson, R.H. Pearce, J.L. Bert, Size of a plasma protein affects its content in postmortem human dermis. *Microvascular Research*, **32**, pp. 224-229 (1986).

[219] A.K. Mathur, S.K. Khanna, Dermal toxicity due to industrial chemicals. *Skin Pharmacology and Applied Skin Physiology*, **15**, pp. 147–153 (2002).

[220] H.N. Mayrovitz, Skin capillary metrics and hemodynamics in the hairless mouse. *Microvascular Research*, **43**, pp. 46–59 (1992).

[221] S.C. Mehta et al., Relationship of skin target site free drug concentration (C*) to the in vivo efficacy: An extensive evaluation of the predictive value of the C* concept using acyclovir as a model drug. *Journal of Pharmaceutical Sciences*, **86**, pp. 797–801 (1997).

[222] M.M. Mershon, Barrier surfaces of skin, pp. 41–73 in *Applied Chemistry at Protein Interfaces, Advances in Chemistry Series* 145, Ed. R.F. Gould, American Chemical Society, Washington D.C. (1975).

[223] H. Metzger, Geometric considerations in modeling oxygen transport processes in tissue. *Advances in Experimental and Medicinal Biology*, **37b**, pp. 761–772 (1973).

[224] A.S. Michaels, S.K. Chandrasekaran, J.E. Shaw, Drug permeation through human skin: theory and in-vitro experimental measurement. *AIChE Journal*, **21**, pp. 985–996 (1975).

[225] C.C. Michel, Capillary permeability and how it may change. *Journal of Physiology*, **404**, pp. 1–29 (1988).

[226] C.C. Michel, Transport of macromolecules through microvascular walls. *Cardiovascular Research*, **32**, pp. 644–653 (1996).

[227] C.C. Michel, Starling: The formulation of his hypothesis of microvascular fluid exchange and its significance after 100 years. *Experimental Physiology*, **82**, pp. 1–30 (1997).

[228] C.C. Michel, F.E. Curry, Microvascular permeability. *Physiological Reviews*, **79**, pp. 703–761 (1999).

[229] M. Mihara et al., Scanning electron microscopy of the epidermal lamina densa in normal human skin. *Journal of Investigative Dermatology*, **99**, pp. 572–578 (1992).

[230] S.R Miselnicky, J.L. Lichtin, A. Sakr, R.L. Bronaugh, The influence of solubility, protein binding, and percutaneous absorption on reservoir formation in skin. *Journal of the Society of Cosmetic Chemists*, **39**, pp. 169–177 (1988).

[231] W. Montagna, A.M. Kligman, K.S. Carlisle, Atlas of normal human skin. Springer-Verlag, New York (1992).

[232] N.A. Monteiro-Riviere et al., Interspecies and interregional analysis of the comparative histologic thickness and laser doppler blood flow measurements at five cutaneous sites in nine species. *The Journal of Investigative Dermatology*, **95**, pp. 582–586 (1990).

[233] N.A. Monteiro-Riviere et al., Topical penetration of piroxicam is dependent on the distribution of the local cutaneous vasculature. *Pharmaceutical Research*, **10**, pp. 1326–1331 (1993).

[234] C.J. Morgan, A.G. Renwick, P.S. Friedman, The role of stratum corneum and dermal microvascular perfusion in penetration and tissue levels of water-soluble drugs investigated by microdialysis. *British Journal of Dermatology*, **148**, pp. 434–443 (2003).

[235] D.J. Morgan, Permeability of myocardial capillaries to hydrophilic drugs: The paracellular pathway. *Clinical and Experimental Pharmacology and Physiology*, **23**, pp. 975–979 (1996).

[236] L. Moore, Y.W. Chien, Transdermal drug delivery: A review of pharmaceutics, pharmacokinetics, and pharmacodynamics. *CRC Critical Reviews in Therapeutic Drug Carrier Systems*, **4**, pp. 285–349 (1988).

[237] C.J. Morgan, A.G. Renwick, P.S. Friedman, The role of stratum corneum and dermal microvascular perfusion in penetration and tissue levels of water-soluble drugs investigated by microdialysis. *British Journal of Dermatology*, *148*, pp. 434–443 (2003).

[238] Y. Morimoto, K. Sugibayashi and H. Natsume, The transdermal drug delivery system and transcutaneous absorption. *Acta Dermatologica e Venereolica (Stockholm)*, **74**, Suppl. 185, pp. 15–17 (1994).

[239] N.G. Nerella, L.H. Block, P.K. Noonan, The impact of lag time on the estimation of pharmacokinetic parameters. I. One - compartment open model. *Pharmaceutical Research*, **10**, pp. 1031–1036 (1993).

[240] J.M. Nitsche, On Brownian dynamics with hydrodynamic wall effects: A problem in diffusion near a fiber, and the meaning of the no-flux boundary condition. *Chemical Engineering Communications*, **148–150**, pp. 623–651 (1996).

[241] G.F. Odland, Structure of the Skin, pp. 3–63 in: *Biochemistry and Physiology of the Skin*, Ed. L.A. Goldsmith, Oxford University Press, New York - Oxford **I** (1983).

[242] T. Ogiso et al., A pharmacokinetic model for the percutaneous absorption of Indomethacin and the prediction of drug disposition kinetics. *Journal of Pharmaceutical Sciences*, **78**, pp. 319–322 (1989).

[243] A.G. Ogston, The spaces in a uniform random suspension of fibers. *Transactions of the Faraday Society*, **54**, pp. 1754–1757 (1958).

[244] A.G. Ogston, B.N. Preston, J.D. Wells, On the transport of compact particles through solutions of chain-polymers. *Proceedings of the Royal Society of London A*, **333**, pp. 297–316 (1973).

[245] A. Oikarinen, A. Knuutinen, Mechanical properties of human skin: Biochemical aspects, pp. 3–16 in *Bioengineering of the Skin*, Ed. P. Elsner, E. Berardesca, K.P. Wilhelm, H.I. Maibach, CRC Press, Boca Raton-London-New York-Washington D.C. (2002).

[246] H. Okamoto et al., Analysis of drug penetration through the skin by the two layer skin model. *Pharmaceutical Research*, **6**, pp. 931–937 (1989).

[247] W.S. Opong, A.L. Zydney, Effect of membrane structure and protein concentration on the osmotic reflection coefficient. *Journal of Membrane Science*, **72**, pp. 277–292 (1992).

[248] S.G. Owen, H.W. Francis, M.S. Roberts, Disappearance kinetics of solutes from synovial fluid after intra-articular injection. *British Journal of Clinical Pharmacology*, **38**, pp. 349–355 (1994).

[249] H. Oxlund, J. Manschot, A. Viidik, The role of elastin in the mechanical properties of skin. *Journal of Biomechanics*, **21**, pp. 213–218 (1988).

[250] W.P. Paaske, Capillary permeability in cutaneous tissue. *Acta Physiologica Scandinavica*, **98**, pp. 492–499 (1976).

[251] W.P. Paaske, Absence of restricted diffusion in cutaneous capillaries. *Acta Physiologica Scandinavica*, **100**, pp. 332–339 (1977).

[252] W.P. Paaske, P. Sejrsen, Permeability of continuous capillaries. *Danish Medical Bulletin*, **36**, pp. 570–590 (1989).

[253] G.E. Palade, M. Simionescu, N. Simionescu, Structural aspects of the permeability of the microvascular endothelium. *Acta Physiologica Scandinavica, Suppl.*, **463**, pp. 11–32 (1979).

[254] H.D. Papenfuss, J.F. Gross, Transluminal Filtration, pp. 41–62 in *Mathematics in Microcirculation Phenomena*, Ed. J.F. Gross, A. Popel, Raven Press, New York (1980).

[255] J.R. Pappenheimer, E.M. Renkin, L.M. Borrero, Filtration, diffusion and molecular sieving through peripheral capillary membranes. *American Journal of Physiology*, **167**, pp. 13–46 (1951).

[256] J.C. Parker, M.A. Perry, A.E. Taylor, Permeability of the microvascular barrier, pp. 143–187 in: *Edema* Ed. N.C. Staub, A.E. Taylor, Raven Press, NY (1984).

[257] D.A.D. Parry, A.S. Craig, Collagen fibrils during development and maturation and their contribution to the mechanical attributes of connective tissue, pp. 1–23 in *Collagen, Vol II: Biochemistry and Biomechanics*, Ed. M.E. Nimni, CRC Press, Boca Raton (1988).

[258] R.H. Pearce, Glycosaminoglycans and glycoproteins in skin, pp. 149–193 in *The Amino Sugars. Vol IIA, Distribution and Biological Role*, Ed. E.A. Balazs, R.W. Jeanloz, Academic Press, New York-London (1965).

[259] R.H. Pearce, B.J. Grimmer, Age and the chemical constitution of normal human dermis. *The Journal of Investigative Dermatology*, **58**, pp. 347–361 (1972).

[260] R.H. Pearce, B.J. Grimmer, The Nature of the Ground Substance, pp. 89–100.

[261] K.D. Peck, A.-H. Ghanem, W.I. Higuchi, Hindered diffusion of polar molecules through and effective pore radii estimates of intact and ethanol treated epidermal membrane. *Pharmaceutical Research*, **11**, pp. 1306–1314 (1994).

[262] K.D. Peck, A.-H. Ghanem, W.I. Higuchi, The effect of temperature upon the permeation of polar and ionic solutes through human epidermal membrane. *Journal of Pharmaceutical Sciences*, **84**, pp. 975–982 (1995).

[263] W. Perl, Modified filtration-permeability model of transcapillary transport-a solution of the Pappenheimer pore puzzle? *Microvascular Research*, **3**, pp. 233–251 (1971).

[264] W. Perl, A friction coefficient, series-parallel channel model for transcapillary flux of nonelectrolytes and water. *Microvascular Research*, **6**, pp. 169–193 (1973).

[265] W. Perl, Convection and permeation of albumin between plasma and interstitium. *Microvacular Research*, **10**, pp. 83–94 (1975).

[266] W.T. Perrins, D.R. McKenzie, R.C. McPhedran, Transport properties of regular arrays of cylinders. *Proceedings of the Royal Society of London A*, **369**, pp. 207–225 (1979).

[267] R.J. Phillips, A hydrodynamic model for hindered diffusion of proteins and micelles in hydrogels. *Biophysical Journal*, **79**, pp. 3350–3354 (2000).

[268] R.J. Phillips, W.M. Deen, J.F. Brady, Hindered transport of spherical macromolecules in fibrous membranes and gels. *AIChE Journal*, **35**, pp. 1761–1769 (1989).

[269] R.J. Phillips, W.M. Deen, J.F. Brady, Hindered transport on fibrous membranes and gels: Effect of solute size and fiber configuration. *Journal of Colloid and Interface Science*, **139**, pp. 363–372 (1990).

[270] S.R. Pinnell, S. Murad, Collagen, pp. 385–410 in: *Biochemistry and Physiology of the Skin*, Ed. L.A. Goldsmith, Oxford University Press, New York - Oxford, **I** (1983).

[271] G.E. Plante et al., Consequences of alteration in capillary permeability. *Canadian Journal of Physiology and Pharmacology*, **74**, pp. 824–833 (1996).

[272] T.S. Poet, J.N. McDougal, Skin absorption and human risk assessment. *Chemico-Biological Interactions*, **140**, pp. 19–34 (2002).

[273] A.S. Popel, Analysis of capillary-tissue diffusion in multicapillary systems. *Mathematical Biosciences*, **39**, pp. 187–211 (1978).

[274] A.S. Popel, Mathematical modeling of convective and diffusive transport in the microcirculation, pp. 63–88 in *Mathematics of Microcirculation Phenomena*, Ed. J.F. Gross and A. Popel, Raven Press, NY (1980).

[275] R.O. Potts and M.L. Francoeur, Influence of stratum corneum morphology on water permeability. *Journal of Investigative Dermatology*, **96**, pp. 495–499 (1991).

[276] R.O. Potts and R.M. Guy, Predicting skin permeability. *Pharmaceutical Research*, **9**, pp. 663–669 (1992).

[277] R.O. Potts and R.M. Guy, A predictive algorithm for skin permeability: the effects of molecular size and hydrogen bond activity. *Pharmaceutical Research*, **12**, pp. 1628–1633 (1995).

[278] C.A. Poulain, B.A. Finlayson, J.B. Bassingthwaighte, Efficient numerical methods for nonlinear-facilitated transport and exchange in a blood-tissue exchange unit. *Annals of Biomedical Engineering*, **25**, pp. 547–564 (1997).

[279] P. Poulin, K. Schoenlein, F.P. Theil, Prediction of adipose tissue: Plasma partition coefficients for structurally unrelated drugs. *Journal of Pharmaceutical Sciences*, **90**, pp. 436–447 (2001).

[280] M.R. Prausnitz, Overcoming skin's barrier: The search for effective and user-friendly drug delivery. *Diabetes Technology and Therapeutics*, **3**, pp. 233–236 (2001).

[281] E.J. Purcell, pp. 584–587 in : Calculus, with analytic geometry. Appleton-Century-Crofts, New York (1965).

[282] R.D. Purves, Multiple solutions, illegal parameter values, local minima of the sum of squares, and anomalous parameter estimates in least-squares fitting of the two-compartment pharmacokinetic model with absorption. *Journal of Pharmacokinetics and Biopharmaceutics*, **24**, pp. 79–101 (1996).

[283] G.L. Qiao, P.L. Williams, J.E. Riviere, Percutaneous absorption, biotransformation, and systemic disposition of parathion in vivo in swine. I. Comprehensive pharmacokinetic model. *Drug Metabolism and Disposition*, **22**, pp. 459–471 (1994).

[284] Lord Rayleigh, Sec.R.S. In the influence of obstacles arranged in rectangular order upon the properties of a medium. *Philosophical Magazine and Journal of Science*, **36**, pp. 481–503 (1892).

[285] R.K. Reed, B.D. Bowen, J.E. Bert, Microvascular exchange and interstitial volume regulation in the rat: implications of the model. *American Journal of Physiology*, **257**, pp. H2081–H2091 (1989).

[286] R.K. Reed, S. Lepsœ, H. Wiig, Interstitial exclusion of albumin in rat dermis and subcutis in over- and dehydration. *American Journal of Physiology*, **257**, pp. H1819-H1827 (1989).

[287] R.C. Reid, The properties of gases and liquids. *Ed. R.C. Reid, J.M. Prausnitz, B.E. Poling*, 4th edition, McGraw-Hill, New York (1987).

[288] M.S. Rendell et al., A comparison of the cutaneous microvascular properties of the spontaneously hypertensive rat and the Wistar-Kyoto rat. *Comparative Biochemistry and Physiology Part A*, **122**, pp. 399–406 (1999).

[289] D.D. Reneau, M.H. Knisely, A mathematical simulation of oxygen transport in the human brain under conditions of countercurrent capillary blood flow. *Chemical Engineering Progress*, **67**, pp. 18–27 (1971).

[290] E.M. Renkin, Transport of large molecules across capillary walls. *Physiologist*, **7**, pp. 13–28 (1964).

[291] E. Renkin, Relation of capillary morphology to transport of fluid and large molecules: a review. *Acta Physiologica Scandinavica, Suppl.*, **463**, pp. 81–91 (1979).

[292] A. Rescigno, Brief retrospectives in pharmacokinetics. *Journal of Pharmacokinetics and Biopharmaceutics*, **22**, pp. 255–257 (1994).

[293] B. Rippe, B. Haraldsson, Capillary permeability in rat hindquarters as determined by estimations of capillary reflection coefficients. *Acta Physiologica Scandinavica*, **127**, pp. 289–303 (1986).

[294] W.A. Ritschel and A.S. Hussain, The principles of permeation of substances across the skin. *Methods and Findings in Experimental and Clinical Pharmacology*, **10**, pp. 39–56 (1988).

[295] J.E. Riviere, M.C. Heit, Electrically-assisted transdermal drug delivery. *Pharmaceutical Research*, **14**, pp. 687–697 (1997).

[296] J.E. Riviere, B. Sage, P.L. Williams, Effects of vasoactive drugs on transdermal lidocaine iontophoresis. *Journal of Pharmaceutical Sciences*, **80**, pp. 615–620 (1991).

[297] C.C. Roberts et al., Skin microvascular architecture and perfusion studied in human postmastectomy oedema by intravital video-capillaroscopy. *International Journal of Microcirculation*, **14**, pp. 327-337 (1994).

[298] M.S. Roberts, Targeted drug delivery to the skin and deeper tissues: Role of physiology, solute structure and disease. *Clinical and Experimental Pharmacology and Physiology*, **24**, pp. 874–879 (1997).

[299] M.S. Roberts, Personal communication, September 2001.

[300] M.S. Roberts, Personal communication, September 2003.

[301] M.S. Roberts, S.E. Cross, A physiological pharmacokinetic model for solute disposition in tissues below a topical application site. *Pharmaceutical Research*, **16**, pp. 1392–1398 (1999).

[302] M.S. Roberts, K.A. Walters, The relationship between structure and barrier function in skin, pp. 1–42 in *Dermal Absorption and Toxicity Assessment*, Ed. M.S. Roberts, K.A. Walters, Marcel Dekker Inc., New York-Basel-Hong Kong (1998).

[303] D. Robertshaw, Apocrine Sweat Glands, pp. 642–653 in: *Biochemistry and Physiology of the Skin*, Ed. L.A. Goldsmith, Oxford University Press, New York - Oxford **I** (1983).

[304] R.J. Roselli, T.R. Harris, A four phase model of capillary tracer exchange. *Annals of Biomedical Engineering*, **7**, pp. 203–238 (1979).

[305] J. Rosenbloom, W.R. Abrams, R. Mecham, Extracellular matrix 4: The elastic fiber. *FASEB Journal*, **7**, pp. 1208–1218 (1993).

[306] N. Rossing, A.M. Worm, Interstitial fluid: Exchange of macromolecules between plasma and skin interstitium. *Clinical Physiology*, **1**, pp. 275–284 (1981).

[307] P. Rous, H.P. Gilding, F. Smith, The gradient of vascular permeability. *Journal of Experimental Medicine*, **51**, pp. 807–830 (1930).

[308] M. Rowland, A. McLachlan, Pharmacokinetic considerations of regional administration and drug targeting: Influence of site of input in target tissue and flux of binding protein. *Journal of Pharmacokinetics and Biopharmaceutics*, **24**, pp. 369–387 (1996).

[309] M. Rucker, F. Roesken, B. Vollmar, M.D. Menger, A novel approach for comparative study of periosteum, muscle, subcutis, and skin microcirculation by intravital fluorescence microscopy. *Microvascular Research*, **56**, pp. 30–42 (1998).

[310] T.J. Ryan, pp. 578–625 in *The Physiology & Pathophysiology of the Skin, Vol II: The Nerves and Blood Vessels* Ed. A. Jarrett, Academic Press, London-New York (1973).

[311] T.J. Ryan, Permeability and responses of blood vessels in skin, pp. 681–718 in *The Physiology & Pathophysiology of the Skin, Vol II: The Nerves and Blood Vessels* Ed. A. Jarrett, Academic Press, London-New York (1973).

[312] T.J. Ryan, The Lymphatics of the Skin, pp. 1755–1780 in *The Physiology and Pathophysiology of the Skin, Vol V*, Ed. A. Jarrett, Academic Press, London-New York, (1978).

[313] T.J. Ryan, Cutaneous circulation, pp. 817–877 in *Biochemistry and Physiology of the Skin*, Ed. L.A. Goldsmith, Oxford University Press, New York - Oxford **II** (1983).

[314] T.J. Ryan, Distinguishing lymphatics from blood vessels in normal and diseased skin. *Lymphology*, **20**, pp. 179–181 (1987).

[315] E.P. Salathe, Convection and diffusion in the extravascular phase. *Mathematics of Microcirculation Phenomena*, Ed. J.F. Gross, A. Popel, Raven Press, New York (1980).

[316] J.E. Sanders et al., Image processing techniques for quantitative analysis of skin structures. *Computer Methods and Programs in Biomedicine*, **59**, pp. 167–180 (1999).

[317] A.S. Sangani, A. Acrivos, Slow flow past periodic arrays of cylinders with application to heat transfer. *International Journal of Multiphase Flow*, **8**, pp. 193–206 (1982).

[318] A.S. Sangani, C. Yao, Transport properties in random arrays of cylinders. I. Thermal conduction. *Physics of Fluids*, **31**, pp. 2426–2434 (1988).

[319] K. Sato, The Physiology and Pharmacology of the Eccrine Sweat Gland, pp. 596–641 in: *Biochemistry and Physiology of the Skin*, Ed. L.A. Goldsmith, Oxford University Press, New York - Oxford **I** (1983).

[320] K. Sato et al., Estimation of blood concentration of drugs after topical application from in vitro skin permeation data. I. Prediction by convolution and confirmation by deconvolution. *Chemical and Pharmaceutical Bulletin*, **36**, pp. 2232–2238 (1988).

[321] V.C. Scanlon, T. Sanders, pp. 234–255 in *Essentials of Anatomy and Physiology*, 3rd Edn., F.A. Davis Company, Philadelphia (1999).

[322] W. Schalla, H. Schaefer, Mechanism of penetration of drugs into the skin, pp. 41–72 in *Dermal and Transdermal Absorption, 1st International Symposium, January 12-14, 1981, Munich*, Ed. R. Brandau, B.H. Lippold, Wissenschaftlichte Verlagsgesellschaft mbH, Stuttgart (1982).

[323] R.J. Scheuplein, Mechanism of percutaneous absorption. *The Journal of Investigative Dermatology*, **48**, pp. 79–88 (1967).

[324] R.J. Scheuplein, I.H. Blank, Permeability of the skin. *Physiological Reviews*, **51**, pp. 702–746 (1971).

[325] R.J. Scheuplein, R.L. Bronaugh, Percutaneous absorption, pp. 1255–1295 in: *Biochemistry and Physiology of the Skin*, Ed. L.A. Goldsmith, Oxford University Press, New York - Oxford **II** (1983).

[326] G.W. Schmid-Schönbein, Microlymphatics and lymph flow. *Physiological Reviews*, **70**, pp. 987–1028 (1990).

[327] A.T.M. Serajuddin, C.I. Jarowski, Effect of diffusion layer pH and solubility on the dissolution rate of pharmaceutical acids and their sodium salts II : Salicylic acid, theophylline and benzoic acid. *Journal of Pharmaceutical Sciences*, **74**, pp. 148–154 (1985).

[328] E.H. Serne et al., Impaired skin capillary recruitment in essential hypertension is caused by both functional and structural capillary rarefaction. *Hypertension*, **38**, pp. 238–242 (2001).

[329] J.C. Shah, Application of kinetic model to in vitro percutaneous permeation of drugs. *International Journal of Pharmaceutics*, **133**, pp. 179–189 (1996).

[330] D. Shanks, Non-linear transformations of divergent and slowly convergent sequences. *Journal of Mathematical Physics*, **34**, pp. 1–42 (1955).

[331] O. Siddiqui, Physicochemical, physiological, and mathematical considerations in optimizing percutaneous absorption of drugs. *Critical Reviews in Therapeutic Drug Carrier Systems*, **6**, pp. 1–38 (1989).

[332] A. Silberberg, Microcirculation and the extravascular space. *Microcirculation in Inflammation, Bibliotheca Anatomica*, **17**, pp. 54–65 (1979).

[333] J.E. Silbert, Structure and metabolism of proteoglycans and glycosaminoglycans. *The Journal of Investigative Dermatology*, **79**, pp. 31s–37s (1982).

[334] L. Simonsen, M.B. Petersen, L. Groth, In vivo skin penetration of salicylic compounds in hairless rats. *European Journal of Pharmaceutical Sciences*, **17**, pp. 95–104 (2002).

[335] R.T. Sims, The Epidermis, pp. 61–75 in: *An Introduction to the Biology of Skin*, Ed. R.H, Champion, T. Gillman, A.J. Rook, R.T. Sims, Blackwell Scientific Publications, Oxford-Edinburgh (1970).

[336] P. Singh, M.S. Roberts, Iontophoretic transdermal delivery of salicylic acid and lidocaine to local subcutaneous structures. *Journal of Pharmaceutical Sciences*, **82**, pp. 127–131 (1993).

[337] P. Singh, M.S. Roberts, Dermal and underlying tissue pharmacokinetics of salicylic acid after topical application. *Journal of Pharmacokinetics and Biopharmaceutics*, **21**, pp. 337–373 (1993).

[338] P. Singh, M.S. Roberts, Effects of vasoconstriction on dermal pharmacokinetics and local tissue distribution of compounds. *Journal of Pharmaceutical Sciences*, **83**, pp. 783–791 (1994).

[339] P. Singh, M.S. Roberts, Local deep tissue penetration of compounds after dermal application: Structure-tissue penetration relationships. *The Journal of Pharmacology and Experimental Therapeutics*, **279**, pp. 908–917 (1996).

[340] S. Singh et al. , Accelerating the convergence of series representing the free space periodic Green's function. *IEEE Transactions on Antennas and Propagation*, **38**, pp. 1958–1962 (1990).

[341] S. Singh, J. Singh, Transdermal drug delivery by passive diffusion and iontophoresis: A review. *Medicinal Research Reviews*, **13**, pp. 569–621 (1993).

[342] S. Singh, R. Singh, Efficient computation of the free-space periodic Green's function. *IEEE Transactions on Microwave Theory and Techniques*, **39**, pp. 1226–1229 (1991).

[343] R. Skalak, Mechanics of the Microcirculation pp. 457–499 in *Biomechanics, Its Foundations and Objectives*, Ed. Y.C. Fung, N. Perrone, M. Anliker, Prentice-Hall Inc. Englewood Cliffs, NJ (1970).

[344] R. Skalak, Blood rheology, pp. 109–139 in *Lectures in Applied Mathematics*, **19** - Mathematical Aspects of Physiology, Ed. F.C. Hoppensteadt, American Mathematical Society, Providence, Rhode Island (1981).

[345] K.B. Sloan, K.G. Siver, S.A.M. Koch, The effect of vehicle on the diffusion of salicylic acid through hairless mouse skin. *Journal of Pharmaceutical Sciences*, **75**, pp. 744–749 (1986).

[346] D.M. Smith, Restricted diffusion through pores with periodic restrictions. *AIChE Journal*, **32**, pp. 1039–1042 (1986).

[347] L.T. Smith, K.A. Holbrook, P.H. Byers, Structure of the dermal matrix during development and in the adult. *The Journal of Investigative Dermatology*, **79**, pp. 93s–104s (1982).

[348] R.I.C. Spearman, Structure and Function of Subcutaneous Tissue, pp. 2251-2281 in: *The Physiology and Pathophysiology of the Skin*, Ed. A. Jarrett, Academic Press, London-New York, **VII**(1982).

[349] M. Spiegel et al. Pressure of lymphatic capillaries in human skin. *American Journal of Physiology*, **262**, pp. H1208–H1210 (1992).

[350] E.H. Starling, On the absorption of fluids from the convective tissue spaces. *Journal of Physiology*, **19**, pp. 312–326 (1896).

[351] A.J. Staverman, The theory of measurement of osmotic pressure. *Recueil des Travaux Chimiques des Pays-Bas - Journal of the Royal Netherlands Chemical Society*, **70**, pp. 344–352 (1951).

[352] R.B. Stoughton, Topical antibiotics for acne vulgaris. *Archives of Dermatology*, **115**, pp. 486–489 (1979).

[353] J.S. Strauss, D.T. Downing, F.J. Ebling, Sebaceous Glands, pp. 569–595 in *Biochemistry and Physiology of the Skin*, Ed. L.A. Goldsmith, Oxford University Press, New York - Oxford **I** (1983).

[354] Syracuse Research Corporation, KowWin (LogKow) Log P calculation. http://esc.syrres.com/interkow/kowdemo.htm (2003).

[355] Z. Taira, H. Terada, Specific and non-specific ligand binding to serum albumin. *Biochemical Pharmacology*, **34**, pp. 1999–2005 (1985).

[356] D.A. Tata, B.J. Anderson, A new method for the investigation of capillary structure. *Journal of Neuroscience Methods*, **113**, pp. 199–206 (2002).

[357] N. El Tayar et al., Percutaneous penetration of drugs: a quantitative structure-permeability relationship study. *Journal of Pharmaceutical Sciences*, **80**, pp. 744–749 (1991).

[358] A.E. Taylor, Capillary fluid filtration, Starling forces and lymph flow. *Circulation Research*, **49**, pp. 558–575 (1981).

[359] A.E. Taylor, T.M. Moore, Capillary fluid exchange. *American Journal of Physiology*, **277**, pp. S203–S210 (1999).

[360] D.G. Taylor, J.L. Bert, B.D. Bowen, A mathematical model of interstitial transport. *Microvascular Research*, **39**, pp. 253–278 (1990).

[361] J.P.K. Tillett, Axial and transverse Stokes flow past slender axisymmetric bodies. *Journal of Fluid Mechanics*, **44**, pp. 401–417 (1970).

[362] M.S. Titcombe, M.J. Ward, An asymptotic study of oxygen transport from multiple capillaries to skeletal muscle tissue. *SIAM Journal of Applied Mathematics*, **60**, pp. 1767–1788 (2000).

[363] K. Tojo, Brick model for drug transport across stratum corneum. *Journal of Pharmaceutical Sciences*, **76**, pp. 889–891 (1987).

[364] K. Tojo, Mathematical modeling of skin permeation of drugs. pp. 1265–1270 (1986).

[365] K. Tojo, Mathematical modeling of transdermal drug delivery. *Journal of Chemical Engineering of Japan*, **20**, pp. 300–308 (1987).

[366] K. Tojo, A.R.C. Lee, A method for predicting steady-state rate of skin penetration in vivo. *Journal of Investigative Dermatology*, **92**, pp. 105–108 (1989).

[367] K. Tojo, A.R.C. Lee, Penetration and bioconversion of drugs in the skin. *Journal of Chemical Engineering of Japan*, **24**, pp. 297–301 (1991).

[368] R.T. Tregear, pp. 21–36 in *Physical Functions of Skin*, Academic Press, London-New York (1966).

[369] R. Tsay, S. Weinbaum, R. Pfeffer, A new model for capillary filtration based on recent electron microscopic studies of endothelial junctions. *Chemical Engineering Communications*, **82**, pp. 67–102 (1989).

[370] E.H. Twizell, The global extrapolation of numerical methods for computing concentration profiles in percutaneous drug absorption. *Computers in Biology and Medicine*, **19**, pp. 163-171 (1989).

[371] G. Tzeghai, S. Weinbaum, R. Pfeffer, A steady-state filtration model for transluminal water movement in small and large blood vessels. *Journal of Biomechanical Engineering*, **107**, pp. 123–130 (1985).

[372] U.S Pharmacist, Clinical review of appropriate uses for albumin. http://www.uspharmacist.com/CE/Albumin/lesson.htm (2003).

[373] J. Uitto, et al., Elastic fibers in human skin: Quantitation of elastic fibers by computerized digital image analyses and determination of elastin by radioimmunoassay of desmosine. *Laboratory Investigation*, **49**, pp. 499–505 (1983).

[374] J. Uitto, D.R. Olsen, M.J. Fazio, Extracellular matrix of the skin: 50 years of progress. *The Journal of Investigative Dermatology*, **92**, pp. 61s–77s (1989).

[375] J.J. Vallner, Binding of drugs by albumin and plasma protein. *Journal of Pharmaceutical Sciences*, **66**, pp. 447–465 (1977).

[376] D. Verotta, L.B. Sheiner, A general conceptual model for non-steady state pharmacokinetic / pharmacodynamic data. *Journal of Pharmacokinetics and Biopharmaceutics*, **23**, pp. 1–4 (1995).

[377] A. Viani, M. Cappiello, G.M. Pacifici, Binding of diazepam, salicylic acid and digitoxin to albumin isolated from fetal and adult serum. *Developmental Pharmacology and Therapeutics*, **17**, pp. 100–108 (1991).

[378] L. Vitellaro-Zuccarello et al., Stereological analysis of collagen and elastic fibers in the normal human dermis: Variability with age, sex, and body region. *The Anatomical Record*, **238**, pp. 153–162 (1994).

[379] B. Vollmar et al., Skin microvascular adaptations during maturation and aging of hairless mice. *American Journal of Physiology*, **279**, pp. H1591–H1599 (2000).

[380] S.M. Wallace, G. Barnett, Pharmacokinetic analysis of percutaneous absorption: evidence of parallel penetration pathways for methotrexate. *Journal of Pharmacokinetics and Biopharmaceutics*, **6**, pp. 315–325 (1978).

[381] C.Y. Wang, Stokes flow through an array of rectangular fibers. *International Journal of Multiphase Flow*, **22**, pp. 185–194 (1996).

[382] W. Wang, A critical parameter for transcapillary exchange of small solutes in countercurrent systems. *Journal of Biomechanics*, **33**, pp. 543–548 (2000).

[383] R.R. Warner, M.C. Myers, D.A. Taylor, Electron probe analysis of human skin: Determination of the water concentration profile. *Journal of Investigative Dermatology*, **90**, pp. 218–224 (1988).

[384] P.D. Watson, F.S. Grodins, An analysis of the effects of the interstitial matrix on plasma-lymph transport. *Microvascular Research*, **16**, pp. 19–41 (1978).

[385] S. Weinbaum, R. Tsay, F.E. Curry, A three-dimensional junction-pore-matrix model for capillary permeability. *Microvascular Research*, **44**, pp. 85–111 (1992).

[386] M. Weiss, M.S. Roberts, Tissue distribution kinetics as determinant of transit time dispersion of drugs in organs: Application of a stochastic model to the rat hindlimb. *Journal of Pharmacokinetics and Biopharmaceutics*, **24**, pp. 173–196 (1996).

[387] R.C. Wester et al., Percutaneous absorption of salicylic acid, theophylline, 2,4-dimethylamine, diethyl hexyl pthalic acid, and p-aminobenzoic acid in the isolated perfused porcine skin flap compared to man in vivo. *Toxicology and Applied Pharmacology*, **151**, pp. 159–165 (1998).

[388] S. Whitaker, Diffusion in packed beds of porous particles. *AIChE Journal*, **34**, pp. 679–683 (1988).

[389] J.W. Wiechers, The barrier function of skin in relation to percutaneous absorption of drugs. *Pharmaceutisch Weekblad Scientific Edition*, **11**, pp. 185–198 (1989).

[390] C.A. Wiederhielm, The Interstitial Space, pp. 273–286 in *Biomechanics, Its Foundations and Objectives*, Ed. Y.C. Fung, N. Perrone, M. Anliker, Prentice-Hall Inc. Englewood Cliffs, NJ (1970).

[391] M.G. Wientjes et al., Penetration of Mitomycin C in human bladder. *Cancer Research*, **53**, pp. 3314–3320 (1993).

[392] H. Wiig, M. DeCarlo, L. Sibley, E.M. Renkin, Interstitial exclusion of albumin in rat tissues measured by a continuous infusion method. *American Journal of Physiology*, **263**, pp. H1222-H1233 (1992).

[393] S.M. Willans, I.D. McCarthy, Distributed model of blood-bone exchange. *Journal of Biomedical Engineering*, **8**, pp. 235–243 (1986).

[394] P.L. Williams, J.E. Riviere, A biophysically based dermatopharmacokinetic model for quantifying percutaneous penetration and absorption of topically applied agents. I. Theory. *Journal of Pharmaceutical Sciences*, **84**, pp. 599–608 (1995).

[395] A. Wilschut, W.F. ten Berge, P.J. Robinson and T.E. McKone, Estimating skin permeation. The validation of five mathematical skin permeation models. *Chemosphere*, **30**, pp. 1275–1296 (1995).

[396] B.M. Wong, D.W. Reeve, Diffusion in fibre beds. *Journal of Pulp and Paper Science*, **16**, pp. J72–J76 (1990).

[397] D.T. Woodley, Importance of the dermal-epidermal junction and recent advances. *Dermatologica*, **174**, pp. 1–10 (1987).

[398] J.D. Wright, F.D. Boudinot, M.R. Ujhelyl, Measurement and analysis of unbound drug concentrations. *Clinical Pharmacokinetics*, **30**, pp. 445–462 (1996).

[399] S.L. Xie et al., A model of human microvascular exchange. *Microvascular Research*, **49**, pp. 141–162 (1995).

[400] F. Yamashita, M. Hashida, *In vivo* and *in vitro* analysis of skin penetration enhancement based on a two-layer diffusion model with polar and nonpolar routes in the stratum corneum. *Pharmaceutical Research*, **11**, pp. 185–191 (1994).

[401] J.R. Yates, Mechanism of Water Uptake by Skin, in *Biophysical Properties of the Skin*, Ed. H.R. Elden, Wiley-Interscience, New York-London-Sydney-Tokyo (1971).

[402] A. Yen and I.M. Braverman, Ultrastructure of the human dermal microcirculation: The horizontal plexus of the papillary dermis. *Journal of Investigative Dermatology*, **86**, pp. 131-142 (1976).

[403] K. Yoneto, et al., A mechanistic study of the effects of the 1-alkyl-2-pyrrolidones on bilayer permeability of stratum corneum lipid liposomes: a comparison with hairless mouse skin studies. *Journal of Pharmaceutical Sciences*, **84**, pp. 853–861 (1995).

[404] W. Zhenxi and W. Ziqiang, External application of drugs: absorption and mechanism. *Journal of Traditional Chinese Medicine*, **13**, pp. 46–49 (1993).

[405] B.W. Zweifach, Permeability aspects of blood tissue exchange. *Investigative Opthalmology*, **4**, pp. 1065–1074 (1965).